UNIVERSIDAD DE SALAMANCA

DOCTORAL THESIS

Dark matter in dense astrophysical objects

Author:
Marina Cermeño Gavilán

Supervisor:
Dr. M Ángeles Pérez-García

Departamento de Física Fundamental, Universidad de Salamanca,
Plaza de la Merced s/n, Salamanca, España

May, 2019

VNiVERSiDAD D SALAMANCA
CAMPUS DE EXCELENCIA INTERNACIONAL

VNiVERSiDAD D SALAMANCA 1218 - 2018

La Dra. M. Ángeles Pérez García, profesora del Departamento de Física Fundamental de la Facultad de Ciencias de la Universidad de Salamanca

Hace constar:

Que la tesis doctoral titulada "Dark matter in dense astrophysical objects" de la que es autora Dña. Marina Cermeño Gavilán ha sido realizada bajo mi dirección y cumple las condiciones formales y académicas exigidas por la legislación vigente para optar al título de Doctor por la Universidad de Salamanca con Mención Internacional, por lo que autoriza su presentación, mediante compendio de publicaciones, a fin de que pueda ser defendida ante el tribunal correspondiente.

Y para que así conste, y a los efectos oportunos, firmo el presente documento en Salamanca a 6 de mayo de 2019.

Dra. M. Ángeles Pérez García

Publicaciones

La presente tesis doctoral incluye seis trabajos originales publicados en revistas científicas cuyas referencias completas, autores y afiliciones de éstos se detallan a continuación

1. Marina Cermeño, María Ángeles Pérez-García and Joseph Silk,
   Physical Review D **94** (2016) 023509.
2. Marina Cermeño, María Ángeles Pérez-García and Joseph Silk,
   Physical Review D **94** (2016) 063001.
3. Marina Cermeño, María Ángeles Pérez-García and Joseph Silk,
   Publications of the Astronomical Society of Australia (PASA) **34** (2017) e043.
4. Marina Cermeño, María Ángeles Pérez-García and Roberto Lineros,
   Astrophysical Journal **863** (2018) 157.
5. Marina Cermeño and María Ángeles Pérez-García,
   Physical Review D **98** (2018) 063002.
6. Marina Cermeño, Jorge Carro, Antonio López Maroto and María Ángeles Pérez-García,
   Astrophysical Journal **872** (2019) 130.

- Marina Cermeño Gavilán
  Departamento de Física Fundamental, Universidad de Salamanca,
  Plaza de la Merced s/n, Salamanca, España
- María Ángeles Pérez-García
  Departamento de Física Fundamental, Universidad de Salamanca,
  Plaza de la Merced s/n, Salamanca, España
- Joseph Silk
  Institut d'Astrophysique, UMR 7095 CNRS, Université Pierre et Marie Curie,
  98bis Blvd Arago, 75014 Paris, France
  Department of Physics and Astronomy, The Johns Hopkins University,
  Homewood Campus, Baltimore MD 21218, USA
  Beecroft Institute of Particle Astrophysics and Cosmology, Department of Physics,
  University of Oxford, Oxford OX1 3RH, UK
- Roberto A. Lineros
  Departamento de Física, Universidad Católica de Chile,
  Av. V. Mackenna 4860, Santiago, Chile
- Jorge Carro Maroto
  Departamento de Física Teórica, Universidad Complutense de Madrid,
  Plaza Ciencias, 1, 28040 Madrid, España
- Antonio López Maroto
  Departamento de Física Teórica, Universidad Complutense de Madrid,
  Plaza Ciencias, 1, 28040 Madrid, España

Acknowledgements

Firstly, I would like to thank my supervisor, M. Ángeles Pérez-García. It has been an honor to be her first Ph.D. student. Thanks for your patience and for being always accesible to me. Apart from the knowledge about our research field I have learnt from you, you have taught me how to do a good research work. What questions I have to ask myself and how to look for the answers. You have also taught me to be more demanding on myself and more independent. I appreciate all the time you have spent with me and your efforts to help me grow profesionally giving me the opportunity to attend a lot of meetings related with this research area and visit other institutions. Thanks for making me a better physicist and for your trust during these four years.

I am also very grateful to the MULTIDARK Consolider project CSD2009-00064 for giving me the opportunity of being part it, allowing me to know many people working on the dark matter field, some of whom I have had the opportunity to collaborate scientifically. Thanks for the funding provided during my Master Thesis and the first seven months of my Ph.D. studies. This thesis is, to a large extent, due to you.

After the months supported by the MULTIDARK project, I was awarded with the pre-doctoral fellowship of the University of Salamanca and Banco Santander (project SA083417). I must thank both of them for allowing me to continue with my research. I also thank the national project FIS2015-65140-P, of which I have been part during these years, for the support to attend international congresses and visit other institutions.

I want to thank Fernando Atrio Barandela for being always willing to help and lend a hand to me. I would also like to thank David Rodríguez Entem and Marc Mars Lloret for helping me with all bureaucratic issues which I have had, making everything very easy.

The research work carried out during these years would not have been possible without the persons who have collaborated with my supervisor and me. Thanks to Joseph Silk, Roberto Lineros, Antonio López Maroto and Jorge Carro. It has been very easy and stimulating to work with you. I also want to thank Jose Cembranos for his help when I became interested in the dark matter field and whenever I have needed his advice.

Thanks to Joakim Edsjö for giving me the chance to visit the Department of Physics at the Oskar Klein Center for Cosmoparticle Physics at the Stokholm University during three months and for teaching me how a big code such as DarkSUSY works. I am really grateful that you make my stay there so pleasant.

I would like also to thank David G. Cerdeño for giving me the opportunity of visiting the Institute for Particle Physics Phenomenology in Durham (UK) and for our interesting discussions. Thanks for your help too.

These years would just not be the same without my officemates. Thanks Paz, Carlos and Alberto for helping me both academically and personally. Thanks Mario, because although I met you when everything was about to finish you are part of this

too. Thanks Christina because from the very beginning you where able to see I could carry out this research. Thanks for your unconditional help.

I thank my friends Roberto, Fer and Josepa for having shared so many things with me during these years. Thanks for being a support. Thanks Leti, Laura and Vero, because you have been by my side always. Isma, thanks for being not only my classmate and flatmate but also my friend and an inspiration for me. And, talking about classmates, I have also to thank my friend Jb for everything we have shared since we started to study physics. I do not know what would have been without you.

I want to thank my friends from Alcalá, who have been all the time close although I was not living there anymore. Specially to Antoñito, Natalia, Paula, Marta, Patry, Bea, Susana and Jorge. Elia, thank you too for coming along with me always. And, of course, thanks Paloma, Julia, Elisa, Blanca and Miguel, the little piece of Paradinas which have accompanied me during this process. Thanks Nadia, not only for the english lessons but also for all our conversations besides those. I am going to miss them. Thanks all of you for being part of this.

Adri, thank you for being with me at every step. Everything is easier having you by my side.

Lastly, I would like to thank my family for all their love and encouragement. Specially to my parents, Carmen and Joaquín, and sister, Carmen, who have never doubted that I could do anything that I decided. Thank to my aunts, Paloma and María Jesús, because you have lived my day to day helping me with anything I have needed. Germán and Sara, thanks you too for being not only my cousins but also my friends. And, I want also to thank Jesús and María for their support during these years.

Thank all of you and many other people who has shared with me all this period.

Agradecimientos

Primero de todo, me gustaría dar las gracias a mi directora de tesis, M. Ángeles Pérez García. Ha sido un honor ser tu primera estudiante de doctorado. Gracias por tu paciencia y por estar siempre accesible y disponible para cualquier cosa que he necesitado. Aparte de los conocimientos que he adquirido gracias a ti, me has enseñado cómo llevar a cabo un buen trabajo de investigación. Qué preguntas debo hacerme y cómo buscar las respuestas. Gracias a ti he aprendido a ser más exigente conmigo misma y más independiente. Agradezco mucho todo el tiempo que me has dedicado y tus esfuerzos por ayudarme a crecer profesionalmente dándome la oportunidad de acudir a gran cantidad de congresos relacionados con este campo de investigación y de visitar otras instituciones. Gracias por ayudarme a ser una mejor física y por tu confianza durante estos cuatro años.

Me gustaría dar las gracias también al proyecto Consolider MULTIDARK CSD2009-00064 por darme la oportunidad de forma parte del mismo, permitiéndome conocer a una gran cantidad gente que trabaja en el campo de la materia oscura, con algunos de los cuales he tenido la oportunidad colaborar después. Gracias por la financiación que me proporcionasteis durante el máster y durante los primeros siete meses de mis estudios de doctorado. Esta tesis es, en gran medida, gracias a vosotros.

Tras los meses de investigación financiados por el proyecto MULTIDARK, la Universidad de Salamanca me concedió un contrato predoctoral cofinanciado por el Banco Santander (proyecto SA083417). Debo agradecerle a ambas entidades el permitirme continuar con mi trabajo de investigación. También agradezco al proyecto FIS2015-65140-P, del que he formado parte durante estos años, la financiación para asistir a congresos internacionales y visitar otras instituciones.

Me gustaría, además, dar las gracias a Fernando Atrio Barandela por estar siempre dispuesto a echarme una mano con cualquier cosa que he necesitado. Gracias también a David Rodríguez Entem y a Marc Mars Lloret por ayudarme con muchos de los asuntos burocráticos que he tenido que solucionar durante estos años. Agradezco vuestra disponibilidad y que hayáis ayudado a que todo fuera fácil.

El trabajo de investigación que he realizado durante estos años tampoco hubiera sido posible sin las personas con las que hemos colaborado mi directora de tesis y yo. Gracias Joseph Silk, Roberto Lineros, Antonio López Maroto y Jorge Carro. Ha sido muy fácil y estimulante trabajar con vosotros. También me gustaría dar las gracias a Jose A. Ruiz Cembranos por su ayuda en el momento en el que comencé a estar interesada en el campo de la materia oscura y siempre que he necesitado su consejo.

Quiero también agradecer a Joakim Edsjö el darme la oportunidad de visitar el Departamento de Física en el Oskar Klein Center for Cosmoparticle Physics en la Universidad de Estocolmo durante tres meses. Gracias por enseñarme cómo funciona un código tan potente y extenso como es DarkSUSY. Estoy realmente agradecida por tu acogida y que hicieras que mi estancia fuera tan agradable.

Gracias también a David G. Cerdeño por darme la oportunidad de visitar the Institute for Particle Physics Phenomenology en Durham (Reino Unido) y por todas nuestras interesantes discusiones. Gracias también por tu ayuda.

Estos años no hubieran sido lo mismo sin mis compañeros de despacho. Gracias Paz, Carlos y Alberto por ayudarme tanto académicamente como personalmente. Gracias Mario, porque, aunque llegaste cuando todo estaba acabando, eres parte de esto también. Gracias Christina, porque desde el principio supieste que podría continuar con esta investigación. Gracias por tu ayuda incondicional.

También quiero agradecer a mis amigos Roberto, Fer y Josepa todo lo que hemos compartido durante estos años. Gracias por ser un apoyo tan grande, sobran las palabras. Gracias Leti, Laura y Vero, porque habéis estado siempre a mi lado, cualquier cosa que os diga se queda corta. Isma, gracias por ser no sólo mi compañero de clase y de piso, sino también mi amigo y una inspiración para mí. Y, hablando de compañeros de clase, tengo que darle las gracias a mi amigo Jb por todo lo compartido durante la carrera y también después. No sé qué hubiera hecho sin ti.

Me gustaría dar las gracias también a mis amigos de Alcalá, que han estado siempre cerca aunque ya no estuviera viviendo allí. Especialmente a Antoñito, Natalia, Paula, Marta, Patry, Bea, Susana y Jorge. Antoñito, gracias por leer mis primeros artículos aunque no entendieras nada. Natalia, Paula y Marta, gracias por estar en mi día a día y preocuparos siempre por cómo estaba. Patry, gracias por interesarte siempre por lo que he hecho. Bea, gracias por no irte jamás y convertirme en una prioridad. Susana, gracias por seguir a mi lado después de tantos años. Jorge, gracias por sacar siempre un hueco para venir de visita y para tratar mi espalda en los momentos críticos.

Elia, gracias por seguir agarrando mi mano.

Quiero dar las gracias también al trocito de Paradinas que me ha acompañado durante todo este proceso. Gracias a Paloma, Julia, Elisa, Blanca y Miguel. Sois un apoyo incondicional.

Gracias Nadia, no sólo por el inglés, sino también por nuestras conversaciones. Las voy a echar de menos.

Y, por supuesto, gracias a ti, Adri, por estar conmigo en cada paso. Todo es más fácil contigo a mi lado.

Por último, me gustaría agradecerle a mi familia su amor y su apoyo. En especial a mis padres, Carmen y Joaquín, y a mi hermana, Carmen. Gracias por no haber dudado nunca que pudiera hacer cualquier cosa que me propusiera. Gracias a mis tías, Paloma y María Jesús, porque habéis vivido mi día a día ayudándome en todo lo que he necesitado. Germán y Sara, gracias por ser, no sólo mis primos sino también mis amigos. Y gracias también a Jesús y a María por el apoyo durante estos años.

Gracias a todos vosotros y a muchas otras personas que me han acompañado durante todo este periodo.

Contents

List of Figures

Chapter 1

Thesis report

1.1 Why Dark Matter?

Nowadays, one of the most important challenges in cosmology and particle physics is the understanding of the dark matter (DM) nature. Many astrophysical and cosmological observations [1–9] support the existence of a great amount of non-baryonic DM which constitutes the most abundant type of the matter in the presently accepted cosmological model for our Universe (the ΛCDM model [10]). Its density is experimentally well-determined by recent analysis of the Planck Collaboration [11], $\Omega_{CDM}h^2 = 0.120 \pm 0.001$. They have also specified the value of the baryonic density, $\Omega_b h^2 = 0.0224 \pm 0.0001$, and that of the total matter density, $\Omega_m h^2 = 0.1430 \pm 0.0011$. Despite this fact, its true identity remains still an open question, see for example a discussion in [12]. The current theoretical efforts are aimed at finding extensions of the Standard Model (SM) of particle physics looking for dark candidates since under its present form it cannot explain the DM nature.

1.1.1 Evidence for DM

As early as the 1930s, F. Zwicky came to the conclusion that it was required a bigger amount of matter than the visible one so that galaxies in the Coma Cluster remained joined [1, 2]. Therefore, it was necessary the existence of another type of matter with negligible or no electromagnetic but gravitational interaction.

However, it was not until 1977, year in which Vera Cooper Rubin measured the rotation curves of spiral galaxies, when the most convincing and direct evidence for DM was achieved. Observed rotational curves exhibited a flat behavior at large distances against what was expected [3]. In other words, if it is considered that the galaxy mass distribution is gathered in the visible part of the galaxy, far from the galactic disk the gravitational field is that created by a point-like mass. In this way, the velocity of the stars will have to decrease at large distances as $v(r) \propto \frac{1}{\sqrt{r}}$. On the contrary, it was obtained that $v(r) \sim$ constant, see Figure 1.1. This fact implies a mass halo $M(r) \propto r$. Hence, galaxies should be inside an enormous halo of dark and unknown matter.

Since then, a big amount of proofs have been exhibited. The General Relativity (GR) theory postulates that masses distort the space-time and, consequently, a photon passing close to a massive object will deviate its otherwise straight trajectory. Thus, some clusters and elliptical galaxies act like gravitational lenses curving the light trajectory, see Figure 1.2. Using this method, masses of clusters and galaxies can be measured and what is obtained is that only $\sim$ 20% of the mass deduced by gravitational lenses can be observed (luminous matter).

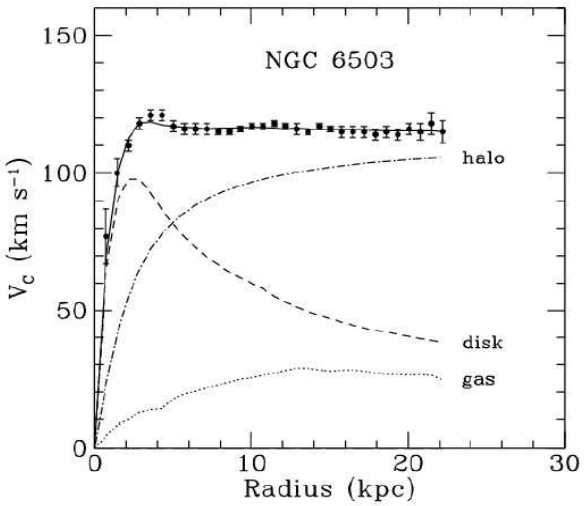

FIGURE 1.1: Rotation curve of NGC 6503 from [13]. The dotted, dashed and dash-dotted lines are the contributions of gas, disk and DM, respectively.

Another striking DM evidence is that provided by the Bullet Cluster [4–6]. This cluster is part of two colliding clusters of galaxies, being the smaller subcluster moving away from the larger one. It has been demonstrated that this cluster pair is mainly compound by three different types of matter. One of them is DM, whose abundance can be measured using gravitational lensing. On the other hand, the stars of the galaxies are observable in visible light and it can be seen that they are not greatly affected by the collision although gravitationally slowed. Another component of the Bullet Cluster is the hot gas, emitting X-rays, which constitutes most of the baryonic matter in the cluster pair and moves much slower than the stars due to the electromagnetic interaction. The key point here is that, during collision, these three components behave differently and can be studied separately. It can be observed that, whereas both gases collide creating a shock wave, the centers of gravitational masses of the subclusters do not collide. See Figure 1.3. This fact cannot be explained in theories involving a pure gravitational effect such as Modified Newtonian Dynamics (MOND) [14, 15] since, in this case, the centers of masses would be expected to follow the baryonic matter.

Besides these indications of the DM existence, there are other ones at cosmological scales. One powerful window into the early Universe is the Cosmic Microwave Background (CMB) [7–9]. This background radiation was originated at the time in which radiation and matter decoupled, when the age of the Universe was ~ 380000 years and baryonic matter started to collapse and to generate structures. Nowadays, CMB is observed to follow an almost perfect black body spectrum, isotropic at 10^{-5} level, corresponding to a temperature $T = 2.725$K [16]. Its small anisotropies are intimately related with the structure formation and, from their analysis, it is possible to test cosmological models and get information about the cosmological parameters. In this way, assuming the ΛCMD model for our Universe, both the abundance of baryons and total matter are determined [11] obtaining that $\sim 85\%$ of the total matter content does not possess a baryonic nature. Besides, it can be concluded that baryonic matter has not been able alone to create the present Universe. DM would

have to decouple from radiation before than ordinary matter to prompt the big structures that we detect.

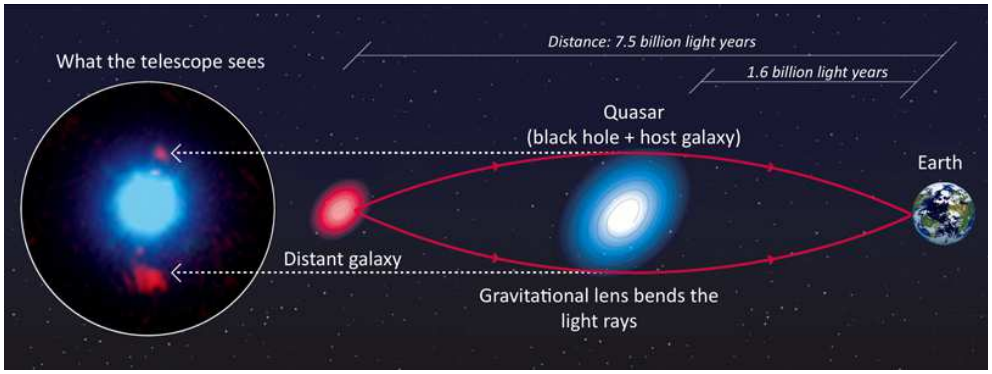

FIGURE 1.2: Gravitational lens. Figure taken from [17].

1.1.2 Candidates

As it has been previously reviewed, the evidence for DM is mainly based on gravitational effects and it can not be explained only by baryonic matter. At the moment, the problem has been circumvented by postulating a new type of matter which interacts gravitationally but negligibly electromagnetically [12]. As another explanation, modifications of gravity have also been suggested as the answer for the total missing gravitational matter. Nevertheless, apart from the problem for some modified gravity (MG) theories like MOND to explain the dynamics of the Bullet Cluster [6], the impossibility to reproduce large-scale structure formation and the anisotropies in the CMB rules out most of them [18–20]. Despite this, newer MG theories aim to match ΛCDM model on cosmological scales solving the before mentioned problems [21, 22]. However, a recent paper [23] concludes that internal motions of Dwarf Galaxies can only be understood by adding cold DM (CDM). They postulate that if two galaxies with the same mass profiles exist, then, they will have to exhibit the same internal dynamics as one another since the law of gravity is the same for both of them. In their study they find that there are at least two galaxies with almost the same mass profiles but largely different gravitational effects.

In this context, the new dark particles that we are looking for have to fulfill some requirements. First of all, DM particles have to be stable against decay or be long lasting, having a lifetime comparable or longer than the age of the Universe, $\tau_U \sim 10^{17}$ s. They should be non-relativistic (as proposed by the paradigm of CDM) at the epoch of structure formation to allow the rise of big structures. In addition, if our candidate is a leading DM constituent, its density has to be consistent with the relic density deduced from the CMB fluctuations [11]. One possibility for its identity is that it is a thermal relic from the early Universe. This points to a weakly interacting particle with a thermally averaged annihilation cross section $\langle \sigma_a v \rangle \sim 3\ 10^{-26}\ \mathrm{cm}^3/\mathrm{s}$ [24]. As another condition, DM should be mostly collisionless in order to be compatible with constraints on structure formation and observations of galaxy cluster systems [25]. However, this could be also satisfied for strongly self interacting DM created thermally via 2 to 3 or 2 to 4 processes (providing the correct relic density) as long as its mass is in the appropriate range, see [26–29]. Finally, it is generally

argued that DM particles must be electrically neutral or slightly charged [30]. Otherwise they would scatter off photons and thus not be dark.

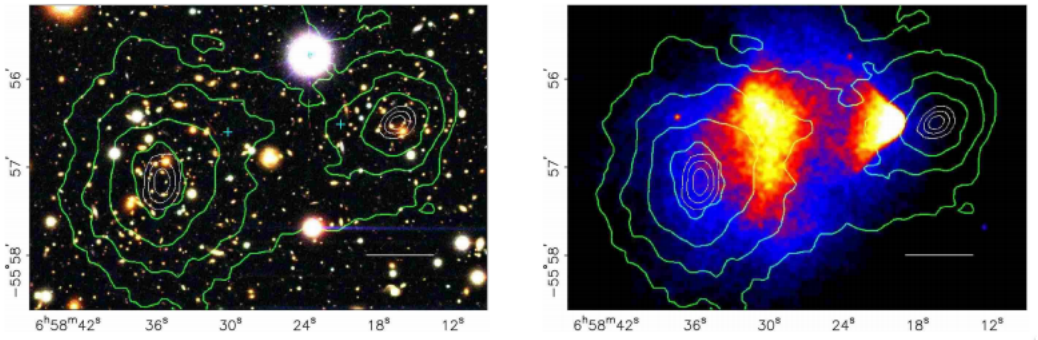

FIGURE 1.3: Bullet globular cluster. Galaxy distribution (left) and gas distribution in X-rays (right) are shown [6]. Green lines depict gravitational equipotential lines which indicate the DM location.

One of the best motivated candidates are the WIMPs (Weakly Interacting Massive Particles) [24] which interact with SM particles through weak interaction. This can be understood as an interaction given by the Fermi theory, with a coupling $G_F \sim 10^{-5}$ GeV^{-2} [31], or just a (sub)weak but non negligible coupling. The motivation for them comes from the assumption that DM particles were created thermally in the early Universe providing the known relic abundance, although other WIMP production mechanisms exist, see [24, 32]. In addition, these requirements can be fulfilled by strongly interacting massive particles (SIMPs) as long as they provide $\langle \sigma_a v \rangle \sim 3\ 10^{-26}$ cm^3/s. These candidates with interaction cross sections with SM particles significantly larger than those of the weak interactions have been studied in the literature by many authors [33–35]. On the other hand, apart from this requirement, values for both DM mass and cross sections with baryonic matter have to be in concordance with constraints coming from the so-called direct, indirect and collider searches. This will be discussed later.

A vast amount of well motivated models can be used to describe the phenomenology of these WIMP and SIMP candidates (Supersymmetric DM [36], Scalar DM [37], secluded DM [38]...). It is out of the scope of this work to discuss the details of all of them. We will restrict our discussion to the models considered during the research presented in this thesis dissertation.

An useful approach is describing the interactions of DM with SM particles by effective operators making minimal assumptions on the DM particle nature and its couplings with SM particles [39, 40]. In their validity range (low momentum transferred) these Effective Field Theories (EFTs) have demonstrated to successfully describe the main features of generic WIMP candidates, having predictive power for direct and collider experiments.

On the other hand, some theories propose a DM particle which interacts with SM particles through metastable mediators providing an almost negligible rate for direct detection (DD) and collider production due to the reduction of its couplings to SM particles by this intermediate state. This scenario is known as secluded DM. In the context of these theories there is a vast amount of models described by different lagrangians, see Tables I and II from [41].

One of the motivations for studying this scenario is the fact that, although direct and collider searches could be not sensitive to these candidates, indirect signals

from their annihilation may be observed. Besides, if the annihilation of DM into SM particles via metastable mediators happens inside stellar objects, the indirect signal coming from this reaction may be enhanced. This would happen due to the fact that the finite lifetime of these mediators may decrease the attenuation of the SM final products passing through the interstellar medium [42–44]. There are also other authors studying the possibility that these candidates annihilate into long lived particles in the galactic center providing an excess of SM particles (coming from the decay of these mediators) far away from the point in which the annihilation takes place [45]. Short lived mediators are also taken into account in the context of indirect detection (ID) [46] demonstrating that the signal is highly dependent not only on the DM annihilation cross section and annihilation final states, but also on the mediator mass.

In particular, some models propose that DM particles could communicate with the visible sector through a pseudoscalar mediator, a, which couples both to DM and SM particles i.e. with interaction lagrangians $\mathcal{L}_{a\chi} = ig_\chi a\bar{\chi}\gamma_5\chi$ and $\mathcal{L}_{af} = ig_f a\bar{f}\gamma_5 f$, where g_χ and g_f are the effective couplings to DM, χ, and SM fermions, f, respectively. These models belong to a set of the so-called simplified type, which possesses a minimal particle content and are understood as part of a more detailed theory [47–51]. One important feature of this type of coupling is the existence of a velocity suppressed χ-nucleon (N) cross section, $\sigma_{\chi,N} \sim \left(\frac{v}{v_0}\right)^4$, in the context of direct searches, since $v \sim 10^{-3}$ (taking the light speed $c = 1$). This means that they will be difficult to test by DD experiments. Nevertheless they can be testable by indirect searches [42, 48, 52, 53].

In the first four published articles presented in this work [54–57] we consider EFT models with non-secluded DM (Chapters 2 and 3) and secluded DM ones (Chapters 4 and 5).

Specifically, in the articles *Diffusion of dark matter in a hot and dense nuclear environment*, M. Cermeño, M. A. Pérez-García and J. Silk, Phys. Rev. D 94 (2016) 023509 [54] and *Light dark matter scattering in outer neutron star crusts*, M. Cermeño, M. A. Pérez-García and J. Silk, Phys. Rev. D 94 (2016) 063001 [55] (Chapters 2 and 3) our candidates are fermionic light DM (LDM) particles, $m_\chi \lesssim 1$ GeV, with Lorentz scalar and vector effective couplings to SM particles in the low momentum transfer limit [58]. These interactions are equivalent to considering a Fermi four-fermion weak interaction model [31]. Here, the effective couplings of mass dimension (-2) are obtained by integrating out the propagator of a generic mediator ϕ of mass M_ϕ and coupling strength $g^2/M_\phi^2 = 1/M_*^2$ at $q^2 \ll M_\phi^2$, with q the transferred four-momentum. Therefore, it is a good approximation to treat them as point-like interactions. Generically, operators containing two fermionic DM fields can be categorized as shown in [59]. In particular, we will focus on those labeled D1 and D5, both contributing to the spin independent (SI) interaction. In addition, for our range of masses it is a good approximation to assume that DM particles do not see the quark structure since the associated wavelength for the incoming DM particles is $\lambda \gtrsim 1$ fm. Typically, elastic scattering (rather than inelastic) is considered as it is the case relevant for DD.

In the Chapter 4, the work *Enhanced Neutrino Emissivities in Pseudoscalar-mediated Dark Matter Annihilation in Neutron Stars*, M. Cermeño, M. A. Pérez-García and R. A. Lineros, Astrophysical Journal 863 (2) (2018) 157 [56] is presented. Here, we consider secluded fermionic WIMPs interacting with SM particles via a pseudoscalar

coupling. These candidates, on the contrary, provide a spin dependent (SD) interaction.

In the article *Gamma rays from dark mediators in white dwarfs*, M. Cermeño and M. A. Pérez-García, Phys. Rev. D 98 (2018) 063002 [57] of Chapter 5 we also take our candidates to be secluded SIMPs but in a mostly independent framework, without considering any specific lagrangian in order to make minimal assumptions.

It is important to remark that, apart from the type of coupling considered, the main difference between the works shown in the Chapters 2 and 3 and those in the Chapters 4 and 5 is the fact that, whereas in the first two articles point-like interactions are studied, neglecting the influence of the mediator over the scattering, in the second two the metastable mediator lifetime and energy losses play a key role.

1.1.3 DM searches and current constraints

In this context, it is necessary to talk about experimental searches and current constraints for our DM candidates.

It is likely that if our galaxy resides inside an enormous DM halo, these particles may be crossing the Earth continuously making possible their detection via interaction with a terrestial target provided a non-zero cross section exists. DD experiments search for a scattering signal due to the interaction between DM particles and SM ones. In particular, most of these settings try to detect particles with masses $m_\chi \gtrsim 1$ GeV by measuring an energy of recoiling nuclei $E_r \sim$ keV in the detector [60]. Other types of direct searches that are starting to be increasingly significant are those which look for DM in the sub-GeV mass range. Such light masses are unreachable for nuclear recoil DD experiments, but may be detected through the small ionization signals caused by DM-electron scattering [61].

Another method of search is attempting to detect DM particles indirectly, via their annihilation or decay into SM products, such as neutrinos [63, 64], gamma rays [65] or antiprotons and positrons [66] above those present in the astrophysical background. An excess of their annihilation products is trying to be observed in regions of increased DM density such as the galactic center and dwarf spheroidal galaxies.

Yet as another strategy, DM is searched as final product in annihilation of SM particles at colliders, see [67] for a review. These experiments alone are not be able to detect DM, they would detect the existence of an invisible particle providing clues for direct and indirect detection experiments. However, they can put constraints on certain models, see Figures 7 and 8 from [67]. Besides, existing models from supersymmetric theories predict favoured regions in the space of parameters which can be complemented by DD and ID bounds, see Figure 8 from [68]. If DM can be produced in particle accelerators, it would be a powerful tool to understand the connection of ordinary matter to DM and to comprehend how the two sectors interacted shortly after the Big Bang.

So far, despite direct and indirect search experiments are increasingly more sensitive and colliders such as the LHC [69] are running at energies close to 13 TeV center-of-mass energies, no signal coming from DM particles has been detected. However, exclusion limits have been established both for nucleon-DM [62] and electron-DM [70] cross sections versus DM mass values. In Figure 1.4 from [71] contraints on DM-nucleon SI cross section versus DM mass are shown.

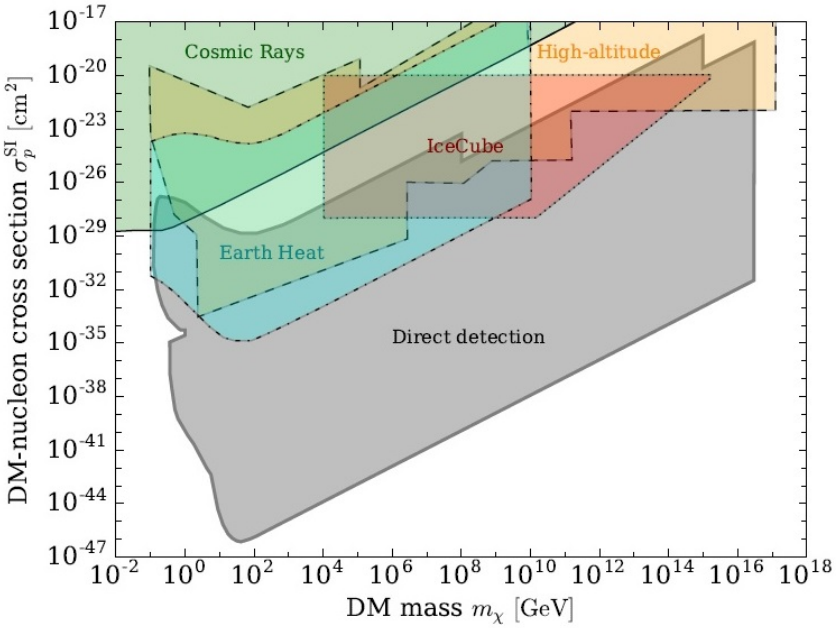

FIGURE 1.4: Summary of constraints on DM from [62]. The solid grey region shows constraints from surface and underground DD experiments. The orange region (dashed line) is excluded by high-altitude experiments. Complementary constraints from IceCube (red region, dotted line), Earth's heat flux (cyan region, dot-dashed line) and DM-cosmic ray interactions (green region, solid line) are also shown.

1.2 Dark Matter inside compact objects

In spite of the variety of detection experiments, some popular candidates are yet difficult to test and they may be well suited to be studied indirectly in astrophysical scenarios. To illustrate, LDM particles with masses smaller than that of the nucleon can only provide kinematical recoil energies at the E_r ∼eV range, below the E_r ∼keV threshold for current conventional terrestrial searches in DD experiments. Nevertheless, they could yet have an impact on the properties of astrophysical objects and provide new indirect signals.

On the other hand, there are many DM candidates displaying interactions with ordinary matter which are momentum suppressed, i.e. their scattering cross sections with normal matter $\sigma_{\chi,N} \sim \mathcal{O}(q^2)$ or $\sigma_{\chi,N} \sim \mathcal{O}(q^4)$, see [72, 73]. This fact makes them almost impossible to test via DD experiments due to the fact that in this context $q \to 0$. On the contrary, these interactions can be important inside dense objects, such as neutron stars (NSs) or white dwarfs (WDs), in which transferred momentum could be higher due to typical temperatures, 10^{-4} MeV $\lesssim T \lesssim 1$ MeV (setting the Boltzmann constant $k_B = 1$), since it is likely that DM particles gain energy from the medium during the interaction. Besides, collisions will not be much coherent because of the boost of DM particles provided by these compact stars.

Yet as another motivation to test DM in these compact scenarios, velocity suppressed annihilation channels, i.e those in which $\sigma v \sim \mathcal{O}(v^2)$, in vacuum or inside the Earth or the Sun, where $v^2 \sim 10^{-6}$, arise from some particular type of DM-SM couplings, see tables I and II of [41] for some examples. These channels could be important if happen inside compact objects in which once DM has thermalized

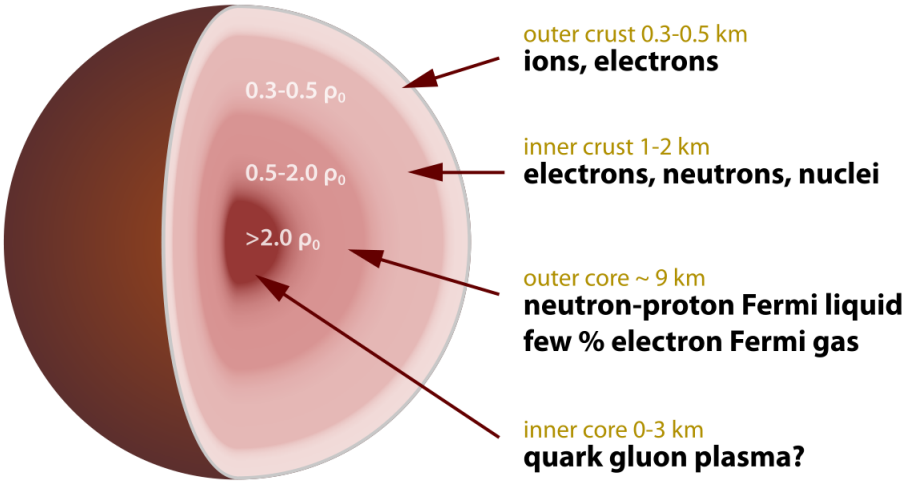

FIGURE 1.5: Neutron Star Section from [74].

$v^2 \sim \frac{T}{m_\chi}$. Therefore, whereas these reactions are not likely to happen in vacuum, they may impact on properties of compact objects or even provide indirect signatures coming from them.

Finally, the fact that both density and compactness (mass-to-radius ratio) of these dense stars is so high combined with the DM local density enhancement with respect to the solar neighborhood value make them better DM accretors than the Earth or the Sun, allowing bigger capture rates. We will focus on these aspects later.

1.2.1 Neutron Stars and White Dwarfs

Both NSs and WDs are formed at the end of the life of a luminous star. The fate of a star with a mass $0.4M_\odot \lesssim M \lesssim 8M_\odot$ is a WD with a degenerate core of Carbon (C) and Oxygen (O), whereas stars with masses $M \gtrsim 8\ M_\odot$ will end their lives becoming NSs or black holes depending on the remnant mass.

NSs are the smallest and densest stars known, with a radius of $R \sim 10$ km and being $\sim 10^{14}$ times denser than the Earth. Into such a small object there is an enclosed mass of $M \sim 1.5M_\odot$.

The notion of NSs as the remnants of supernova (SN) explosions [75], very energetic events in which the previous star releases its outer layers producing electromagnetic emissions, neutrinos and gravitational waves, was suggested for the first time by Baade and Zwicky in 1934. They proposed that the source of these explosions, some of which are visible in daylight for weeks, was the gravitational binding energy of the NS progenitor. On the other hand, NSs can acquire high angular velocities due to the angular momentum conservation of the progenitor and strong magnetic fields through magnetic flux conservation during the collapse of luminous stars. These two features were those which made these objects suitable to be detected for the first time in 1967 due to the beamed periodic signal of pulsars [76].

These compact stars are mostly constituted by nucleons ($\sim$ 90% of the star), which support the star against collapse due to the Fermi pressure, forming a central core at a density in excess of nuclear saturation density, $\rho_0 = 2.4\ 10^{14}\ \mathrm{g/cm^3}$ [77]. The rest of the star is composed by an outer and an inner crust [78]. The

outer crust is formed by periodically arranged nuclei, with increasing baryonic number, A, from Iron (Fe) to Krypton (Kr), with typical densities ranging from $\rho_B \sim 2\ 10^6 - 4\ 10^{11}$ g/cm^3. At these high densities, electrons form a degenerate Fermi sea and very neutron rich nuclei are immersed in a gas of dripped neutrons. This ~ 1 km thick layer forms the inner crust. See Figure 1.5 from [74] where the section of a NS is shown.

In addition, NSs are born hot in SN explosions, achieving internal temperatures around $T \sim 10^{11}$ K. During the first minute after its birth the star becomes transparent for neutrinos generated in its interior [79, 80]. In the following stage NSs cool by emitting neutrinos from their body (mainly from the core) and by heating transport through the envelope to the surface, where electromagnetic emission takes place. In a hundred of years the NS crust and core become thermally adjusted and the NS interior can be considered isothermal. Emission of neutrinos mainly cools the star over the next million years making the star to reach temperatures $T \sim 10^7$ K.

A less dense star example is that of a WD. WDs are the core remnants of medium and low-mass stars after a thermal expansion of their envelope. They are constituted by nuclei immersed in a degenerate electron gas, which supports the star against gravitational collapse due to the degeneracy pressure of electrons. Because of the Pauli exclusion principle, which postulates that two fermions with same quantum numbers cannot occupy the same state, collapse of a WD will increase the kinetic energy of the electrons and, accordingly, the pressure. Densities of these objects are ranging $\rho_B \sim 10^5 - 10^9$ g/cm^3, with masses between $M \sim 0.4 M_\odot$ and $M \sim 1.2 M_\odot$ and an average mass of $M \sim 0.6 M_\odot$ compacted in radii of $\sim 1\%$ of the solar radius.

WDs show a layered structure: in most cases it consists of a C and O degenerate and nearly isothermal core surrounded by a very thin almost pure Hydrogen (H) layer on top of a Helium (He) one, both non-degenerate [81]. These outer layers constitute $\sim 1\%$ of the total radius of the star and, although thin, they determine its thermal evolution. Whereas most of the WD mass is at almost the same temperature, $T \sim 10^6 - 10^7$ K, the surface temperature drops significantly reaching values between $T \sim 10^3 - 10^4$ K [82, 83].

With respect to the equation of state (EoS), for NSs microscopic theories of dense matter are model dependent and provide a large list of possibilities [84], ranging from stiff to soft ones, with different compositions of inner NS cores. A stiff EoS is understood as one in which pressure increases fast when density increases, being the matter described by this equation hard to compress. Conversely, a soft EoS provides a smaller increase of pressure for the same change in density.

On the other hand, for WDs it can be a good estimation to use a polytropic EoS, which relates pressure and density through an equation of the form $P = K\rho^{1+\frac{1}{n}}$, with K a constant with appropriate units and n the index of the equation. It can be easily demonstrated that a non-relativistic Fermi gas of degenerate electrons can be described by an EoS with $n = \frac{3}{2}$, whereas for the relativistic case the correspondent index is $n = 3$. Thus, a WD with non-relativistic electrons could be described by a polytropic EoS of index $n = \frac{3}{2}$. Above a certain density, electrons will become relativistic as they are pushed up to higher momenta by the Pauli exclusion principle. In this case, the index needed will be $n = 3$. See [85–88] for more details.

1.2.2 Capture of Dark Matter particles by dense stars

As it has been mentioned before, the large ratio M/R of compact stars makes them better DM accretors than less dense objects, i.e the Earth or the Sun [89, 90].

On the other hand, it should be noted that the distribution of NSs in our galaxy peaks at distances $\langle r \rangle \lesssim 4$ kpc [91] where the local DM mass density ρ_χ is enhanced with respect to the solar neighborhood value, for which we have used in our works $\rho_{\chi,0}^{ambient} = 0.3$ GeV/cm^3. Although a recent estimate [92] finds $\rho_{\chi,0}^{ambient} = 0.385 \pm 0.027$ GeV/cm^3. In addition, some globular clusters (GCs), such as M4 from which experimental data of stellar magnitudes and distances are available [93], are though to have a core DM density of $\rho_\chi \sim 100 \frac{\text{GeV}}{\text{cm}^3}$ as it has been derived in [94, 95]. Both old WDs [93, 96] and pulsars [97] have been observed in the inner parts of GCs, therefore, it is a good assumption to consider that in many cases ρ_χ around these compact objects will be much higher than the value near the solar system. This fact will also contribute to the enhancement of the capture rate.

Yet as another difference with respect to the terrestrial case, DM approaching NSs can reach relativistic velocities $\beta_{NS} = \sqrt{\frac{2GM_{NS}}{R_{NS}}} \sim 0.6$ (with G the Newtonian gravitational constant), whereas in WDs typically $\beta_{WD} \sim 10^{-2}$ as a result of the gravitational velocity boost. Therefore, the speed value of DM when reaching a WD can be approximately an order of magnitude higher than that for the Earth, $\beta_{Earth} \sim 10^{-3}$, while NSs are suitable to test an intermediate energy range between direct and collider searches.

In this context, after reaching the star, DM could be effectively accreted and retained if it looses enough energy via interaction with baryonic matter. The DM capture rate can be written as [98–100]

$$\Gamma_{\text{capt}} = \frac{8}{3}\pi^2 \frac{\rho_\chi}{m_\chi} \frac{GMR}{1 - \frac{2GM}{R}} \bar{v}^2 \left(\frac{3}{2\pi\bar{v}^2}\right)^{\frac{3}{2}} f, \tag{1.1}$$

where $\bar{v}$ is the average χ velocity in the existing DM distribution at the star location and f is the fraction of particles that undergo one or more scatterings while inside the star. f saturates to ~ 1 if $\sigma_{\chi,i} \gtrsim \sigma_0$, where $\sigma_{\chi,i}$ is the cross section between DM and the SM particle of i-th type (with mass m_i) which constitutes the star and $\sigma_0 = \frac{\pi m_i R^2}{M}$ is the geometrical cross section associated to the stellar object. Otherwise, for $\sigma_{\chi,i} < \sigma_0$, it has been estimated that $f \sim 0.45 \frac{\sigma_{\chi,N}}{\sigma_0}$ for the case of a NS [99] and $f \sim \frac{\sigma_{\chi,A}}{\sigma_0}$ for WDs [100], where $\sigma_{\chi,A}$ is the DM-nucleus cross section.

For NSs, the capture rate can be written numerically as [98]

$$\Gamma_{\text{capt}} \simeq 6 \times 10^{25} \left(\frac{M}{1.5M_\odot}\right) \left(\frac{R}{12\,\text{km}}\right) \left(\frac{1\,\text{GeV}}{m_\chi}\right) \left(\frac{\rho_\chi}{\rho_{\chi,0}^{ambient}}\right) f \text{ s}^{-1}. \tag{1.2}$$

In the same way, for a WD

$$\Gamma_{\text{capt}} \simeq 6 \times 10^{27} \left(\frac{M}{0.6M_\odot}\right) \left(\frac{R}{0.01R_\odot}\right) \left(\frac{1\,\text{GeV}}{m_\chi}\right) \left(\frac{\rho_\chi}{\rho_{\chi,0}^{ambient}}\right) f \text{ s}^{-1}. \tag{1.3}$$

Note that whereas the DM-nucleon cross section needed to get an efficient capture, i.e. DM scatters at least once per star crossing, for the case of NSs is $\sigma_{\chi N} \gtrsim 10^{-45}$ cm^2, for WDs one should have $\sigma_{\chi N} \gtrsim 10^{-39}$ cm^2. Therefore, NSs are more sensitive to test smaller values of the χ-N cross section.

On the other hand, it is important to remark that although DM could be in principle accreted by the star not only during the collapsed stage but also during its previous stellar lifetime, the capture in the compact star stage is generally more efficient due to the high compactness of the object. Still, for cases in which DM particles have

extremely small annihilation cross sections, the amount of DM accumulated during the progenitor lifetime, $N_{0,\chi}$, could be of the order of the number of DM particles accreted by the compact object. See [98, 101, 102] for an estimation of this quantity using Eq. (1.1). It is worth mentioning that there are two competing effects. Whereas mass and radius of the progenitors are larger, allowing more DM particles to cross the star, smaller compactness makes the probability of scattering to be lower.

Returning to the compact star scenario, its core is effectively opaque to DM and allows to build up an internal DM number density, $n_\chi(r)$, where r is the radial stellar coordinate. The number of DM particles which resides inside the star, N_χ, will depend, in general, on the capture, annihilation (or decay) and evaporation rates, $\Gamma_{\rm capt}$, $\Gamma_{\rm ann}$, $\Gamma_{\rm evap}$, respectively, see for example [103, 104]. However, for DM particles accreted by NSs (WDs) with masses larger than $m_\chi \sim 2$ keV ($m_\chi \sim 2$ MeV) evaporation effects can be safely ignored. The argument is as follows. The limiting evaporation mass, m_{evap}, can be estimated by imposing that the typical DM particle velocity when thermalized, $v_\chi \sim \sqrt{\frac{T_c}{m_\chi}}$, at the dense star central temperature, T_c, is less than the local escape velocity of the star, $v_{\rm esc}$. Thus, m_{evap} will somewhat depend on the thermodynamical properties, mass and radius of the star considered. Therefore, for $m_\chi > m_{evap} = \frac{T_c R}{2GM}$ the number of DM particles inside these compact objects at a given time t can be obtained by solving the differential equation

$$\frac{dN_\chi}{dt} = \Gamma_{\rm capt} - 2\Gamma_{\rm ann}, \tag{1.4}$$

where the annihilation rate can be written as

$$\Gamma_{\rm ann} = \frac{1}{2}\int d^3\vec{r}\; n_\chi^2(\vec{r})\langle\sigma_a v\rangle = \frac{1}{2}C_a N_\chi^2. \tag{1.5}$$

Besides, the DM number density inside the star verifies $\int d^3\vec{r}\; n_\chi(\vec{r}) = N_\chi$ at a given time. Supposing that thermalization times are much smaller than dynamical cooling times, once inside, DM is believed to diffuse toward the denser central stellar regions and to distribute according to the exponential law

$$n_\chi(r) = n_{0,\chi} e^{-\frac{m_\chi}{T}\Phi(r)}, \tag{1.6}$$

with $n_{0,\chi}$ the central value and $\Phi(r) = \int_0^r \frac{GM(r')dr'}{r'^2}$ the gravitational potential. Taking the density in this volume to be constant and equal to the central value, $\rho(r) = \rho_c$, it is verified $n_\chi(r) = n_{0,\chi} e^{-(r/r_{\rm th})^2}$ with $r_{\rm th} = \sqrt{\frac{9T}{8\pi G\rho_c m_\chi}}$ the thermal radius [104]. In this way, if DM particles self-annihilate, these reactions will be more likely to happen inside compact stars than in vacuum or less dense objects because of the higher DM densities in their central core. In addition, solving Eq. (1.4) for $t \gg \tau_{\rm eq} = 1/\sqrt{\Gamma_{\rm capt} C_a}$, where $\tau_{\rm eq}$ is an equilibrium time-scale set by the competing processes of capture and annihilation, it is obtained $\Gamma_{\rm capt} = 2\Gamma_{\rm ann}$ as a steady solution.

It is worth mentioning that for asymmetric DM, i.e. DM which does not self-annihilates, there is a critical value of the amount of accumulated DM mass. This limit comes from the fact that the star could be destroyed forming a black hole as it has been studied in [98, 105, 106] both for fermionic and bosonic candidates. Even so, it is important to note that the fraction of DM inside the star remains tiny at all times. For asymmetric DM, case in which the fraction of DM will be greater as compared to the self-annihilating case, the number of DM particles inside the star can be estimated as $N_\chi(t) \approx N_{0,\chi} + \Gamma_{\rm capt} t$. For example, for the case of an old NS with

a lifetime $t \sim 10^9$ yr, using the expression of Eq. (1.2) and taking $N_{0,\chi}$ of the same order than $\Gamma_{\text{capt}} t$ (in general it will be of the same order or smaller), we can estimate $N_\chi(t)$. As the number of baryons in the star is $N_B \simeq 2\ 10^{57}$, the ratio between the number of DM particles and nucleons yields $Y_\chi = N_\chi / N_B < 2\ 10^{-13}$. In the same way, for typical WDs with ages $t \sim 10^9$ yr, the number of baryons is $N_B \simeq 7\ 10^{56}$, therefore $Y_\chi = N_\chi / N_B < 5\ 10^{-11}$.

At this point, it should be pointed out that in the works presented in this dissertation [54–57] both no-thermalized (Chapters 2 and 3) and thermalized DM (Chapters 4 and 5) scenarios inside compact stars have been studied.

The work *Diffusion of dark matter in a hot and dense nuclear environment*, M. Cermeño, M. A. Pérez-García and J. Silk, Phys. Rev. D 94 (2016) 023509 [54] (Chapter 2) considers the interaction of DM which reaches a NS at $\beta_{NS} \sim 0.6$ with nucleons of the inner core, whereas in the article *Light dark matter scattering in outer neutron star crusts*, M. Cermeño, M. A. Pérez-García and J. Silk, Phys. Rev. D 94 (2016) 063001 [55] (Chapter 3) the effect of the interactions of these relativistic DM particles with nuclei of the outer crust is analyzed.

On the other hand, in the articles *Enhanced Neutrino Emissivities in Pseudoscalar-mediated Dark Matter Annihilation in Neutron Stars*, M. Cermeño, M. A. Pérez-García and R. A. Lineros, Astrophysical Journal 863 (2) (2018) 157 and *Gamma rays from dark mediators in white dwarfs*, M. Cermeño and M. A. Pérez-García, Phys. Rev. D 98 (2018) 063002 [56, 57] (shown in Chapters 4 and 5) consequences of DM which has had time to thermalize inside NSs and WDs are studied. In Chapter 6 a review of DM inside NSs titled *Fermionic Light Dark Matter particles and the New Physics of Neutron Stars*, M. Cermeño, M. A. Pérez-García and J. Silk, PASA 34 (2017) e043 [107] is presented.

Finally, the effect of MG theories in different properties of low-mass stars and WDs is studied in the work presented in Chapter 7, *Modified Gravity at Astrophysical Scales*, M. Cermeño, J. Carro, A. L. Maroto and M. A. Pérez-García, Astrophysical Journal 872 (2019) 130 [108].

1.3 Review of the contributions presented in this thesis dissertation

The research presented in this dissertation is focused on the interaction of DM with ordinary matter inside dense objects, such as NSs and WDs, and measurable consequences from indirect signals arising from them.

The dense and hot nuclear medium of proto-NS interior effects in the cross section of boosted fermionic LDM scattering off nucleons have been studied in the article *Diffusion of dark matter in a hot and dense nuclear environment*, M. Cermeño, M. A. Pérez-García and J. Silk, Phys. Rev. D 94 (2016) 023509 [54] (Chapter 2). In this contribution, we considered LDM which couples to nucleons via scalar and vector effective interactions, i.e with an interaction Lagrangian under the form

$$\mathcal{L}_{\mathcal{I}} = \sum_{N=n,p} \frac{G_{s,N}}{\sqrt{2}} \chi \overline{\chi} N \overline{N} + \sum_{N=n,p} \frac{G_{v,N}}{\sqrt{2}} \chi \gamma^\mu \overline{\chi} N \gamma_\mu \overline{N}, \tag{1.7}$$

where γ_μ are the Dirac matrices and $G_{s,N}, G_{v,N}$ are the scalar and vector coupling constants to nucleons. We assumed a point-like interaction similar to the Fermi theory [31] of weak interaction, as we studied low energy momentum transfer events inside the star.

In order to take into account nuclear medium effects, first of all, Fermi-Dirac distribution functions for the nucleon sector, $f_N(E) = \frac{1}{1+e^{(E-\mu_N^*)/k_BT}}$, must to be considered. They introduce dependencies on the effective nucleon chemical potential, μ_N^*, the nucleon energy E and T. The role of these functions is to partially restrict the outgoing nucleon phase space in the $\chi N \to \chi N$ reaction according to the Pauli exclusion principle. We assumed that all outgoing DM particles states are in principle allowed because it can be easily verified (Section 1.2.2) that the fraction of DM inside the star remains tiny at all times. Another density effect was taken into account through the effective values of the nucleon chemical potential and mass, m_N^*, which differ from the nude values, μ_N and $m_N \geq m_N^*$, by the presence of meson fields [109]. In addition, temperature effects were considered by adding the detailed balance factor [110], $S(q_0, T) = \frac{1}{1-e^{-\frac{|q_0|}{k_BT}}}$, which accounts for positive and negative values of the energy transferred, q_0, during the interaction due to the finite value of the medium temperature.

In order to check the influence of the medium in the LDM scattering events, we calculated the $\chi - N$ differential cross section per unit volume taking into account the medium effects mentioned before. Using the known general expression for this quantity [111]

$$d\sigma = \frac{|\overline{\mathcal{M}}_{\mathcal{N}}|^2}{4\sqrt{(pk)^2 - {m^*}_N^2 m_\chi^2}} d\Phi(p, p', k, k') f_N(E)(1 - f_N(E'))S(q_0), \tag{1.8}$$

where the phase space volume element is

$$d\Phi(p, p', k, k') = (2\pi)^4 \delta^{(4)}(p + k - p' - k') \frac{d^3\vec{p'}}{(2\pi)^3 2E'} \frac{d^3\vec{k'}}{(2\pi)^3 2\omega'}, \tag{1.9}$$

and

$$\begin{aligned} |\overline{\mathcal{M}}_N|^2 &\simeq 4g_{Ns}^2(E'E + {m^*}_N^2)(\omega'\omega + m_\chi^2) \\ &+ 8g_{Nv}^2(2{m^*}_N^2 m_\chi^2 - {m^*}_N^2 \omega\omega' - m_\chi^2 E'E + 2E'\omega' E\omega) \\ &+ 8g_{Ns}g_{Nv}m_N^* m_\chi(E\omega + E\omega' + E'\omega + E'\omega') \end{aligned} \tag{1.10}$$

is the squared scattering amplitude of the process considered, which was obtained using the Feynman rules and retaining the lowest order in particle velocities. We denoted $p'^\mu = (E', \vec{p'})$ and $p^\mu = (E, \vec{p})$ as the four-momentum for the outgoing and incoming nucleon, respectively, and $k'^\mu = (\omega', \vec{k'})$ and $k^\mu = (\omega, \vec{k})$ the analogous for the DM particle. The transferred four-momentum is defined as $q^\mu = (q_0, \vec{q}) = p'^\mu - p^\mu = k^\mu - k'^\mu$.

Once these modifications to the vacuum expression were considered, the cross section per unit volume, i.e the inverse of the mean free path $\lambda_\chi^{-1} = \frac{\sigma(\omega)}{V}$, could be written as

$$\lambda_\chi^{-1} = \frac{m_N^*}{4(2\pi)^3} \int_0^{\omega - m_\chi} dq_0 \int_{|\vec{k}| - |\vec{k'}|}^{|\vec{k}| + |\vec{k'}|} d|\vec{q}| \int_{|\vec{p}_-|}^{\infty} d|\vec{p}| \frac{|\overline{\mathcal{M}}_{\mathcal{N}}|^2 |\vec{p}| f_N(E)(1 - f_N(E'))S(q_0, T)}{4E'|\vec{k}|\sqrt{E^2\omega^2 - {m^*}_N^2 m_\chi^2}}, \tag{1.11}$$

with

$$|\vec{p}_-|^2 = \frac{{m_N^*}^2}{|\vec{q}|^2}\left(q_0 - \frac{|\vec{q}|^2}{2m_N^*}\right)^2. \tag{1.12}$$

This lower integration limit for $\vec{p}$ given by Eq. (1.12) comes from the imposition of the energy conservation, $q_0 = E' - E$, in the non-relativistic limit, which provides a value for the angle between $\vec{p}$ and $\vec{q}$, defined by

$$cos\ \theta_0 = \frac{m_N^*}{|\vec{p}||\vec{q}|}\left(q_0 - \frac{|\vec{q}|^2}{2m_N^*}\right), \tag{1.13}$$

and from the restriction $|cos\ \theta_0| \leq 1$.

Calculating Eq. (1.11) numerically, we found sizable modifications of the mean free path in medium with respect to the vacuum value (Figures 5, 6 and 7 from Chapter 2), which has been found to be a good approximation for interactions inside less dense objects like the Sun or the Earth [90, 112].

We obtained that both temperature and density effects greatly affect our final results (Figures 6 and 7 from Chapter 2). The first one diminishing the mean free path (Figure 6), although the most important changes come from the effect of smaller effective nucleon masses, or, in other words, the finite density of matter (Figure 7). A steady decrease of λ_χ when increasing density can be observed in the case in which no effective nucleon mass was considered. Conversely, when we took into account the effective value of the nucleon mass, we found that above a certain density value the decreasing behaviour changes providing higher values of λ_χ. It is important to note that temperature effects come not only from the detailed balance factor but also from the Fermi Dirac distribution functions at finite temperature.

In addition, although our values for λ_χ are found to be higher than those for the vacuum scenario due to the fact that we are restricting part of the outgoing phase space, we get $\lambda_\chi \ll R$ both for warm and cold NSs. This indicates that it is likely that LDM particles get trapped inside the star, contrary to the case of standard neutrinos, which after the first ~ 10 s of the NS birth ($T \lesssim 10$ MeV) will escape from the star. This fact could provide some modifications of internal energy in cooling processes.

After having studied the interaction of LDM with nucleons of the NS core, where the baryonic density reaches its highest value, a follow up work, *Light dark matter scattering in outer neutron star crusts*, M. Cermeño, M. A. Pérez-García and J. Silk, Phys. Rev. D 94 (2016) 063001 [55] (Chapter 3), considers the scattering of relativistic incoming LDM off the lattice of nuclei in the outer crust of NSs. From this interaction, the possibility of excitation of phonons with momentum $|\vec{k}|$ and polarization λ and potential consequences on NS outer layers is studied. We explored this scenario for the same type of interaction than in the previous work, i.e same interaction lagrangian given by Eq. (1.7).

Restricting the phase space to DM particles with masses $m_\chi \lesssim 500$ MeV, the scattering off nuclei can be treated as elastic and coherent. Besides, acoustic phonons, which follow a linear dispersion relation $\omega_{k,\lambda} = c_{l,\lambda}|\vec{k}|$ with $c_{l,\lambda} = \frac{T_p/3}{(6\pi^2 n_A)^{\frac{1}{3}}}$ the sound speed of the mode, may be excited. Where $T_p = \sqrt{\frac{4\pi n_A Z^2 e^2}{m_A}}$ is the plasma temperature associated to a medium of ions with number density n_A, baryonic number A and electric charge Ze [113]. In order to analyze this, the single acoustic phonon

excitation rate was calculated using the Fermi golden rule

$$R_{\vec{k},\lambda} = 2\pi\delta(E_f - E_i)|\langle f|\mathcal{V}|i\rangle|^2, \tag{1.14}$$

where i and f are the initial and final states considered. $\mathcal{V} = \sum_j \delta^3(\vec{r} - \vec{r}_j)\frac{2\pi a}{m_\chi}$ is the interaction potential felt by an incoming DM particle with energy $E_\chi = \sqrt{|\vec{p}_\chi|^2 + m_\chi^2}$ when approaching a nucleus in the periodic lattice. It is important to remark that the interaction potential only takes this form in the Born approximation ($|\vec{k}| \ll \frac{1}{a}$), in which the $\chi - A$ cross section in the center of mass frame can be estimated as $\sigma_{\chi,A} \simeq 4\pi a^2$ with a the scattering length. In this way, in order to know the phonon excitation rate, it is needed to calculate the parameter a for our type of interaction. This value can be got by performing the squared matrix element, $|\overline{\mathcal{M}}_{\chi A}|^2$, since the cross section in the center of mass frame can also be obtained from $\frac{d\sigma_{\chi,A}}{d\Omega}|_{CM} = \frac{|\overline{\mathcal{M}}_{\chi A}|^2}{64\pi^2 s}$, where s is the Mandelstam variable corresponding to the squared center of mass energy. In other words,

$$4\pi a^2 = m_A^2 \frac{\left(\frac{Z}{m_p}\sqrt{|\tilde{\mathcal{M}}_p|^2} + \frac{(A-Z)}{m_n}\sqrt{|\tilde{\mathcal{M}}_n|^2}\right)^2}{16\pi(m_\chi + m_A)^2}, \tag{1.15}$$

with $\int_{-1}^{1} 2\pi d(cos\ \theta_\chi)|\overline{\mathcal{M}}_{\chi \mathrm{N}}|^2 \equiv |\tilde{\mathcal{M}}_{\mathrm{N}}|$. The squared matrix element for the interaction with nucleons ($N = p, n$), $|\overline{\mathcal{M}}_{\chi \mathrm{N}}|^2$, can be calculated in the same way that it was done in the previous work to obtain Eq. (1.10) from the lagrangian of Eq. (1.7). The only difference here is that we did not neglect $|\vec{p}_\chi|^2$ terms with respect to m_χ^2.

After performing some calculations, the single phonon excitation rate (per unit volume) in the lattice can be cast into the form

$$R_k^{(0)} = \frac{8\pi^4 n_A^2}{(2\pi)^6 m_\chi^2 m_A c_l}\int_0^\infty |\vec{p}_\chi| d |\vec{p}_\chi| f_\chi(\vec{p}_\chi) |E_\chi - |\vec{k}| c_l| a^2, \tag{1.16}$$

where $f_\chi(\vec{p}_\chi) = \frac{n_\chi \mu}{4\pi m_\chi^3 K_2(\mu)} e^{-\mu\sqrt{1+\frac{|\vec{p}_\chi|^2}{m_\chi^2}}}$ is the Maxwell-Jüttner distribution function [114] for a local number density n_χ of relativistic incoming DM particles. $\mu = \frac{m_\chi}{k_B T} \approx 6.7$ for $\sqrt{< v^2 >} \sim 0.6$, see [115] and [116], and $K_2(\mu)$ is the modified Bessel function of second kind.

Once we had evaluated the expression in Eq. (1.16) numerically, we obtained that this quantity does not depend on the phonon momentum, since $|\vec{k}| c_l \ll E_\chi$, contrary to the case of cosmological neutrinos in which there is a strong dependence on $\vec{k}$ [117, 118] that can be fit as $R_\nu^0(|\vec{k}|) = R_{\nu 0} e^{-b|\vec{k}|}$, with $R_{\nu 0} = R_\nu^0(0)$ and b a constant value. Therefore, looking at Figure 1 from Chapter 3, in which the phonon excitation rates due to LDM and neutrinos are shown for $|\vec{k}| \to 0$, it can be seen that our rate could be actually more important than that due to cosmological neutrinos for a finite value of $|\vec{k}|$. In addition, we verified that considering the full relativistic phase distribution functions for the incoming DM particles provides a non-negligible correction to the local phonon excitation rate (monochromatic approximation) of $\sim 20\%$.

In order to analyze astrophysical consequences, we estimated the contribution of LDM to the modification of the acoustic phonon population and its effect on the thermal conductivity in the outer crust. Global thermal conductivity, κ, is the sum

of a contribution from ions, κ_i, and from electrons, κ_e. Besides, the ion-thermal conductivity reads as $\kappa_i^{-1} = \kappa_{ii}^{-1} + \kappa_{ie}^{-1}$. Where κ_{ii} is the ion-ion thermal conductivity, i.e the thermal conductivity due to the interaction between phonons in the lattice, and κ_{ie} is the ion-electron thermal conductivity due to the interaction between electrons and phonons.

In the scenario studied in our work we assumed a BCC lattice and the temperature range verifies $T_U < T < T_D$ for each density considered. $T_U \simeq 0.07 T_D$ is the minimum temperature for which the approximation of free electrons holds [119, 120] and $T_D \simeq 0.45 T_p$ is the Debye temperature. This upper limit for T assures that only acoustic phonons will be excited by thermal mechanisms. Besides, from [120] we know that in this range of temperatures ion-electron conductivity dominates over the standard ion-ion one. The idea here is to analyze if the modification of the ion-ion thermal conductivity due to LDM scattering off nuclei in the lattice can modify this fact.

The ion-ion thermal conductivity can be written under the form [119]

$$\kappa_{ii} = \frac{1}{3} k_{\mathrm{B}} C_A n_A c_l L_{ph}, \tag{1.17}$$

where $C_A = 9 \left(\frac{T}{T_D}\right)^3 \int_0^{T_D/T} \frac{x^4 e^x dx}{(e^x-1)^2}$ is the phonon (dimensionless) heat capacity (per ion) and L_{ph} is an effective phonon mean free path. Typically, L_{ph} is related to the thermal phonon number at temperature T as $L_{ph} \sim \delta t / N_{0,k\lambda} = \delta t (e^{\omega_{k\lambda}/k_{\mathrm{B}}T} - 1)$, where δt is the time unit. In our case, we considered $L_{ph} \sim \delta t / N_{k\lambda}$, where $N_{k\lambda}$ is the total number of phonons, both standard thermal ones and those coming from scattering excitation and stimulated emission [117]. Note that the last ones act diminishing $N_{k\lambda}$. In a 4-volume element $\delta V \delta t$, this quantity is written as

$$N_{k\lambda} \simeq N_{0,k\lambda} + R_k^{(0)} \delta V \delta t - \int \frac{d^3\vec{p}}{n_\chi} f_\chi(\vec{p}) \tilde{R}_k^{(0)} N_{0,k\lambda} e^{(\omega_{k,\lambda} + \vec{k}.\vec{v})/(E_\chi - m_\chi)} \delta V \delta t, \tag{1.18}$$

where $\tilde{R}_k^{(0)}$ is the single phonon excitation rate for each particular momentum value (not averaged over incoming χ momenta). Besides, the Doppler shift due to the relative motion of the NS with respect to the LDM flux was taken into account by adding the term $\vec{k}.\vec{v}$ in the exponential factor, being $v \equiv v_{NS} \sim 10^{-2}$ the galactic NS drift velocity.

Once we had obtained the net number of phonons taking into account LDM interactions in the outer crust, we followed to numerically calculate values for the ion-ion thermal conductivity. On the one hand, we obtained that depending on the value of $|\vec{k}|$ and m_χ the total number of phonons in the lattice will be able to be higher than the standard thermal result (scattering excitation dominates) or lower (stimulated emission caused by the interaction between the new phonons and the standard ones dominates). In the first case, κ_{ii} can be lower than κ_{ie} and, therefore, it will be able to be more important than the latter affecting the total ion conductivity by diminishing it. In the other case, in which κ_{ii} is of the same order or higher than κ_{ie}, κ_{ii} will only affect the total ion conductivity (making it lower) when it is of the same order than κ_{ie}. As an example, in Figure 2 of Chapter 3 we show the enhancement with respect to the standard thermal result of the ion-ion thermal conductivity at large baryonic densities, $\rho_B \gtrsim 10^{11}$ g/cm^3, fixing $m_\chi = 100$ MeV and $|\vec{k}| = 0.01/a$.

After having analized that, considering the existence of magnetic fields in NSs,

we compared our results with electron thermal conductivity in magnetized realistic scenarios. We observed that the ion-ion thermal conductivity can surpass electron thermal conductivity, κ_e, in the perpendicular direction to the magnetic field for $n_\chi \sim 100 n_{0,\chi}$ and $\rho_B \gtrsim 3.5\ 10^{11}$ g/cm^3, where $n_{0,\chi} = \frac{\rho_{\chi,0}^{ambient}}{m_\chi}$ is the solar neighborhood value. This can be seen in Figure 3 of Chapter 3. For this example we took $m_\chi = 65$ MeV and $|\vec{k}| = 0.01/a$, but, as we have mentioned before, other values of m_χ and $|\vec{k}|$ provide the opposite behaviour. Note that in this case what is being compared is only κ_{ii}. Besides, it should be noted that, for magnetized NSs, in the cases in which κ_{ii} is lower or of the same order of κ_{ie}, the LDM effect over the global conductivity in the outer crust will influence on the difference in heat conduction between perpendicular and parallel directions to the magnetic field [121–123].

Once we have analyzed the impact of relativistic DM particles interacting with nuclear matter when they reach NSs, another interesting topic is to study the effect of self-annihilating DM captured by NSs after thermalizing in the NS core. In this way, in our next contribution, *Enhanced Neutrino Emissivities in Pseudoscalar-mediated Dark Matter Annihilation in Neutron Stars*, M. Cermeño, M. A. Pérez-García and R. A. Lineros, Astrophysical Journal 863 (2) (2018) 157 [56] (Chapter 4), we considered the annihilation of secluded DM particles which interact with SM particles via a pseudoscalar mediator, a. In this context, the enhancement of neutrino emissivities from NSs due to these annihilations was studied.

The interaction lagrangian of this model reads [48, 52]

$$\mathcal{L}_\mathcal{I} = -i\frac{g_\chi}{\sqrt{2}} a \bar{\chi}\gamma_5\chi - i g_0 \frac{g_f}{\sqrt{2}} a \bar{f}\gamma_5 f\,, \tag{1.19}$$

where g_χ is the DM-mediator coupling, g_f corresponds to the couplings to the SM fermions, f, and g_0 is an overall scaling factor. We took $g_f = 1$ for all SM fermions, i.e a flavour-universal coupling type, although other schemes are valid [52].

As we have mentioned, we were interested in restricting our final states to neutrinos. In the range $m_\chi < m_{\text{Higgs}}$ and $m_a < m_\chi$, where m_a is the pseudoscalar mass, the relevant annihilation processes are given by a S-wave channel, $\chi\chi \to \nu\nu$, and a P-wave channel via pseudoscalar mediators, $\chi\chi \to aa$, which subsequently decay into neutrinos, $a \to \nu\nu$. The local energy emissivity, energy produced per unit volume per unit time, through a prescribed particle physics reaction, reads [124]

$$Q_E = 4\int d\Phi(E_1+E_2)\,|\overline{\mathcal{M}}|^2\, f(f_1,f_2,f_3,f_4). \tag{1.20}$$

With

$$d\Phi = \frac{d^3\vec{p}_1}{2(2\pi)^3E_1}\frac{d^3\vec{p}_2}{2(2\pi)^3E_2}\frac{d^3\vec{p}_3}{2(2\pi)^3E_3}\frac{d^3\vec{p}_4}{2(2\pi)^3E_4}\,(2\pi)^4\delta^4(p_1+p_2-p_3-p_4) \tag{1.21}$$

the 4-body ($12 \to 34$) phase space element and $|\overline{\mathcal{M}}|^2$ the spin-averaged squared matrix element of the reaction considered. The additional factor $f(f_1,f_2,f_3,f_4)$ accounts for the global phase space blocking due to the initial and final particle distribution functions, f_i, $i = 1,...,4$.

For the S-channel

$$f(f_1,f_2,f_3,f_4) = f_\chi(E_1)f_{\bar{\chi}}(E_2)(1-f_\nu(E_3))(1-f_{\bar{\nu}}(E_4)). \tag{1.22}$$

Since DM Fermi energy is much smaller than the NS temperature, i.e. $E_{F,\chi} \ll T$ with $E_{F,\chi} = \frac{(3\pi^2 n_\chi)^{\frac{2}{3}}}{2m_\chi}$, f_χ can be approximated by a Maxwell Boltzmann distribution function, $f_\chi = f_\chi^{MB}(|\vec{p}_i|, r) = \left(\frac{1}{2\pi m_\chi T}\right)^{\frac{3}{2}} n_\chi(r) e^{\frac{-|\vec{p}_i|^2}{2m_\chi T}}$, $i = 1, 2$. Note that the DM number density at the position r inside the star $n_\chi(r)$ is given by Eq. (1.6). For the particular case of neutrinos we assumed they do not get trapped inside the star, therefore $f_\nu \sim 0$.

On the other hand, for the annihilation into pseudoscalars, the phase space factor reads

$$f(f_1, f_2, f_3, f_4) = f_\chi(E_1) f_{\bar{\chi}}(E_2) f_a(E_3) f_a(E_4). \tag{1.23}$$

On this occasion, DM particles annihilate into bosons, thus there is no Pauli blocking for the a component and we took $f_a(E) \sim 1$ for simplicity.

In order to compute Eq. (1.20) for both reactions, as it has been done in our previous works [54, 55], the squared matrix elements have to be calculated from the lagrangian described by Eq. (1.19).

For the S-wave channel

$$|\overline{\mathcal{M}}_{f\bar{f}}|^2 = \frac{g_\chi^2 g_f^2}{4} \frac{s^2}{(s - m_a^2)^2 + E_{\vec{q}}^2 \Gamma^2}, \tag{1.24}$$

where $s = (p_1 + p_2)^2 = (p_3 + p_4)^2$, $E_{\vec{q}} = \sqrt{|\vec{q}|^2 + m_a^2}$ is the pseudoscalar energy and Γ its decay width through the reaction $a \to f\bar{f}$.

For the P-wave channel

$$\begin{aligned} |\overline{\mathcal{M}}_{aa}|^2 = \frac{-g_\chi^4}{2} \Bigg\{ & \frac{(t - m_a^2)^2 - m_\chi^2(m_\chi^2 + 2m_a^2)}{(t - m_\chi^2)^2} + \frac{(u - m_a^2)^2 - m_\chi^2(m_\chi^2 + 2m_a^2)}{(u - m_\chi^2)^2} \\ + \quad & 2\frac{2m_\chi^2 - s}{u - m_\chi^2} + \frac{(s - 2m_\chi^2)(2m_a^2 - s) + 2m_\chi^2(m_\chi^2 + 2m_a^2 - 2s) - 2(t - m_a^2)^2}{(t - m_\chi^2)(u - m_\chi^2)} \Bigg\} \end{aligned} \tag{1.25}$$

where $t = (p_1 - p_3)^2 = (p_4 - p_2)^2$ and $u = 2m_\chi^2 + 2m_a^2 - s - t$.

Integration details for both S-wave and P-wave channel emissivities can be checked in Chapter 4.

After computing these expressions numerically, the emissivity due to the reaction $\chi\chi \to aa$, and the subsequent decay $a \to \nu\nu$, was found to be higher than that due to the direct production of neutrinos, $\chi\chi \to \nu\nu$, see Figures 2 and 3 from Chapter 4. Besides, our energy emissivity can be enhanced orders of magnitude compared to that due to Modified URCA (MURCA) standard neutrino processes for parameter sets (m_χ, m_a, g_χ y g_0) which respect DD constraints, cosmological bounds or even tighter rare meson decay bounds. This can be also checked from Figures 2 and 3 in Chapter 4. This comparison is important since during the first $\sim 10^5$ years after the birth of typical NSs they cool off due to the emission of neutrinos via URCA and Modified URCA processes [125, 126]. In our work, however, we do not take into account URCA processes due to the fact that stellar central densities considered are lower than those needed to indeed open these reaction channels [127]. At this point it is important to remark that the emitting region is found to be localized in a tiny fraction of the star (less than 7% of the total stellar volume for $T \lesssim 10^{10}$ K). Still, even in that small region, energy injections could distort the standard energetic mechanisms as it has been shown in [128].

On the other hand, we provide a phenomenological fit of emissivities depending on temperature and DM particle number inside the star as

$$Q_E(T, N_\chi) = Q_0 \left(\frac{N_\chi}{N_{0,\chi}}\right)^2 \left(\frac{T}{1\,\mathrm{MeV}}\right)^{-3}, \tag{1.26}$$

where

$$N_{\chi,0} \simeq 1.5 \times 10^{39} \left(\frac{\rho_\chi}{\rho_{\chi,0}^{ambient}}\right) \left(\frac{1\,\mathrm{GeV}}{m_\chi}\right) \left(\frac{\sigma_{\chi,N}}{10^{-43}\,\mathrm{cm}^2}\right) \tag{1.27}$$

is the initial DM population when the protoNS is born [101]. Using [48] and appendix D in [52] at one-loop in the appropriate kinematical limit, the $\chi - N$ scattering cross section can be written as $\sigma_{\chi,N} \simeq \frac{9}{64\pi} \frac{|\vec{q}|^4 \mu^2 g_N^2 g_\chi^2}{m_N^2 m_\chi^2 (m_a^2+q^2)^2}$, with g_N the DM-nucleon coupling and $\mu = \frac{m_N m_\chi}{m_N + m_\chi}$ the $\chi-$N reduced mass.

One should realize that N_χ depends on temperature indirectly through the temporal variable t. However, although a fully detailed cooling simulation would be needed to explore the temporal sequence, in our work we give instead an estimate on the time duration of the dominance of the neutrino emissivities coming from DM annihilation over local MURCA processes. After doing this, we obtained that these processes can last the entire lifetime of the NS for some of our sets of parameters ($m_\chi = 30$ GeV, $m_a = 1$ GeV).

Having studied the impact of self-annihilating secluded DM with pseudoscalar couplings to SM particles inside NSs, in our following work, *Gamma rays from dark mediators in white dwarfs*, M. Cermeño and M. A. Pérez-García, Phys. Rev. D 98 (2018) 063002 [57] (presented in Chapter 5), we were interested in a related study of secluded DM self-annihilation into metastable mediators, Y, and their subsequent decay into photons, Y$\to \gamma\gamma$, inside WDs. In this case we did not consider any specific lagrangian to get a mostly model independent analysis.

The motivation to consider these less dense stars is the wish of comparing our results with available experimental data. Internal luminosities of WDs in the GC M4 can be derived from experimental measurements of magnitudes and distances [95]. Thus, if we calculate internal luminosities of WDs in this GC due to the annihilation of DM particles and we compare our results with experimental luminosities we can obtain constraints for some of our model parameters.

In this context, we considered sub-GeV DM captured by WDs of mass M_{WD} and radius R_{WD} due to their interaction with C and O nuclei constituting the core of the star. We assumed that the main DM annihilation channel is that producing two generic metastable mediators, $\chi\bar{\chi} \to$ Y Y, which have a finite lifetime at rest $\tau_{rest} \lesssim 1$ s (in order to fulfill constraints from early Universe) and mass $m_Y \leq m_\chi$. These mediators, with velocity $v_\mathrm{Y} = \frac{p_\mathrm{Y}}{E_\mathrm{Y}}$, where E_Y is its energy and $p_\mathrm{Y} = \sqrt{E_\mathrm{Y}^2 - m_\mathrm{Y}^2}$ its momentum modulus, before decaying into photons, may loose energy due to their interaction with nuclei provided that their lifetime, $\tau = \gamma_Y \tau_{rest}$ (with γ_Y the Lorentz factor), is higher than their interaction mean free path, λ_{int}. In other words, Y will scatter off nuclei only if $\frac{1}{\sqrt{1-v_\mathrm{Y}^2}}\tau_{rest} > \frac{1}{\sigma_{\mathrm{Y},A}\, n(r)}$, where $\sigma_{\mathrm{Y},A} = A^2 \sigma_{\mathrm{Y},N}$ is the Y-nucleus cross section, $\sigma_{\mathrm{Y},N}$ the Y-nucleon cross section and $n(r)$ is the nuclei number density. Since the WD is supported by pressure due to degenerate electrons, $n(r)$ can be described by a polytropic EoS. For central densities $\rho_c \ll 10^6$ g/cm^3 the non-relativistic Fermi gas approach is a good estimation. Therefore, restricting our densities to this value, we can take the index $n = \frac{3}{2}$, and $n(r) = \frac{\rho_c}{A m_N} \int_0^r \omega(r')^{\frac{3}{2}} dr'$,

where $\omega(r)$ is the approximated analytic solution of the Lane-Emden equation, accurate to 1% to the numerical full solution [129].

It is clear that when the mediator particle is created, its energy can be written as $E_{Y,0} = E_\chi \simeq m_\chi$, being its momentum modulus $p_{Y,0} = \sqrt{m_\chi^2 - m_Y^2}$. After suffering one interaction, the mediator will loose a momentum fraction, $p_Y = q p_{Y,0}$, with $0 < q < 1$. Thus, approximating these energy losses as continuous, the mediator momentum modulus after travelling a distance r can be obtained by solving

$$\frac{dp_Y}{dr} = \frac{\Delta p_Y}{\lambda_{int}(r)} = \frac{-(1-q)p_Y}{\lambda_{int}(r)}, \tag{1.28}$$

therefore

$$p_Y(r) = \sqrt{m_\chi^2 - m_Y^2}\, exp\left\{\frac{-(1-q)A\sigma_{Y,N}\rho_c}{m_N}\int_0^r \omega(r')^{\frac{3}{2}}dr'\right\}, \tag{1.29}$$

and, accordingly, its energy will also have a radial dependence, $E_Y(r) = \sqrt{p_Y(r)^2 + m_Y^2}$.

On the other hand, attenuation will also be important for the calculation of the mediator decay probability density inside the star. In this occasion, the equation which has to be solved is

$$\frac{dP_{\rm dec}}{dr} = \frac{-P_{\rm dec}}{\gamma_Y \tau_{\rm rest}} = \frac{-P_{\rm dec} m_Y}{\tau_{\rm rest} E_Y(r)}, \tag{1.30}$$

yielding

$$P_{\rm dec}(r) = N\, e^{-\int_0^r \frac{m_Y dr'}{\tau_{\rm rest} E_Y(r')}}, \tag{1.31}$$

which has to fulfill the normalization condition $\int_0^\infty P_{\rm dec} dr = 1$. This implies

$$N\left(\int_0^R e^{-\int_0^r \frac{m_Y dr'}{\tau_{\rm rest} E_Y(r')}} dr + \int_R^\infty e^{-\int_0^r \frac{m_Y dr'}{\tau_{\rm rest} E_Y(R)}} dr\right) = 1. \tag{1.32}$$

Once attenuation had been parametrized, both the energy flux at a given distance d outside the WD, $E_\gamma^2 \frac{d\Phi}{dE_\gamma}$, and the internal luminosity, L_χ, due to annihilation of secluded DM particles into photons through metastable mediators could be obtained.

Following [44], when expressions for solar photon energy flux due to secluded DM annihilation are given, the photon flux reads

$$E_\gamma^2 \frac{d\Phi}{dE_\gamma} = \frac{\Gamma_{\rm ann}}{4\pi d^2} E_\gamma^2 \frac{dN_\gamma}{dE_\gamma}(R) P_{\rm d,out}^Y, \tag{1.33}$$

where

$$P_{\rm d,out}^Y = \frac{N\tau_{rest} E_Y(R)}{m_Y} e^{-\frac{m_Y R}{\tau_{rest} E_Y(R)}}\left(1 - e^{-\frac{m_Y (d-R)}{\tau_{rest} E_Y(R)}}\right) \tag{1.34}$$

is the probability that the mediator decays at a distance d from the star center.

It is worth mentioning that ages of typical WDs in the GC M4, $t \sim 12$ Gyr, are much higher than thermalization times, $\tau_{\rm eq} \lesssim 22$ yr. Therefore, $\Gamma_{\rm capt} = 2\Gamma_{\rm ann}$. Thus, the annihilation rate is fully determined by the rate of DM captured by the star, which, apart from other dependencies, depends on $\sigma_{\chi,N}$, see Eq. (1.1).

On the other hand, the energy spectrum in the decay process $Y \to \gamma\gamma$ is given by a box-type shape

$$\frac{dN_\gamma}{dE_\gamma}(r) = \frac{4}{\Delta E}\theta(E_\gamma - E_-)\theta(E_+ - E_\gamma), \tag{1.35}$$

with energy ranging from E_- to E_+, where $E_\pm = \frac{1}{\gamma_Y(r)}\frac{m_Y}{2}(1 \mp v_Y(r))^{-1}$ and $\Delta E = E_+ - E_-$.

This can be easily understood having in mind that each of the four photons emitted per annihilation has a monochromatic energy in the rest frame of the mediator given by $\frac{m_Y}{2}$. However, in the laboratory frame there will be a dependence on the angle α between the momentum of the mediator and the photon emitted $E_\gamma = \frac{1}{\gamma_Y}\frac{m_Y}{2}(1 - v_Y \cos\alpha)^{-1}$ with $\cos\alpha \in [-1, 1]$.

Knowing that, the internal luminosity can be written as

$$L_\chi = \Gamma_{\text{ann}} \int_0^{R_{\text{WD}}} N\, e^{-\int_0^r \frac{m_Y dr'}{\tau_{rest} E_Y(r')}} \left[\int_{E_-(r)}^{E_+(r)} E_\gamma \frac{dN_\gamma(r)}{dE_\gamma} dE_\gamma\right] dr. \tag{1.36}$$

Note that in the limiting case in which $m_Y \sim m\chi$, $v_Y(r) \to 0$ and $\gamma_Y(r) \to 1$, therefore, $E_- \to E_+$ and $\Delta E \to 0$. On the other hand, this scenario can also be achieved due to the mediator attenuation if $\sigma_{Y,N}$ is high enough to stop the mediator.

In order to check both the impact of the mediator lifetime and the attenuation on the internal luminosity L_χ, we evaluated Eq. (1.36) numerically.

We found that, for lower values of the Y decay lifetime at rest, L_χ is higher as more photons are deposited inside the star. In addition, L_χ increases when $m_Y/m_\chi \to 1$, due to the fact that in this limiting case the mediator is created at rest and the probability of decaying inside the star is ~ 1. Both effects can be checked in Figure 3 from Chapter 5.

On the other hand, the effect of energy losses is retained in the $\sigma_{Y,N}$ value, see Figure 1 from Chapter 5, providing higher luminosities as it grows.

After analyzing both effects on the internal luminosity due to the self-annihilation of secluded DM, we compared our results with experimental luminosities of the GC M4 and put constraints on the mediator lifetime. We made this by imposing that our luminosities cannot be higher than the experimental ones. We obtained that the lower allowed value for τ_{rest} (we named it as τ_{limit}) is monotically increasing with m_Y/m_χ as it was expected since L_χ increases with m_Y/m_χ. Besides, the τ_{limit} dependence on m_Y/m_χ changes for different values of $\sigma_{Y,N}$ and $\sigma_{\chi,N}$, i.e different attenuation and capture rate. See Figure 5 from Chapter 5.

In this way, it is possible to obtain different exclusion regions for τ_{rest} versus $\sigma_{\chi,N}$ depending on the values of m_Y/m_χ and $\sigma_{Y,N}$. The most restrictive scenario can be achieved for $m_Y/m_\chi = 1$, case in which there is no attenuation since the mediator is created at rest and, therefore, results will not depend on $\sigma_{Y,N}$. The exclusion plot for this specific case is shown in Figure 4 from Chapter 5. For this choice, it can be seen that the lower limit of τ_{rest} remains constant for $\sigma_{\chi,N} \gtrsim \frac{\sigma_0}{A^2}$ since the only dependence of L_χ on $\sigma_{\chi,N}$ is through $\Gamma_{\text{ann}} = \frac{1}{2}\Gamma_{\text{capt}}$, which saturates to a constant value when $\sigma_{\chi,A} \gtrsim \sigma_0$. On the other hand, for $\sigma_{\chi,N} < \frac{\sigma_0}{A^2}$, $\Gamma_{\text{capt}} \propto \frac{A^2\sigma_{\chi,N}}{\sigma_0}$ and τ_{limit} decreases with $\sigma_{\chi,N}$.

In conclusion, we have been able to obtain constraints for the decay lifetime of the mediator at rest vs the χ-N cross section. This has been done for a model independent study of secluded DM which self-annihilate into two metastable mediators inside WDs taking into account the attenuation of the mediator inside the compact

object.

After that, in Chapter 6, a review of the first three works [54–56] mentioned before (presented in Chapters 2, 3 and 4) titled *Fermionic Light Dark Matter particles and the New Physics of Neutron Stars*, M. Cermeño, M. A. Pérez-García and J. Silk, PASA 34 (2017) e043 [107] is included.

So far, in the works previously presented [54–57] the framework considered has been that of the GR theory. However, in the article *Modified Gravity at Astrophysical Scales*, M. Cermeño, J. Carro, A. L. Maroto and M. A. Pérez-García, Astrophysical Journal 872 (2019) 130 [108] (which can be seen in Chapter 7) a more general scenario in which the hypothesis of the need to consider modifications of gravity is analyzed inside low-density (solar-type) and high-density stars (WDs). In this article, stellar structure equations considering MG theories are solved using a perturbative approach and describing the interior of these stars with a polytropic EoS of index $n = 3$. This choice for the index is a good assumption to model both main sequence stars, at least in the radiation zone, corresponding to the Eddington Standard Model of stellar structure [86, 87, 130], and WDs with relativistic electrons ($\rho_c \gg 10^6$ g/cm^3) [86, 87]. The goal of this work was to analyze variations in their masses and radii due to the modification of the gravity theory and, as a consequence, in their luminosities. In addition, this allowed us to check if variations in the luminosity from the standard case are higher due to DM or MG effects in a perturbative approach.

In the context of MG models, following [131–133], which try to describe large scale structures using a cosmological perturbation theory in Fourier space, we considered lineal scalar perturbations to the Minkowski metric in the Newtonian gauge. The line element reads

$$d\tau^2 = g_{\mu\nu}dx^\mu dx^\nu = -(1+2\psi(r))dt^2 + (1-2\phi(r))(dr^2 + r^2 d\Omega^2), \tag{1.37}$$

where linear scalar perturbations are introduced through the radial potentials $\psi(r)$ and $\phi(r)$ in the weak field approximation, $\psi(r) \ll 1$, $\phi(r) \ll 1$. From this metric, $g_{\mu\nu}$, and considering a perfect fluid, the energy momentum tensor reads

$$T_{\mu\nu} = (\rho + P)U_\mu U_\nu + P g_{\mu\nu}, \tag{1.38}$$

where ρ is the energy density, P the pressure and U^μ the fluid four-velocity.

We assumed a static solution for the four-velocity and took $U^\mu U_\mu = -1$. Besides, we approximated the spatial diagonal component of the energy momentum tensor as $T_{ii} = P(1-2\phi) \approx P$. Thus, the Einstein's equations yield the Tolman-Oppenheimer-Volkoff equations,

$$\nabla^2\phi = 4\pi G\rho, \tag{1.39}$$

$$\frac{d\psi}{dr} = \frac{Gm(r) + 4\pi G r^3 P}{r^2}, \tag{1.40}$$

with $m(r)$ the mass enclosed in a radius r in the star.

After this, from the continuity equation $\nabla_\mu T^{\mu\nu} = 0$, it can be obtained

$$\frac{dP}{dr} = -(\rho + P)\frac{d\psi}{dr}. \tag{1.41}$$

It is important to remark that, in a first order perturbation theory $\psi \sim \phi \sim -\frac{GM(r)}{r}$ and $P \sim 0$. Therefore, whereas ρ and ψ are first order functions in perturbation theory, P is a second order function in perturbations. In this way, Eqs. (1.40) and (1.41) can be rewritten as

$$\frac{d\psi}{dr} = \frac{Gm(r)}{r^2}, \tag{1.42}$$

and

$$\frac{dP}{dr} = -\rho\frac{d\psi}{dr}. \tag{1.43}$$

At this point, two functions, $\mu(k)$ and $\gamma(k)$, in the Fourier k-space which modify the equations for the potentials, ψ, ϕ, can be introduced as it is done in [131–133]. Thus, the Poisson equation can be rewritten as

$$\nabla^2\psi = 4\pi G\mu\rho \tag{1.44}$$

and

$$\phi = \gamma\psi. \tag{1.45}$$

Where $\mu(k)$ acts modifying the value of the gravitational constant. Following [133], the most general expression for this parameter is

$$\mu(k) = \frac{1 + p_3k^2}{p_4 + p_5k^2}. \tag{1.46}$$

Or, equivalently, in the position space

$$\mu(r) = \frac{1 - p_3\nabla^2}{p_4 - p_5\nabla^2}, \tag{1.47}$$

with p_3, p_4, p_5 constant parameters, from which p_3 and p_5 have units of squared length and p_4 is dimensionless. Besides, for our study we took $\gamma(k) = 1$.

As we were interested in small perturbations from GR, our parameters verify $p_3\nabla^2$, $p_5\nabla^2 \ll 1$ and $p_4 \sim 1$. In this way, the differential operator μ^{-1} is given by

$$\mu^{-1} = p_4(1 - \xi\nabla^2), \tag{1.48}$$

where

$$\xi = -p_3 + \frac{p_5}{p_4}. \tag{1.49}$$

After that, the Tolman-Oppenheimer-Volkoff equations in a first order perturbation theory read

$$\frac{d\psi}{dr} = \frac{Gm(r)}{p_4r^2} + \frac{\xi G}{p_4}\left(\frac{m''(r)}{r^2} - \frac{2m'(r)}{r^3}\right) \tag{1.50}$$

and

$$\frac{dP}{dr} = -\rho\frac{Gm(r)}{p_4r^2} - \frac{\xi\rho G}{p_4}\left(\frac{m''(r)}{r^2} - \frac{2m'(r)}{r^3}\right), \tag{1.51}$$

which are the modified versions of Eqs. (1.42) and (1.43). Notice that, in order to be consistent with the laboratory measured value of the Newton constant G, we have

to impose $p_4 = 1$. Thus the combination G/p_4 appearing in the obtained structure equations inside the stellar body will effectively take the value G.

At this point, we restricted our study to a polytrope with index $n = 3$. The EoS for this specific polytrope takes the form

$$P = K\rho^{\frac{4}{3}}. \tag{1.52}$$

Therefore, the density profile can be obtained as

$$\rho(r) = \left(\frac{-\psi}{4K}\right)^3. \tag{1.53}$$

Introducing Eq. (1.53) into Eq. (1.44) and using a perturbative approach, we considered a solution under the form $\psi = \psi_0 + \psi_1$, with $|\psi_1| \ll |\psi_0|$. The equations which had to be figured out are

$$\psi_0'' + \frac{2}{r}\psi_0' = \frac{-\pi G}{16}\left(\frac{\psi_0}{K}\right)^3, \tag{1.54}$$

and

$$\psi_1'' + \frac{2}{r}\psi_1' = \frac{-\pi G}{16K^3}\left[\xi\nabla^2(\psi_0)^3 + 3(\psi_0)^2\psi_1\right]. \tag{1.55}$$

After solving numerically these differential equations, we found that our perturbative approach restricts the value of the parameter ξ. More specifically, imposing $|\psi_1| \leq 0.1|\psi_0|$, we got a lower limit for $|\xi|$ which depends on the central density of our star. In this way, for solar-type stars $|\xi| \lesssim 1.2\ 10^{19}$ cm^2.

Once we had obtained the solution $\psi(r)$, which would provide us the value of the density ρ through Eq. (1.53), the radius R of the star was obtained by imposing $\psi(R) = 0$, since both pressure and density vanish for $r = R$. After that, the total mass of the star, $M(R)$, was calculated through the integration

$$M(R) = \int_0^R 4\pi r^2 \rho dr. \tag{1.56}$$

Evaluating these expressions numerically we obtained the $M - R$ diagrams, from which we can observe how the curvature varies from the constant solution of the GR case ($\xi = 0$). Besides, the behaviour of $M(R)$ changes when ξ goes from positive to negative values, corresponding the latter to metastable stellar configurations. This means that negative values of ξ are not going to be allowed since they provide non physical solutions. See Figures 2 and 3 for low-mass stars and Figure 7 for WDs in Chapter 7.

As a consequence, these modifications of M and R values have an impact on the stellar luminosity

$$L = \int_0^R \epsilon(r) dm(r) = \int_0^R 4\pi r^2 \rho(r)\epsilon(r) dr, \tag{1.57}$$

where $\epsilon(r)$ is the nuclear energy generation rate in units of erg g^{-1} s^{-1}. For low mass solar-type stars with active pp chain of neutrino production, $\epsilon(r)$ takes the form [87]

$$\epsilon(r) = 2.46 \times 10^6 \,\text{erg g}^{-1}\,\text{s}^{-1}\,\rho(r)X^2\left(\frac{T(r)}{10^6\ \text{K}}\right)^{-\frac{2}{3}} e^{-33.81\left(\frac{T(r)}{10^6\ \text{K}}\right)^{-\frac{1}{3}}}, \tag{1.58}$$

where X is the H fraction and $T(r)$ is the temperature at a position r inside the star.

In our work, we considered stars mainly dominated by gas pressure, i.e $P \approx P_g = \frac{\rho k_B T}{\bar{\mu} m_H}$, with $\bar{\mu}$ the mean molecular weight and m_H the H mass. Therefore, for a $n = 3$ polytropic star, temperature yields

$$T = \frac{\bar{\mu} m_H K \rho^{\frac{1}{3}}}{k_B}. \tag{1.59}$$

When we computed values for the stellar luminosity, we obtained that it is enhanced with respect to the GR case for $\xi > 0$ (stable configurations) being higher for greater values of ξ (Figure 5 from Chapter 7). We derived as a conclusion that this could cause objects to appear brighter although it seems hard to measure experimentally. Besides, even if it were possible, it appears to be challenging to disentangle this effect from other standard effects such as proper fluctuations of the star.

We also explored the luminosity-effective temperature, T_{eff}, correlation finding a weak and non-trivial dependence on ξ. Writing our correlation under the form $\text{Log}\,\text{L} = \alpha \text{Log}\,[\text{T}_{\text{eff}}(\text{R})] + \text{C}$ we observed a weak variation of $\sim 0.6\%$ in the slope. This can be checked from Figure 6 in Chapter 7. It is important to remark that in our case we have obtained T_{eff} by varying R, therefore we do not expect to recover the usual value $\alpha = 4$ but only to check the dependence on ξ.

After having studied possible variations of the luminosity due to both the self-annihilation of DM inside WDs and the effect of MG theories in a perturbative approach, we have come to the conclusion that the presence of DM will probably affect more this quantity than modifications of gravity in a weak field approximation.

Chapter 1

Memoria de la tesis

1.1 ¿Por qué Materia Oscura?

Hoy en día, uno de los retos más importantes en el ámbito de la cosmología y la física de partículas es la comprensión de la naturaleza de la materia oscura (DM, por sus siglas en inglés). Multitud de observaciones cosmológicas y astrofísicas [1–9] evidencian la existencia de una gran cantidad de DM no bariónica que constituye la mayor parte de la materia en el modelo cosmológico actualmente aceptado para nuestro Universo (modelo ΛCDM [10]). Su densidad está determinada experimentalmente con gran exactitud por análisis recientes de la colaboración Planck [11], $\Omega_{CDM}h^2 = 0.120 \pm 0.001$, así como la densidad bariónica, $\Omega_b h^2 = 0.0224 \pm 0.0001$, y la total, $\Omega_m h^2 = 0.1430 \pm 0.0011$. A pesar de este hecho, su verdadera identidad continúa siendo una cuestión no resuelta, ver por ejemplo una discusión sobre esto en [12]. Desde un punto de vista teórico, actualmente, los esfuerzos se centran en encontrar extensiones del Modelo Estándar (SM, por sus siglas en inglés) de física de partículas buscando nuevos candidatos, ya que éste en su forma actual no puede explicar la naturaleza de la DM.

1.1.1 Algunas evidencias

Ya en 1933, F. Zwicky llegó a la conclusión de que, para que las galaxias del Cúmulo de Coma permanecieran unidas, se requería una cantidad de materia mayor que la que se observada debido a la emisión electromagnética (materia luminosa) [1, 2]. Por lo tanto, era necesaria la existencia de otro tipo de materia cuya interacción electromagnética fuera despreciable o inexistente pero que sí interaccionara gravitacionalmente.

Sin embargo, no fue hasta 1977, año en el que Vera Cooper Rubin midió las curvas de rotación de galaxias espirales, que se logró la evidencia más directa y convincente. Las curvas de rotación observadas mostraban un comportamiento plano a grandes distancias del centro galáctico, contrariamente a lo que se esperaba [3]. En otras palabras, si se considera que la distribución de masa de la galaxia está agrupada en la parte visible de ésta, lejos del disco galáctico el campo gravitacional puede ser descrito por el de una masa puntual. De esta forma, la velocidad de las estrellas tendrá que disminuir a grandes distancias de la forma $v(r) \propto \frac{1}{\sqrt{r}}$. Por el contrario, lo que se obtuvo fue que $v(r) \sim$ constante, ver Figura 1.1. Este hecho implica que debe haber un halo cuya masa $M(r) \propto r$. Es decir, las galaxias deben estar dentro de un halo enorme de materia oscura y desconocida.

Desde entonces, se han obtenido una gran cantidad de evidencias. La teoría de la Relatividad General (GR, por sus siglas en inglés) postula que las masas deforman el espacio-tiempo y, como consecuencia, un fotón pasando cerca de un objeto masivo desviará su trayectoria, que en otro caso seguiría una línea recta. De esta forma,

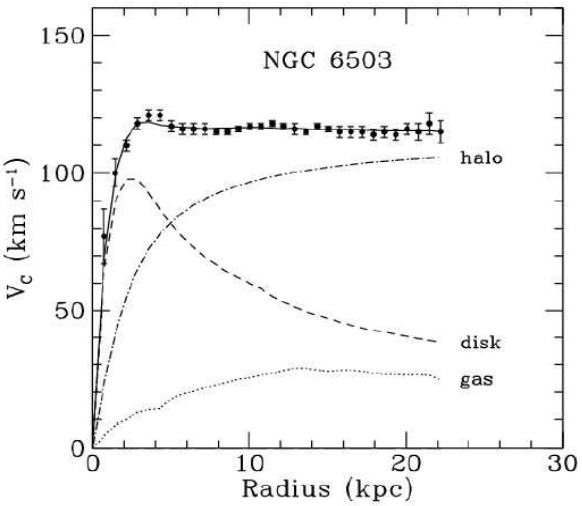

FIGURE 1.1: Curva de rotación de NGC 6503 tomada de [13]. Las líneas punteadas, rayadas y las rayadas con puntos son las contribuciones del gas, disco y DM, respectivamente.

algunos cúmulos y galaxias elípticas actúan como lentes gravitacionales curvando la trayectoria de la luz, ver Figura 1.2. Usando este método se pueden medir masas de cúmulos y galaxias y lo que se obtiene es que sólo un $\sim$ 20% de la masa deducida mediante lentes gravitacionales está constituida por materia luminosa.

Otra evidencia importante es aquella que proviene del Cúmulo de Bala [4–6]. Este cúmulo es parte de dos cúmulos de galaxias que están en colisión, estando el subcúmulo menor alejándose del mayor. La cantidad de DM del cúmulo puede medirse usando el método de lente gravitacional. Por otro lado, las estrellas de las galaxias, que no se ven muy afectadas por la colisión a pesar de que su movimiento es algo decelerado gravitacionalmente, son observadas en el visible. Otro componente del Cúmulo de Bala es el gas caliente emitido en rayos X. Éste constituye la mayor parte de la materia bariónica del sistema de cúmulos y se desplaza mucho más lentamente que las estrellas debido a la interacción electromagnética. El punto importante aquí es que, durante la colisión, estos tres componentes se comportan de forma diferente, pudiendo estudiarse por separado. Se puede observar que, mientras que los gases colisionan creando una onda de choque, los centros de las masas gravitacionales, que no se encuentran donde están los gases de rayos X sino en dos regiones separadas cerca de las galaxias visibles, no se ven afectados por la colisión. Ver Figura 1.3. Este hecho no puede ser explicado mediante teorías que involucran efectos puramente gravitacionales como la Dinámica Newtoniana Modificada (MOND, por sus siglas en inglés) [14, 15] puesto que, en ese caso se esperaría que la lente gravitacional ocurriera gracias a la materia bariónica.

Además de estas evidencias, existen otras a escalas cosmológicas. Una potente ventana hacia el Universo primitivo es el Fondo Cósmico de Microondas (CMB, por sus siglas en inglés) [8, 9]. Esta radiación de fondo fue originada en el momento en el que se desacoplaron la materia bariónica y la radiación, cuando el Universo tenía $\sim$ 380000 años y la materia bariónica empezó a colapsar y a dar lugar a estructuras. Hoy en día observamos que el CMB sigue un espectro de cuerpo negro prácticamente perfecto, isótropo a un nivel de 10^{-5}, con una temperatura $T = 2.725$K. Sus

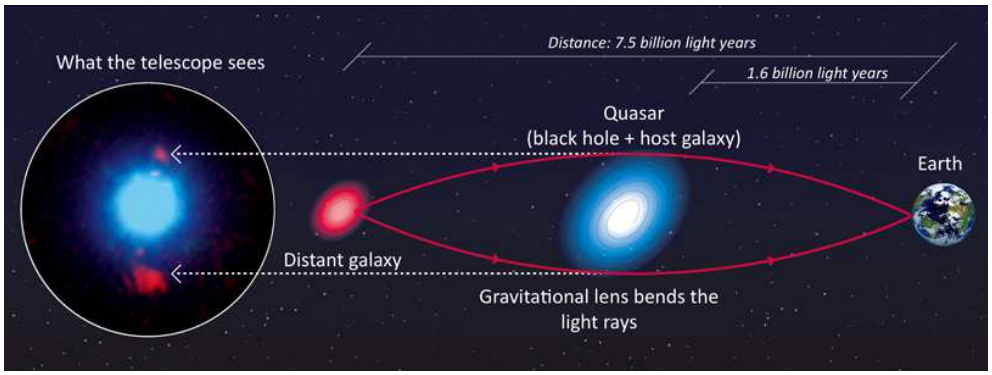

FIGURE 1.2: Lente gravitacional. Figura tomada de [17].

pequeñas anisotropías están íntimamente relacionadas con la formación de estructuras y, de su análisis, es posible testear modelos cosmológicos y obtener información sobre los denominados parámetros cosmológicos. De esta forma, asumiendo el modelo ΛCDM para nuestro Universo, tanto la abundancia de bariones como la de la materia total pueden ser determinadas, obteniendo que $\sim 85\%$ de la materia total no posee una naturaleza bariónica [11]. Además, se puede concluir que la materia bariónica por sí sola no ha tenido tiempo de crear el Universo actual. La DM tendría que haberse desacoplado de la radiación antes que la materia ordinaria para constituir las estructuras tan grandes que detectamos.

1.1.2 Candidatos

Como hemos visto en la sección anterior, estas evidencias están basadas principalmente en efectos gravitacionales que no pueden ser explicados únicamente por la materia bariónica. Hasta el momento, el problema se ha sorteado postulando la existencia de un nuevo tipo de materia que interacciona gravitacionalmente pero cuya interacción electromagnética es despreciable [12]. Como otra alternativa, se ha sugerido que la explicación a la materia que falta podría venir dada por modificaciones de la gravedad. Sin embargo, aparte del problema que presentan algunas teorías de gravedad modificada (MG, por sus siglas en inglés) como MOND a la hora de explicar la dinámica del Cúmulo de Coma [6], la imposibilidad para reproducir la formación de estructuras a grandes escalas y las anisotropías del CMB descarta la mayor parte de estas teorías [18–20]. A pesar de ello, es cierto que teorías más modernas logran coincidir con el modelo ΛCDM a escalas cosmológicas, resolviendo estos dos problemas [21, 22]. Sin embargo, un paper reciente [23] llega a la conclusión de que los movimientos internos de galaxias enanas solo pueden entenderse añadiendo materia oscura fría (CDM, por sus siglas en inglés). Su planteamiento es que si existen dos galaxias con el mismo perfil de materia, entonces, ambas tendrán que presentar la misma dinámica interna, debido a que la ley de la gravedad es la misma para ambas. En su estudio encuentran que hay al menos dos galaxias con prácticamente el mismo perfil de materia pero con efectos gravitacionales diferentes.

En este contexto, las nuevas partículas que buscamos tienen que satisfacer ciertas condiciones. Primero, la DM tiene que ser estable, en el sentido de que no debe decaer en otras partículas, o de larga vida, siendo ésta comparable o mayor que la edad del Universo, $\tau_U \sim 10^{17}$ s. Debe ser no relativista (como propone el paradigma de

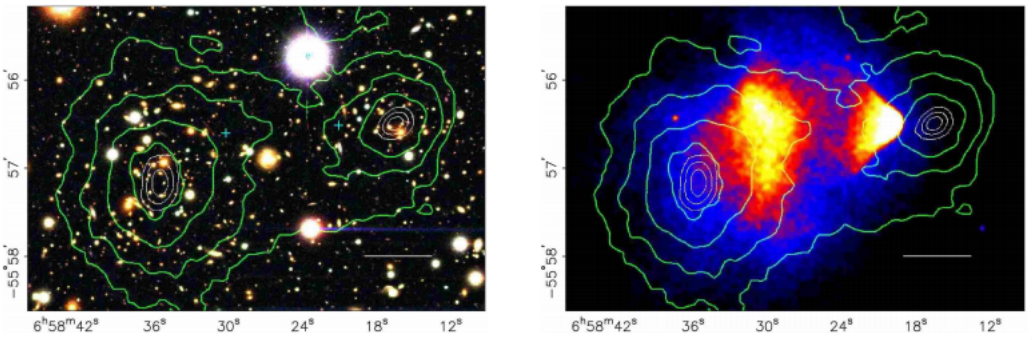

FIGURE 1.3: Cúmulo globular de Bala. Se pueden ver la distribución galáctica en el visible (izquierda) y la del gas en rayos X (derecha). Las líneas verdes representan los equipotenciales gravitatorios que indican la localización de la DM. Imagen tomada de [6].

CDM) en el momento en el que la materia empieza a colapsar, permitiendo el crecimiento de grandes estructuras. Además, si nuestro candidato es uno de los componentes principales de la DM, su densidad tiene que ser consistente con la abundancia de materia total (densidad reliquia) deducida de las fluctuaciones del CMB [11]. Una posibilidad es que estas partículas sean reliquias térmicas del Universo primitivo. Esto apunta a partículas débilmente interaccionantes con una sección eficaz de aniquilación promediada térmicamente $\langle \sigma_a v \rangle \sim 3\ 10^{-26}$ cm^3/s [24]. Como otra condición, la DM no debería tener apenas autointeracción para que sea compatible con los límites de formación de estructuras y las observaciones de sistemas de cúmulos de galaxias [25]. Aunque estos requerimientos podrían satisfacerlos también partículas con autointeracciones fuertes creadas térmicamente mediante procesos de 3 a 2 o de 4 a 2 partículas (proporcionando además el valor correcto de la densidad reliquia) siempre y cuando su masa se encuentre en el rango apropiado, ver [26–29]. Finalmente, en general se argumenta que las partículas de DM deben ser eléctricamente neutras o ligeramente cargadas [30]. En otro caso, interaccionarían con los fotones y no serían oscuras.

Uno de los candidatos a DM mejor motivados son los denominados WIMPs, por sus siglas en inglés (Partículas Masivas Débilmente Interaccionantes), que interaccionan con las partículas del SM a través de una interacción débil [24]. Pudiendo ésta ser entendida como una interacción dada por la Teoría de Fermi, con un acoplo $G_F \sim 10^{-5}$ GeV^{-2} [31], o simplemente como una con un acoplo menor que el de la teoría electrodébil sin ser éste despreciable. La motivación para estos candidatos viene de suponer que estas partículas fueron creadas térmicamente en el Universo primitivo dando lugar a la densidad reliquia conocida, aunque existen otro tipo de mecanismos de producción, ver [24, 32]. Además, estas condiciones pueden cumplirlas también partículas masivas fuertemente interaccionantes (SIMPs, por sus siglas en inglés) siempre y cuando $\langle \sigma_a v \rangle \sim 3\ 10^{-26}$ cm^3/s. Estos candidatos, cuyas secciones eficaces con las partículas del SM son considerablemente mayores que aquellas dadas por interacciones débiles, han sido estudiados en la literatura por numerosos autores [33–35]. Aparte de esta motivación, tanto los valores de la masa de la DM como los de su sección eficaz con la materia bariónica tienen que respetar los límites de exclusión obtenidos mediante experimentos de búsqueda directa o indirecta de DM, así como los debidos a colisionadores de partículas. Esto será discutido más adelante.

Existe una gran cantidad de modelos bien motivados que pueden ser usados

para describir la fenomenología de los WIMPs y de los SIMPs (Supersimetría [36], DM escalar [37], secluded DM [38]...). Entrar a discutir los detalles de todos estos modelos no forma parte de los objetivos de este trabajo pero se introducirán aquellos que se han considerado en los artículos que componen esta tesis.

Una aproximación de gran utilidad es la de describir las interacciones de la DM con las partículas del SM a través de operadores efectivos, haciendo suposiciones mínimas acerca de la naturaleza de la DM y sus acoplos con las partículas del SM [39, 40]. En su rango de validez (bajo momento transferido) se ha demostrado que estas Teorías de Campo Efectivo (EFTs, por sus siglas en inglés) describen satisfactoriamente las principales características de los WIMPs, teniendo poder de predicción sobre experimentos de detección directa y colisionadores de partículas.

Por otro lado, algunas teorías sugieren que las partículas de DM podrían interaccionar con las del SM a través de mediadores metaestables, dando lugar a tasas de detección directa (DD) y de producción en aceleradores de partículas prácticamente nulas debido a la reducción de su acoplo a las partículas del SM causado por la existencia de este estado intermedio. Este escenario es conocido como secluded DM. En el contexto de estas teorías hay una gran cantidad de modelos descritos por distintos lagrangianos, ver Tablas I y II de [41].

Una de las motivaciones para estudiar este escenario es el hecho de que, aunque la búsqueda mediante experimentos de DD y colisionadores de partículas podría no ser sensible a estos candidatos, sí que podrían observarse señales indirectas de su aniquilación. Además, si la aniquilación de DM en partículas del SM a través de mediadores metaestables ocurre dentro de objetos estelares, la señal indirecta proveniente de estas reacciones podría aumentar con respecto a la de una interacción puntual. Esto es así debido a que la vida finita del mediador podría hacer que los productos finales de aniquilación sufrieran menos atenuación dentro de la estrella [42–44]. Otros autores estudian la posibilidad de que estos candidatos se aniquilen en el centro galáctico produciendo partículas metaestables de larga vida que al decaer proporcionarían un exceso de partículas del SM lejos del punto en el que tiene lugar la aniquilación [45]. También se tienen en cuenta mediadores de corta vida en el contexto de la detección indirecta (ID, por sus siglas en inglés) [46] y, se puede demostrar, que la señal debida a ellos depende, no sólo de la sección eficaz de aniquilación de DM y de los estados finales, sino de la masa del mediador.

En particular, algunos de estos modelos proponen que las partículas de DM podrían comunicarse con el sector visible a través de un mediador pseudoescalar, a, que se acopla tanto a la DM como a las partículas del SM, es decir, con lagrangianos de interacción de la forma $\mathcal{L}_{a\chi} = ig_\chi a\bar{\chi}\gamma_5\chi$ y $\mathcal{L}_{af} = ig_f a\bar{f}\gamma_5 f$, donde g_χ y g_f son los acoplos efectivos de a con la DM y con los fermiones del SM, respectivamente. Estos modelos pertenecen a los denominados modelos simplificados, los cuales poseen un contenido mínimo de partículas y son entendidos como parte de una teoría más completa [47–51]. Una característica importante de este acoplo es la de proporcionar una sección eficaz χ-nucleón (N) suprimida por su dependencia con la velocidad, $\sigma_{\chi,N} \sim \left(\frac{v}{v_0}\right)^4$, en el contexto de búsqueda directa en el que $v \sim 10^{-3}$ (tomando la velocidad de la luz $c = 1$). Esto implica que este tipo de candidatos serán difíciles de testear mediante experimentos de DD, siendo la ID mucho más efectiva [42, 48, 52, 53].

En los primeros cuatro artículos publicados presentados en este trabajo [54–57] consideramos modelos del tipo EFT con interacciones puntuales de DM no secluded (Capítulos 2 y 3) y modelos de secluded DM (Capítulos 4 y 5).

En particular, en los artículos *Diffusion of dark matter in a hot and dense nuclear environment*, M. Cermeño, M. A. Pérez-García and J. Silk, Phys. Rev. D 94 (2016) 023509 [54] y *Light dark matter scattering in outer neutron star crusts*, M. Cermeño, M. A. Pérez-García and J. Silk, Phys. Rev. D 94 (2016) 063001 [55] (Capítulos 2 y 3) nuestros candidatos son partículas de DM ligeras (LDM, por sus siglas en inglés), $m_\chi \lesssim 1$ GeV, y fermiónicas que se acoplan a las partículas del SM con acoplos efectivos de tipo escalar y vectorial en el límite de bajo momento transferido [58]. Estas interacciones son equivalentes a considerar el modelo Fermi de interacción débil con un cuadrifermión [31]. En este caso, los acoplos efectivos poseen dimensión de masa (-2) y se obtienen integrando el propagador de un mediador genérico ϕ de masa M_ϕ con una intensidad de acoplo $g^2/M_\phi^2 = 1/M_*^2$ en el caso en el que $q^2 \ll M_\phi^2$. Por tanto, en este contexto, tratar las interacciones como puntuales es una buena aproximación. Típicamente, se consideran colisiones elásticas (en lugar de inelásticas) debido a que éstas son las relevantes para los experimentos de detección directa. Generalmente, operadores que contienen dos campos de DM fermiónica pueden ser clasificados como se muestra en [59]. Más específicamente, nosotros nos centramos en los denominados tipo D1 y D5, que contribuyen ambos a interacciones independientes del espín (SI, por sus siglas en inglés).

En el Capítulo 4 se presenta el trabajo *Enhanced Neutrino Emissivities in Pseudoscalar-mediated Dark Matter Annihilation in Neutron Stars*, M. Cermeño, M. A. Pérez-García and R. A. Lineros, Astrophysical Journal 863 (2018) 157 [56] en el que se consideran secluded WIMPs de tipo fermiónico que interaccionan con partículas del SM a través de un acoplo pseudoescalar. Estos candidatos, por el contrario, proporcionan interacciones dependientes del espín (SD, por sus siglas en inglés).

En el artículo que se muestra en el Capítulo 5, *Gamma rays from dark mediators in white dwarfs*, M. Cermeño and M. A. Pérez-García, Phys. Rev. D 98 (2018) 063002 [57], los candidatos que tenemos en cuenta son secluded SIMPs, aunque en este caso no se toma ningún lagrangiano específico para hacer las mínimas suposiciones posibles. De este modo, se puede decir que nuestros cálculos son prácticamente independientes de la modelización.

Es importante destacar que, aparte del tipo de acoplo, la principal diferencia entre los trabajos expuestos en los Capítulos 2 y 3 y los que se encuentran en los Capítulos 4 y 5 es que, mientras que en los dos primeros artículos se consideran interacciones puntuales, despreciando la influencia del mediador en el scattering, en los dos siguientes la vida media del mediador y las pérdidas de energía de éste juegan un papel importante.

1.1.3 La búsqueda de la DM y límites actuales de exclusión

En este contexto, es necesario hablar acerca la búsqueda experimental de DM y de los límites actuales de exclusión.

Es evidente que, si nuestra galaxia se encuentra dentro de un enorme halo de DM, estas partículas estarán atravesando la Tierra continuamente, haciendo posible su detección a través de la interacción de éstas con blancos terrestres, siempre y cuando la sección eficaz sea no nula. Los experimentos de DD buscan señales en sus detectores debidas a la colisión entre las partículas de DM y las del SM. En particular, la mayoría de estos están construidos con vistas a detectar partículas con $m_\chi \gtrsim 1$ GeV midiendo la energía de retroceso de los núcleos del detector, que es del orden de $E_r \sim$ keV [60]. Otro tipo de búsqueda directa que está ganando importancia es aquella que trata de detectar la DM en un rango en el que $m_\chi \lesssim 1$ GeV. Estas partículas tan ligeras no pueden ser testeadas con experimentos de DD

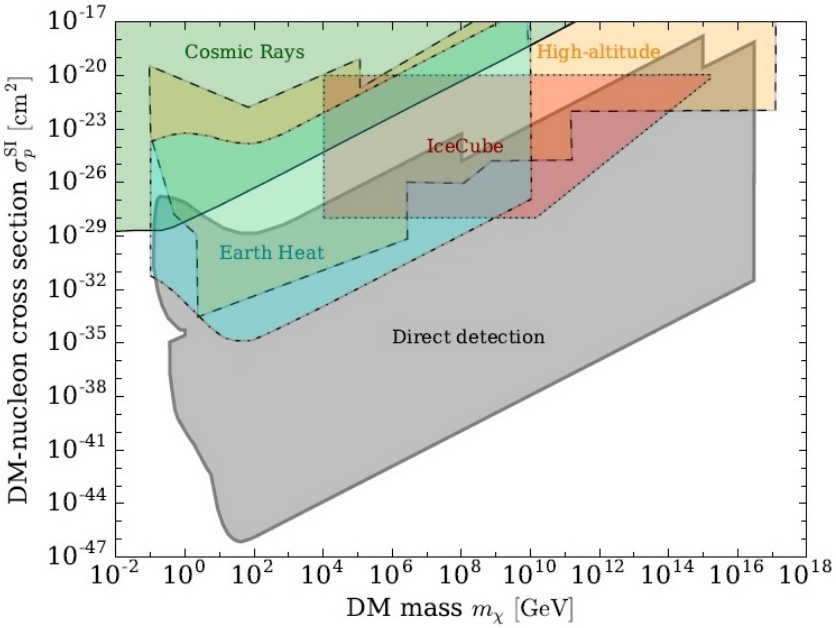

FIGURE 1.4: Resumen de los límites de exclusión de DM tomada de [62]. La región gris muestra los límites de exclusión provenientes de experimentos de DD, tanto de aquellos que se encuentran en la superficie terrestre como bajo Tierra. La región naranja (línea rayada) es excluida por experimentos de ID de gran altitud. Se muestran además límites complementarios de IceCube (región roja, línea punteada), del flujo de calor de la Tierra (región cian, línea de trazos discontínuos de puntos y rayas) y interacciones de DM y rayos cósmicos (región verde, línea sólida).

basados en retrocesos nucleares, pero podrían ser detectadas a través de pequeñas señales de ionización debidas a la colisión de partículas de DM con los electrones de los núcleos del detector [61].

Otro método de búsqueda es tratar de detectar la DM indirectamente, a través de sus productos de decaimiento o aniquilación, suponiendo que éstos fueran partículas del SM. El objetivo de estos experimentos es detectar un exceso de estados finales tales como neutrinos [63, 64], rayos gamma [65], antiprotones o positrones [66] sobre el fondo astrofísico conocido de partículas. Este exceso intenta ser observado principalmente en regiones en las que hay un aumento de la densidad de DM con respecto a la vecindad solar, como el centro galáctico o en galaxias esféricas enanas.

Por último, se intenta también detectar la DM como producto final de aniquilación de partículas del SM en colisionadores de partículas, ver [67] para un repaso actualizado sobre este tipo de búsqueda. Estos experimentos por sí solos no son capaces de detectar la DM, lo que detectarían sería la existencia de una partícula invisible proporcionando pistas para los experimentos de DD e ID. Si la DM se pudiera producir en aceleradores de partículas, tendríamos una poderosa herramienta para entender la conexión entre la materia ordinaria y la DM y para comprender cómo estos dos sectores se relacionaron poco después del Big Bang.

Hasta el momento, a pesar de que tanto los experimentos de DD como los de ID van aumentando su sensibilidad y que los aceleradores de partículas son cada vez más energéticos, alcanzando energías en el centro de masas de 13 TeV en el caso

del LHC [69], no se ha detectado ninguna señal debida a la existencia de la DM. Sin embargo, se han establecido límites de exclusión tanto para los valores de la sección eficaz DM-nucleón [62] como para los de la DM-electrón [70] frente a los de la masa de la DM. En la Figura 1.4 obtenida de [71] se pueden ver las regiones excluidas para los valores de la sección eficaz SI DM-nucleón frente a los de la masa de la DM.

1.2 Materia Oscura dentro de objetos compactos

A pesar de la variedad de experimentos que existen tratando de detectar la DM, algunos candidatos bien motivados son difíciles de testear en detectores convencionales y podría proporcionarnos más información estudiarlos en escenarios astrofísicos.

Por ejemplo, las partículas de LDM con masas menores que la del nucleón sólo pueden proporcionar energías cinéticas de retroceso en el rango del $E_r \sim$eV, por debajo del umbral de energía, $E_r \sim$keV, de los experimentos de DD habituales. Sin embargo, éstas podrían provocar un impacto en propiedades de objetos astrofísicos proporcionando nuevas señales indirectas.

Por otro lado, muchos candidatos de DM exhiben interacciones con la materia ordinaria que están suprimidas por su dependencia en el momento transferido durante la colisión, es decir, su sección eficaz con la materia bariónica verifica $\sigma_{\chi,N} \sim \mathcal{O}(q^2)$ o $\sigma_{\chi,N} \sim \mathcal{O}(q^4)$, ver, por ejemplo, [72, 73]. Este hecho hace que estas partículas sean prácticamente imposibles de testear mediante experimentos de DD puesto que en ellos $q \to 0$. Por el contrario, estas interacciones podrían ser importantes dentro de objetos densos, tales como las estrellas de neutrones (NSs, por sus siglas en inglés) o las enanas blancas (WDs, por sus siglas en inglés). Esto se debe a que el momento transferido durante la interacción podría ser mayor debido las temperaturas típicas de estas estrellas, 10^{-4} MeV $\lesssim T \lesssim 1$ MeV (tomando la constante de Boltzmann $k_B = 1$), ya que existe una probabilidad no nula de que estas partículas ganen energía del medio durante la interacción. Además, en estos objetos, las colisiones no serán, en general, totalmente coherentes debido a la aceleración proporcionada a las partículas de DM por el alto campo gravitatorio creado por estos objetos densos.

Otra motivación para estudiar la DM en estos escenarios compactos es el hecho de que existen modelos con canales de aniquilación que están suprimidos en vacío o en objetos como la Tierra o el Sol debido a su dependencia en velocidades, $\sigma v \sim \mathcal{O}(v^2)$ [134], ya que en estos escenarios $v^2 \sim 10^{-6}$, véanse las Tablas I y II de [41] para algunos ejemplos. Estos canales podrían ser significativos si la aniquilación ocurriese dentro de estrellas densas, una vez que la DM ha termalizado $v^2 \sim \frac{T}{m_\chi}$. De esta forma, mientras que estas reacciones difícilmente ocurrirán en vacío, es muy probable que ocurran dentro de estos medios densos pudiendo tener impacto en sus propiedades o incluso proporcionar señales indirectas provenientes de ellos.

Finalmente, el hecho de que tanto la densidad como la compactificación (ratio entre la masa y el radio) de estas estrellas sean tan altas hace que sean mejores acretores de DM que la Tierra y el Sol, proporcionando una tasa de captura mayor. Estos aspectos serán discutidos más adelante.

1.2.1 Estrellas de Neutrones y Enanas Blancas

Tanto las NSs como las WDs se crean al acabar la vida de una estrella luminosa. El destino de una estrella cuya masa está en el rango $0.4M_\odot \lesssim M \lesssim 8M_\odot$ tras fusionar todo su combustible es desprenderse de sus capas externas quedando tan sólo un

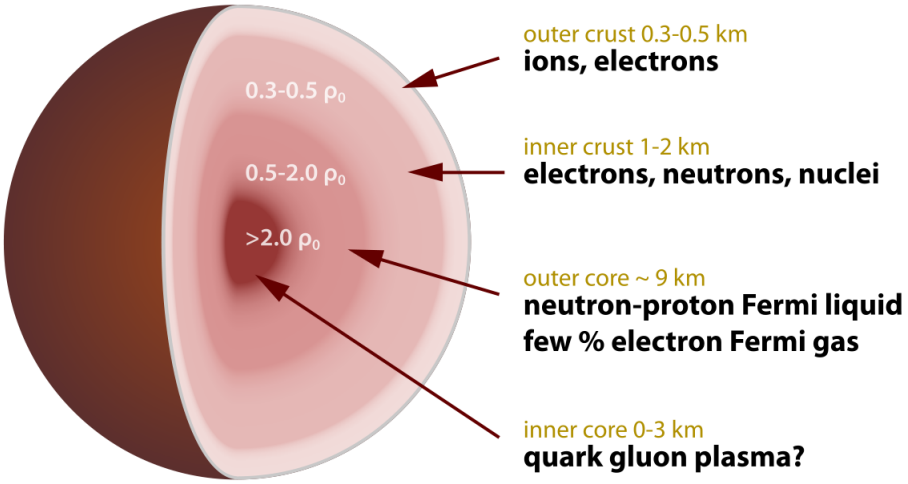

FIGURE 1.5: Sección de una estrella de neutrones tomada de [74].

núcleo degenerado de Carbón (C) y Oxígeno (O), es decir, convirtiéndose en una WD. Por otro lado, las estrellas con masas $M \gtrsim 8\ M_\odot$ terminarán dando lugar a NSs o agujeros negros, dependiendo de la masa del remanente estelar.

Las NSs son las estrellas más pequeñas y densas que se conocen hasta el momento, con un radio de $R \sim 10$ km y siendo $\sim 10^{14}$ veces más densas que la Tierra. En estos objetos se encuentra concentrada una masa de $M \sim 1.5 M_\odot$.

La noción de NS como el remanente de una explosión de supernova (SN) [75], evento en las que la estrella previa se desprende de sus capas externas produciendo emisiones electromagnéticas, neutrinos y ondas gravitacionales, fue propuesta por primera vez por Baade and Zwicky en 1934. Ellos sugerían que la fuente de estas explosiones, que pueden ser visibles a la luz del día durante semanas, era la energía gravitacional que mantiene ligadas a las estrellas progenitoras. Por otro lado, las NSs pueden adquirir velocidades angulares muy altas debido a la conservación del momento angular del progenitor y fuertes campos magnéticos a través de la conservación del flujo magnético durante el colapso de éste. Estas dos características fueron las que hicieron que estos objetos pudieran ser detectados por primera vez en 1967 mediante la intensa señal periódica emitida por púlsares [76].

Estas estrellas compactas están mayoritariamente constituidas por neutrones ($\sim$ 90% de la estrella), los cuales sostienen la estrella contra el colapso gravitacional gracias a la presión de Fermi, permitiendo que se forme un núcleo central que alcanza densidades mayores que la de saturación nuclear, $\rho_0 = 2.4\ 10^{14}\ \mathrm{g/cm^3}$ [77]. El resto de la estrella está compuesto por una corteza externa y otra interna [78]. La corteza externa está formada por una red periódica de núcleos, cuyos números bariónicos, A, van de menos a más, desde Hierro (Fe) hasta Kriptón (Kr), con densidades típicas en el rango de $\rho_B \sim 2\ 10^6 - 4\ 10^{11}\ \mathrm{g/cm^3}$. Cuando se alcanzan las densidades más altas de la corteza, los electrones comienzan a formar un mar de Fermi degenerado y los núcleos, muy ricos en neutrones, están inmersos en un gas de neutrones libres. Esta fina capa de $\sim$ 1 km forma la corteza interna. Véase la Figura 1.5 obtenida de [74] donde se muestra la sección de una NS.

Como hemos comentado previamente, las NSs nacen en explosiones de SN, llegando a alcanzar temperaturas internas de $T \sim 10^{11}$ K. Durante sus primeros minutos de vida, la NS comienza a volverse transparente para los neutrinos generados en su interior [79, 80]. Tras esto, empieza a enfriarse debido a la emisión de neutrinos (principalmente provenientes del núcleo de la estrella) y al transporte de calor entre la corteza y la superficie, donde tiene lugar la emisión electromagnética. En cien años, la corteza y el núcleo intercambian calor llegando a alcanzar prácticamente la misma temperatura y pudiéndose considerar el interior de la NS isotérmico. La emisión de neutrinos enfría la estrella durante los siguientes millones de años haciendo que la estrella alcance temperaturas de $T \sim 10^7$ K.

Otro ejemplo de estrella compacta, pero menos densa que las NSs, es el de las WDs. Estos objetos son remanentes de los núcleos de estrellas con $M \lesssim 8M_\odot$ tras la expansión térmica de su envoltura. Están constituidas por núcleos inmersos en un gas de electrones degenerado, que sostienen la estrella contra el colapso gravitacional gracias a la presión de degeneración. Debido al principio de exclusión de Pauli, que postula que dos fermiones con los mismos números cuánticos no pueden ocupar el mismo estado, el colapso de una WD incrementará la energía cinética de los electrones y, por lo tanto, la presión. Las densidades de estos objetos están en el rango de $\rho_B \sim 10^5 - 10^9$ g/cm^3 con masas entre $M \sim 0.4M_\odot$ y $M \sim 1.2M_\odot$ y una masa media de $M \sim 0.6M_\odot$ compactificada en un radio de $\sim 1\%$ del radio solar.

Las WDs muestran una estructura de capas: en la mayoría de los casos consiste en un núcleo de C y O degenerado y prácticamente isotermo rodeado de una capa muy fina de Hidrógeno (H) por encima de una de Helio (He), ambos no degenerados [81]. Estas capas externas de H y He constituyen el $\sim 1\%$ del radio total de la estrella y, aunque sean muy finas, determinan la evolución térmica de la WD. Mientras que la mayoría de la masa de la estrella permanece más o menos a la misma temperatura, $T \sim 10^6 - 10^7$ K, la temperatura de la superficie desciende significativamente, alcanzando valores entre $T \sim 10^3 - 10^4$ K [82, 83].

En lo que respecta a la ecuación de estado (EoS), en el caso de las NSs las teorías microscópicas de materia densa son variadas y difieren dependiendo de la composición del núcleo, proporcionando una larga lista de posibles ecuaciones [84]. Éstas van desde las denominadas rígidas (stiff) hasta las designadas blandas (soft). Una EoS rígida es aquella en la que la presión aumenta rápidamente al aumentar la densidad y, por lo consiguiente, la materia es más difícil de ser comprimida. Por el contrario, una EoS blanda proporciona un incremento pequeño de la presión cuando la densidad aumenta, siendo más fácil comprimir el material. Por otro lado, en el caso de las WDs se puede obtener una buena descripción del interior estelar usando una EoS politrópica, que son aquellas que relacionan presión y densidad a través de una ecuación de la forma $P = K\rho^{1+\frac{1}{n}}$, donde K es una constante con las unidades apropiadas. Se puede demostrar fácilmente que un gas de Fermi no relativista de electrones degenerados puede ser descrito por una EoS de índice $n = \frac{3}{2}$, mientras que para el caso relativista el índice correspondiente es $n = 3$. De esta forma, una WD constituida por electrones no relativistas puede ser descrita por una EoS de índice $n = \frac{3}{2}$. A partir de un cierto valor de la densidad, los electrones pasarán a ser relativistas y, en tal caso, el índice que deberá usarse será $n = 3$. Ver [85–88] para más detalles sobre esto.

1.2.2 Materia Oscura capturada por estrellas densas

Como se ha mencionado antes, las estrellas compactas son, en general, mejores acretores de DM que otros objetos menos densos como la Tierra y el Sol debido a que

poseen valores mayores del ratio M/R [89, 90].

Por otro lado, es importante darse cuenta de que el máximo de la distribución de NSs en nuestra galaxia se encuentra a distancias $\langle r \rangle \lesssim 4$ kpc [91] donde ρ_χ es mayor que en la vecindad solar, para la cual en nuestros trabajos hemos tomado un valor de $\rho_{\chi,0}^{ambient} = 0.3$ GeV/cm^3. Aunque estimaciones más recientes [92] encuentran que $\rho_{\chi,0}^{ambient} = 0.385 \pm 0.027$ GeV/cm^3. Además de esto, se cree que algunos cúmulos globulares (GCs, por sus siglas en inglés), tales como M4 del que se conocen datos experimentales de magnitudes y distancias estelares [93], poseen una densidad de DM en su núcleo de $\rho_\chi \sim 100$ GeV/cm^3, como se concluye en [94, 95]. Tanto WDs evolucionadas [93, 96] como púlsares [97] han sido observados en el interior de GCs, por lo tanto, es una buena hipótesis considerar que en muchos casos ρ_χ alrededor de estos objetos compactos será mucho mayor que alrededor de el Sol o la Tierra.

Otra diferencia con respecto al caso terrestre es el hecho de que la DM acelerada gravitacionalmente por las NSs puede alcanzar velocidades relativistas $\beta_{NS} = \sqrt{\frac{2GM_{NS}}{R_{NS}}} \sim 0.6$ (con G la constante gravitatoria Newtoniana). En el caso de WDs las velocidades alcanzadas son típicamente $\beta_{WD} \sim 10^{-2}$, es decir, aproximadamente un orden de magnitud mayores que para la Tierra, $\beta_{Earth} \sim 10^{-3}$. Por su parte, las NSs permiten testear energías intermedias entre las relativas a los experimentos de DD y aquellas alcanzadas en los colisionadores de partículas.

En este contexto, una vez han alcanzado la estrella, las partículas de DM podrían ser acretadas y capturadas de forma efectiva si pierden la suficiente energía a través de interacciones con la materia bariónica. La tasa de captura de DM puede escribirse como [98–100]

$$\Gamma_{\text{capt}} = \frac{8}{3}\pi^2 \frac{\rho_\chi}{m_\chi} \frac{GMR}{1 - \frac{2GM}{R}} \bar{v}^2 \left(\frac{3}{2\pi\bar{v}^2}\right)^{\frac{3}{2}} f, \tag{1.1}$$

donde $\bar{v}$ es la velocidad media de χ en la distribución de DM existente alrededor de la estrella y f es la fracción de partículas que experimentan uno o más choques con la materia ordinaria dentro de la estrella. $f \sim 1$ si $\sigma_{\chi,i} \gtrsim \sigma_0$, donde $\sigma_{\chi,i}$ es la sección eficaz entre la DM y la partícula del SM de tipo i que constituye la estrella y $\sigma_0 = \frac{\pi m_i R^2}{M}$ es la sección eficaz geométrica asociada al objeto estelar. En caso contrario, $\sigma_{\chi,i} < \sigma_0$, se ha estimado que $f \sim 0.45\frac{\sigma_{\chi,N}}{\sigma_0}$ para el caso de captura por NSs [99] y $f \sim \frac{\sigma_{\chi,A}}{\sigma_0}$ para WDs [100], donde $\sigma_{\chi,A}$ es la sección eficaz DM-núcleo.

Evaluando numéricamente la tasa de captura, para NSs obtenemos [98]

$$\Gamma_{\text{capt}} \simeq 6 \times 10^{25} \left(\frac{M}{1.5M_\odot}\right) \left(\frac{R}{12\,\text{km}}\right) \left(\frac{1\,\text{GeV}}{m_\chi}\right) \left(\frac{\rho_\chi}{\rho_{\chi,0}^{ambient}}\right) f \text{ s}^{-1}. \tag{1.2}$$

De la misma forma, para WDs

$$\Gamma_{\text{capt}} \simeq 6 \times 10^{27} \left(\frac{M}{0.6M_\odot}\right) \left(\frac{R}{0.01R_\odot}\right) \left(\frac{1\,\text{GeV}}{m_\chi}\right) \left(\frac{\rho_\chi}{\rho_{\chi,0}^{ambient}}\right) f \text{ s}^{-1}. \tag{1.3}$$

Nótese que mientras que la sección eficaz DM-nucleón necesaria para una captura eficiente, es decir, para que la DM haga scattering al menos una vez por cada vez que cruza la estrella, en el caso de NSs es $\sigma_{\chi N} \gtrsim 10^{-45}$ cm^2, mientras que para WDs $\sigma_{\chi N} \gtrsim 10^{-39}$ cm^2. Por tanto, las NSs serán más sensibles a la hora de testear valores menores de la sección eficaz DM-nucleón.

Por otro lado, es importante resaltar que la DM podría en principio ser acretada

por la estrella no sólo durante la época en la que ya ha colapsado, sino también durante su vida estelar anterior. No obstante, la captura durante la etapa de estrella compacta será en general más eficiente debido la gran compactificación del objeto. Aún así, para casos en los que la DM tiene una sección eficaz de aniquilación extremadamente pequeña, la cantidad de DM acumulada durante la vida del progenitor, $N_{0,\chi}$, podría ser del mismo orden que la acretada por el objeto compacto. Ver [98, 101, 102] para una estimación de esta cantidad usando la Eq. (1.1). Merece la pena mencionar además, que habrá dos efectos compitiendo. Mientras que tanto la masa como el radio del progenitor son mayores que los del objeto compacto, permitiendo que más partículas de DM crucen la estrella, una menor compactificación de éstos hace que la probabilidad de scattering sea menor.

Volviendo a la acreción en la etapa de estrella compacta, el núcleo de la estrella es opaco para la DM, permitiendo que se construya una densidad de DM en su interior, $n_\chi(r)$, donde r es la coordenada estelar radial. El número de partículas de DM que reside dentro de la estrella, N_χ, dependerá, en general, de las tasas de captura, aniquilación (o decaimiento) y evaporación, $\Gamma_{\rm capt}$, $\Gamma_{\rm ann}$, $\Gamma_{\rm evap}$, respectivamente, ver por ejemplo [103, 104]. Sin embargo, para partículas de DM acretadas por NSs (WDs) con masas mayores que $m_\chi \sim 2$ keV ($m_\chi \sim 2$ MeV) los efectos de evaporación pueden ser ignorados. El argumento es el siguiente. La masa límite a partir de la cual los efectos de evaporación han de tenerse en cuenta, m_{evap}, puede ser estimada considerando que, para que esto ocurra, la velocidad típica de la partícula de DM termalizada, $v \sim \sqrt{\frac{T_c}{m_\chi}}$, a la temperatura central de la estrella, T_c, debe ser mayor que la velocidad de escape local de la estrella, $v_{\rm esc}$. De esta forma, m_{evap} dependerá de las propiedades termodinámicas de la estrella, de su masa y de su radio. Una vez hemos tenido en cuenta esto, para $m_\chi > m_{evap} = \frac{T_c R}{2GM}$ el número de partículas de DM dentro de estos objetos compactos a un tiempo t determinado puede ser obtenido resolviendo la ecuación diferencial

$$\frac{dN_\chi}{dt} = \Gamma_{\rm capt} - 2\Gamma_{\rm ann}, \tag{1.4}$$

donde

$$\Gamma_{\rm ann} = \frac{1}{2}\int d^3\vec{r}\, n_\chi^2(\vec{r})\langle\sigma_a v\rangle = \frac{1}{2}C_a N_\chi^2. \tag{1.5}$$

Además, la densidad de DM en el interior de la estrella ha de verificar $\int d^3\vec{r}\, n_\chi(\vec{r}) = N_\chi$ en cada momento. Suponiendo que el tiempo de termalización es mucho menor que los tiempos de la dinámica del enfriamiento estelar, una vez dentro, la DM se dispersará hacia las regiones estelares más densas y estará distribuida de acuerdo con la ley exponencial

$$n_\chi(r) = n_{0,\chi} e^{-\frac{m_\chi}{T}\Phi(r)}, \tag{1.6}$$

con $n_{0,\chi}$ el valor de densidad central y $\Phi(r) = \int_0^r \frac{GM(r')dr'}{r'^2}$ el potencial gravitatorio. Tomando la densidad constante en el volumen estelar e igual a la densidad central, $\rho(r) = \rho_c$, la densidad de DM puede escribirse como $n_\chi(r) = n_{0,\chi} e^{-(r/r_{\rm th})^2}$ con un radio térmico $r_{\rm th} = \sqrt{\frac{9T}{8\pi G\rho_c m_\chi}}$ [104]. De esta forma, si las partículas de DM se autoaniquilan, será más probable que lo hagan dentro de objetos compactos que en vacío o en objetos menos densos, debido a que la densidad de DM será mayor en el núcleo de estrellas más densas. Además, para tiempos $t \gg \tau_{\rm eq} = 1/\sqrt{\Gamma_{\rm capt} C_a}$, donde $\tau_{\rm eq}$ es una escala temporal de equilibrio establecida por los dos procesos que compiten en el interior estelar, la captura y la aniquilación, resolviendo la Eq. (1.4), se obtiene que $\Gamma_{\rm capt} = 2\Gamma_{\rm ann}$ en todo momento.

Merece la pena mencionar que para DM asimétrica, es decir, DM que no sufre autoaniquilación, existe un valor crítico de la cantidad de masa de DM acumulada. Este límite viene del hecho de que la estrella podría ser destruida creando un agujero negro, como se ha estudiando en [98, 105, 106] tanto para candidatos de tipo fermiónico como bosónico. Aún así, es importante puntualizar que, en general, la fracción de DM dentro de la estrella es muy pequeña en todo momento. Para DM que no se autoaniquila, caso en el que la fracción de DM será mayor que en el caso contrario, el número de partículas de DM dentro de la estrella puede ser estimado como $N_\chi(t) \approx N_{0,\chi} + \Gamma_{\rm capt} t$. Por ejemplo, para una NS evolucionada con una edad de $t \sim 10^9$ años, usando la expresión de la Eq. (1.2) y tomando $N_{0,\chi}$ del mismo orden que $\Gamma_{\rm capt} t$ (en general será menor o, como mucho, del mismo orden), podemos estimar $N_\chi(t)$. Dado que el número de bariones en la estrella es $N_B \simeq 2\ 10^{57}$, el ratio entre el número de partículas de DM y bariones es $Y_\chi = N_\chi / N_B < 2\ 10^{-13}$. De la misma forma, para WDs típicas cuya edad es $t \sim 10^9$ años, el número de bariones es $N_B \simeq 7\ 10^{56}$, y, por lo tanto, $Y_\chi = N_\chi / N_B < 5\ 10^{-11}$.

Llegados a este punto, deberíamos mencionar que, en los trabajos presentados en esta tesis [54–57] se estudia tanto el escenario en el que la DM no ha tenido tiempo de termalizar (Capítulos 2 y 3) como el de DM termalizada (Capítulos 4 y 5) dentro de estrellas compactas.

El trabajo *Diffusion of dark matter in a hot and dense nuclear environment*, M. Cermeño, M. A. Pérez-García and J. Silk, Phys. Rev. D 94 (2016) 023509 [54] (Capítulo 2) considera la interacción de DM que alcanza una NS con velocidad $\beta_{NS} \sim 0.6$ con los nucleones del núcleo interno de ésta, mientras que en el artículo *Light dark matter scattering in outer neutron star crusts*, M. Cermeño, M. A. Pérez-García and J. Silk, Phys. Rev. D 94 (2016) 063001 [55] (Capítulo 3) se analiza el efecto de las interacciones de esta DM relativista con los núcleos de la corteza externa de la estrella.

Por otro lado, en los artículos *Enhanced Neutrino Emissivities in Pseudoscalar-mediated Dark Matter Annihilation in Neutron Stars*, M. Cermeño, M. A. Pérez-García and R. A. Lineros, Astrophysical Journal 863 (2018) 157 y *Gamma rays from dark mediators in white dwarfs*, M. Cermeño and M. A. Pérez-García, Phys. Rev. D 98 (2018) 063002 [56, 57] (Capítulos 4 y 5) se estudian las consecuencias de la existencia de DM que ha tenido tiempo de termalizar dentro de NSs y WDs.

En el Capítulo 6 se muestra un repaso sobre trabajos relacionados con la presencia de DM dentro de NSs titulado *Fermionic Light Dark Matter particles and the New Physics of Neutron Stars*, M. Cermeño, M. A. Pérez-García and J. Silk, PASA 34 (2017) e043 [107].

Finalmente, los efectos de considerar teorías de MG en diferentes propiedades (masa, radio, luminosidad) de estrellas poco masivas y WDs son analizados en el artículo presentado en el Capítulo 7, *Modified Gravity at Astrophysical Scales*, M. Cermeño, J. Carro, A. L. Maroto and M. A. Pérez-García, Astrophysical Journal 872 (2019) 130 [108].

1.3 Análisis de las contribuciones presentadas en esta tesis

El trabajo de investigación presentado en esta tesis se centra en la interacción de DM con materia ordinaria dentro de objetos densos, tales como NSs y WDs, y las posibles consecuencias medibles en forma de señales indirectas provenientes de ellos.

Un primer paso para nuestro estudio fue considerar los efectos de un medio nuclear denso y caliente en la sección eficaz de LDM fermiónica que interacciona con

nucleones en el interior de una proto-NS una vez ha alcanzado la estrella a velocidades $\beta_{NS} \sim 0.6$. Este análisis es presentado en el artículo *Diffusion of dark matter in a hot and dense nuclear environment*, M. Cermeño, M. A. Pérez-García and J. Silk, Phys. Rev. D 94 (2016) 023509 [54] (Capítulo 2). En esta contribución se consideró LDM que se acopla a los nucleones a través de interacciones efectivas de tipo escalar y vectorial, es decir, con un lagrangiano de interacción de la forma

$$\mathcal{L}_{\mathcal{I}} = \sum_{N=n,p} \frac{G_{s,N}}{\sqrt{2}} \chi\overline{\chi} N\overline{N} + \sum_{N=n,p} \frac{G_{v,N}}{\sqrt{2}} \chi\gamma^{\mu}\overline{\chi} N\gamma_{\mu}\overline{N}, \tag{1.7}$$

donde γ_μ son las matrices de Dirac y $G_{s,N}, G_{v,N}$ las constantes de acoplo a los nucleones de tipo escalar y vectorial, respectivamente. Asumimos una interacción puntual similar a la de la teoría de Fermi [31] de la interacción débil, puesto que consideramos que el momento transferido es pequeño dentro de la estrella.

Para tener en cuenta los efectos del medio nuclear, primeramente, deben incluirse las funciones de distribución de Fermi-Dirac para los nucleones, $f_N(E) = \frac{1}{1+e^{(E-\mu_N^*)/k_BT}}$. Éstas introducen dependencias en el potencial químico efectivo de los nucleones, μ_N^*, en su energía E y en la temperatura de la estrella. Su papel es el de restringir parcialmente el espacio de fases del nucleón saliente en interacciones del tipo $\chi N \to \chi N$, basándose en el principio de exclusión de Pauli. Asumimos además que todos los estados salientes de la DM están en principio permitidos ya que puede verificarse fácilmente (ver Sección 1.2.2) que la fracción de DM dentro de la estrella es muy pequeña en todo momento. Otro efecto de densidad fue introducido a través de los valores efectivos del potencial químico y de la masa del nucleón, m_N^*, que difieren de los valores desnudos, μ_N y $m_N \geq m_N^*$, por la presencia de campos mesónicos [109]. Además, también se consideraron efectos de temperatura por medio del factor de balance detallado [110], $S(q_0, T) = \frac{1}{1-e^{-\frac{|q_0|}{k_BT}}}$, que tiene en cuenta valores de la energía transferida, q_0, tanto positivos como negativos debido al valor finito de la temperatura del medio.

Para analizar la influencia del medio en los eventos de scattering de las partículas de LDM, se calculó la sección eficaz diferencial $\chi - N$ por unidad de volumen teniendo en cuenta los efectos del medio mencionados anteriormente. Usando la expresión general [111]

$$d\sigma = \frac{|\overline{\mathcal{M}}_{\mathcal{N}}|^2}{4\sqrt{(pk)^2 - {m^*}_N^2 m_\chi^2}} d\Phi(p, p', k, k') f_N(E)(1 - f_N(E'))S(q_0) \tag{1.8}$$

donde el elemento de volumen del espacio de fases viene dado por

$$d\Phi(p, p', k, k') = (2\pi)^4 \delta^{(4)}(p + k - p' - k') \frac{d^3\vec{p'}}{(2\pi)^3 2E'} \frac{d^3\vec{k'}}{(2\pi)^3 2\omega'}, \tag{1.9}$$

y

$$\begin{aligned} |\overline{\mathcal{M}}_N|^2 &\simeq 4g_{Ns}^2(E'E + {m^*}_N^2)(\omega'\omega + m_\chi^2) \\ &+ 8g_{Nv}^2(2{m_N^*}^2 m_\chi^2 - {m^*}_N^2\omega\omega' - m_\chi^2 E'E + 2E'\omega' E\omega) \\ &+ 8g_{Ns}g_{Nv}m_N^* m_\chi(E\omega + E\omega' + E'\omega + E'\omega') \end{aligned} \tag{1.10}$$

es la amplitud de scattering al cuadrado del proceso considerado, que fue obtenida usando las reglas de Feynman y quedándonos al orden más bajo en las velocidades

de las partículas. Denotamos $p'^{\mu} = (E', \vec{p'})$ y $p^{\mu} = (E, \vec{p})$ como los cuadrimomentos de los nucleones salientes y entrantes, respectivamente, y $k'^{\mu} = (\omega', \vec{k'})$ y $k^{\mu} = (\omega, \vec{k})$ los análogos para la partículas de DM. El cuadrimomento transferido se define como $q^{\mu} = (q_0, \vec{q}) = p'^{\mu} - p^{\mu} = k^{\mu} - k'^{\mu}$.

Una vez se consideraron estas modificaciones con respecto al caso en vacío, la sección eficaz por unidad de volumen, es decir, la inversa del recorrido libre medio, $\lambda_{\chi}^{-1} = \frac{\sigma(\omega)}{V}$, pudo ser escrita como

$$\lambda_{\chi}^{-1} = \frac{m_N^*}{4(2\pi)^3} \int_0^{\omega - m_{\chi}} dq_0 \int_{|\vec{k}|-|\vec{k'}|}^{|\vec{k}|+|\vec{k'}|} d|\vec{q}| \int_{|\vec{p}_-|}^{\infty} d|\vec{p}| \frac{|\overline{\mathcal{M}}_{\mathcal{N}}|^2 |\vec{p}| f_N(E)(1 - f_N(E'))S(q_0, T)}{4E'|\vec{k}|\sqrt{E^2\omega^2 - {m_N^*}^2 m_{\chi}^2}}, \tag{1.11}$$

donde

$$|\vec{p}_-|^2 = \frac{{m_N^*}^2}{|\vec{q}|^2}\left(q_0 - \frac{|\vec{q}|^2}{2m_N^*}\right)^2. \tag{1.12}$$

El límite inferior de integración para $\vec{p}$ dado por la Eq. (1.12) viene de la imposición de la conservación de la energía, es decir de $q_0 = E' - E$, en el límite no relativista, que proporciona un valor para el ángulo entre $\vec{p}$ y $\vec{q}$, definido por

$$cos\ \theta_0 = \frac{m_N^*}{|\vec{p}||\vec{q}|}\left(q_0 - \frac{|\vec{q}|^2}{2m_N^*}\right), \tag{1.13}$$

y de la restricción $|cos\ \theta_0| \leq 1$.

Evaluando la Eq. (1.11) numéricamente, encontramos modificaciones notables del recorrido libre medio de la partícula de DM en el medio con respecto al resultado en vacío (Figuras 5, 6 y 7 del Capítulo 2), que ha demostrado ser una buena aproximación para interacciones dentro de objetos menos densos como el Sol o la Tierra [90, 112]. Obtenemos que tanto los efectos de temperatura como los de densidad afectan significativamente a nuestros resultados finales. Los primeros lo hacen disminuyendo el recorrido libre medio de la DM (Figura 6), aunque las variaciones más importantes obtenidas vienen del efecto de considerar masas efectivas menores que las del valor desnudo de la masa del nucleón, o, en otras palabras, del efecto de la densidad finita de materia (Figura 7). Una continua disminución de λ_{χ} al aumentar la densidad se puede observar en el caso en el que no se tiene en cuenta la masa efectiva de los nucleones. Por el contrario, cuando ésta se tiene en cuenta, encontramos que a partir de un valor específico de la densidad el comportamiento decreciente cambia proporcionando valores mayores de λ_{χ}. Es importante notar que los efectos de temperatura provienen, no sólo del factor de balance detallado, sino también de las funciones de distribución de Fermi Dirac a temperatura finita.

Por otro lado, aunque los valores encontrados para el recorrido libre medio son mayores que los que se darían en vacío, debido a que estamos restringiendo parte del espacio de parámetros de los nucleones salientes, se ha obtenido que $\lambda_{\chi} \ll R$ tanto para NSs calientes (jóvenes) como frías (evolucionadas). Esto indica que es muy probable que las partículas de LDM queden atrapadas dentro de la estrella, contrariamente a lo que ocurre en el caso de neutrinos estándar a partir de los primeros ~ 10 s tras el colapso, cuando la temperatura de la estrella es $T \lesssim 10$ MeV. Este hecho podría proporcionar modificaciones de la energía interna en procesos de enfriamiento.

Tras haber estudiado la interacción de LDM con los nucleones del núcleo interno de una NS, donde la densidad bariónica alcanza su valor máximo, nuestro siguiente trabajo, *Light dark matter scattering in outer neutron star crusts*, M. Cermeño, M. A.

Pérez-García and J. Silk, Phys. Rev. D 94 (2016) 063001 [55] (Capítulo 3), considera el scattering de LDM relativista con la red de núcleos de la corteza externa de una NS. En este trabajo se estudia la posibilidad de excitar fonones con momento $|\vec{k}|$ y polarización λ en la corteza externa debido a estas interacciones y sus potenciales consecuencias. Analizamos este escenario para el mismo tipo de interacción que la del trabajo anterior, es decir, mismo lagrangiano de interacción dado por la Eq. (1.7).

Restringiendo el espacio de fases a partículas de DM con masas $m_\chi \lesssim 100$ MeV, el scattering con núcleos puede ser tratado como elástico y coherente. Debido a estas interacciones podrían excitarse fonones acústicos, es decir, aquellos que siguen una relación lineal de dispersión de la forma $\omega_{k,\lambda} = c_{l,\lambda}|\vec{k}|$, con $c_{l,\lambda} = \frac{T_p/3}{(6\pi^2 n_A)^{\frac{1}{3}}}$ la velocidad del sonido del modo. Donde $T_p = \sqrt{\frac{4\pi n_A Z^2 e^2}{m_A}}$ es la temperatura del plasma asociada a un medio de iones de densidad n_A, número bariónico A y carga eléctrica Ze [113]. Para analizar esto, calculamos la tasa de excitación de fonones acústicos usando la regla de oro de Fermi

$$R_{\vec{k},\lambda} = 2\pi\delta(E_f - E_i)|\langle f|\mathcal{V}|i\rangle|^2, \tag{1.14}$$

donde i y f son los estados iniciales y finales considerados. $\mathcal{V} = \sum_j \delta^3(\vec{r} - \vec{r_j})\frac{2\pi a}{m_\chi}$ es el potencial de interacción sentido por una partícula de DM entrante cuando se aproxima a un núcleo de la red periódica. Es importante remarcar que el potencial de interacción sólo toma esta forma en la aproximación de Born ($|\vec{k}| \ll \frac{1}{a}$), en la que la sección eficaz $\chi - A$ en el centro de masas puede ser estimada como $\sigma_{\chi,A} \simeq 4\pi a^2$, siendo a un parámetro de longitud que da cuenta del alcance del scattering. De esta forma, para conocer la tasa de excitación de fonones, es necesario calcular el parámetro a para nuestro tipo de interacción. Para esto se debe hallar el elemento de matriz, $|\overline{\mathcal{M}}_{\chi A}|^2$, ya que la sección eficaz en el centro de masas también puede obtenerse de $\frac{d\sigma_{\chi,A}}{d\Omega}|_{CM} = \frac{|\overline{\mathcal{M}}_{\chi A}|^2}{64\pi^2 s}$, donde s es la variable de Mandelstam correspondiente a la energía del centro de masas al cuadrado. En otras palabras,

$$4\pi a^2 = m_A^2 \frac{\left(\frac{Z}{m_p}\sqrt{|\tilde{\mathcal{M}}_p|^2} + \frac{(A-Z)}{m_n}\sqrt{|\tilde{\mathcal{M}}_n|^2}\right)^2}{16\pi(m_\chi + m_A)^2}, \tag{1.15}$$

con $\int_{-1}^{1} 2\pi d(cos\ \theta_\chi)|\overline{\mathcal{M}}_{\chi \mathrm{N}}|^2 \equiv |\tilde{\mathcal{M}}_{\mathrm{N}}|$. El elemento de matriz al cuadrado para la interacción con los nucleones ($N = p, n$), $|\overline{\mathcal{M}}_{\chi \mathrm{N}}|^2$, puede calcularse de la misma forma que en el trabajo anterior a la hora de obtener la Eq. (1.10) del lagrangiano de la Eq. (1.7). La única diferencia es que en este caso no despreciamos los términos $|\vec{p_\chi}|^2$ con respecto a m_χ^2.

Tras llevar a cabo algunos cálculos, la tasa de excitación de fonones (por unidad de volumen) en la corteza pudo escribirse como

$$R_k^{(0)} = \frac{8\pi^4 n_A^2}{(2\pi)^6 m_\chi^2 m_A c_l}\int_0^\infty |\vec{p_\chi}|d|\vec{p_\chi}|f_\chi(\vec{p_\chi})|E_\chi - |\vec{k}|c_l|a^2, \tag{1.16}$$

donde $f_\chi(\vec{p_\chi}) = \frac{n_\chi \mu}{4\pi m_\chi^3 K_2(\mu)} e^{-\mu\sqrt{1+\frac{|\vec{p_\chi}|^2}{m_\chi^2}}}$ es la función de distribución de Maxwell-Jüttner [114] para una densidad local n_χ de partículas entrantes de DM relativistas. Con $\mu = \frac{m_\chi}{k_B T} \approx 6.7$ para $\sqrt{< v^2 >} \sim 0.6$, ver [115] y [116], y $K_2(\mu)$ la función de Bessel modificada de segundo orden.

Una vez hubimos evaluado la expresión de la Eq. (1.16) numéricamente, se obtuvo que esta cantidad no depende del momento del fonón, ya que $|\vec{k}|c_l \ll E_\chi$. Esto es contrario a lo que ocurre en el caso de neutrinos cosmológicos, en el que hay una fuerte dependencia en $\vec{k}$ [117, 118] que puede ajustarse como $R^0_\nu(|\vec{k}|) = R_{\nu 0}e^{-b|\vec{k}|}$, con $R_{\nu 0} = R^0_\nu(0)$ y b una constante. Así, de la Figura 1 del Capítulo 3, donde se muestran las tasas de excitación de fonones debidos a LDM y a neutrinos para $|\vec{k}| \to 0$, se puede ver que nuestra tasa puede ser más importante que la debida a neutrinos para valores finitos de $|\vec{k}|$. Además, comprobamos que el hecho de considerar el espacio de fases total usando las funciones de distribución de Maxwell Jüttner para las partículas de DM entrantes, en vez de tomar la aproximación monocromática, nos da una corrección del $\sim 20\%$.

Con vistas a analizar consecuencias astrofísicas, estimamos la contribución de la modificación de la población de fonones acústicos debido a las interacciones de LDM a la conductividad térmica en la corteza externa. La conductividad térmica global, κ, es la suma de una contribución de iones, κ_i, y otra de electrones, κ_e. Además, la conductividad térmica debida a iones se puede escribir como $\kappa_i^{-1} = \kappa_{ii}^{-1} + \kappa_{ie}^{-1}$. Donde κ_{ii} es la conductividad térmica ión-ión, o lo que es lo mismo, la conductividad térmica debida a la interacción entre fonones en la red, y κ_{ie} es la conductividad térmica ión-electrón debida a la interacción entre electrones y fonones.

En el escenario estudiado en nuestro trabajo asumimos una red de tipo BCC y el rango de temperaturas verifica $T_U < T < T_D$ para cada densidad considerada. $T_U \simeq 0.07T_D$ es la temperatura mínima para la cual la aproximación de electrones libres funciona [119, 120] y $T_D \simeq 0.45T_p$ es la temperatura de Debye. Este límite superior asegura que mediante mecanismos térmicos sólo serán excitados fonones acústicos. Además, de [120] sabemos que, en este rango de temperaturas, o bien las conductividades estándar ión-electrón e ión-ión son del mismo orden de magnitud, o la primera domina sobre la segunda (esto dependerá de la densidad bariónica). La idea aquí es analizar si la modificación de la conductividad térmica ión-ión debida al scattering entre partículas de LDM y los núcleos de la corteza puede modificar este hecho.

En general, la conductividad térmica ión-ión puede escribirse de la forma [119]

$$\kappa_{ii} = \frac{1}{3}k_{\rm B}C_A n_A c_l L_{ph}, \tag{1.17}$$

donde $C_A = 9\left(\frac{T}{T_D}\right)^3 \int_0^{T_D/T} \frac{x^4 e^x dx}{(e^x-1)^2}$ es la capacidad calorífica (por ión y adimensional) de fonones y L_{ph} es el recorrido libre medio efectivo de los fonones. Típicamente, L_{ph} está relacionado con el número de fonones térmicos a temperatura T de la forma $L_{ph} \sim \delta t/N_{0,k\lambda} = \delta t(e^{\omega_{k\lambda}/k_{\rm B}T} - 1)$, donde δt es la unidad de tiempo. En nuestro caso consideramos $L_{ph} \sim \delta t/N_{k\lambda}$, con $N_{k\lambda}$ el número total de fonones, donde se tienen en cuenta tanto los fonónes térmicos estándar como los que provienen de la excitación y de la emisión estimulada debidos al scattering de LDM [117]. Nótese que estos últimos actúan disminuyendo $N_{k\lambda}$. En un elemento de cuadrivolumen $\delta V \delta t$, esta cantidad queda como

$$N_{k\lambda} \simeq N_{0,k\lambda} + R_k^{(0)}\delta V\delta t - \int \frac{d^3\vec{p}}{n_\chi} f_\chi(\vec{p})\tilde{R}_k^{(0)} N_{0,k\lambda} e^{(\omega_{k,\lambda}+\vec{k}.\vec{v})/(E_\chi - m_\chi)}\delta V\delta t, \tag{1.18}$$

donde $\tilde{R}_k^{(0)}$ es la tasa de excitación de fonones para cada valor particular del momento (sin promediar sobre los momentos de las χ entrantes). Además, el corrimiento Doopler debido al movimiento relativo de la NS con respecto al flujo de LDM tiene que tenerse en cuenta a través del factor $\vec{k}.\vec{v}$ de la exponencial, siendo $v \equiv v_{NS} \sim 10^{-2}$ la velocidad galáctica de deriva de la NS.

Una vez hubimos obtenido el número neto de fonones teniendo en cuenta las interacciones de las partículas de LDM en la corteza externa de la estrella, calculamos numéricamente la conductividad térmica ión-ión. Por un lado, obtuvimos que, dependiendo de los valores de $|\vec{k}|$ y m_χ, el número total de fonones en la corteza podrá ser mayor que en el caso térmico estándar (la excitación de fonones debido al scattering domina) o menor (domina la emisión estimulada causada por la interacción de los nuevos fonones con los estándares). En el primer caso, κ_{ii} puede ser menor que κ_{ie} y, por tanto, más importante que ésta, afectando la conductividad iónica total haciendo que disminuya. En otro caso, cuando κ_{ii} es del mismo orden o mayor que κ_{ie}, κ_{ii} sólo afectará la conductividad iónica total (disminuyéndola) cuando sea del mismo orden que κ_{ie}. Como ejemplo de estas modificaciones de κ_{ii}, en la Figura 2 del Capítulo 3, se muestra el aumento con respecto al resultado térmico estándar de la conductividad térmica ión-ión para densidades bariónicas altas, $\rho_B \gtrsim 10^{11}$ g/cm^3, fijando $m_\chi = 100$ MeV y $|\vec{k}| = 0.01/a$.

Tras haber analizado esto, considerando la existencia de campos magnéticos en NSs, comparamos nuestros resultados con la conductividad térmica eléctrica en un escenario realista magnetizado. Observamos que la conductividad térmica ión-ión puede sobrepasar a la debida a electrones, κ_e, en la dirección perpendicular al campo magnético para $n_\chi \sim 100 n_{0,\chi}$ y $\rho_B \gtrsim 3.5\ 10^{11}$ g/cm^3, donde $n_{0,\chi} = \frac{\rho_{\chi,0}^{ambient}}{m_\chi}$ es el valor de la densidad de DM en la vecindad solar. Esto puede verse en la Figura 3 del Capítulo 3. Para este ejemplo se tomó $m_\chi = 65$ MeV y $|\vec{k}| = 0.01/a$, pero, como hemos mencionado antes para otros valores de m_χ y $|\vec{k}|$ se obtiene el comportamiento opuesto. Nótese que en este caso lo que se está comparando es solamente κ_{ii}. Es importante darse cuenta de que, para NSs magnetizadas, en los casos en los que κ_{ii} es menor o del mismo orden que κ_{ie}, el efecto de la LDM sobre la conductividad térmica global en la corteza externa tendrá influencia en la diferencia de conducción del calor entre las direcciones paralela y perpendicular al campo magnético [121–123].

Una vez estudiado el impacto de DM relativista que interacciona con la materia nuclear al alcanzar NSs, nos interesó analizar el efecto de la autoaniquilación de DM capturada por NSs una vez ha tenido tiempo de termalizar en el núcleo de la estrella. De esta forma, en nuestra siguiente contribución, *Enhanced Neutrino Emissivities in Pseudoscalar-mediated Dark Matter Annihilation in Neutron Stars*, M. Cermeño, M. A. Pérez-García and R. A. Lineros, Astrophysical Journal 863 (2) (2018) 157 [56] (Capítulo 4), se consideró la aniquilación de partículas de DM de tipo secluded que interaccionan con las partículas del SM a través de un mediador pseudoescalar, a. En este contexto, se estudió el aumento de la emisividad de neutrinos de estos objetos compactos debido este tipo de aniquilaciones.

El lagrangiano de interacción de este modelo puede escribirse como [48, 52]

$$\mathcal{L}_\mathcal{I} = -i\frac{g_\chi}{\sqrt{2}} a\bar{\chi}\gamma_5\chi - ig_0\frac{g_f}{\sqrt{2}} a\bar{f}\gamma_5 f\,, \tag{1.19}$$

donde g_χ es el acoplo DM-mediador, g_f corresponde al acoplo del mediador con los fermiones, f, y g_0 es un factor de escala que afecta a todo tipo de fermiones. Para

nuestro estudio tomamos $g_f = 1$ para todos los fermiones del SM, es decir, un acoplo de tipo flavour-universal, aunque otras elecciones son válidas, ver por ejemplo [52].

Como ya hemos mencionado, estuvimos interesados en restringir los estados finales de aniquilación a neutrinos. En el rango $m_\chi < m_{\rm Higgs}$ y $m_a < m_\chi$, donde m_a es la masa del mediador pseudoescalar, los procesos de aniquilación relevantes están dados por un canal onda-S, $\chi\chi \to \nu\nu$, y un canal onda-P a través de dos mediadores pseudoescalares, $\chi\chi \to aa$, con su posterior decaimiento a neutrinos, $a \to \nu\nu$. La emisividad de energía local (energía producida por unidad de volumen y de tiempo a través de una reacción específica) viene dada por [124]

$$Q_E = 4 \int d\Phi (E_1 + E_2) \, |\overline{\mathcal{M}}|^2 \, f(f_1, f_2, f_3, f_4). \tag{1.20}$$

Con

$$d\Phi = \frac{d^3\vec{p}_1}{2(2\pi)^3 E_1} \frac{d^3\vec{p}_2}{2(2\pi)^3 E_2} \frac{d^3\vec{p}_3}{2(2\pi)^3 E_3} \frac{d^3\vec{p}_4}{2(2\pi)^3 E_4} (2\pi)^4 \delta^4(p_1 + p_2 - p_3 - p_4) \tag{1.21}$$

el elemento del espacio de fases de una reacción de cuatro cuerpos ($12 \to 34$) y $|\overline{\mathcal{M}}|^2$ el elemento de matriz al cuadrado del proceso considerado promediado a los espines de las partículas entrantes. El factor adicional $f(f_1, f_2, f_3, f_4)$ da cuenta del bloqueo del espacio de fases global debido a las funciones de distribución de las partículas iniciales y finales, f_i, $i = 1, ..., 4$.

Para el canal onda-S

$$f(f_1, f_2, f_3, f_4) = f_\chi(E_1) f_{\bar{\chi}}(E_2)(1 - f_\nu(E_3))(1 - f_{\bar{\nu}}(E_4)), \tag{1.22}$$

donde f_χ puede aproximarse por una función de distribución de Maxwell-Boltzmann, $f_\chi = f_\chi^{MB}(|\vec{p}_i|, r) = \left(\frac{1}{2\pi m_\chi T}\right)^{\frac{3}{2}} n_\chi(r) e^{\frac{-|\vec{p}_i|^2}{2m_\chi T}}$, $i = 1, 2$. Esto es así debido a que la energía de Fermi de la DM es mucho menor que la temperatura de la NS, $E_{F,\chi} \ll T$, con $E_{F,\chi} = \frac{(3\pi^2 n_\chi)^{\frac{2}{3}}}{2m_\chi}$. Nótese que la densidad de DM en la posición r dentro de la estrella $n_\chi(r)$ viene dada por la Eq. (1.6). Para el caso particular en el que el estado final está dado por neutrinos, asumimos que éstos no se quedan atrapados dentro de la estrella, de este modo, $f_\nu \sim 0$.

Por otro lado, para la aniquilación en dos pseudoescalares, el factor del espacio de fases es

$$f(f_1, f_2, f_3, f_4) = f_\chi(E_1) f_{\bar{\chi}}(E_2) f_a(E_3) f_a(E_4). \tag{1.23}$$

En esta ocasión, las partículas de DM se aniquilan en bosones, por lo tanto, no hay que tener en cuenta el bloqueo de Pauli para los estados salientes de tipo a y tomamos $f_a(E) \sim 1$ por simplicidad.

Con el objetivo de evaluar la Eq. (1.20) para ambas reacciones, como ya se ha hecho en los trabajos anteriores [54, 55], se calcularon los elementos de matriz a partir del lagrangiano descrito por la Eq. (1.19).

Para el canal onda-S

$$|\overline{\mathcal{M}}_{f\bar{f}}|^2 = \frac{g_\chi^2 g_f^2}{4} \frac{s^2}{(s - m_a^2)^2 + E_{\vec{q}}^2 \Gamma^2}, \tag{1.24}$$

donde $s = (p_1 + p_2)^2 = (p_3 + p_4)^2$, $E_{\vec{q}} = \sqrt{|\vec{q}|^2 + m_a^2}$ es la energía de la partícula pseudoescalar y Γ su anchura de decaimiento a través de la reacción $a \to f\bar{f}$.

Para el canal onda-P

$$|\overline{\mathcal{M}}_{aa}|^2 = \frac{-g_\chi^4}{2}\left\{\frac{(t-m_a^2)^2 - m_\chi^2(m_\chi^2+2m_a^2)}{(t-m_\chi^2)^2} + \frac{(u-m_a^2)^2 - m_\chi^2(m_\chi^2+2m_a^2)}{(u-m_\chi^2)^2}\right.$$
$$\left. + \quad 2\frac{2m_\chi^2 - s}{u-m_\chi^2} + \frac{(s-2m_\chi^2)(2m_a^2-s) + 2m_\chi^2(m_\chi^2+2m_a^2-2s) - 2(t-m_a^2)^2}{(t-m_\chi^2)(u-m_\chi^2)}\right\}, \quad (1.25)$$

donde $s = k^2 = (p_1+p_2)^2$, $t = (p_1-p_3)^2 = (p_4-p_2)^2$ y $u = 2m_\chi^2 + 2m_a^2 - s - t$.

Los detalles de la integración para las emisividades debidas tanto a la reacción onda-S como a la onda-P pueden verse en el Capítulo 4.

Tras calcular estas cantidades numéricamente, encontramos que la emisividad debida a la reacción $\chi\chi \to aa$, con su posterior decaimiento $a \to \nu\nu$, alcanza valores mayores que aquella debida a la producción directa de neutrinos, $\chi\chi \to \nu\nu$. Ver Figuras 2 y 3 del Capítulo 4. Además, nuestra emisividad de energía puede aumentar órdenes de magnitud con respecto a aquella debida a procesos URCA Modificados (MURCA, por sus siglas en inglés) estándares de neutrinos para conjuntos de parámetros (m_χ, m_a, g_χ y g_0) que respetan los límites de detección directa, los cosmológicos o incluso aquellos deducidos de decaimientos poco frecuentes de mesones. Esto puede observarse también de las Figuras 2 y 3. La importancia de esta comparación se debe a que durante los primeros $\sim 10^5$ años tras el nacimiento de NSs típicas, éstas se enfrían debido a la emisión de neutrinos a través de procesos de tipo URCA y MURCA [125, 126]. En nuestro trabajo, sin embargo, no comparamos nuestros resultados con las emisividades debidas a los procesos URCA ya que las densidades centrales estelares que usamos son menores que las necesarias para que este tipo de reacciones ocurran [127]. Llegados a este punto, es importante mencionar que la región donde se produciría la emisión de estos neutrinos debidos a la aniquilación de DM estaría localizada en una fracción de la estrella muy pequeña (menor que aproximadamente el 7% del total del volumen estelar a temperaturas $T \lesssim 10^{10}$ K).

Por otro lado, proporcionamos un ajuste fenomenológico para las emisividades dependiente de la temperatura y del número de partículas de DM dentro de la estrella dado por

$$Q_E(T, N_\chi) = Q_0 \left(\frac{N_\chi}{N_{0,\chi}}\right)^2 \left(\frac{T}{1\,\mathrm{MeV}}\right)^{-3}, \quad (1.26)$$

donde

$$N_{\chi,0} = 1.5\times 10^{39}\left(\frac{\rho_\chi}{\rho_{\chi,0}^{ambient}}\right)\left(\frac{1\,\mathrm{GeV}}{m_\chi}\right)\left(\frac{\sigma_{\chi,N}}{10^{-43}\,\mathrm{cm}^2}\right) \quad (1.27)$$

es la población inicial de DM cuando nace la protoNS [101]. Siguiendo [48] y el apéndice D de [52] y restringiéndonos a procesos a un loop en el límite cinemático apropiado para nuestra descripción, la sección eficaz del scattering $\chi - N$ puede escribirse como $\sigma_{\chi,N} \simeq \frac{9}{64\pi}\frac{|\vec{q}|^4\mu^2 g_N^2 g_\chi^2}{m_N^2 m_\chi^2 (m_a^2+q^2)^2}$, con g_N el acoplo DM-nucleón y $\mu = \frac{m_N m_\chi}{m_N+m_\chi}$ la masa reducida del sistema $\chi-$N.

Es importante darse cuenta de que N_χ depende de la temperatura indirectamente a través de la variable temporal t. Sin embargo, aunque una simulación detallada del enfriamiento sería necesaria para explorar la secuencia temporal, en nuestro estudio estimamos el tiempo que puede durar el hecho de que las emisividades de neutrinos que provienen de la aniquilación de DM dominen sobre las debidas a procesos MURCA. Tras hacer esto, obtuvimos que esto puede ocurrir durante toda la vida de

la NS para algunos casos estudiados ($m_\chi = 30$ GeV, $m_a = 1$ GeV).

Una vez analizado el impacto de la autoaniquilación de DM de tipo secluded a través de un acoplo pseudoscalar con las partículas del SM dentro de NSs, en nuestro siguiente trabajo, *Gamma rays from dark mediators in white dwarfs*, M. Cermeño and M. A. Pérez-García, Phys. Rev. D 98 (2018) 063002 [57] (presentado en el Capítulo 5), estuvimos interesadas en un estudio relativo. Consideramos DM de tipo secluded que se autoaniquila en mediadores metaestables, Y, con su posterior decaimiento en fotones, Y$\rightarrow \gamma\gamma$, dentro de WDs. En este caso, no asumimos ningún lagrangiano de interacción específico para obtener un análisis prácticamente independiente del modelo.

La motivación de considerar para este artículo estrellas menos densas es la voluntad de comparar nuestros resultados con los datos experimentales existentes. Las luminosidades internas de las WDs del GC M4 pueden ser extraídas de medidas experimentales de sus magnitudes aparentes y distancias [95]. De esta forma, si calculamos las luminosidades internas de WDs en este GC debidas a la aniquilación de partículas de DM y comparamos nuestros resultados con las luminosidades experimentales, podemos obtener límites de exclusión para algunos parámetros de nuestro modelo.

En este contexto, se consideraron partículas de DM con masas de sub-GeV capturadas por WDs, de masas M_{WD} y radios R_{WD}, debido a su interacción con los nucleos de C y O que constituyen el núcleo de la estrella. Asumimos que el principal canal de aniquilación es aquel que produce dos mediadores genéricos metaestables, $\chi\bar{\chi} \rightarrow$ Y Y, con una vida media en reposo que verifica $\tau_{rest} \lesssim 1$ s (para satisfacer los límites del Universo temprano) y cuya masa $m_Y \leq m_\chi$. Estos mediadores, con velocidades $v_\mathrm{Y} = \frac{p_\mathrm{Y}}{E_\mathrm{Y}}$, donde E_Y es su energía y $p_\mathrm{Y} = \sqrt{E_\mathrm{Y}^2 - m_\mathrm{Y}^2}$ el módulo de su momento, antes de decaer a fotones, podrían perder energía debido a su interacción con los núcleos, siempre y cuando su vida media, $\tau = \gamma_Y \tau_{rest}$ (con γ_Y el factor de Lorentz), sea mayor que el recorrido libre medio de la interacción, λ_{int}. En otras palabras, Y interaccionará con los núcleos sólo si $\frac{1}{\sqrt{1-v_\mathrm{Y}^2}}\tau_{rest} > \frac{1}{\sigma_{Y,A} n(r)}$, donde $\sigma_{Y,A} = A^2 \sigma_{Y,N}$ es la sección eficaz Y-núcleo, $\sigma_{Y,N}$ la sección eficaz Y-nucleón y $n(r)$ es la densidad de núcleos en una posición r dentro de la estrella. Como la WD está sostenida por la presión de electrones degenerados, $n(r)$ puede ser descrita por una ecuación de estado politrópica. Para densidades centrales $\rho_c \ll 10^6$ g/cm^3 la aproximación de gas de Fermi no relativista es una buena estimación y, por tanto, restringiendo nuestras densidades a este valor, podemos tomar el índice $n = \frac{3}{2}$, y $n(r) = \frac{\rho_c}{A m_N} \int_0^r \omega(r')^{\frac{3}{2}} dr'$. Aquí, $\omega(r)$ es la solución analítica aproximada de la ecuación de Lane-Emden, precisa hasta el 1% comparada con la solución numérica exacta [129].

Es claro que, cuando el mediador es creado, su energía puede escribirse como $E_{\mathrm{Y},0} = E_\chi \simeq m_\chi$, siendo el módulo de su momento $p_{\mathrm{Y},0} = \sqrt{m_\chi^2 - m_\mathrm{Y}^2}$. Tras sufrir una interacción, el mediador perderá una fracción de su momento, pudiendo escribirse $p_Y = q p_{\mathrm{Y},0}$, con $0 < q < 1$. De este modo, si aproximamos estas pérdidas de energía como continuas, el módulo del momento del mediador tras haber viajado una distancia r puede obtenerse resolviendo

$$\frac{dp_\mathrm{Y}}{dr} = \frac{\Delta p_\mathrm{Y}}{\lambda_{int}(r)} = \frac{-(1-q)p_\mathrm{Y}}{\lambda_{int}(r)}. \tag{1.28}$$

Así,

$$p_Y(r) = \sqrt{m_\chi^2 - m_Y^2}\,\exp\left\{\frac{-(1-q)A\sigma_{Y,N}\rho_c}{m_N}\int_0^r \omega(r')^{\frac{3}{2}}dr'\right\}, \tag{1.29}$$

y, de la misma manera, su energía tendrá también una dependencia radial, $E_Y(r) = \sqrt{p_Y(r)^2 + m_Y^2}$.

Por otro lado, la atenuación será además importante a la hora de calcular la densidad de probabilidad de decaimiento del mediador dentro de la estrella. En esta ocasión, la ecuación a resolver es

$$\frac{dP_{\rm dec}}{dr} = \frac{-P_{\rm dec}}{\gamma_Y \tau_{\rm rest}} = \frac{-P_{\rm dec} m_Y}{\tau_{\rm rest} E_Y(r)}, \tag{1.30}$$

que nos proporciona

$$P_{\rm dec}(r) = N\, e^{-\int_0^r \frac{m_Y dr'}{\tau_{\rm rest} E_Y(r')}}. \tag{1.31}$$

Evidentemente, la densidad de probabilidad de decaimiento del mediador ha de satisfacer la condición de normalización $\int_0^\infty P_{\rm dec} dr = 1$. Esto implica

$$N\left(\int_0^R e^{-\int_0^r \frac{m_Y dr'}{\tau_{\rm rest} E_Y(r')}} dr + \int_R^\infty e^{-\int_0^r \frac{m_Y dr'}{\tau_{\rm rest} E_Y(R)}} dr\right) = 1. \tag{1.32}$$

Una vez parametrizamos la atenuación, pudimos obtener tanto el flujo de energía a una distancia d fuera de la WD, $E_\gamma^2 \frac{d\Phi}{dE_\gamma}$, como la luminosidad interna, L_χ, debidos a la aniquilación de partículas de tipo secluded DM en fotones a través de mediadores metaestables.

Siguiendo [44], donde se dan expresiones para el flujo de energía de fotones provenientes de la aniquilación de DM dentro del Sol, el flujo de fotones para nuestro caso puede escribirse como

$$E_\gamma^2 \frac{d\Phi}{dE_\gamma} = \frac{\Gamma_{\rm ann}}{4\pi d^2} E_\gamma^2 \frac{dN_\gamma}{dE_\gamma}(R) P^Y_{\rm d,out}, \tag{1.33}$$

donde

$$P^Y_{\rm d,out} = \frac{N\tau_{rest} E_Y(R)}{m_Y} e^{-\frac{m_Y R}{\tau_{rest} E_Y(R)}}\left(1 - e^{-\frac{m_Y(d-R)}{\tau_{rest} E_Y(R)}}\right) \tag{1.34}$$

es la probabilidad de que el mediador decaiga a una distancia d del centro de la estrella.

Merece la pena mencionar que la edad típica de las WDs en el GC M4 es $t \sim 12$ Gyr, que es mucho mayor que el tiempo de termalización, $\tau_{\rm eq} \lesssim 22$ yr. En este caso, por tanto, se verifica $\Gamma_{\rm capt} = 2\Gamma_{\rm ann}$ y la tasa de aniquilación está completamente determinada por la tasa de DM capturada por la estrella, que dependerá de $\sigma_{\chi,N}$ aparte de otros parámetros, véase la Eq. (1.1).

Por otro lado, el espectro de energías del proceso de decaimiento $Y \to \gamma\gamma$ puede describirse de la forma

$$\frac{dN_\gamma}{dE_\gamma}(r) = \frac{4}{\Delta E}\theta(E_\gamma - E_-)\theta(E_+ - E_\gamma), \tag{1.35}$$

con energías que van desde E_- a E_+, siendo $E_\pm = \frac{1}{\gamma_Y(r)}\frac{m_Y}{2}(1 \mp v_Y(r))^{-1}$ y $\Delta E = E_+ - E_-$. Esto puede entenderse fácilmente teniendo en mente que cada uno de los cuatro fotones emitidos por aniquilación tendrá una energía monocromática en el sistema

de referencia en reposo del mediador dada por $\frac{m_Y}{2}$. Mientras que en el sistema de laboratorio existirá una dependencia en el ángulo α entre el momento del mediador y del fotón emitido de la forma $E_\gamma = \frac{1}{\gamma_Y}\frac{m_Y}{2}(1 - v_Y \cos\,\alpha)^{-1}$, con $\cos\alpha \in [-1, 1]$.

Sabiendo esto, la luminosidad interna puede escribirse como

$$L_\chi = \Gamma_{\rm ann} \int_0^{R_{\rm WD}} N\, e^{-\int_0^r \frac{m_Y dr'}{\tau_{rest} E_Y(r')}} \left[\int_{E_-(r)}^{E_+(r)} E_\gamma \frac{dN_\gamma(r)}{dE_\gamma} dE_\gamma\right] dr. \tag{1.36}$$

Nótese que, en el caso límite en el que $m_Y \sim m\chi$, $v_Y(r) \to 0$ y $\gamma_Y(r) \to 1$. Por tanto, $E_- \to E_+$ y $\Delta E \to 0$. A su vez, este mismo escenario puede alcanzarse debido a la atenuación del mediador si $\sigma_{Y,N}$ es lo suficientemente grande como para frenarle hasta el reposo.

Con el objetivo de analizar tanto el impacto de la vida media del mediador como el de la atenuación en la luminosidad interna L_χ, la Eq. (1.36) fue evaluada numéricamente. Una vez hecho esto, encontramos que para valores pequeños de la vida media del mediador, L_χ toma valores mayores, ya que habrá más fotones que serán creados en el interior de la estrella. Además, L_χ aumenta cuando $m_Y/m_\chi \to 1$, debido a que en este caso límite el mediador es creado en reposo y la probabilidad de que decaiga dentro de la estrella es ~ 1. Ambos efectos pueden observarse en la Figura 3 del Capítulo 5. Por otro lado, el efecto de las pérdidas de energía está contenido en el valor de $\sigma_{Y,N}$, ver Figura 1 del Capítulo 5, proporcionando luminosidades mayores cuando ésta aumenta.

Una vez hubimos analizado estos efectos en la luminosidad interna debida a la autoaniquilación de secluded DM, comparamos nuestros resultados con las luminosidades experimentales del GC M4 y pusimos límites de exclusión a la vida media del mediador. Esto lo hicimos imponiendo que nuestras luminosidades no puedan ser mayores que las experimentales. Lo que obtuvimos es que el menor valor permitido para τ_{rest} (lo que llamamos τ_{limit}) aumenta monótonamente con m_Y/m_χ, como era de esperar, ya que L_χ aumenta con m_Y/m_χ. Además, la dependencia de τ_{limit} en m_Y/m_χ cambia para distintos valores de $\sigma_{Y,N}$ y $\sigma_{\chi,N}$, es decir, para diferente atenuación y tasa de captura. Ver Figura 5 del Capítulo 5. De esta forma, es posible obtener diferentes regiones de exclusión para τ_{rest} frente a $\sigma_{\chi,N}$ dependiendo de los valores de m_Y/m_χ y $\sigma_{\rm Y,N}$. El escenario más restrictivo se obtendrá para $m_Y/m_\chi = 1$, caso en el que no hay atenuación ya que el mediador es creado en reposo y, por tanto, los resultados no dependen de $\sigma_{\rm Y,N}$. Esta región de exclusión se muestra en la Figura 4 del Capítulo 5. Para esta elección se puede observar que el límite inferior de τ_{rest} permanece constante para $\sigma_{\chi,N} \gtrsim \frac{\sigma_0}{A^2}$, puesto que la única dependencia de L_χ en $\sigma_{\chi,N}$ es a través de $\Gamma_{\rm ann} = \frac{1}{2}\Gamma_{\rm capt}$ que satura a un valor constante cuando $\sigma_{\chi,A} \gtrsim \sigma_0$. Por otro lado, para $\sigma_{\chi,N} < \frac{\sigma_0}{A^2}$, $\Gamma_{\rm capt} \propto \frac{A^2\sigma_{\chi,N}}{\sigma_0}$ y τ_{limit} disminuye cuando lo hace $\sigma_{\chi,N}$.

En conclusión, se han obtenido restricciones para los valores de la vida media del mediador en reposo frente a la sección eficaz $\chi-$N. Esto se ha hecho para un estudio independiente de modelos específicos de secluded DM que se aniquila en dos mediadores metaestables dentro de WDs teniendo en cuenta la atenuación del mediador en el medio denso.

Tras esto, en el Capítulo 6 se incluye el review publicado con el título *Fermionic Light Dark Matter particles and the New Physics of Neutron Stars*, M. Cermeño, M. A. Pérez-García and J. Silk, PASA 34 (2017) e043 [107]. En él se analizan los primeros tres trabajos [54–56] anteriormente mencionados y presentados en los Capítulos 2, 3 y 4, además de un breve repaso acerca de la captura de DM por NSs.

Hasta el momento, en los trabajos presentados previamente [54–57] el marco considerado fue el de la GR. Sin embargo, en el artículo *Modified Gravity at Astrophysical Scales*, M. Cermeño, J. Carro, A. L. Maroto and M. A. Pérez-García, Astrophysical Journal 872 (2019) 130 [108] (Capítulo 7) analizamos un escenario más general en el que se explora la hipótesis de la necesidad de considerar modificaciones de la gravedad dentro de estrellas de baja densidad (tipo solar) y estrellas de densidad mayor (WDs). En este artículo se resuelven las ecuaciones de estructura estelares teniendo en cuenta teorías de MG en una aproximación perturbativa y describiendo el interior de las estrellas a través una EoS politrópica de índice $n = 3$. Se puede demostrar que el uso de este índice es una buena estimación tanto para estrellas de la secuencia principal (al menos en la zona radiativa), descritas por el Modelo Estándar de estructura estelar [86, 87, 130], como para WDs con electrones relativistas ($\rho_c \gg 10^6$ g/cm^3) [86, 87]. El objetivo de este trabajo fue analizar las variaciones en las masas y radios de estas estrellas debido a la modificación de la teoría de la gravedad y, como consecuencia, en sus luminosidades. Además, esto nos permitió chequear si las variaciones de la luminosidad son mayores debidas a la aniquilación de DM o a los efectos de MG en el límite perturbativo.

En el contexto de modelos de MG, siguiendo [131–133], donde tratan de describir estructuras a grandes escalas usando una teoría perturbativa cosmológica en el espacio de Fourier, consideramos perturbaciones escalares lineales a la métrica de Minkowski en el gauge Newtoniano. El elemento de línea queda de la forma

$$d\tau^2 = g_{\mu\nu}dx^\mu dx^\nu = -(1+2\psi(r))dt^2 + (1-2\phi(r))(dr^2 + r^2 d\Omega^2), \tag{1.37}$$

donde las perturbaciones escalares lineales se introducen a través de los potenciales radiales $\psi(r)$ y $\phi(r)$ en la aproximación de campo débil, $\psi(r) \ll 1$, $\phi(r) \ll 1$.

De esta métrica $g_{\mu\nu}$ y considerando la aproximación de fluido perfecto, el tensor energía momento se puede escribir como

$$T_{\mu\nu} = (\rho + P)U_\mu U_\nu + P g_{\mu\nu}, \tag{1.38}$$

donde ρ es la densidad de energía, P la presión y U^μ la cuadrivelocidad del fluido.

Una vez hecho esto, se consideró una solución estática para la cuadrivelocidad y se tomó $U^\mu U_\mu = -1$. Además, usando la aproximación para la componente diagonal espacial del tensor energía momento $T_{ii} = P(1-2\phi) \approx P$, las ecuaciones de Einstein nos proporcionaron las siguientes expresiones para las ecuaciones de Tolman-Oppenheimer-Volkoff

$$\nabla^2\phi = 4\pi G\rho, \tag{1.39}$$

$$\frac{d\psi}{dr} = \frac{Gm(r) + 4\pi G r^3 P}{r^2}. \tag{1.40}$$

Donde $m(r)$ es la masa contenida en un radio r dentro de la estrella. Tras esto, usando la ecuación de continuidad $\nabla_\mu T^{\mu\nu} = 0$, se obtuvo

$$\frac{dP}{dr} = -(\rho + P)\frac{d\psi}{dr}. \tag{1.41}$$

Es importante resaltar que, en una teoría perturbativa a primer orden se verifica $\psi \sim \phi \sim -\frac{GM(r)}{r}$ y $P \sim 0$. Esto es debido a que, mientras que ρ and ψ son funciones de primer orden en perturbaciones, P es una función de segundo orden. De esta

forma, las Eqs. (1.40) y (1.41) pueden reescribirse como

$$\frac{d\psi}{dr} = \frac{Gm(r)}{r^2}, \tag{1.42}$$

y

$$\frac{dP}{dr} = -\rho\frac{d\psi}{dr}. \tag{1.43}$$

Llegados a este punto, introducimos dos funciones, $\mu(k)$ y $\gamma(k)$, en el espacio k de Fourier, como se hace en [131–133], que modifican las ecuaciones para los potenciales, ψ, ϕ. Quedando la ecuación de Poisson de la forma

$$\nabla^2\psi = 4\pi G\mu\rho \tag{1.44}$$

y, además,

$$\phi = \gamma\psi. \tag{1.45}$$

Se puede ver que $\mu(k)$ actúa modificando el valor de la constante gravitatoria. Siguiendo [133], la expresión más general para este parámetro es

$$\mu(k) = \frac{1 + p_3k^2}{p_4 + p_5k^2}. \tag{1.46}$$

O, equivalentemente, en el espacio de posiciones

$$\mu(r) = \frac{1 - p_3\nabla^2}{p_4 - p_5\nabla^2}, \tag{1.47}$$

con p_3, p_4, p_5 parámetros constantes, de los cuales p_3 y p_5 tienen unidades de longitud al cuadrado y p_4 es adimensional. Además, para nuestro estudio tomamos $\gamma(k) = 1$.

Como estábamos interesados en pequeñas perturbaciones de la teoría de GR, nuestros parámetros verifican $p_3\nabla^2, p_5\nabla^2 \ll 1$ y $p_4 \sim 1$. En este sentido, el operador diferencial μ^{-1} se puede escribir como

$$\mu^{-1} = p_4(1 - \xi\nabla^2), \tag{1.48}$$

donde

$$\xi = -p_3 + \frac{p_5}{p_4}. \tag{1.49}$$

Así, las ecuaciones de Tolman-Oppenheimer-Volkoff a primer orden en teoría de perturbaciones quedan de la forma

$$\frac{d\psi}{dr} = \frac{Gm(r)}{p_4r^2} + \frac{\xi G}{p_4}\left(\frac{m''(r)}{r^2} - \frac{2m'(r)}{r^3}\right) \tag{1.50}$$

y

$$\frac{dP}{dr} = -\rho\frac{Gm(r)}{p_4r^2} - \frac{\xi\rho G}{p_4}\left(\frac{m''(r)}{r^2} - \frac{2m'(r)}{r^3}\right), \tag{1.51}$$

que son las versiones modificadas de las Eqs. (1.42) y (1.43). Nótese que, para ser consistente con el valor medido de la constante de Newton G, tenemos que imponer

$p_4 = 1$. De esta forma, la combinación G/p_4 que aparece en las ecuaciones de estructura obtenidas dentro del objeto estelar tomarán un valor idéntico a G.

Llegados a este punto, nos restringimos a estudiar un polítropo de índice $n = 3$. La EoS para este polítropo específico toma la forma

$$P = K\rho^{\frac{4}{3}}. \tag{1.52}$$

Así, el perfil de densidad se puede obtener como

$$\rho(r) = \left(\frac{-\psi}{4K}\right)^3. \tag{1.53}$$

Introduciendo la Eq. (1.53) en la Eq. (1.44) y usando una aproximación perturbativa en la que se considera una solución de la forma $\psi = \psi_0 + \psi_1$, con $|\psi_1| \ll |\psi_0|$. Las ecuaciones que han de resolverse son

$$\psi_0'' + \frac{2}{r}\psi_0' = \frac{-\pi G}{16}\left(\frac{\psi_0}{K}\right)^3, \tag{1.54}$$

y

$$\psi_1'' + \frac{2}{r}\psi_1' = \frac{-\pi G}{16K^3}\left[\xi\nabla^2(\psi_0)^3 + 3(\psi_0)^2\psi_1\right]. \tag{1.55}$$

Una vez resolvimos numéricamente estas ecuaciones diferenciales, encontramos que nuestra aproximación perturbativa restringe el valor del parámetro ξ. De forma más específica, si imponemos $|\psi_1| \leq 0.1|\psi_0|$, se obtiene un límite inferior para $|\xi|$ que depende del valor de la densidad central de nuestra estrella. De esta forma, para estrellas de tipo solar $|\xi| \lesssim 1.2\ 10^{19}$ cm^2.

Obtenida la solución $\psi(r)$, que proporciona el valor de la densidad ρ a través de la Eq. (1.53), se pudo hallar el valor del radio R de la estrella imponiendo $\psi(R) = 0$, ya que la presión y la densidad se hacen nulas para $r = R$. Tras esto, la masa total de la estrella, $M(R)$, se calculó a través de la integración

$$M(R) = \int_0^R 4\pi r^2 \rho dr. \tag{1.56}$$

Evualuando estas expresiones numéricamente se obtuvieron los diagramas $M - R$, de los que se puede observar cómo varía la curvatura partiendo de la solución constante del caso de GR ($\xi = 0$). Además, el comportamiento de $M(R)$ cambia cuando ξ pasa de valores positivos a valores negativos, correspondiendo estos últimos a configuraciones estelares metaestables. De este modo, como valores negativos de ξ proporcionan soluciones no físicas, podemos decir que no estarán permitidos. Ver Figuras 2 y 3 del Capítulo 7 para estrellas de baja masa y la Figura 7 para el caso de WDs.

Estas modificaciones en los valores de las masas y radios de las estrellas afectan, como consecuencia, a la luminosidad estelar, que puede obtenerse integrando

$$L = \int_0^R \epsilon(r) dm(r) = \int_0^R 4\pi r^2 \rho(r)\epsilon(r) dr, \tag{1.57}$$

donde $\epsilon(r)$ es la tasa de generación de energía nuclear en unidades de erg g^{-1} s^{-1}.

Para estrellas de tipo solar de baja masa con un canal activo de producción de neutrinos en la cadena pp $\epsilon(r)$ toma la forma [87]

$$\epsilon(r) = 2.46 \times 10^6 \,\mathrm{erg\ g^{-1}\ s^{-1}}\, \rho(r) X^2 \left(\frac{T(r)}{10^6\ \mathrm{K}}\right)^{-\frac{2}{3}} e^{-33.81\left(\frac{T(r)}{10^6\ \mathrm{K}}\right)^{-\frac{1}{3}}}, \tag{1.58}$$

con X la fracción de H y $T(r)$ la temperatura interior de la estrella a una distancia r del centro de la misma.

Para este trabajo, se consideraron estrellas dominadas principalmente por la presión del gas, es decir, $P \approx P_g = \frac{\rho k_B T}{\bar{\mu} m_H}$, con $\bar{\mu}$ el peso molecular y m_H la masa del H. Así, para un polítropo con $n = 3$ la temperatura queda de la forma

$$T = \frac{\bar{\mu} m_H K \rho^{\frac{1}{3}}}{k_B}. \tag{1.59}$$

Cuando evaluamos la luminosidad estelar se obtuvo que ésta aumenta con respecto al caso de GR para $\xi > 0$ (configuraciones estables), siendo mayor cuanto mayor es ξ (Figura 5 del Capítulo 7). Podríamos pensar, por tanto, que esto causará un aumento en el brillo de estas estrellas. Sin embargo, lo cierto es que, aunque fuera así, sería muy difícil separar este efecto de las fluctuaciones propias de las estrellas de similar magnitud.

Exploramos también la correlación luminosidad-temperatura efectiva, T_{eff}, encontrando una dependencia débil y no trivial en ξ. Escribiendo esta correlación bajo la forma $\mathrm{Log\,L} = \alpha \mathrm{Log}\left[\mathrm{T_{eff}(R)}\right] + \mathrm{C}$ se puede observar una variación del $\sim 0.6\%$ en la pendiente. Esto se puede ver de la Figura 6 del Capítulo 7. Es importante resaltar que en nuestro caso hemos obtenido T_{eff} al variar R, por tanto, no esperamos recuperar el valor usual de $\alpha = 4$ sino únicamente chequear la dependencia en ξ.

Tras haber estudiado las posibles variaciones de luminosidad debidas tanto a la aniquilación de DM dentro de WDs como a la consideración de teorías de MG en el marco de una aproximación perturbativa, podemos concluir que la presencia de DM probablemente afectará más a esta cantidad que las modificaciones de la gravedad en aproximación de campo débil.

Chapter 2

Diffusion of dark matter in a hot and dense nuclear environment

Resumen

En este trabajo se ha calculado el recorrido libre medio, o lo que es lo mismo, la inversa de la sección eficaz de scattering por unidad de volumen, de una partícula de DM fermiónica y ligera, $m_\chi \lesssim 5$ GeV, debido a interacciones efectivas de tipo escalar y vectorial con nucleones en un medio denso y caliente. Nos centramos en los efectos debidos a la densidad y la temperatura en el medio nuclear con el fin de evaluar la importancia del principio de exclusión de Pauli en el proceso de scattering. Tras hacer esto, encontramos que tanto la sección eficaz de interacción diferencial como la integrada se ven afectadas de manera importante por los efectos de densidad de la materia nuclear, concretamente por el hecho de considerar una masa efectiva para los nucleones $m_N^* < m_N$. Los efectos de temperatura son también importantes aunque en menor medida que los de densidad. Éstos se tienen en cuenta considerando un factor adicional de balance detallado.

Una vez hecho esto, discutimos cualitativamente sus posibles implicaciones en la opacidad de objetos estelares nucleares, tales como las NSs, donde una fracción de DM podría ser acretada gravitacionalmente. La estimación típica para el recorrido libre medio, $\lambda_\chi \simeq 1/\sigma_{\chi,N} n$, no tiene en cuenta la dependencia del espacio de fases en el proceso de scattering, la cual hemos comprobado que introduce cambios significativos en el valor de éste. El hecho de tener en cuenta las funciones de distribución de los nucleones restringe los estados salientes posibles, haciendo que $\frac{\sigma_{\chi,N}}{V}$ disminuya con respecto a la estimación de vacío aumentando λ_χ. En este artículo se muestra que la aproximación de comportamiento difusivo de la DM a densidad y temperatura finita en el interior de NSs está bien fundamentada y que la DM podría contribuir al transporte de energía dentro de la estrella.

PHYSICAL REVIEW D **94,** 023509 (2016)

Diffusion of dark matter in a hot and dense nuclear environment

Marina Cermeño,[1,*] M. Ángeles Pérez-García,[1,†] and Joseph Silk[2,3,4,‡]

[1]*Department of Fundamental Physics, University of Salamanca, Plaza de la Merced s/n 37008 Salamanca, Spain*

[2]*Institut d'Astrophysique, UMR 7095 CNRS, Université Pierre et Marie Curie, 98bis Boulevard Arago, 75014 Paris, France*

[3]*Department of Physics and Astronomy, The Johns Hopkins University, Homewood Campus, Baltimore, Maryland 21218, USA*

[4]*Beecroft Institute of Particle Astrophysics and Cosmology, Department of Physics, University of Oxford, Oxford OX1 3RH, United Kingdom*

(Received 12 November 2015; revised manuscript received 20 May 2016; published 7 July 2016)

We calculate the mean free path in a hot and dense nuclear environment for a fermionic dark matter particle candidate in the ∼GeV mass range interacting with nucleons via scalar and vector effective couplings. We focus on the effects of density and temperature in the nuclear medium in order to evaluate the importance of the final state blocking in the scattering process. We discuss qualitatively possible implications for opacities in stellar nuclear scenarios, where dark matter may be gravitationally accreted.

DOI: 10.1103/PhysRevD.94.023509

I. INTRODUCTION

There are multiple indications pointing toward a model containing cold dark matter (DM) as the best explanation for the universe we see at different scales. In particular, the importance of the dark sector component of matter on stellar scales has been less extensively studied and has mainly focused on the sun, planets, white dwarfs [1–3], and compact stars [4]. This is due to the expected moderate capability of gravitational accretion by these individual celestial bodies from an existing DM galactic distribution. Although the current situation of DM searches has greatly benefited from a world-wide experimental effort, at the present time, there still remains a relatively vast DM phase space to explore. Regarding possible values for DM particle masses within the weak interaction sector (*wimp* scenario), most popular candidates range from the sub-GeV region up to ∼100 TeV. As for the interaction cross sections with nuclear matter (i.e., nucleons, N), there are at least five orders of magnitude in the ∼GeV mass range remaining to be fully tested, namely, $\sigma_{\chi N} \sim 10^{-43}$–$10^{-48}$ cm^2 as quoted by direct detection searches [5].

Apart from this, concerning the nature of the DM particle, in the case of a Majorana candidate, the expected indirect signal involving gamma rays or neutrino final products is still under debate [6]. In this same direction, we may cite other astrophysical effects such as the modification of the emissivity of Standard Model neutrinos from solar reaction chains that have been recently suggested [7]. In the case of asymmetric candidates, accretion of DM mass beyond a critical value, i.e., the Chandrasekhar mass, could induce a dramatic fate for the star where DM accumulates over time [8–10] and eventually collapses to a black hole. Another catastrophic event could be triggered following compact object formation via DM seeding. In case of a Majorana candidate, it could induce spark formation energetic enough to nucleate stable bubbles of deconfined quark matter leading to a softening of the nucleon equation of state. This would drive a neutron star to quark star conversion [11–13]. In addition, unstable DM can also be constrained by structural stability of accreting objects [14].

However, aside from a pure particle physics description, from the thermodynamical point of view, average magnitudes incorporating the effect of a novel dark sector could be, in principle, determined by evaluating the interplay of both types of matter in a common environment. Typically, the possible dark self-interaction effects are expected to be small as long as the numbers of DM particles remain tiny at all times, with respect to the baryons, and their relative fraction $Y_\chi = N_\chi/N_B \ll 1$. This could be important, however, for a precise determination of the critical dark matter mass capable of being sustained in a star [8].

As mentioned before, for a given candidate, $\sigma_{\chi N}$ mainly determines the relative fraction of DM to be captured by a compact-sized (spherical) object of mass M and radius R. Once inside, it is believed to diffuse toward the denser central stellar regions according to the exponential law $\sim e^{-m_\chi \phi(r)/k_B T(r)}$, being $T(r)$ a local temperature, $\phi(r)$ the gravitational potential and r the radial coordinate [15].

As an order-of-magnitude estimate, the mean free path of a DM particle, λ_χ, is quoted as $\lambda_\chi \simeq 1/\sigma_{\chi N} n$, where n is the ordinary nucleon number density. This is usually considered as being sufficient to obtain knowledge about the most

*marinacgavilan@usal.es
†mperezga@usal.es
‡silk@iap.fr

efficient opaque environments. For example, a dense nuclear medium such as the central core in a neutron star (with a content $\gtrsim 90\%$ neutrons) exhibits densities well in excess nuclear saturation density $n_0 \simeq 0.17$ fm^{-3}. It is important to note, however, that in-medium effects are mostly absent from the previous rough estimate. Let us briefly comment on some of the missing corrections. To begin with, Fermi blocking due to partial restriction of the outgoing nucleon phase space can play a role diminishing the χN cross section. Finite temperature effects will additionally allow the population of higher energy states in the nucleon sector with respect to the vanishing temperature case to provide the opposite effect. Let us remind ourselves here that temperatures in the range of $T \lesssim 50$ MeV are usually achieved in the very early stages of proto-neutron star evolution [16]. Later, after a primary neutrino cooling era, temperatures fall to the ∼keV range. This will effectively set at large times a $T \approx 0$ configuration, as thermal energies are indeed much smaller than nucleon Fermi energies $k_B T \ll E_{FN}$ in the dense medium.

Motivated for the need to compare bounds from the colliders to direct detection, one can describe interactions between DM and fermions with effective operators in the context of effective field theories (EFT). In direct detection searches, for example, a nonrelativistic incoming χ particle with low Maxwellian velocity, $v/c \ll 1$, is considered. However, collider searches can constrain the high energy part of the interaction as particles are increasingly more relativistic $v/c \sim 1$ allowing, in addition, higher values of $\sqrt{s}$ and momentum transfer ∼TeV. Typically, all the quoted interactions have been largely explored in very low density or vacuum conditions. In particular, scalar, vector, and pseudoscalar couplings can play a crucial role as seen in [17,18]. To test increasing relativistic velocity ranges, natural sources of acceleration can be provided by gravitational boosting near compact stars. In this way, (neutral) DM particles can acquire large velocities $v \sim c$ and scatter very dense macroscopic regions of size nearly the radius of the star $R \sim 10$–12 km. This extent has so far only been marginally explored [19,20]. In this work, we focus on the impact of the relativistic contribution of scalar and vector χN couplings to the spin-independent (SI) diffusion of DM inside a dense and hot nuclear medium.

The structure of this contribution is as follows. In Sec. II, we present the effective field theory Lagrangian model using dark matter-nucleon contact interaction via scalar and vector couplings in a relativistic framework. Later, we compute the doubly differential and integrated χN cross sections at finite nucleon chemical potential and temperature. We especially focus on the resulting diffusive behavior of weakly interacting DM particles. In Sec. III, we discuss the obtained dependencies by presenting the figures for selected cases. Finally, in Sec. IV, we give our conclusions.

II. DARK MATTER MODEL AND CROSS SECTIONS

We consider a fermionic dark matter particle of Dirac type, χ, with scalar and vector couplings to the nucleon field N (protons and neutrons). We can write the interaction Lagrangian under the form

$$\mathcal{L}_{\mathcal{I}} = \sum_{N=n,p} g_{Ns}\chi\bar{\chi}N\bar{N} + g_{Nv}\chi\gamma^{\mu}\bar{\chi}N\gamma_{\mu}\bar{N}, \tag{1}$$

where γ_μ are the Dirac matrices and g_{Ns}, g_{Nv} are the scalar and vector coupling constants, respectively. This treatment is already used in direct detection at low energies with nonrelativistic effective field theory operators as shown in [21]. Typically, elastic scattering (rather than inelastic) is considered as it is the case relevant for direct detection. Generically, operators containing two fermionic dark matter fields can be categorized as shown in [5,22]. In particular, we focus on those labeled D1 and D5, both contributing to the SI interaction. This interaction is equivalent to considering a Fermi four-fermion interaction model, where the effective couplings of mass dimension (-2) for these operators are obtained by integrating out the propagator of a generic ϕ mediator with mass M_ϕ. Motivated by the need to compare bounds from colliders to direct detection, we describe interactions of DM with quarks $q = u, d$, and averaging in terms of nucleon fields, we can write for the vector case $g_{Nv}/M_\phi^2 \sim 1/{\Lambda_v}^2$ and $g_{Ns}/M_\phi^2 \sim m_q/{\Lambda_s}^3$, where Λ_v (Λ_s) is the suppression mass scale for the vector (scalar) case. As usual, we are assuming the effective couplings are of order $O(1)$ and can be absorbed into $\Lambda_{s,v}$ [23]. Using bounds from CMS and ATLAS [24,25], we set $\Lambda_v \gtrsim 1$ TeV and $\Lambda_s \gtrsim 100$ GeV. At this point, it is worth mentioning that a larger parameter range can be considered by means of a multiplicative factor in each coupling, g_{Ns}, g_{Nv}. We have selected these values as they refer to families of phenomenological models that are currently allowed.

Usually, the incoming DM particle is supposed to be thermalized in the galaxy with the Maxwellian mean velocities $\bar{v} \sim 220$ km/s. However, in the scenario we consider, an accreting dense star (typically with the mass and dimensions of a neutron star), general relativistic effects are non-negligible and are capable of providing a sizable gravitational boost to the incoming DM particle [19,26]. Let us consider, in order to be concrete, a canonical neutron star of mass $M_{\rm NS} \simeq 1.5\, M_\odot$ and radius $R_{\rm NS} \simeq 12$ km. Expliciting the ratio used as unity, $\frac{GM_{\rm NS}}{c^2} = 1$, the velocity modulus v at the star surface is given by

$$\beta = \frac{v}{c} = \sqrt{\frac{2GM_{\rm NS}}{rc^2}} \approx 0.6\sqrt{\left(\frac{12\text{ km}}{R_{\rm NS}}\right)\left(\frac{M_{\rm NS}}{1.5\, M_\odot}\right)}, \tag{2}$$

yielding a minimum Lorentz factor at the surface $\gamma = 1/\sqrt{1-\beta^2} \approx 1.26$. If scattering happens well inside the core, the previous value is a lower limit, then $\gamma \gtrsim 1.26$. The associated wavelength of the incoming DM particle is $\lambda = \frac{2\pi\hbar c}{\sqrt{\gamma^2-1}m_\chi c^2}$. This expression sets, in practice, a measure of the validity of our calculation since matter is tested to sizes around $\lambda \sim 1$ fm, i.e., in the DM mass range $m_\chi \lesssim 5$ GeV. Although further modeling would be required for the description of the inner hadron structure, the use of nuclear form factors can somewhat mitigate the short-range correlations arising in our calculation as we see later in the manuscript.

In order to calculate the differential cross section per unit volume for the DM-nucleon scattering, we use the interaction terms appearing in Eq. (1). We denote $p'^\mu = (E', \vec{p}')$ and $p^\mu = (E, \vec{p})$ as the four-momentum for the outgoing and incoming nucleon of effective mass m_N^*, respectively, and $k'^\mu = (\omega', \vec{k}')$ and $k^\mu = (\omega, \vec{k})$ analogous for the DM particle of mass m_χ. Momentum transfer is denoted by $q^\mu = p'^\mu - p^\mu = k^\mu - k'^\mu$. In this way, $q_0 = E' - E = \omega - \omega'$ and $\vec{q} = \vec{p}' - \vec{p} = \vec{k} - \vec{k}'$. The general expression can be written as [27,28]

$$d\sigma = \frac{|\overline{\mathcal{M}}_{\mathcal{N}}|^2}{4\sqrt{(pk)^2 - m^{*2}_N m^2_\chi}} d\Phi(p, p', k, k') \mathcal{F}_{\mathcal{FB}}, \quad (3)$$

where the phase space volume element is

$$d\Phi(p, p', k, k') = (2\pi)^4 \delta^{(4)}(p + k - p' - k') \frac{d^3\vec{p}'}{(2\pi)^3 2E'} \frac{d^3\vec{k}'}{(2\pi)^3 2\omega'}. \quad (4)$$

Here, $|\overline{\mathcal{M}}_{\mathcal{N}}|^2$ is the square of the scattering amplitude of the process considered in our interaction model that we discuss in detail later. The four-dimensional delta assures the conservation of momentum and energy in the collision. The factor $\mathcal{F}_{\mathcal{FB}}$ accounts for the Fermi blocking term that takes into account the occupation of states and in our calculation affects only to the nucleon sector (protons or neutrons) $\mathcal{F}_{\mathcal{FB}} = f_N(E)(1 - f_N(E'))$ with $f_i(E) = \frac{1}{1+e^{(E-\mu_i^*)/k_B T}}$ $i = \mathrm{p}, \mathrm{n}$. Also, μ_i^* is the effective nucleon chemical potential for a particle with isospin of ith-type. From this point and in what follows, we consider $\hbar = c = 1$. Let us remark that for the dark sector we assume that all outgoing DM particles states are, in principle, allowed and $1 - f_\chi(\omega') \approx 1$ since the fraction of DM inside the star remains tiny at all times. The validity of this approximation is given by the estimate of DM particles inside the object as $N_\chi(t) \approx N_{0\chi} + C_\chi \delta t$. Using $C_\chi \simeq 6 \times 10^{25} (\frac{M}{1.5 M_\odot})(\frac{R}{12\ \mathrm{km}})(m_\chi)\left(\frac{\rho_\chi^{\mathrm{ambient}}}{0.3 \frac{\mathrm{GeV}}{\mathrm{cm}^3}}\right)\left(\frac{\sigma_{\chi N}}{\sigma_0}\right)$ s^{-1} [8] and the number of nucleons in the star $N_N = N_B \simeq 10^{58}$, we obtain $Y_\chi = N_\chi/N_N < 10^{-20}$ for an old neutron star with a lifetime $\delta t \sim 10^6$ yr. We assume a cross section $\sigma_{\chi N} > \sigma_0$ larger than the geometrical or critical cross section [2] $\sigma_0 \simeq \pi R^2_{\mathrm{NS}} m_N / M_{\mathrm{NS}} \sim 10^{-45}$ cm^2 so the star can effectively scatter and capture DM. Let us mention here that the cross section ratio $\sigma_{\chi N}/\sigma_0$ could be, in principle, even smaller than unity, but in that case, the scattering scenario we present would be mostly insensitive to dark matter, assuming cross sections compatible with the range of currently allowed experimental constraints, $\sigma_{\chi N}/\sigma_0 > 1$, however. DM population in the NS (after the supernova explosion) should not be negligible since the massive progenitor $8\ M_\odot \lesssim M_{\mathrm{progenitor}} \lesssim 15\ M_\odot$ can be efficient in the DM accretion process [14]. Then, $N_{0\chi} \lesssim 10^{39}$ for an environment with ambient DM density $\rho_\chi^{\mathrm{ambient}} \simeq 0.3$ GeV/cm^3. Effective values of nucleon mass and chemical potential define the *quasi-particle* nature of the nucleon in the medium and differ from the nude values by the presence of average meson fields. In this work, we consider this correction as obtained in the existing literature and refer for further reading to [29].

Since we are interested in calculating the DM particle mean free path, we also consider the differential and integrated cross section *per unit volume*, and thus, we must integrate over the incoming nucleon phase space [27]. Then, our expression reads

$$\frac{d\sigma(\omega)}{V} = \frac{1}{(2\pi)^5} \int d^3\vec{p} \int d^3\vec{k}' \delta(E + \omega - E - \omega') \times \frac{|\overline{\mathcal{M}}_{\mathcal{N}}|^2}{16\omega' E' \sqrt{E^2\omega^2 - m^{*2}_N m^2_\chi}} \mathcal{F}_{\mathcal{FB}}, \quad (5)$$

where we have performed a partial integration over three-dimensional momentum space. The flux expression appearing in the denominator in Eq. (5) as well as the scattering amplitude we discuss later in the manuscript have, in general, momentum dependences. In the cross-section calculation, we have retained only the lowest order terms following [27] since $v_\chi^2 \sim v_N^2 \ll 1$ given $\frac{|\vec{p}_i|}{E_i} = v_i$, $i = \chi, N$ from reference values $v_\chi \sim 0.6$, and nucleon Fermi velocities $v_N \sim v_{FN} = |\vec{p}_{FN}|/E_{FN} \sim 0.4$ at $n = \frac{|\vec{p}_{FN}|^3}{3\pi^2} = n_0$. In particular, for the flux, this leads to the final expression $\sqrt{(pk)^2 - m_N^2 m_\chi^2} = \sqrt{(E\omega - \vec{p}\,\vec{k})^2 - m_N^2 m_\chi^2} \simeq \sqrt{E^2\omega^2 - m_N^2 m_\chi^2}$.

Let us further rewrite Eq. (5) using a dispersion angle θ for the outgoing DM particle. In this way, we obtain $d^3\vec{k}' = |\vec{k}'|^2 2\pi d(\cos\theta) d|\vec{k}'| = 2\pi |\vec{q}| \frac{\omega'}{|\vec{k}|} d|\vec{q}| dq_0$. This follows from $\omega' d\omega' = |\vec{k}'| d|\vec{k}'|$ and $d(\cos\theta) = \frac{|\vec{q}|d|\vec{q}|}{|\vec{k}||\vec{k}'|}$. Finally, we obtain after a trivial partial integration,

$$\frac{d\sigma(\omega)}{V} = \frac{1}{(2\pi)^4}\int d^3\vec{p}\int d|\vec{q}|\int dq_0\delta(q_0+E-E') \times \frac{|\vec{q}|}{|\vec{k}|}\frac{|\overline{\mathcal{M}}_{\mathcal{N}}|^2}{16E'\sqrt{E^2\omega^2 - m^{*2}_N m^2_\chi}}\mathcal{F}_{\mathcal{FB}}. \quad (6)$$

In this calculation, we restrict ourselves to temperatures and densities typical for the thermodynamical evolution of the stellar core region, that is, $T \lesssim 50$ MeV and $n \simeq (1-3)n_0$. Due to the fact that squared Fermi nucleon velocities are $v^2_{FN} \ll 1$, we perform an expansion of the single particle energies for the incoming and outgoing nucleon states

$$E = m^*_N + \frac{|\vec{p}|^2}{2m^*_N}, \qquad E' = m^*_N + \frac{|\vec{q}+\vec{p}|^2}{2m^*_N}. \quad (7)$$

In order to perform the integral in Eq. (6), we express the energy delta function as

$$\delta(q_0+E-E') = \frac{m^*_N}{|\vec{p}||\vec{q}|}\delta(\cos\theta-\cos\theta_0)\Theta(|\vec{p}|^2-|\vec{p}_-|^2), \quad (8)$$

where

$$\cos\theta_0 = \frac{m^*_N}{|\vec{p}||\vec{q}|}\left(q_0 - \frac{|\vec{q}|^2}{2m^*_N}\right), \quad (9)$$

and

$$|\vec{p}_-|^2 = \frac{m^{*2}_N}{|\vec{q}|^2}\left(q_0 - \frac{|\vec{q}|^2}{2m^*_N}\right)^2. \quad (10)$$

Let us now discuss the range of the integration variables. For the energy transfer range $-\infty < q_0 < \omega - m_\chi$ since $m_\chi < \omega' < \infty$ and $|\vec{k}| - |\vec{k}'| < |\vec{q}| < |\vec{k}| + |\vec{k}'|$ from the constraint of a real-valued angle. Instead, at $T = 0$, the energy transfer cannot be negative, so that $q_0 > 0$ and $0 < q_0 < \omega - m_\chi$, and for the incoming nucleon, it follows $|\vec{p}_-| < |\vec{p}| < \infty$. Note that for $T = 0$ in the limit of vanishing kinetic energy for the incoming DM particle, the q_0 range reduces to zero as the outgoing states are all occupied, therefore providing a null cross section, while this is not true in the finite T case as more channels are available.

Finally, if we are interested in the doubly differential cross section, this can be obtained as

$$\frac{1}{V}\frac{d\sigma}{d\Omega dq_0} = \frac{1}{(2\pi)^4}\int_{|\vec{p}_-|}^{\infty}\frac{d|\vec{p}||\vec{p}|}{4E'}\frac{m^*_N|\vec{k}'|}{|\vec{q}|}\delta(\cos\theta-\cos\theta_0) \times \Theta(|\vec{p}|^2-|\vec{p}_-|^2)\mathcal{M}, \quad (11)$$

with

$$\mathcal{M} = \frac{|\overline{\mathcal{M}}_{\mathcal{N}}|^2 f_N(E)(1-f_N(E'))}{4\sqrt{E^2\omega^2 - m^{*2}_N m^2_\chi}}. \quad (12)$$

The sum of scalar(s) and vector(v) contributions from the Lagrangian in Eq. (1) gives a scattering amplitude $\mathcal{M}_N = \mathcal{M}_s + \mathcal{M}_v$, and therefore,

$$|\overline{\mathcal{M}}_N|^2 = \frac{1}{4}\sum_{\text{spins}}\mathcal{M}_N\mathcal{M}^*_N = |\overline{\mathcal{M}}_s|^2 + |\overline{\mathcal{M}}_v|^2 + \frac{1}{2}\sum_{\text{spins}}\mathcal{M}^*_s\mathcal{M}_v, \quad (13)$$

where

$$|\overline{\mathcal{M}}_s|^2 = 4g^2_{Ns}(p'p + m^{*2}_N)(k'k + m^2_\chi),$$
$$|\overline{\mathcal{M}}_v|^2 = 8g^2_{Nv}[2m^{*2}_N m^2_\chi - m^{*2}_N k'k - m^2_\chi p'p + (p'k')(pk) + (p'k)(pk')],$$

and

$$\frac{1}{2}\sum_{\text{spins}}\mathcal{M}^*_s\mathcal{M}_v = 8g_{Ns}g_{Nv}m^*_N m_\chi(pk + pk' + p'k + p'k').$$

As a further correction at short ranges, we can model the structure of the nucleon with a form factor $F(|\vec{q}|)$. We consider a monopolar form with a cutoff parameter $\Lambda = 1.5$ GeV. Then, we replace $g_{Ns} \to g_{Ns}F(|\vec{q}|^2)$ and $g_{Nv} \to g_{Nv}F(|\vec{q}|^2)$ with $F(|\vec{q}|^2) = \frac{\Lambda^2}{\Lambda^2+q^2}$ so that $F(0) = 1$.

Retaining the lowest order in particle velocities in the averaged squared matrix element, we obtain

$$|\overline{\mathcal{M}}_N|^2 \simeq 4g^2_{Ns}(E'E + m^{*}{}^2_N)(\omega'\omega + m^2_\chi) + 8g^2_{Nv}(2m^{*2}_N m^2_\chi - m^{*2}_N\omega\omega' - m^2_\chi E'E + 2E'\omega' E\omega) + 8g_{Ns}g_{Nv}m^*_N m_\chi(E\omega + E\omega' + E'\omega + E'\omega').$$

Let us note that if finite temperature is considered detailed balance factors must be added to the medium response to weak probes [30,31] under the form

$$S(q_0,T) = \frac{1}{1-e^{-\frac{|q_0|}{k_B T}}}. \quad (14)$$

This factor provides the relation between the dynamical nuclear structure factor for positive and negative energy transfers q_0 as the thermodynamic environment can donate energy to the outgoing particle.

As we are interested in obtaining the total integrated cross section per unit volume $\frac{\sigma(\omega)}{V}$ and the inverse of it, i.e., the mean free path, $\lambda_\chi = (\frac{\sigma(\omega)}{V})^{-1}$, we must integrate over all

possible outgoing energy transfer values and solid angle. In this way, we obtain

$$\lambda_\chi^{-1} = \frac{\sigma(\omega)}{V} = \frac{m_N^*}{4(2\pi)^3}\int_0^{\omega-m_\chi} dq_0 \int_{|\vec{k}|-|\vec{k}'|}^{|\vec{k}|+|\vec{k}'|} d|\vec{q}| \times \int_{|\vec{p}_-|}^{\infty} d|\vec{p}|\, \frac{|\overline{\mathcal{M}}_{\mathcal{N}}|^2 |\vec{p}| f_N(E)(1-f_N(E'))S(q_0,T)}{4E'|\vec{k}|\sqrt{E^2\omega^2 - {m_N^*}^2 m_\chi^2}}. \quad (15)$$

III. RESULTS

In this section, we present the results. We start by discussing the low T regime. We set $g_{Ns} \sim 10^{-15}$ MeV^{-2} and $g_{Nv} \sim 10^{-13}$ MeV^{-2} and a cutoff parameter $\Lambda = 1.5$ GeV. In order to include the effect of the medium, we replace vacuum nucleon mass and chemical potential values by the effective ones at each baryonic density and T [29]. The ith-type isospin is obtained according to $n_i = \frac{2}{(2\pi)^3}\int_0^\infty \frac{4\pi p^2 dp}{1+e^{(\sqrt{p^2+{m_N^*}^2}-\mu_i^*)/k_B T}}$.

In Fig. 1, we show the differential cross section per unit volume as a function of the energy transfer q_0 for different values of $|\vec{q}| = 20$, 41, 207, and 290 MeV with dash-dotted, dashed, dotted, and solid lines, respectively, for a pure neutron system with $n = n_0$. We use $m_\chi = 0.5$ GeV setting $T = 0$. The limiting upper value of the energy transfer is $\omega - m_\chi \approx 130$ MeV. The triangular shape is due to the Heaviside Fermi distribution at $T = 0$. Beyond q_0 values limited by real-valued angles in Eq. (9), the scattered states are not allowed since it is kinematically impossible to scatter a nucleon due to lack of empty states.

In Fig. 2, we show the differential cross section per unit volume as a function of the energy transfer q_0 for different values of the nucleon number density $n = (0.5, 1, 2)n_0$ with dotted, dashed, and solid lines, respectively, for

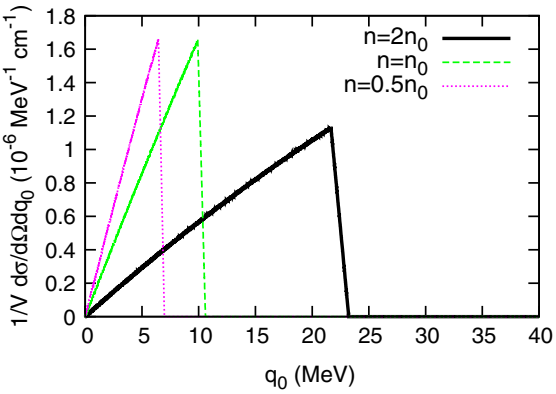

FIG. 2. Differential cross section per unit volume as a function of the energy transfer q_0 for nucleon densities $n = (0.5, 1, 2)n_0$. We set $|\vec{q}| = 20$ MeV and $m_\chi = 0.5$ GeV at $T = 0$.

$|\vec{q}| = 20$ MeV. We use $m_\chi = 0.5$ GeV setting $T = 0$ and effective nucleon masses $m_N^*/m_N \simeq 0.85$, 0.7 and 0.4 for the increasing density set. A combined effect of the density dependence of nucleon masses and the nucleon Fermi momentum value provide a rapid increase in the maximum q_0 value.

In order to test the variability with the dark probe mass, we depict in Fig. 3 the differential cross section per unit volume as a function of q_0 for mass values $m_\chi = 0.5$, 1, and 5 GeV. We set $T = 0$ and $n = n_0$ at $|\vec{q}| = 20$ MeV. The curve with $m_\chi = 5$ GeV has been decreased by a factor of 10 to make the trend more clear.

Finite temperature effects can be observed in Fig. 4, where the detailed balance factors have been included. We use values of temperature $T = 0$, 5, and 10 MeV with solid, dashed, and dotted lines, respectively, for $|\vec{q}| = 20$ MeV. We set a fixed value of the chemical potential $\mu = E_{FN}$ at $n = n_{\rm sat}$. This corresponds to densities $n = 0.170$, 0.174, and 0.209 fm^{-3} setting $m_\chi = 0.5$ GeV. At temperatures

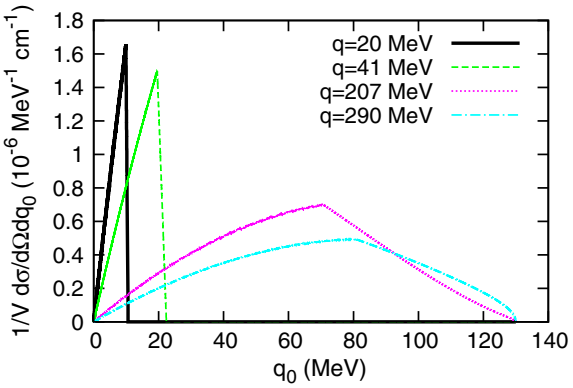

FIG. 1. Differential cross section per unit volume as a function of the energy transfer q_0 for values of $|\vec{q}| = 20$, 41, 207, and 290 MeV. The DM particle mass is $m_\chi = 0.5$ GeV, and $T = 0$ at $n = n_0$.

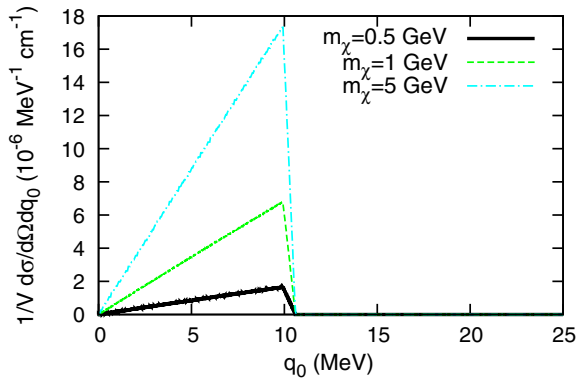

FIG. 3. Differential cross section per unit volume as a function of the energy transfer q_0 for a nucleon density $n = n_0$. We set $|\vec{q}| = 20$ MeV at $T = 0$. The $m_\chi = 5$ GeV case has been decreased by a factor of 10 in this plot.

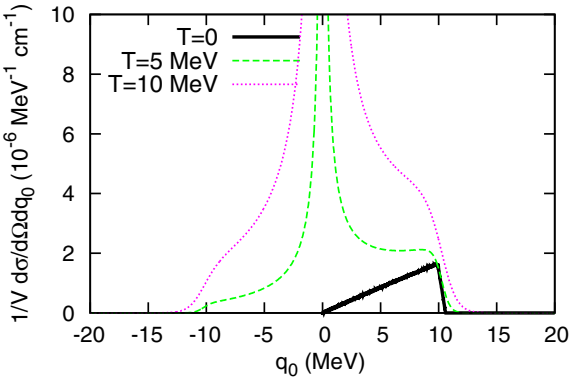

FIG. 4. Differential cross section per unit volume as a function of the energy transfer q_0 at $T = 0$, 5, 10 MeV for a nucleon density $n = n_0$. We set $|\vec{q}| = 20$ MeV and $m_\chi = 0.5$ GeV.

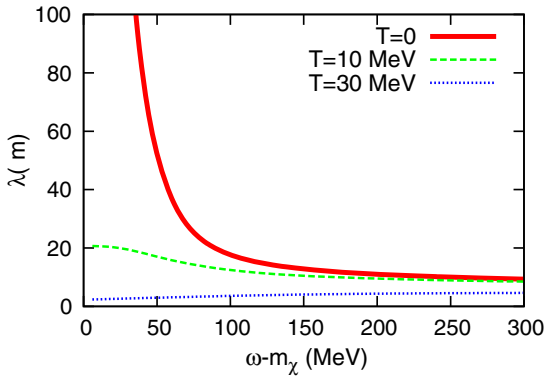

FIG. 6. DM particle mean free path as a function of kinetic energy for $m_\chi = 1$ GeV at $n = n_0$ for $T = 0$, 10, and 30 MeV.

$T > 0$, the negative energy transfer states get increasingly populated, and the sharp nucleon distribution is smoothed. As $q_0 \to 0$, the inverse detailed balance factor $S^{-1}(q_0, T) \to 0$. The corresponding divergence will, however, be integrable in order to obtain a finite integrated cross section.

In Fig. 5, we show the mean free path for the χ particle as a function of kinetic energy $K = \omega - m_\chi$ for three mass values $m_\chi = 0.5$, 1, and 5 GeV with solid, dashed, and dotted lines, respectively. We set $n = n_0$ and $T = 0$. We can see that in this DM mass range scattering is diffusive to very good approximation as $\lambda/R \ll 1$. We show with the dot-dashed line that the simplified estimate yields a constant value $\lambda_\chi \simeq 1/\sigma_{\chi N} n \sim 5.9$ m, assuming sensitivities $\sigma_{\chi N} \sim 10^{-41}$ cm^2. For our choice of couplings strengths, fixed K energy, a Standard Model neutrino displays typical mean free path somewhat smaller [27,30,32], however, being an efficient heat carrier inside the star. The larger the mass of the DM particle the more opaque is the medium to it. Note that as $\omega \to m_\chi$ the phase space available for the outgoing particles vanishes as the energy transferred $q_0 \to 0$. As all the outgoing states are all occupied in the nucleon sea at $T = 0$, this provides a null value of the integrated cross-section value for the DM-nucleon interaction. This behavior is shown in Fig. 6, where we plot the variation of the mean free path with kinetic energies for temperatures $T = 0$ (solid line), $T = 10$ MeV (dashed line), and $T = 30$ MeV (dotted line). We consider $m_\chi = 1$ GeV and $n = n_0$. At $T = 0$ and vanishing kinetic energy, the mean free path goes arbitrary large as the integrated cross section also vanishes due to filled population levels. This behavior is smoothed at finite temperature, where a nonvanishing mean free path value is recovered.

In Fig. 7, the variation of the DM particle mean free path is shown as a function of density (in units of n_0) for two values of temperature, $T = 0$ (solid line) and $T = 10$ MeV (dashed line). We use $m_\chi = 1$ GeV, and effective nucleon masses have been considered for the $T = 0$ case, while not for the finite temperature case in order to estimate competitive effects. A steady decrease is obtained in case the

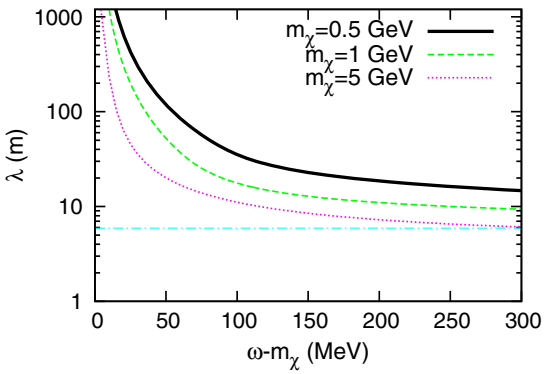

FIG. 5. Dark matter mean free path as a function of kinetic energy for $m_\chi = 0.5$, 1, and 5 GeV at $T = 0$ and $n = n_{\rm sat}$. Dot-dashed line shows that the simplified estimate yields a constant value $\lambda_\chi \simeq 1/\sigma_{\chi N} n \sim 5.9$ m, assuming current experimental sensitivities $\sigma_{\chi N} \sim 10^{-41}$ cm^2. See text for details.

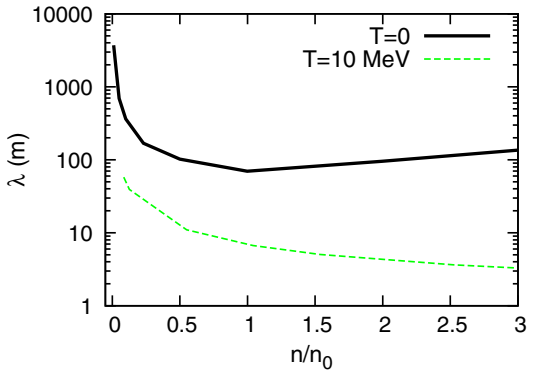

FIG. 7. DM particle mean free path as a function of density (in units of n_0) for two values of temperature, $T = 0$ and $T = 10$ MeV. Effective (naked) nucleon mass has been used in the zero (finite) T calculation.

naked nucleon mass is considered. Incoming energy has been fixed to $\omega = 1.26 m_\chi$ for each case. Temperature effects, which are relevant in the early stages of dense star evolution, tend to increase the opacity of nucleon matter to prevent DM nearly free streaming.

In order to qualitatively compare our findings with existing current experiments, we consider generic sensitivities constrained from direct and collider searches. In this part, our aim is to see how our results fit in the global present picture of relativistic scattering of DM coming from a complementary and different scenario.

From our earlier discussion, the scenario we present in our work is meaningful for a χN cross section larger than that of the geometrical cross section $\langle \sigma_{\chi N} \rangle \sim \sigma_0 \simeq \pi R^2 m_n / M \sim 10^{-45}$ cm^2. Typical constrained values in current experiments are larger than this value. In order to compare strengths, we consider a typical reference value of central baryonic density in the star $n = 2n_0$ and estimate integrated cross sections *per particle*, averaging over the nucleon particle density, as $\langle \sigma_{\chi N} \rangle \simeq \frac{\sigma_{\chi N}/V}{n}$.

Using our set of generic couplings g_{Ns}, g_{Nv} we obtain scalar and vector contributions $\langle \sigma_{s,\chi N} \rangle \sim 10^{-47}$, $\langle \sigma_{v,\chi N} \rangle \sim 10^{-43}$ cm^2 for masses in the range $m_\chi \sim$ GeV. These results must be considered as an averaged value in momentum space and are consistent with existing collider constraints on D1 and D5 couplings [24,25] at the $m_\chi \sim$ GeV range derived in the context of EFT. Note that these quoted constraints on collider and direct searches should be however taken with caution since they present some already well-known problems, i.e., (over-) under-estimates and inconsistencies with the thermal relic density for m_χ ranges outside a $m_\chi \sim (170\text{–}500)$ GeV range, see the discussion in [33,34]. The energy range that we describe in the relativistically boosted scenario accounts for center-of-mass energies of $\sqrt{s} \lesssim 6$ GeV for DM candidates with $m_\chi \lesssim 5$ GeV scattering target nucleons in a dense nuclear sea. However, as stated in [34], it is also the momentum transfer and mediator mass, M_ϕ, that provide the validity of interpretation of EFT as it must fulfill $q^2 \ll M_\phi^2$.

In the current status of the direct detection DM search in the low mass range region, CDMS [35] and SuperCDMS SNOLAB [36] provide the best limits up to date with a sensitivity of $\sigma_{\chi N} \sim 10^{-41}$ cm^2 for a limiting value $m_\chi \sim 5$ GeV. Below this mass, collider searches can provide better sensitivities than direct searches because the momentum transfer becomes small and the nuclear recoil energy falls below experimental thresholds. We expect, nevertheless, that a more refined model of the hadron structure or the mediators in the interaction will provide a richer contribution to be determined in the future, as this is far from the present scope of this work. We consider that, despite indirectly, dense astrophysical sites can contribute to probing the low mass region of the DM phase space.

IV. CONCLUSIONS

In summary, we have calculated dark matter scattering cross sections in an environment of dense and hot nucleon matter. We have considered a fermionic DM particle with scalar and vector effective couplings. In this scattering scenario, we have tested a low mass region $m_\chi \lesssim 5$ GeV. Examples for this setting are the interiors of neutron stars, where core densities range typically exceed $n/n_0 \gtrsim 1$ and temperatures $T \lesssim 50$ MeV. We have included the nuclear medium effects through Fermi-Dirac distributions for the nucleon sector, assuming the amount of DM mass in the star remains tiny at all times. To partially correct for the fact that we consider a point-like interaction, we use monopolar form factors for the hadron structure. We find that the differential and integrated cross sections are greatly affected by the finite density of matter, namely, by the effect of a smaller effective nucleon mass $m_N^* < m_N$. Temperature effects are taken into account with additional detailed balance factors and are found to be important, although to a lesser extent relative to density. The mean free path for a DM particle is found to be larger than the typical values of those found for Standard Model neutrinos with vector-axial couplings. The simplified estimate for the mean free path, $\lambda_\chi \simeq 1/\sigma_{\chi N} n$, lacks the rich dependence on the phase space of the scattering process. In this paper, we show that the diffusive behavior approximation at finite density and temperature in the interior of NS is well grounded and DM can contribute to the energy transport in their interior. While a specific application to proto-neutron stars is deferred to a later paper, here, we have discussed the interest of dense neutron stars to expose the importance of the medium effects in the interaction of ordinary and dark matter.

ACKNOWLEDGMENTS

M. A. P.-G. acknowledges interesting discussions with C. Albertus, R. Lineros, and J. Horvath. This research has been partially supported by University of Salamanca, Grants No. FIS2012-30926 and No. FIS2015-65140, MULTIDARK MINECO projects, and at IAP by the ERC project 267117 (DARK) hosted by Université Pierre et Marie Curie—Paris 6 and at JHU by NSF Grant No. OIA-1124403. M. C. is supported by a fellowship from the Consolider MULTIDARK project and Universidad de Salamanca.

[1] M. McCullough and M. Fairbairn, Phys. Rev. D **81**, 083520 (2010); D. Hooper, D. Spolyar, A. Vallinotto, and N. Y. Gnedin, Phys. Rev. D **81**, 103531 (2010).
[2] W. H. Press and D. N. Spergel, Astrophys. J. **296**, 679 (1985).
[3] A. Peter, Ph.D. Thesis, Princeton University, 2008.
[4] A. Gould, Astrophys. J. **321**, 571 (1987); I. Goldman and S. Nussinov, Phys. Rev. D **40**, 3221 (1989); C. Kouvaris, Phys. Rev. D **77**, 023006 (2008).
[5] D. Bauer *et al.*, arXiv:1310.8327v2; M. Klasen, M. Pohl, and G. Sigl, Prog. Part. Nucl. Phys. **85**, 1 (2015).
[6] M. Cirelli, Pramana **79**, 1021 (2012).
[7] I. Lopes and J. Silk, Science **330**, 462 (2010).
[8] C. Kouvaris and P. Tinyakov, Phys. Rev. D **83**, 083512 (2011).
[9] S. D. McDermott, H.-B. Yu, and K. M. Zurek, Phys. Rev. D **85**, 023519 (2012).
[10] J. Bramante, K. Fukushima, and J. Kumar, Phys. Rev. D **87**, 055012 (2013).
[11] M. A. Perez-Garcia, J. Silk, and J. R. Stone, Phys. Rev. Lett. **105**, 141101 (2010).
[12] M. A. Pérez-García and J. Silk, Phys. Lett. B **711**, 6 (2012).
[13] M. A. Pérez-García, F. Daigne, and J. Silk, Astrophys. J. **768**, 145 (2013).
[14] M. A. Pérez-García and J. Silk, Phys. Lett. B **744**, 13 (2015).
[15] S. Ritz and D. Seckel, Nucl. Phys. **B304**, 877 (1988).
[16] D. Page, J. M. Lattimer, M. Prakash, and A. W. Steiner, Astrophys. J. **155**, 623 (2004).
[17] H. Y. Cheng and C. W. Chiang, J. High Energy Phys. 07 (2012) 009.
[18] A. Alvesa, A. Berlin, S. Profumo, and F. S. Queiroz, J. High Energy Phys. 10 (2015) 076.
[19] M. Cannoni, M. E. Gómez, M. A. Pérez-García, and J. D. Vergados, Phys. Rev. D **85**, 115015 (2012).
[20] B. Bertoni, A. E. Nelson, and S. Reddy, Phys. Rev. D **88**, 123505 (2013).
[21] A. L. Fitzpatrick, W. Haxton, E. Katz, N. Lubbers, and Y. Xu, J. Cosmol. Astropart. Phys. 02 (2013) 004.
[22] J. Goodman, M. Ibe, A. Rajaraman, W. Spherd, T. M. P. Tait, and H. Yu, Phys. Rev. D **82**, 116010 (2010).
[23] K. Cheung, P. Tseng, Y. S. Tsai, and T. Yuan, J. Cosmol. Astropart. Phys. 05 (2012) 001.
[24] G. Aad *et al.*, Phys. Rev. D **90**, 012004 (2014); G. Aad *et al.*, Phys. Rev. D **91**, 012008 (2015).
[25] V. Khachatryan *et al.* (CMS Collaboration), Eur. Phys. J. C **75**, 235 (2015); Phys. Lett. B **755**, 102 (2016).
[26] M. Bañados, J. Silk, and S. M. West, Phys. Rev. Lett. **103**, 111102 (2009).
[27] S. Reddy, M. Prakash, and J. M. Lattimer, Phys. Rev. D **58**, 013009 (1998).
[28] K. A. Olive *et al.* (Particle Data Group Collaboration), Chin. Phys. C **38**, 090001 (2014).
[29] B. D. Serot and J. D. Walecka, *Advances in Nuclear Physics*, edited by J. W. Negele and E. Vogt (Plenum, New York, 1986).
[30] C. J. Horowitz and M. A. Perez-Garcia, Phys. Rev. C **68**, 025803 (2003).
[31] C. J. Horowitz and K. Wehrberger, Phys. Lett. B **266**, 236 (1991).
[32] M. A. Perez-Garcia, Eur. Phys. J. A **44**, 77 (2010).
[33] Y. Bai, P. J. Fox, and R. Harnik, J. High Energy Phys. 12 (2010) 048.
[34] O. Buchmueller, M. J. Dolan, and C. McCabe, J. High Energy Phys. 01 (2014) 025.
[35] R. Agnese *et al.* (CDMS Collaboration), Phys. Rev. Lett. **111**, 251301 (2013).
[36] R. Agnese *et al.* (SuperCDMS Collaboration), Phys. Rev. Lett. **112**, 041302 (2014).

Chapter 3

Light dark matter scattering in outer neutron star crusts

Resumen

En el artículo que se muestra a continuación se calcula por primera vez la tasa de excitación de fonones acústicos en la corteza externa de una NSs debido a la interacción de partículas de LDM que han sido aceleradas gravitacionalmente hacia la estrella hasta alcanzarla a velocidades relativistas. Se consideran partículas de DM con $m_\chi \lesssim 1$ GeV que hacen scattering con una red periódica de núcleos a través de interacciones efectivas de tipo escalar-vector con nucleones. Se encuentra que la colisión elástica de LDM con los núcleos de la corteza causa una modificación en el número neto de fonones en la red en comparación con los fonones térmicos estándar. Esta variación es mayor que en el caso en el que las excitaciones fueran producidas debidas a neutrinos cosmológicos. Además, estimamos la contribución de esta modificación del número neto de fonones acústicos debida a la DM a la conductividad térmica ión-ión en la capa más externa de la estrella y encontramos que esta cantidad puede aumentar significativamente en el caso en el que la densidad de DM alrededor de la estrella sea $n_\chi \sim 100 n_{0,\chi}$, densidad en el máximo de la distribución de NSs en nuestra galaxia. Nuestros resultados implican que para NSs con campos magnéticos elevados el aumento de la conductividad térmica global en la corteza externa podría reducir las diferencias en la conducción del calor entre las direcciones paralelas y perpendiculares al campo magnético.

PHYSICAL REVIEW D **94,** 063001 (2016)

Light dark matter scattering in outer neutron star crusts

Marina Cermeño,[1,*] M.Ángeles Pérez-García,[1,†] and Joseph Silk[2,3,4,‡]

[1]*Department of Fundamental Physics, University of Salamanca, Plaza de la Merced s/n, 37008 Salamanca, Spain*

[2]*Institut d'Astrophysique, UMR 7095 CNRS, Université Pierre et Marie Curie, 98bis Boulevard Arago, 75014 Paris, France*

[3]*Department of Physics and Astronomy, The Johns Hopkins University, Homewood Campus, Baltimore, Maryland 21218, USA*

[4]*Beecroft Institute of Particle Astrophysics and Cosmology, Department of Physics, University of Oxford, Oxford OX1 3RH, United Kingdom*

(Received 19 May 2016; published 2 September 2016)

We calculate for the first time the phonon excitation rate in the outer crust of a neutron star due to scattering from light dark matter (LDM) particles gravitationally boosted into the star. We consider dark matter particles in the sub-GeV mass range scattering off a periodic array of nuclei through an effective scalar-vector interaction with nucleons. We find that LDM effects cause a modification of the net number of phonons in the lattice as compared to the standard thermal result. In addition, we estimate the contribution of LDM to the ion-ion thermal conductivity in the outer crust and find that it can be significantly enhanced at large densities. Our results imply that for magnetized neutron stars the LDM-enhanced global conductivity in the outer crust will tend to reduce the anisotropic heat conduction between perpendicular and parallel directions to the magnetic field.

DOI: 10.1103/PhysRevD.94.063001

I. INTRODUCTION

Dark matter constitutes the most abundant type of matter in our Universe, and its density is now experimentally well determined $\Omega_{\rm CDM}h^2 = 0.1199 \pm 0.0027$ [1]. Worldwide efforts to constrain its nature and interactions have led the community to a puzzling situation where null results coexist with direct detection experiments that find high significance excesses [2]. In particular, in the low mass region of dark matter (DM) candidates, i.e., $m_\chi < 1$ GeV/c^2, cosmological, astrophysical and collider constraints seem to be the most important; see, for example, a discussion in Ref. [3]. Direct detection searches of thermalized galactic DM are mostly based on nuclear recoils on selected targets. In this scenario, light dark matter (LDM) particles with masses much smaller than that of the nucleon, $m_\chi \ll m_N$, can only provide energies ∼eV which are below the ∼keV threshold for conventional terrestrial searches. If one, instead, considers LDM scattering off bound electrons, energy transfer can cause excitation or even ionization and thus seems promising for exploring the phase space in a complementary way in the near future [4]. DM hitting terrestrial targets is expected to have low velocities $v_\chi \sim 10^{-3}$ (we use $c = \hbar = 1$ units) as the gravitational boost is small for the Earth, i.e., its Lorentz factor $\gamma_\oplus = 1/\sqrt{1-\beta_\oplus^2} \sim 1$ with $\beta_\oplus = \sqrt{\frac{2GM_\oplus}{R_\oplus}}$. However, for compact objects, such as neutron stars (NSs) with typical masses $M_{\rm NS} \simeq 1.5\ M_\odot$ and radius $R_{\rm NS} \simeq 12$ km, $\gamma_{\rm NS} \sim 1.26$ providing $v_\chi \sim 0.7$ as a result of the gravitational velocity boost. Contrary to what happens around other less compact celestial bodies this mechanism allows to boost particles from tiny velocities to relativistic values or, accordingly, test the same length scales as in direct detection searches with smaller projectile masses. In particular, the outer crusts in NSs are formed by periodically arranged nuclei with typical densities ranging from $\rho \simeq 210^6$–410^{11} g/cm^3. In the single-nucleus description [5], a series of nuclei with increasing baryonic number, A, from Fe to Kr form a lattice before neutrons start to leak out of nuclei. At these high densities, electrons form a degenerate Fermi sea. At even larger densities and up to nuclear saturation density, around $\rho_0 \simeq n_0 m_N \simeq 2.410^{14}$ g/cm^3, a number of different nuclear structures called *pasta* phases appear [6].

In this work, we study the effect of LDM scattering in the production of quantized lattice vibrations (phonons) in the outer NS crust. Later, we will discuss how this result can impact subsequent quantities of interest, such as the ion thermal conductivity, that are relevant for computing the cooling behavior of NSs. Phonons are quantized vibrational modes characterized by a momentum $\vec{k}$ and polarization vector $\vec{\epsilon}_\lambda$ appearing in a nuclear periodic system [7]. They can have a number of different sources. They can be excited due to nonzero temperature T in the medium. The Debye temperature allows us to evaluate the importance of the ion motion quantization. For a body-centered cubic (bcc) lattice [8], for example, $T_D \simeq 0.45 T_p$, with $T_p = \omega_p/k_B = \sqrt{\frac{4\pi n_A Z^2 e^2}{k_B^2 m_A}}$ geing the plasma temperature

*marinacgavilan@usal.es
†mperezga@usal.es
‡silk@iap.fr

associated to a medium of ions with number density n_A, baryonic number A, electric charge Ze and mass m_A. k_B is the Boltzmann constant. At low temperatures $T < T_D$, the quantization becomes increasingly important, and the thermal phonons produced are typically acoustic modes, following a linear dispersion relation $\omega_{k,\lambda} = c_{l,\lambda}|\vec{k}|$, where $c_l = \frac{\omega_p/3}{(6\pi^2 n_A)^{1/3}}$ is the sound speed. In addition, phonon production can be caused by an external scattering agent, for example, standard model neutrinos. In this respect, weak probes such as cosmological neutrinos with densities $n_\nu \sim 116\ \mathrm{cm}^{-3}$ per flavor have been shown to provide small phonon production rates in a crystal target [9,10]. Due to the tiny mass of the neutrino, the experimental signature of this effect seems, however, hard to confirm. The main interest in the astrophysical context we discuss in this contribution follows as phonon excitation in a periodic system, such as the outer crust of a NS, can affect the thermal transport coefficients in the star. The potential modification of transport properties of heat/energy in the external layers in NSs is crucial to possibly identifying relevant distortions in the cooling behavior of these astrophysical objects in rich LDM environments.

The structure of this contribution is as follows. In Sec. II, we present the effective field theory Lagrangian model using dark matter-nucleon contact interactions via scalar and vector couplings in a relativistic framework and compute the single phonon excitation rate, discussing sources of uncertainty. Later, in Sec. III, we compute the thermal conductivity in the outer crust with LDM contributions comparing the results to the standard thermal value and discussing possible astrophysical consequences. Finally, in Sec. IV, we give our conclusions.

II. LIGHT DARK MATTER SCATTERING AND PHONON EXCITATION RATE

In this work, we consider the interaction of an incoming fermionic DM particle, χ, scattering quasielastically with a nucleus in the outer NS crust lattice via scalar and vector couplings [11,12] composed of Z protons (p) and $A-Z$ neutrons (n),

$$\mathcal{L}_{\mathcal{I}} = \sum_{N=n,p} g_{s,N}\chi\overline{\chi}N\overline{N} + g_{v,N}\chi\gamma^\mu\overline{\chi}N\gamma_\mu\overline{N}, \qquad (1)$$

where $g_{s,N}$ ($g_{v,N}$) are the effective scalar (vector) couplings of the DM particle to the nucleon (N) field. We will focus on a weakly interacting candidate (WIMP) with mass in the sub-GeV range. This interaction is equivalent to considering a Fermi four-fermion interaction model, where the effective couplings of mass dimension (-2) for these operators are obtained by integrating out the propagator of a generic ϕ mediator with mass M_ϕ. Let us mention that, indeed, more effective operators for Dirac LDM candidates are possible; see, for example, Table I in Ref. [13] for leading coupling contributions to Standard Model fermions. However, in order to keep our description concise for the sake of clarity, we will restrict here to the spin-independent interaction model used in previous works [12].

Motivated by the need to compare bounds from colliders to direct detection, we describe interactions of DM with quarks $q = u, d$, and averaging in terms of nucleon fields, we can write for the vector case $g_{v,N}/M_\phi^2 \sim 1/{\Lambda_v}^2$ and $g_{s,N}/M_\phi^2 \sim m_q/{\Lambda_s}^3$ where Λ_v (Λ_s) is the suppression mass scale for the vector (scalar) case, assuming the effective couplings are of order $O(1)$ and can be absorbed into $\Lambda_{s,v}$ [14]. Using bounds from CMS and ATLAS [15], we set $\Lambda_v \gtrsim 1$ TeV and $\Lambda_s \gtrsim 100$ GeV.

We denote by $p'^\mu_N = (E'_N, \vec{p'_N})$ and $p^\mu_N = (E_N, \vec{p}_N)$ the four momentum for the outgoing and incoming nucleon and $p'^\mu_\chi = (E'_\chi, \vec{p'_\chi})$ and $p^\mu_\chi = (E_\chi, \vec{p}_\chi)$ as those analogous for the LDM particle, respectively. Momentum transfer is denoted by $q^\mu = p'^\mu_\chi - p^\mu_\chi$.

Generically, given an interaction potential $\mathcal{V}$ felt by an interacting DM particle when approaching a nucleus in the periodic lattice, the single phonon excitation rate *per mode* can be obtained using the Fermi golden rule, $R_{\vec{k},\lambda} = 2\pi\delta(E_f - E_i)|\langle f|\mathcal{V}|i\rangle|^2$, where i and f are the initial and final states considered and $\delta(E_f - E_i)$ assures energy conservation. Given the fact that incoming (outgoing) LDM particles suffer a very moderate perturbation from the plane wave state, we will describe its incoming (outgoing) quantum state as $\Psi_{\vec{p}_\chi}(\vec{r}) = \frac{1}{\sqrt{V}} e^{i\vec{p}_\chi\vec{r}}$ with V the volume of the system. The interaction potential felt by the LDM particle is the sum [9] over lattice sites $\mathcal{V}(\vec{r}) = \sum_j v(\vec{r} - \vec{r}_j)$ that we describe for the sake of simplicity as impenetrable pointlike spheres $v(\vec{r} - \vec{r}_j) = \delta^3(\vec{r} - \vec{r}_j)v_0$. We, nevertheless, comment on corrections to this picture later in the manuscript.

Using the Born approximation, the scattering amplitude for an incident χ particle can be written as

$$f(\vec{p}_\chi, \vec{p'_\chi}) \simeq -\frac{m_\chi}{2\pi}\int e^{i(\vec{p}_\chi - \vec{p'_\chi})\vec{r'}} v(\vec{r'}) d^3\vec{r'}, \qquad (2)$$

and from its squared value, the differential cross section in the center-of-mass frame, $\frac{d\sigma}{d\Omega}|_{\mathrm{CM}} = |f(\vec{p}_\chi, \vec{p'_\chi})|^2$. The validity of the Born approximation is provided by the finite-range potential $\mathcal{V}(\vec{r})$ so the condition $|(\vec{p}_\chi - \vec{p'_\chi}).\vec{r'}| \ll 1$ is fulfilled, with $|\vec{r'}|$ being a typical target size. The effective interaction potential can be obtained from the squared interaction matrix element as calculated from the Lagrangian in Eq. (1) as $\frac{d\sigma}{d\Omega}|_{\mathrm{CM}} = \frac{|\overline{\mathcal{M}}_{\chi N}|^2}{64\pi^2 s}$. First, we compute the scattering amplitude $|\overline{\mathcal{M}}_{\chi N}|^2$ with $s = (p_N + p_\chi)^2$ being the Mandelstam variable. Adding the contribution over proton and neutron amplitudes coherently, we can obtain the LDM particle-nucleus differential cross section and then integrate to find a relation between the total cross section $\sigma_{\chi A} \simeq 4\pi a^2$, or, equivalently, the effective potential

from Eq. (2), and the scattering length, a, at low incident energies. We obtain $v(\vec{r}) = \frac{2\pi a}{m_\chi}\delta(\vec{r})$. Besides, we have used a normalization of the delta function as $\int_{VT}\delta(x)d^4x = 1$. From the Lagrangian in Eq. (1), the spin-averaged scattering amplitude [12] reads

$$\begin{aligned}|\overline{\mathcal{M}}_{\chi\mathrm{N}}|^2 &= 4g_{s,N}^2[(p_N p'_N + m_N^2)(p_\chi p'_\chi + m_\chi^2)] \\ &+ 8g_{v,N}^2[2m_N^2 m_\chi^2 - m_N^2 p'_\chi p_\chi - m_\chi^2 p_N p'_\chi \\ &+ (p'_\chi p'_N)(p_N p_\chi) + (p'_N p_\chi)(p_N p'_\chi)] \\ &+ 8g_{s,N}g_{v,N}[m_N m_\chi(p_N + p'_N)(p_\chi + p'_\chi)]. \end{aligned} \quad (3)$$

Due to the mildly relativistic nature of nucleons inside the nucleus, energy and momentum will lie close to the Fermi surface values $E_{\mathrm{FN}}, |\vec{p}_{\mathrm{FN}}|$ and $|\vec{p}_N|^2 \sim |\vec{p'}_N|^2 \sim |\vec{p}_{\mathrm{FN}}|^2 \ll m_N^2$. We will approximate the product $p'_N p_N = E_N E'_N - |\vec{p}_N||\vec{p}_N{}'|\cos\theta_{\vec{p}_N,\vec{p}_N{}'} \simeq E_{\mathrm{FN}}^2$. On the other hand, for the more relativistic DM particle products, $p_\chi p'_\chi = E_\chi E'_\chi - |\vec{p}_\chi||\vec{p'_\chi}|\cos\theta_{\vec{p}_\chi,\vec{p'_\chi}} = E_\chi^2 - |\vec{p}_\chi|^2\cos\theta_\chi = m_\chi^2 + |p_\chi|^2(1-\cos\theta_\chi)$, where we use $\theta_{\vec{p}_\chi,\vec{p}_\chi{}'} \equiv \theta_\chi$. The density dependence will be retained using a parametrization of the nuclear Fermi momentum $|\vec{p}_{\mathrm{FN}}| \sim (3\pi^2 n_0 Y_N)^{1/3}$ and the nuclear fractions $Y_p = Z/A$, $Y_n = (A-Z)/A$. If we now average over angular variables,

$$\begin{aligned}&\int_{-1}^{1} 2\pi d(\cos\theta_\chi)|\overline{\mathcal{M}}_{\chi\mathrm{N}}|^2 \\ &= 16\pi g_{s,N}^2[(2m_N^2 + |\vec{p}_{\mathrm{FN}}|^2)(2m_\chi^2 + |\vec{p}_\chi|^2)] \\ &+ 32\pi g_{v,N}^2[2E_\chi^2 E_{\mathrm{FN}}^2 - m_N^2|\vec{p}_\chi|^2 - m_\chi^2|\vec{p}_{\mathrm{FN}}|^2] \\ &+ 128\pi g_{s,N}g_{v,N}[m_N m_\chi E_{\mathrm{FN}}E_\chi]. \end{aligned} \quad (4)$$

In the nucleus, we can use the previous expression, Eq. (4), to find the coherent contribution of the A nucleons in a way similar to what is done in direct detection [16],

$$\begin{aligned}&\int_{-1}^{1} 2\pi d(\cos\theta_\chi)|\overline{\mathcal{M}}_{\chi A}|^2 \\ &\simeq m_A^2\left(\frac{Z}{m_p}\sqrt{|\tilde{\mathcal{M}}_p|^2} + \frac{(A-Z)}{m_n}\sqrt{|\tilde{\mathcal{M}}_n|^2}\right)^2, \end{aligned} \quad (5)$$

with $\int_{-1}^{1} 2\pi d(\cos\theta_\chi)|\overline{\mathcal{M}}_{\chi\mathrm{N}}|^2 \equiv |\tilde{\mathcal{M}}_{\mathrm{N}}|$. The Mandelstam variable $s = (p_A + p_\chi)^2 = m_\chi^2 + m_A^2 + 2E_A E_\chi - 2\vec{p}_A\,\vec{p}_\chi$ can be approximated as $s \simeq (m_\chi + m_A)^2$, neglecting the mildly relativistic nuclei momenta. Thus, we can express the cross section in the center-of-mass frame as

$$\sigma_{A,\chi} = 4\pi a^2 = m_A^2\frac{\left(\frac{Z}{m_p}\sqrt{|\tilde{\mathcal{M}}_p|^2} + \frac{(A-Z)}{m_n}\sqrt{|\tilde{\mathcal{M}}_n|^2}\right)^2}{16\pi(m_\chi + m_A)^2}. \quad (6)$$

From a zero-order momentum expansion, we recover the usual expression for direct detection spin independent cross section at low energies [17] for each coupling $\sigma_{A,\chi} \to \frac{\mu_{\chi A}^2}{\pi}(Zg_{s,p} + (A-Z)g_{s,n})^2$ where $\mu_{\chi A} = \frac{m_\chi m_A}{m_\chi + m_A}$ is the reduced $\chi - A$ mass. Note at this point that the $\sim A^2$ enhancement in the obtained cross section remains as the coherence condition $\lambda \geq R_A$ is fulfilled, with R_A being the nuclear radius and $\lambda = h/|\vec{p}_\chi|$ being the De Broglie wavelength. In addition, the contribution of the nuclear lattice will be described by the summations extended over the lattice sites, or, equivalently, by the inclusion of the structure factor $S(q) \sim |\sum_j e^{-i\vec{q}\,\vec{r}_j}|^2$, in the full phonon excitation rate expression as will be shown later in the manuscript. Some studies have included form factors $F^2(q)$ to correct a pointlike nucleus nature approach [17]; however, since we will be focusing on $q \to 0$ limit, we will consider them as unity for the sake of simplicity. In what follows, we will refer to $\vec{p'} \equiv \vec{p'_\chi}$ and $\vec{p} \equiv \vec{p}_\chi$. The single-phonon excitation time rate from the ground state now reads

$$R_{k,\lambda}^{(0)} = \frac{4\pi^2 a^2}{V^2 m_\chi^2}\delta(E_{\vec{p'}} + \omega_{k,\lambda} - E_{\vec{p}})2\pi|\sum_j\langle 1,\vec{k}\lambda|e^{-i\vec{q}\,\vec{r}_j}|0\rangle|^2, \quad (7)$$

where $\vec{r}_j = \vec{x}_j^{(0)} + \vec{u}_j$ with $\vec{x}_j^{(0)}$ the lattice point and $\vec{u}_j$ the displacement vector [18]. We must note at this point that the previous expression includes the squared modulus of the Fourier transform of the periodically arranged lattice sites including thus the usual description in terms of the structure factors $S(q)$. This function provides information on the spatial distribution through a correlation function and presents maxima at the crystal nuclear positions. The contribution of this factor to the global cross section describes coherent scattering from all of the different nuclei as discussed in Ref. [19]. There, the effect of efficient low-energy scattered WIMPS from the interior of the stelar DM distribution was mentioned as an additional factor to prevent DM escaping from the NS once inside. In this way, it thus constitutes a mechanism for *trapping* DM, besides the deep gravitational potential felt by these sub-GeV mass particles.

Beyond this point, we will consider an isotropic medium, and since the Born approximation $|\vec{q}.\vec{r}'| \ll 1$ holds, it is most likely that acoustic modes are excited. It follows that

$$-i\vec{q}\sum_j e^{-i\vec{q}\vec{x}_j^{(0)}}\langle 1,\vec{k}\lambda|\vec{u}_j|0\rangle = -in_A\delta^{(3)}(\vec{k}-\vec{q})\sqrt{\frac{|\vec{k}|}{2m_A c_l}}, \quad (8)$$

where we have used the continuum limit $\sum_j \to n_A\int d^3x$ and the fact that all $\vec{k}$ have a polarization vector that verifies $\vec{\epsilon}_l//\vec{k}$ and the other two vectors are perpendicular to $\vec{k}$. Finally Eq. (7) can be written as

$$R_k^{(0)} = \frac{4\pi^2 a^2}{m_\chi^2 V}\delta(E_{\vec{p}'} + \omega_{k,\lambda} - E_{\vec{p}})2\pi n_A^2 \frac{\delta^{(3)}(\vec{k}-\vec{q})|\vec{k}|}{2m_A c_l}. \quad (9)$$

At this point, we must consider the peculiarities of the incoming LDM phase space distribution $f_\chi(\vec{p})$ as it will impact the averaged final phonon excitation rate. Typically, for the Sun or the Earth, the uncertainties have different sources including the orbital speed of the Sun, escape velocity from the DM halo and the form of the phase space distribution itself. About the latter and in local searches, direct and indirect detection are affected in a different manner. For example, direct detection is sensitive to DM with high velocities [20], while for indirect detection, the low-velocity part of the distribution is tested [21,22].

A popular choice is obtained using an approximation based on an isotropic sphere with density profile $\rho_{\rm DM}(r) \propto r^{-2}$ of collisionless particles, i.e., a Maxwell-Boltzmann type with a local mass density $\rho_{\rm LDM} = 0.3$ GeV cm^{-3}. Uncertainties on the knowledge of the distribution function must be carefully considered as this impacts accuracy when translating event rates to constraints on particle physics models of DM.

In the case we analyze here of a more compact object, it is the high velocity part of the distribution that is tested, as typical values for boosted root-mean-squared velocities are $\langle v^2\rangle \sim 2GM_{\rm NS}/R_{\rm NS} \sim (0.6)^2$. For these relativistic regimes, one must use the Maxwell-Jüttner distribution [23] function and, more properly, take into account the space-time curvature due to the gravitational field created by the NS [24],

$$f_\chi(\vec{p}) = \frac{n_\chi \mu}{4\pi m_\chi^3 K_2(\mu)} e^{-\mu\sqrt{1+g_1(r)\frac{|\vec{p}|^2}{m_\chi^2}}}, \quad (10)$$

where $\mu = \frac{m_\chi}{k_B T}$ and $K_2(\mu)$ is the modified Bessel function of the second kind defined as $K_n(\mu) = (\frac{\mu}{2})^n \frac{\Gamma(1/2)}{\Gamma(n+1/2)} \times \int_0^\infty e^{-\mu y}(y^2-1)^{n-1/2}dy$. The isotropic Schwarzschild metric for the gravitational field created by the NS source is [24] $ds^2 = g_0(r)(dx^0)^2 - g_1(r)\delta_{ij}x^i x^j$, $i, j = 1, 2, 3$.

Note that, in the close vicinity of the NS where we will be interested in assessing our quantities of interest, $r \sim R_{\rm NS}$, and it follows that $g_1(R) = (1+\frac{GM_{\rm NS}}{2R_{\rm NS}})^4 \sim 1.42$, $g_0(R) = (1-\frac{GM_{\rm NS}}{2R_{\rm NS}})^2/(1+\frac{GM_{\rm NS}}{2R_{\rm NS}})^2 \sim 0.69$. The distortion from the flat space with a Minkowski metric effectively sets $g_0(r)$, $g_1(r) \neq 1$ as expected. Furthermore, if we obtain from the above the root-mean-squared $\sqrt{\langle v^2\rangle} \sim 0.6$, this implies $\mu \approx 6.7$ [25,26].

The normalization condition is such that the particle 4-flow J^α can be defined, and taking the $\alpha = 0$ component, we obtain $\int d^3\vec{p} f_\chi(\vec{p})\sqrt{-g}/g_0 = J^0 = n_\chi/\sqrt{g_0}$ with $\sqrt{-g} = \sqrt{g_0 g_1^3}$. n_χ is the DM number density near the NS. Note that at nonrelativistic velocities and flat space we do recover the Maxwell-Boltzmann distribution as expected. Further, we consider all outgoing χ states are allowed as the net number will be tiny as compared to ordinary matter. The phonon excitation time rate must be weighted with the momenta of the *local* χ phase space that, as mentioned, is shifted to the relativistic values

$$R_k^{(0)} = \frac{4\pi^3 n_A^2 V}{m_\chi^2 m_A c_l}\int \frac{d^3\vec{p} f_\chi(\vec{p})}{(2\pi)^3}\int \frac{d^3\vec{p}'}{(2\pi)^3}\delta^{(3)}(\vec{k}-\vec{q}) \times \delta(E_{\vec{p}'} + \omega_{\vec{k},\lambda} - E_{\vec{p}})|\vec{k}|a^2. \quad (11)$$

Computing the zeros of the delta function and expressing the incoming momentum as $|\vec{p}_0| = \sqrt{\gamma^2-1}m_\chi$, we obtain an interval of kinematically allowed $|\vec{k}|$ values $0 \leq |\vec{k}| \leq 2m_\chi(\frac{c_l\gamma}{(c_l^2-1)} + \frac{\sqrt{\gamma^2-1}}{|c_l^2-1|})$, and Eq. (11) takes the form

$$R_k^{(0)} = \frac{8\pi^4 n_A^2 V}{(2\pi)^6 m_\chi^2 m_A c_l}\int_0^\infty |\vec{p}|^2 d|\vec{p}| f_\chi(\vec{p})\frac{|\gamma m_\chi - |\vec{k}|c_l|}{m_\chi\sqrt{\gamma^2-1}}a^2. \quad (12)$$

In Fig. 1, we show the single phonon excitation rate (per unit volume) from the ground state and averaged over χ phase space as a function of density in the outer crust using the single-nucleus table from Ref. [5]. Curves plotted with solid, dashed and dash-dotted lines correspond to the excitation of phonons with $|\vec{k}| \to 0$ for $m_\chi = 500$, 100 and 5 MeV and $n_\chi/n_{0,\chi} = 10$. We also plot for the sake of comparison the specific excitation rate at $|\vec{k}| \to 0$, $R_{\nu 0}$, for neutrinos with masses $m_\nu = 0.1$, 1 eV with dotted and double-dashed lines, respectively. Note, however, that in this later case there is a strong momentum

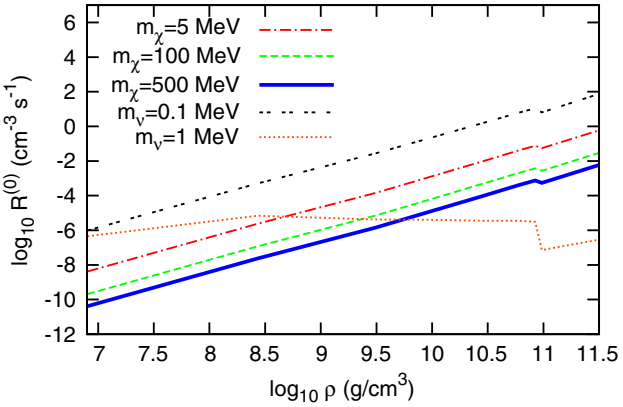

FIG. 1. Averaged single-phonon excitation rate per unit volume as a function of density in the outer crust. DM particle masses $m_\chi = 500$, 100 and 5 MeV are used, and $n_\chi/n_{0,\chi} = 10$. Neutrino contribution at $|\vec{k}| \to 0$, $R_{\nu 0}$ is also shown for $m_\nu = 0.1$, 1 eV. See the text for details.

dependence that declines rapidly. We can fit this behavior for $m_\nu = 0.1$ eV as $R^0_\nu(|\vec{k}|) = R_{\nu 0} e^{(\frac{-1754|\vec{k}|}{1\text{eV}})}$ and for $m_\nu = 1$ eV as $R^0_\nu(|\vec{k}|) = R_{\nu 0} e^{-(\frac{2561.3|\vec{k}|}{1\text{eV}})}$.

We have verified that, since, typically, the speed of the thermalized LDM particles far from the star is essentially $v_\chi \sim v_\infty \sim 10^{-3}$, when hitting the NS, it has already acquired a boosted energy. Using an estimate based on a monochromatic value $E_\chi = \gamma_{\rm NS} m_\chi$, $\gamma_{\rm NS} = 1.26$, we can straightforwardly integrate and obtain the analytical result

$$R^{(0)}_k = \frac{n_\chi n_A^2 V}{4(2\pi)^3 m_\chi^3 m_A c_l} \frac{|\gamma_{\rm NS} m_\chi - |\vec{k}| c_l|}{\sqrt{\gamma^2_{\rm NS} - 1}} a^2 \qquad (13)$$

that underpredicts the exact result by ∼20%. As deduced from the previous expression, Eq. (13), the rate is indeed constant as a function of momentum as the inequality $\gamma_{\rm NS} m_\chi \ll |\vec{k}| c_l|$ is fulfilled. It seems that the contribution of the phase space distribution of LDM may also have a strong impact on the results, as it happens for the Sun or Earth.

III. ASTROPHYSICAL IMPACT ON THERMAL CONDUCTIVITY

Phonon production can be crucial for determining further transport properties, in particular, thermal conductivity in an ion-electron system such as that in the outer NS crust. As an important contribution to the total ion conductivity, κ_i, partial ion conductivities due to ion-ion, $\kappa_{ii} \equiv \kappa_{ph}$, and ion-electron collisions, κ_{ie}, must be added [27] under the prescription $\kappa_i^{-1} = \kappa_{ii}^{-1} + \kappa_{ie}^{-1}$. Standard mechanisms to produce lattice vibrations include thermal excitations, as analyzed in detail in previous works [28,29]. In a NS, the outer crust can be modelled under the one-component-plasma description. This low density solid phase can be classified according to the Coulomb coupling parameter $\Gamma = Z^2 e^2/ak_BT$ where $a = (4\pi n_A/3)^{1/3}$ is the ion sphere radius. It is already known that typically for $\Gamma \geq \Gamma_m \simeq 175$, or below melting temperature $T < T_m$, single-ion systems crystallize [30].

There are a number of processes that can affect thermal conductivity in the medium. The so-called U-processes [7] are responsible for modifying the electron conductivity such that for high temperatures, $T > T_U$, electrons move almost freely. Assuming a bcc lattice, $T_U \simeq 0.07 T_D$. Thus, in the scenario depicted here, the temperature range must be $T_U < T < T_D < T_m$ for each density considered. According to kinetic theory, the thermal conductivity can be written in the form [7]

$$\kappa_{ii} = \frac{1}{3} k_B C_A n_A c_l L_{ph}, \qquad (14)$$

where $C_A = 9(\frac{T}{T_D})^3 \int_0^{T_D/T} \frac{x^4 e^x dx}{(e^x-1)^2}$ is the phonon (dimensionless) heat capacity *per ion* and L_{ph} is an effective phonon mean free path that includes all scattering processes considered: U-processes and impurity (I) scattering processes (both dissipative) and the phonon normal (N) scattering, which are nondissipative $L_{ph}^{-1} = L_U^{-1} + L_I^{-1} + L_N^{-1}$. Typically, the thermal conductivity is related to the thermal phonon number at temperature T, $L_{ph} \sim 1/N_{0,k\lambda}$, where $N_{0,k\lambda} = (e^{\omega_{k\lambda}/k_BT} - 1)^{-1}$. The contribution from DM can be obtained by the net number of phonons that results from the competition of thermal and scattering excitation and stimulated emission [9] in a 4-volume $\delta V \delta t$ using the averaged rate per unit volume, and weighting with the incoming distribution providing the frequencies of different values of momenta, we obtain

$$N_{k\lambda} \simeq N_{0,k\lambda} + R^{(0)}_k \delta V \delta t - \int \frac{d^3\vec{p}}{n_\chi} f_\chi(\vec{p}) \tilde{R}^{(0)}_k N_{0,k\lambda} e^{(\omega_{k,\lambda} + \vec{k}.\vec{v})/K_\chi} \delta V \delta t, \qquad (15)$$

where $K_\chi = (\gamma - 1) m_\chi$ is the χ kinetic energy and $\tilde{R}^{(0)}_k$ is the single phonon excitation rate for each particular momentum value (not averaged over incoming χ momenta). Since the source (NS) is in relative motion to the LDM flux, there is a Doppler shift characterized by the source velocity $v \equiv v_{\rm NS} \sim 10^{-2}$, i.e., galactic NS drift velocity. The distribution of NSs in our Galaxy peaks at distances $\langle r \rangle_{\rm max} \lesssim 4$ Kpc [31]. In this central region DM density is enhanced with respect to the solar neighborhood value $n_{0,\chi} \simeq 0.3$ GeV/cm^3. Thus we will consider density values $n_\chi \simeq (10, 100) n_{0,\chi}$ as prescribed by popular galactic DM distribution profiles. In Fig. 2, we show the phonon thermal conductivity as a function of density (in units of 10^{10} g/cm^3) at $T = 510^7$ K, 510^8 K typical for the base of the crust, for $m_\chi = 100$ MeV. Solid lines are the standard thermal result with no DM. Dash-dotted and dashed lines correspond to

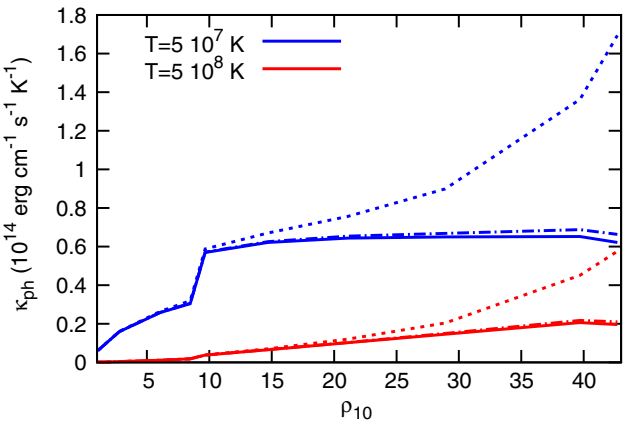

FIG. 2. Phonon thermal conductivity as a function of density (in units of 10^{10} g/cm^3) for temperatures $T = 510^7$ K (blue), 510^8 K (red) and $m_\chi = 100$ MeV. Dash-dotted and dashed lines depict the impact of a LDM density $n_\chi/n_{0\chi} = 10, 100$. Solid lines are the standard thermal result with no DM for each case. See the text for details.

$n_\chi/n_{0,\chi} = 10$, 100, respectively. We see that at the largest LDM local densities considered there is a clear enhancement over the thermal result well inside the outer crust. This corresponds to the site where the DM-induced effects have the most influence [32] as this is the most massive part of the outer crust. Below these densities, there is a negligible change, though. At lower T, the effect of a perturbation over the thermal phonon population is more important. Enhanced (decreased) conductivities at moderate LDM densities are due to a net reduction (increase) of the number of phonons in the lattice as a result of cancellation of modes. As a representative scenario, we have taken $|\vec{k}| = 0.01/a$ at each density since we have verified that this choice verifies the kinematical restrictions on $|\vec{k}|$ when performing the averages over phase space distribution as discussed in Sec. II. Besides, rates are mostly constant at low $|\vec{k}|$. Note that in standard calculations [27] there is no momentum dependence as they replace the frequency mode $\omega_{k\lambda}$ by a constant threshold. We must bear in mind that this result must be compiled with a realistic impurity fraction so that conductivity remains finite. We have considered $L_I \sim 5a$ [27].

In order to understand the significance of our result in the dense stellar context in Fig. 3, we show the phonon thermal conductivity as a function of density (in units of 10^{10} g/cm^3) at $T = 10^8$ K and $m_\chi = 65$ MeV for $|\vec{k}| = 0.01/a$. Solid, dot-dashed and dashed lines correspond to cases with no DM, $n_\chi/n_{0,\chi} = 10$, 100, respectively. Electron thermal conductivity is also shown for magnetized realistic scenarios in the direction perpendicular to a magnetic field B of strength $B = 10^{14}$ G (dotted) and $B = 10^{15}$ G (doble dotted). Ions are mostly not affected by the presence of a magnetic field. The parallel direction electronic contribution is not depicted here since it is typically much larger $k_{e\|} \sim 10^{17}$–10^{19} erg cm^{-1} s^{-1} K^{-1}. Since we perform averages over the χ phase space, we again use $|\vec{k}| = 0.01/a$. On the plot, we can see that the electronic contribution in the perpendicular direction falls below the enhanced $n_\chi/n_{0,\chi} = 100$ DM value for densities $\gtrsim 3.5 10^{11}$ g/cm^3. Note that the low value chosen for $|\vec{k}|$ in this plot is to be understood as a compromise value; larger $|\vec{k}|$ values would imply the impossibility of exciting phonons from low-momenta incoming LDM. Since the global conductivity is $\kappa = \kappa_e + \kappa_{ph}$, the obtained result is expected to contribute to the reduction of the difference in heat conduction in both directions and thus to the isotropization of the NS surface temperature pattern as seen in Ref. [32] for standard physics. Temperatures would be smoothly driven toward more isothermal profiles for latitudes among the pole and equator. It is already known [33] that the outer crust plays an important role in regulating the relation among the temperature in the base of it and the surface. The detailed calculation of this implication for surface temperatures remains, however, for future work.

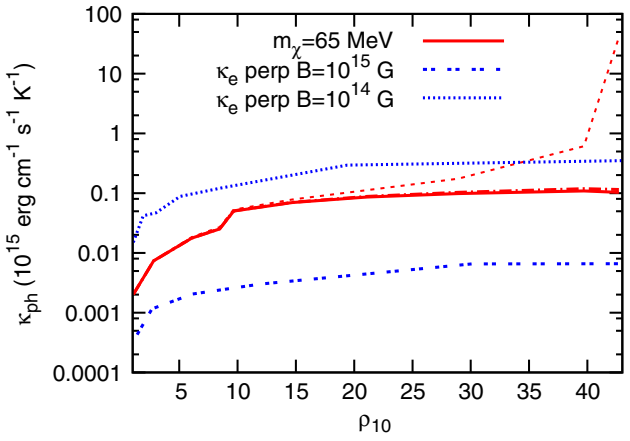

FIG. 3. Phonon thermal conductivity as a function of density (in units of 10^{10} g/cm^3) at $T = 10^8$ K and $m_\chi = 65$ MeV. Solid, dot-dashed and dashed lines correspond to cases with no DM, $n_\chi/n_{0,\chi} = 10$, 100. Perpendicular electron thermal conductivity is also shown for $B = 10^{14}$, 10^{15} G.

IV. CONCLUSIONS

In conclusion, we have derived for the first time the single-phonon excitation rate in the outer NS crust for relativistic LDM particles in the sub-GeV mass range. We have found that this rate is constant with the phonon momentum and much larger than for cosmological neutrinos at finite $|\vec{k}|$. A non-negligible correction to the local phonon excitation rate of ~20% is obtained when full relativistic phase distribution functions are considered for the incoming χ particles with respect to a monochromatic approximation, that underpredicts the result.

As an astrophysical consequence of the previous, we have calculated the ion thermal conductivity in the dense and hot outer envelope, finding that it can be largely enhanced at LDM densities in the maximum of the NS galactic distribution $n_\chi \sim 100 n_{0,\chi}$ due to a net modification of the acoustic phonon population. This effect is non-negligible at densities beyond $\sim 3.5 10^{11}$ g/cm^3 in the base of the outer crust at the level of standard ion-electron or thermal effects [27,28]. We do not expect the degenerate electron contribution to largely modify this result as this would mildly screen nuclear charge in the lattice; however, it remains to be further studied. Although a detailed study of the quantitative effect in the surface temperature pattern remains to be undertaken, it is expected that for magnetized NSs the LDM-enhanced global enhancement of the perpendicular thermal conductivity allows a reduction of the difference of heat transport among parallel and perpendicular directions to the magnetic field. Based on previous works only including standard thermal contributions, we expect that, as a natural consequence, the surface temperature profile would be more isotropic, yielding

flatter profiles for intermediate latitudes, and remains to be calculated in a future contribution.

ACKNOWLEDGMENTS

We acknowledge useful comments from J. Pons and C. Albertus. This research has been partially supported by MULTIDARK and FIS2015-65140 MINECO projects and at IAP by the ERC Project No. 267117 (DARK) hosted by Université Pierre et Marie Curie—Paris 6 and at JHU by NSF Grant No. OIA-1124403. M. Cermeño is supported by a fellowship from the University of Salamanca.

[1] P. Ade *et al.* (Planck Collaboration), Astron. Astrophys. **571**, A16 (2014).
[2] R. Bernabei *et al.* (DAMA and LIBRA Collaborations), Eur. Phys. J. C **67**, 39 (2010).
[3] T. Lin, H.-B. Yu, and K. M. Zurek, Phys. Rev. D **85**, 063503 (2012).
[4] R. Essig, M. Fernández-Serra, J. Mardon, A. Soto, T. Volansky, and T.-T. Yu, J. High Energy Phys. 05 (2016) 046.
[5] S. B. Ruster, M. Hempel, and J. Schaffner-Bielich, Phys. Rev. C **73**, 035804 (2006).
[6] C. J. Horowitz, M. A. Pérez-García, and J. Piekarewicz, Phys. Rev. C **69**, 045804 (2004); M. A. Pérez-García, J. Math. Chem. **48**, 21 (2010).
[7] J. M. Ziman, *Electrons and Phonons* (Oxford University Press, Oxford, 1960).
[8] W. J. Carr, Phys. Rev. **122**, 1437 (1961).
[9] I. Ferreras and I. Wasserman, Phys. Rev. D **52**, 5459 (1995); R. Chandrasekharan, Diploma Thesis, Institute for particle physics, ETHZ, 2003.
[10] M. M. Hedman, J. Cosmol. Astropart. Phys. 09 (2013) 029.
[11] A. L. Fitzpatrick, W. Haxton, E. Katz, N. Lubbers, and Y. Xu, J. Cosmol. Astropart. Phys. 02 (2013) 004.
[12] M. Cermeño, M. A. Pérez-García, and J. Silk, Phys. Rev. D **94**, 023509 (2016).
[13] J. Goodman, M. Ibe, A. Rajaraman, W. Spherd, T. M. P. Tait, and H.-B. Yu, Phys. Rev. D **82**, 116010 (2010).
[14] K. Cheung, P. Tseng, Y. S. Tsai, and T. Yuan, J. Cosmol. Astropart. Phys. 05 (2012) 001.
[15] V. Khachatryan *et al.* (CMS Collaboration) Eur. Phys. J. C **75**, 235 (2015); G. Aad *et al.*, Phys. Rev. D **90**, 012004 (2014); **91**, 012008 (2015).
[16] J.-M. Zheng, Z.-H. Yu, J.-W. Shao, X.-J. Bi, Z. Li, and H.-H. Zhang Nucl. Phys. **B854**, 350 (2012).
[17] V. Gluscevic, M. I. Gresham, S. D. McDermott, A. H. G. Peter, and K. M. Zurek, J. Cosmol. Astropart. Phys. 12 (2015) 057.
[18] N. W. Ashcroft and N. D. Mermin, *Solid State Physics* (Saunders College, Philadelphia, 1976).
[19] C. J. Horowitz, arXiv:1205.3541v1.
[20] A. M. Green, Phys. Rev. D **66**, 083003 (2002); Mod. Phys. Lett. A **27**, 1230004 (2012).
[21] M. Fornasa and A. M. Green, Phys. Rev. D **89**, 063531 (2014).
[22] K. Choi, C. Rott, and Y. Itow, J. Cosmol. Astropart. Phys. 05 (2014) 049.
[23] F. Juttner, Ann. Phys. Chem. **34**, 856 (1911).
[24] G. M. Kremer, J. Stat. Mech. (2013) P04016.
[25] R. Hakim, *Introduction to Relativistic Statistical Mechanics Classical and Quantum* (World Scientific, Singapore, 2011).
[26] C. Cercignani *et al.*, *The Relativistic Boltzmann Equation: Theory and Applications* (Birkhäuser Verlag, Berlin, 2002).
[27] A. I. Chugunov and P. Haensel, Mon. Not. R. Astron. Soc. **381**, 1143 (2007).
[28] J. W. Negele and D. Vautherin, Nucl. Phys. **A207**, 298 (1973); A. Y. Potekhin, G. Chabrier, and D. G. Yakovlev, Astron. Astrophys. **323**, 415 (1997).
[29] D. A. Baiko, A. D. Kaminker, A. Y. Potekhin, and D. G. Yakovlev, Phys. Rev. Lett. **81**, 5556 (1998).
[30] H. Nagara, Y. Nagata, and T. Nakamura, Phys. Rev. A **36**, 1859 (1987).
[31] D. R. Lorimer *et al.*, Mon. Not. R. Astron. Soc. **372**, 777 (2006).
[32] J. F. Pérez-Azorín, J. A. Miralles, and J. A. Pons, Astron. Astrophys. **451**, 1009 (2006).
[33] A. D. Kaminker, D. G. Yakovlev, A. Y. Potekhin, N. Shibazaki, P. S. Shternin, and O. Y. Gnedin, Astrophys. Space Sci. **308**, 423 (2007).

Chapter 4

Enhanced Neutrino Emissivities in Pseudoscalar-mediated Dark Matter Annihilation in Neutron Stars

Resumen

En este trabajo se calcula la emisividad de neutrinos debida a la aniquilación de DM termalizada en el medio denso y caliente del interior estelar de una (proto)NS. Usando un modelo en el que la DM interacciona con los nucleones del núcleo de la estrella a través de un bosón pseudoescalar (a), encontramos que las tasas de producción de neutrinos de los canales de aniquilación dominantes, $\chi\bar{\chi} \to \nu\bar{\nu}$ y $\chi\bar{\chi} \to aa$, con el posterior decaimiento del mediador $a \to \nu\bar{\nu}$, podrían ser comparables localmente o incluso superar en las primeras etapas las de neutrinos estándar provenientes de procesos Urca nucleares modificados. Esta emisión de neutrinos debidos a la aniquilación de DM estaría localizada en una pequeña región de la estrella, un volumen $\lesssim 7\%$ del total estelar para temperaturas $T \lesssim 10^{10}$ K, y el proceso podría durar toda la vida de la estrella para algunos de los casos estudiados. Se discuten además las posibles consecuencias de nuestros resultados en el enfriamiento estelar teniendo en cuenta los límites existentes de DM.

The Astrophysical Journal, 863:157 (9pp), 2018 August 20 https://doi.org/10.3847/1538-4357/aad1ec

Enhanced Neutrino Emissivities in Pseudoscalar-mediated Dark Matter Annihilation in Neutron Stars

M. Cermeño[1], M. A. Pérez-García[1], and R. A. Lineros[2,3,4]
[1] Department of Fundamental Physics, University of Salamanca, Plaza de la Merced s/n, E-37008 Salamanca, Spain; marinacgavilan@usal.es, mperezga@usal.es
[2] Instituto de Física Corpuscular—CSIC/U. Valencia, Parc Científic, calle Catedrático José Beltrán 2, E-46980 Paterna, Spain; rlineros@gmail.com
[3] Space Sciences, Technologies and Astrophysics Research (STAR) Institute, Université de Liége, Bât. B5a, 4000 Liège, Belgium
[4] Departamento de Física, Universidad Católica del Norte, Avda. Angamos 0610, Casilla 1280, Antofagasta, Chile
Received 2018 May 10; revised 2018 June 28; accepted 2018 June 28; published 2018 August 20

Abstract

We calculate neutrino emissivities from self-annihilating dark matter (DM) (χ) in the dense and hot stellar interior of a (proto)neutron star. Using a model where DM interacts with nucleons in the stellar core through a pseudoscalar boson (a) we find that the neutrino production rates from the dominant reaction channels $\chi\chi \rightarrow \nu\bar{\nu}$ or $\chi\chi \rightarrow aa$, with subsequent decay of the mediator $a \rightarrow \nu\bar{\nu}$, could locally match and even surpass those of the standard neutrinos from the modified nuclear URCA processes at early ages. We find that the emitting region can be localized in a tiny fraction of the star (less than a few percent of the core volume) and the process can last its entire lifetime for some cases under study. We discuss the possible consequences of our results for stellar cooling in light of existing DM constraints.

Key words: dark matter – neutrinos – stars: neutron

1. Introduction

Dark matter (DM) is an essential ingredient of the standard cosmological model. We now know it constitutes nearly 85% of the universe matter density. However, despite the tremendous amount of progress that has been made in the search for this missing type of matter, both on theoretical and experimental fronts, its true nature remains an open question. The Standard Model (SM) of particle physics alone cannot explain the nature of DM, suggesting that it must be extended. Many theoretical model proposals have arisen aiming to explain the existing phenomenology (Bertone & Hooper 2016). The possible interplay between ordinary and DM could reveal interesting novel features, thus serving as the smoking gun evidence for the existence of a dark sector. As an example, one could cite a possible contribution to the reionization of the universe and the increase of gas temperature prior to the reionization epoch, leaving a potentially detectable imprint on the cosmological 21 cm signal, as studied in Chuzhoy (2007) and Mapelli et al. (2006). In particular, the production of SM neutrinos from annihilation of proposed dark candidates, generically χ, with energy $E_\nu \lesssim m_\chi$ is of paramount importance for the description of internal dynamics and energetic balance in stellar scenarios. In order to be specific, for example, one can consider the solar context. A DM particle will be gravitationally captured by the Sun if, in scattering against solar nuclei, it falls below the local escape velocity. This accumulation mechanism can lead to a local stellar DM density higher than that of the galactic halo where it resides, potentially providing us with an opportune region in which to search for visible signatures (Kouvaris 2008; Rott et al. 2015; Vincent et al. 2015). Additionally, low density environments in solar-type stars could yield interesting features in the neutrino channel (Palomares-Ruiz & Pascoli 2008; Aartsen et al. 2017).

On the other hand, in denser stellar environments such as those leading to the formation of neutron stars (NSs), neutrinos are vastly produced as they are very efficient at releasing the excess of gravitational energy when a compact stellar object is formed from a more massive progenitor. It has now been more than 30 years since the supernova SN1987A event allowed us to glimpse the complex behavior of the neutrino internal dynamics and obtain confirmation of the existence of a preliminary neutrino trapping phase followed by a transparency era (Gusakov et al. 2004) from the neutrino telescopes on Earth (Yuksel & Beacom 2007). In addition, X-ray satellite measurements have also provided indications of the cooling sequence, for a catalog of isolated cooling NSs (see Vigano et al. 2013 and Yakovlev & Levenfish 1995). Although a global understanding of the extracted temperatures for these objects is still missing, the so-called minimal cooling mechanism has been successful at reproducing the trends of observed cooling curves (Page et al. 2004). When solving for the internal temperature profile $T(r, t)$ as a function of stellar radius r and time t, one of the key ingredients that can dictate the energetic balance is the local energy emissivity, $Q_E = \frac{dE}{dVdt}$, i.e., the energy produced per unit volume per unit time, through a prescribed particle physics reaction.

In this work, we will be interested in obtaining astrophysical neutrino emissivities related to novel reaction channels involving DM undergoing self-annihilation processes inside the star. In particular, we focus on models in which DM particles communicate with the visible sector through a pseudoscalar mediator. These have been quoted to be well-motivated both from theoretical and from phenomenological grounds. Some of these models belong to a set of the so-called *simplified* type including Boehm et al. (2014), Wild (2016), Bauer et al. (2017), and Baek et al. (2017). As mentioned, they extend the SM by (at least) two particles, a DM candidate as well as a state that mediates the DM interactions with the visible sector, and are able to capture, with a minimal set of assumptions, some important features of more ultraviolet-complete (UV) theories while providing a (semi-)consistent

framework in order to analyze the experimental results (Banerjee et al. 2017).

In this setting, we will be interested in the dominant neutrino production processes, i.e., the s-wave process $\chi\chi \to \nu\bar{\nu}$ and the p-wave process $\chi\chi \to aa$, with subsequent decay $a \to \nu\bar{\nu}$. Although the previous reactions constitute the main neutrino emission channels in this model setting, additional reactions like, e.g., radiative a-emission or $\chi\chi \to aaa$ could also happen, but we will not consider them here as they are subdominant. As we will show, the two main reactions could provide a contribution to the standard astrophysical neutrino emissivities in NS environments of sizable magnitude at early times. The observability of such indirect effects caused by DM seems to be difficult nowadays, as it could be critically relying on the finest capabilities of current and future X-ray and gamma satellites (*NICER, eXTP, LOFT, ATHENA, CHANDRA*).

2. Neutrino Emissivities from DM Annihilation

In this work we are interested in calculating neutrino emissivities from DM self-annihilation in dense and hot stellar interiors, i.e., that of a (proto-)NS. In order to carry out our calculation, we choose a model where DM particles interact with SM particles through a pseudoscalar mediator. These kinds of models are well-motivated, both from the theoretical and phenomenological point of view. With direct detection bounds being typically subleading in such scenarios, the main constraints arise from collider searches (meson bounds) and from indirect detection experiments (Banerjee et al. 2017). Examples recently used along this line include the coy DM model of Boehm et al. (2014) and others (Wild 2016; Baek et al. 2017; Bauer et al. 2017). Although popular, we must stress that these simplified models have some limitations, regarding construction itself, and when confronted with bounds from collider searches (Dolan et al. 2015; Goncalves et al. 2017).

We now introduce our concrete model realization. We consider a model where the SM field content is extended by a Dirac fermion, χ, with mass m_χ, which plays the role of a DM candidate, and a pseudoscalar field, a, with mass m_a, which mediates the interaction of ordinary and dark sectors. The interaction Lagrangian of the model reads

$$\mathcal{L}_\mathcal{I} = -i\frac{g_\chi}{\sqrt{2}} a\bar{\chi}\gamma_5\chi - ig_0\frac{g_f}{\sqrt{2}} a\bar{f}\gamma_5 f, \tag{1}$$

where g_χ is the DM-mediator coupling, g_f corresponds to the couplings to the SM fermions, f, and g_0 is an overall scaling factor. From the usual schemes used for matter couplings when introducing Beyond-SM motivated physics we will restrict for simplicity to the so-called flavor-universal, which sets $g_f = 1$ for all SM fermions. Let us recall, however, that there are other schemes where a couples either to quarks or leptons exclusively, and with a flavor structure that will be treated elsewhere.

Typically, in these models DM phenomenology is controlled by four parameters, m_χ, m_a, g_χ, and $g_0 g_f$. In the range of $m_\chi < m_{\rm Higgs}$ and $m_a < m_\chi$, the relevant annihilation processes into two-body final states (Abdullah et al. 2014; Arina et al. 2015) are s-wave $\chi\chi \to f\bar{f}$ and p-wave $\chi\chi \to aa$. As a remark, it is worth mentioning that, as presented, the most straightforward UV-completion of this setup would be in the framework of the two Higgs doublet model or models involving even more extended scalar sectors. However, one should keep in mind that additional interactions with extra scalars arise at tree level and that can introduce important phenomenological model-dependent features (Haber & O'Neil 2011).

Table 1
Parameters Used in This Work as They Appear in the Interaction Lagrangian in Equation (1)

Model[a]	m_χ [GeV]	m_a [GeV]	g_χ	g_0
A	0.1	0.05	7.5×10^{-3}	7.5×10^{-3}
B	1	0.05	1.2×10^{-1}	2×10^{-3}
C	30	1	6×10^{-1}	5×10^{-5}

Note.
[a] We use flavor-universal $g_f = 1$.

Despite the limitations of simplified models, in our particular realization it is reasonable to expect that the very light mediators will not distort the relic density predictions due to the presence of additional annihilation channels involving these extra scalars as discussed in Banerjee et al. (2017).

DM abundance in our universe is likely to be fixed by the thermal freeze-out phenomenon: DM particles, initially present in our universe in thermal equilibrium abundance, annihilate with one another until chemical equilibrium is lost due to the expansion of the universe. The present-day relic density of these particles is predictable and it has been measured by Planck (Ade et al. 2016) to be $\Omega_{\rm CDM}h^2 = 0.1198 \pm 0.0015$.

Due to the pseudoscalar portal considered here, this model provides spin-dependent interactions with nucleons (N) at tree level. In this way, the χ-N interaction considered in direct searches is suppressed because it is momentum dependent, see Freytsis & Ligeti (2011), Cheng & Chiang (2012), and Gresham & Zurek (2014) for details. Instead, the spin-independent cross section is not present at tree level but the effective interaction at one-loop can be constructed (Ipek et al. 2014). Estimations of both cross sections in vacuum are given in Freytsis & Ligeti (2011). Both features regarding the behavior of the cross section impact the capability of the star to capture DM during the stage of the progenitor and in the collapsed configuration, although they can compensate each other in the star lifetime in order to have a finite meaningful amount of DM populating the object (Kouvaris & Tinyakov 2011).

Usual model analysis considers sets of parameters with a variety of bounds at a different level of significance. Here, in order to be definite, we will restrict our analysis to three different sets of flavor-universal parameters that are not in conflict with existing phenomenology to describe light DM ($m_\chi \lesssim 30$ GeV) interactions with ordinary matter. We consider constraints from direct detection experiments (Bertone et al. 2005), cosmological bounds (Zel'dovich 1965), and collider bounds (Dolan et al. 2015). The masses and couplings used in this work appear in Table 1.

Model sets A and B are mainly determined by DM relic abundance since the dark candidate mass is in the region where direct detection experiments are less restrictive (Ipek et al. 2014). The couplings in set C are chiefly constrained by LUX results (Akerib et al. 2017) in spin-independent and spin-dependent cross sections and, in addition, they respect restrictive rare meson decays (Dolan et al. 2015) as well. In the beforementioned cases,

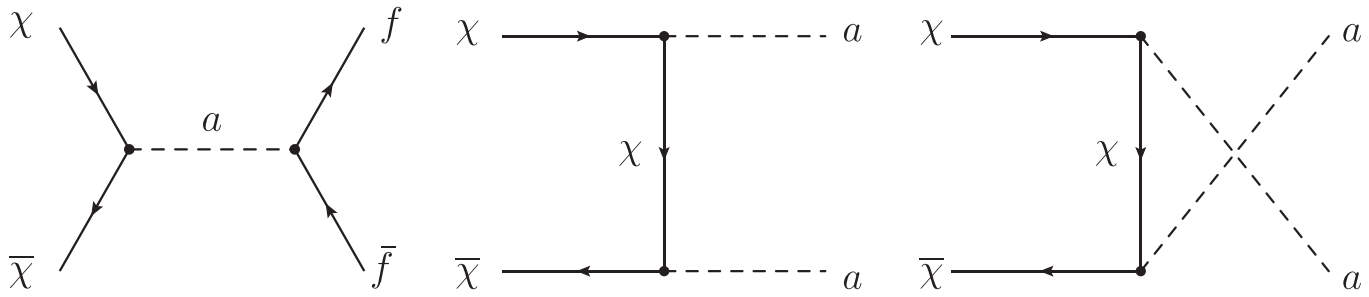

Figure 1. Feynman diagrams for DM annihilation reactions $\chi\chi \to f\bar{f}$ and $\chi\chi \to aa$ considered in this work.

we estimate the parameters using MicroOmegas (Belanger et al. 2010) and direct detection cross sections at one-loop level (Freytsis & Ligeti 2011; Ipek et al. 2014).

According to the current stage of exploration of the phase space of masses and cross sections for DM candidates interacting with nucleons in ordinary matter, dense compact stars are believed to be suitable places to find this kind of matter. NSs are believed to be efficient DM accretors (Gould 1987). One of the key quantities that can dictate their internal stellar energetic balance is the local energy emissivity, $Q_E = \frac{dE}{dVdt}$ (energy produced per unit volume per unit time, through a prescribed particle physics reaction). In this work, we will be interested in the annihilation reactions of DM into two-body fermionic states (f), $\chi\chi \to f\bar{f}$ and two pseudoscalar boson states $\chi\chi \to aa$ with subsequent decay $a \to f\bar{f}$. Furthermore, we will discuss possible astrophysical consequences particularizing to the $f = \nu$ neutrino channel.

Formally, the expression for Q_E generically denotes the energy emission rate per stellar volume arising from fermionic or pseudoscalar pair production and can be written as (Esposito et al. 2002)

$$Q_E = 4\int d\Phi(E_1 + E_2)|\overline{\mathcal{M}}|^2 f(f_1, f_2, f_3, f_4), \tag{2}$$

with

$$d\Phi = \frac{d^3\boldsymbol{p}_1}{2(2\pi)^3 E_1}\frac{d^3\boldsymbol{p}_2}{2(2\pi)^3 E_2}\frac{d^3\boldsymbol{p}_3}{2(2\pi)^3 E_3} \times \frac{d^3\boldsymbol{p}_4}{2(2\pi)^3 E_4}(2\pi)^4\delta(p_1 + p_2 - p_3 - p_4), \tag{3}$$

the 4-body ($12 \to 34$) phase space element and $|\overline{\mathcal{M}}|^2$, the spin-averaged squared matrix element of the reaction considered. The additional factor $f(f_1, f_2, f_3, f_4)$ accounts for the global phase space blocking factor due to the initial and final particle distribution functions, f_i, $i = 1, \ldots, 4$ we will discuss below. $\delta(x)$ is the four-dimensional delta function. We will denote $p_1 = (E_1, \boldsymbol{p}_1)$, $p_2 = (E_2, \boldsymbol{p}_2)$ as the incoming 4-momenta, while $p_3 = (E_3, \boldsymbol{p}_3)$, $p_4 = (E_4, \boldsymbol{p}_4)$ are the outgoing 4-momenta, respectively. The detailed associated Feynman diagrams are shown in Figure 1. Let us note that besides the quoted annihilation processes we consider, there may be additional pseudoscalar boson production s-wave $\chi\chi \to aaa$ (Abdullah et al. 2014), initial/final state radiation and internal bremsstrahlung processes $\chi\chi \to f\bar{f}a$ or $\chi\chi a \to f\bar{f}$ (Bell et al. 2017). However, since the cross sections for these processes are proportional to $g_\chi^2 g_f^4$ and $g_\chi^4 g_f^2$, respectively, they are subdominant in the case of a Dirac fermion DM candidate (Ibarra et al. 2013; Bringmann et al. 2017). Similarly, radiative a-production can arise from the SM particles' interaction inside the star, but this process is found to be only relevant in the case of very light mediators ($\lesssim$eV) like axions or Majorons (Farzan 2003; Sedrakian 2016).

Specifically, for the case of annihilation into fermionic pairs (left diagram in Figure 1) we label the emissivity as $Q_E^{f\bar{f}}$. It includes the expression for the spin-averaged squared matrix element as

$$|\overline{\mathcal{M}}_{f\bar{f}}|^2 = \frac{g_\chi^2 g_f^2}{4}\frac{s^2}{(s - m_a^2)^2 + E_{|\boldsymbol{q}|}^2\Gamma^2}, \tag{4}$$

where $q^2 = s = (p_1 + p_2)^2 = (p_3 + p_4)^2$ is the Mandelstam variable and $E_{|\boldsymbol{q}|} = \sqrt{|\boldsymbol{q}|^2 + m_a^2}$. In this case

$$f(f_1, f_2, f_3, f_4) = f_\chi(E_1) f_{\bar{\chi}}(E_2)(1 - f_f(E_3))(1 - f_{\bar{f}}(E_4)), \tag{5}$$

and f_χ, f_f are the local stellar distribution functions for DM and fermionic particles, respectively, containing density and temperature dependence we will discuss further below. Γ is the pseudoscalar particle decay width in the local medium through the reaction $a \to f\bar{f}$. It is obtained using the optical theorem as

$$\Gamma = \frac{1}{E_{|\boldsymbol{q}|}}\,\mathrm{Im}\,\Pi(\boldsymbol{q}), \tag{6}$$

where $\Pi(\boldsymbol{q})$ is the pseudoscalar polarization insertion given by

$$\Pi(\boldsymbol{q}) = \frac{ig_f^2}{2}\int\frac{d^4k}{(2\pi)^4}\mathrm{tr}[\gamma_5 G^0(k)\gamma_5 G^0(k + q)], \tag{7}$$

and the corresponding cut of the associated tadpole diagram involves the fermion propagator $G^0(k)$ including a vacuum and matter contribution (Chin 1977; Matsui & Serot 1982).

Using Equations (2) and (4), we can obtain an expression for the emissivity produced by the annihilation of DM particles into $f\bar{f}$, $Q_E^{f\bar{f}}$. Let us first deal with the integration over $\boldsymbol{p}_4$ so that

$$\int\frac{d^3\boldsymbol{p}_3}{2E_3(2\pi)^3}\int\frac{d^3\boldsymbol{p}_4}{2E_4(2\pi)^3}(2\pi)^4\delta(p_1 + p_2 - p_3 - p_4) = \int\frac{2\pi|\boldsymbol{p}_4|^2 d|\boldsymbol{p}_4|}{4E_3E_4(2\pi)^2}d(\cos\theta)\delta(q_0 - E_3 - E_4), \tag{8}$$

where θ is the angle between $\boldsymbol{p}_4$ and $\boldsymbol{q}$, and $q_0 = E_1 + E_2$ for this annihilation channel. Besides, we can express the energy

delta function as

$$\delta(q_0 - E_3 - E_4) = \frac{\sqrt{m_f^2 + |\boldsymbol{q}|^2 + |\boldsymbol{p}_4|^2 - 2|\boldsymbol{p}_4||\boldsymbol{q}|\cos\theta}}{|\boldsymbol{p}_4||\boldsymbol{q}|} \times \delta(\cos\theta - \cos\theta_0)\Theta(q^2 \geqslant 4m_f^2), \tag{9}$$

where

$$\cos\theta_0 = \frac{1}{2|\boldsymbol{p}_4||\boldsymbol{q}|}(|\boldsymbol{q}|^2 - q_0^2 + 2q_0E_4), \tag{10}$$

and $q^2 = q_0^2 - |\boldsymbol{q}|^2$. $\Theta(x)$ is the Heaviside function. Equation (9) has been obtained using

$$\delta[f(x)] = \sum_i \frac{\delta(x - x_{0i})}{|f'(x)|_{x_{0i}}|}, \tag{11}$$

with x_{0i} the zeros of $f(x)$. Now, we use $|\boldsymbol{p}_4|d|\boldsymbol{p}_4| = E_4 dE_4$. Imposing $\cos^2\theta_0 \leqslant 1$, we obtain limits for the integration over E_4

$$E_4 \pm = \frac{1}{2}\left(q_0 \pm |\boldsymbol{q}|\sqrt{1 - \frac{4m_f^2}{q^2}}\right). \tag{12}$$

In the same way, we use $|\boldsymbol{p}_1|d|\boldsymbol{p}_1| = E_1 dE_1$ and $|\boldsymbol{p}_2|d|\boldsymbol{p}_2| = E_2 dE_2$. After that, Equation (2) takes the form

$$Q_E^{f\bar{f}} = \frac{1}{2(2\pi)^5}\int_{m_\chi}^\infty dE_1\sqrt{E_1^2 - m_\chi^2}\int_{m_\chi}^\infty dE_2\sqrt{E_2^2 - m_\chi^2} \times \int_{-1}^1 d(\cos\phi)q_0\Theta(q^2 \geqslant 4m_f^2)\int_{E_4-}^{E_4+} dE_4 \times \int_{-1}^1 d\cos\theta\delta(\cos\theta - \cos\theta_0)f(f_1, f_2, f_3, f_4) \times \frac{|\overline{\mathcal{M}}_{f\bar{f}}|^2}{|\boldsymbol{q}|}, \tag{13}$$

where ϕ is the angle between $\boldsymbol{p}_1$ and $\boldsymbol{p}_2$, $E_3 = E_1 + E_2 - E_4$,

$$|\boldsymbol{q}| = \sqrt{|\boldsymbol{p}_1|^2 + |\boldsymbol{p}_2|^2 + 2|\boldsymbol{p}_1||\boldsymbol{p}_2|\cos\phi}, \tag{14}$$

and $|\boldsymbol{p}_1| = \sqrt{E_1^2 - m_\chi^2}$, $|\boldsymbol{p}_2| = \sqrt{E_2^2 - m_\chi^2}$.

Instead, for the DM annihilation into two pseudoscalars (middle and right diagrams in Figure 1), now the emissivity is labeled as Q_E^{aa}. In this case, when calculating the spin averaged matrix element one must note that

$$|\overline{\mathcal{M}}_{aa}|^2 = \frac{1}{2}\frac{1}{2}\sum_{s,s'}|\mathcal{M}_{aa}|^2, \tag{15}$$

where s and s' are the spin states of the DM particle. The squared matrix element finally reads,

$$|\overline{\mathcal{M}}_{aa}|^2 = \frac{-g_\chi^4}{2}\left\{\frac{(t - m_a^2)^2 - m_\chi^2(m_\chi^2 + 2m_a^2)}{(t - m_\chi^2)^2} + \frac{(u - m_a^2)^2 - m_\chi^2(m_\chi^2 + 2m_a^2)}{(u - m_\chi^2)^2} + 2\frac{2m_\chi^2 - s}{u - m_\chi^2} + \frac{(s - 2m_\chi^2)(2m_a^2 - s) + 2m_\chi^2(m_\chi^2 + 2m_a^2 - 2s) - 2(t - m_a^2)^2}{(t - m_\chi^2)(u - m_\chi^2)}\right\}. \tag{16}$$

where $s = k^2 = (p_1 + p_2)^2$, $t = (p_1 - p_3)^2 = (p_4 - p_2)^2$ and $u = 2m_\chi^2 + 2m_a^2 - s - t$.

As we can see, now the matrix element not only depends on s but also on t and u. Dealing with the integration to obtain the emissivity, it is convenient to write these variables as

$$s = 2m_\chi^2 + 2E_1E_2 - 2|\boldsymbol{p}_1||\boldsymbol{p}_2|\cos\theta_{12}, \tag{17}$$

and

$$t = m_\chi^2 + m_a^2 - 2E_1E_3 + 2|\boldsymbol{p}_1||\boldsymbol{p}_3|\cos\theta_{13}, \tag{18}$$

where θ_{ij} is the angle between $\boldsymbol{p}_i$ and $\boldsymbol{p}_j$.

In the same way that we did for the annihilation into fermions, we can write

$$\int\frac{d^3\boldsymbol{p}_3}{2E_3(2\pi)^3}\int\frac{d^3\boldsymbol{p}_4}{2E_4(2\pi)^3}(2\pi)^4\delta(p_1 + p_2 - p_3 - p_4) = \iiint\frac{|\boldsymbol{p}_3|^2 d|\boldsymbol{p}_3|d\phi_3}{4E_3E_4(2\pi)^2}d(\cos\theta_3)\delta(k_0 - E_3 - E_4), \tag{19}$$

where we are denoting the four momentum $k = (k_0, \boldsymbol{k})$ and θ_i as the angle between $\boldsymbol{p}_i$ and $\boldsymbol{k}$. As obtained in Equation (9), we find

$$\delta(k_0 - E_3 - E_4) = \frac{E_4}{|\boldsymbol{p}_3||\boldsymbol{k}|}\delta(\cos\theta_3 - \cos\theta_{3,0}), \tag{20}$$

being

$$\cos\theta_{3,0} = \frac{1}{2|\boldsymbol{p}_3||\boldsymbol{k}|}(|\boldsymbol{k}|^2 + 2k_0E_3 - k_0^2). \tag{21}$$

Now, we can write the emissivity into two pseudoscalars as

$$Q_E^{aa} = \frac{1}{2(2\pi)^6}\int_0^\infty|\boldsymbol{k}|d|\boldsymbol{k}|\int_{m_\chi}^\infty\sqrt{E_2^2 - m_\chi^2}dE_2 \times \int_{-1}^1 d\cos\theta_2\frac{E_1 + E_2}{E_1}\Theta(k^2 - 4m_a^2) \times \int_{E_3-}^{E_3+} dE_3\int_{-1}^1 d\cos\theta_3\delta(\cos\theta_3 - \cos\theta_{3,0}) \times \int_0^{2\pi} d\phi_3 f(f_1, f_2, f_3, f_4)|\overline{\mathcal{M}}_{aa}|^2 \tag{22}$$

where $|\boldsymbol{p}_1| = \sqrt{|\boldsymbol{k}|^2 + |\boldsymbol{p}_2|^2 - 2|\boldsymbol{k}||\boldsymbol{p}_2|\cos\theta_2}$, $t = m_\chi^2 + m_a^2 - 2E_1E_3 + 2|\boldsymbol{p}_3|(|\boldsymbol{k}|\cos\theta_3 - |\boldsymbol{p}_2|\cos\theta_{23})$, and $\cos\theta_{23} = \cos\phi_3\sin\theta_2\sin\theta_3 + \cos\theta_2\cos\theta_3$. We have also used the trigonometric relation $|\boldsymbol{p}_1|\cos\theta_{13} = |\boldsymbol{k}|\cos\theta_3 - |\boldsymbol{p}_2|\cos\theta_{23}$. The limits for the outgoing energy in the integral are

$$E_3 \pm = \frac{1}{2}\left(k_0 \pm |\boldsymbol{k}|\sqrt{1 - \frac{4m_a^2}{k^2}}\right). \tag{23}$$

In the case of annihilation into pseudoscalars the phase space factor reads

$$f(f_1, f_2, f_3, f_4) = f_\chi(E_1)f_{\bar{\chi}}(E_2)f_a(E_3)f_a(E_4). \tag{24}$$

In this case, one should also take into account the further decay of each pseudoscalar into fermionic pairs and the availability of kinematical phase space through and additional Pauli blocking factor. Although not explicit, there is also a further local dependence on the DM density in the distribution function that will be discussed later in the manuscript.

2.1. Dense and Hot Stellar Scenario

In order to explain the physical relevance of the quantities under scrutiny obtained in the previous section, at this point we will particularize to that of a dense and hot stellar scenario. We will focus on a (proto-)NS. Briefly, an NS is mostly constituted by nucleons forming a central core at a density in excess of nuclear saturation density, $\rho_0 \simeq 2.4 \times 10^{14}\,\mathrm{g\,cm^{-3}}$. An average NS has a radius $R \lesssim 12\,\mathrm{km}$ and mass $M \sim (1\text{–}1.5)\,M_\odot$ (mostly in its core) being thus a star with large compactness ratio $\sim M/R$. For the sake of our discussion, we will consider a typical baryonic core density value $\rho_b = \rho_N \sim 2\rho_0$. Regarding internal temperature and composition, NSs are born as hot lepton-rich objects with temperatures $T \sim 20\,\mathrm{MeV}$ evolving into cold $T \sim 10\,\mathrm{keV}$ neutron-rich ones, after a deleptonization era. Assuming dark and ordinary matter has coupling strengths at the level of current experimental search bounds, NSs are believed to be capable of accreting (and retaining) DM particles whose masses are larger than a few GeV from an existing galactic distribution.

Accretion of a dark component will proceed not only during the collapsed stage but also during most of the previous progenitor stellar lifetime at different epoch-dependent capture rates, C_χ. First, in the progenitor stages, the progressively denser nuclear ash central core is effectively opaque to DM and allows build up of an internal finite DM number density over time, $n_\chi(r)$, where r is the radial stellar coordinate. Briefly, the progenitor with a mass $\sim(10\text{–}15)M_\odot$ is able to fuse lighter elements into heavier ones and thus its composition changes through the burning ages. Hydrogen first, and later the He, C, O, and the rest of the heavier elements up to Si proceed through the burning stages. Spin-dependent (mostly from H) as well as spin-independent χ-N cross sections allow the gravitational capture of DM population inside the star. Coherence effects may play a role for slowly moving, low m_χ incoming DM particles scattering nuclei off when their associated de Broglie wavelength is comparable to the nuclear size, and in this case the spin-independent cross section bears a multiplicative factor $\simeq A^2$, where A is the baryonic number. Since the later burning stages proceed rapidly, the He–C–O stage gives the main contribution to the DM capture in the progenitor. As the thermalization times during this set of stages can follow the internal dynamics the collapsed star will have as a result a nonzero, mostly inherited, initial DM population.

In detail, the DM particle population number inside the star, N_χ, will not only depend on the capture rate C_χ (Gould 1987) but also on the self-annihilation rate, C_a. Note that in the range of masses in the parameter sets we consider, evaporation effects (Krauss et al. 1986) as well as decay (Perez-Garcia & Silk 2015) do not substantially modify the DM population as the kinetic to gravitational potential energy ratio remains small.

Then the DM particle number, N_χ, can be obtained as a function of time t by solving the differential equation

$$\frac{dN_\chi}{dt} = C_\chi - C_a N_\chi^2, \tag{25}$$

considering the two competing processes, capture and annihilation (Kouvaris & Tinyakov 2010)

$$N_\chi(t) = \sqrt{\frac{C_\chi}{C_a}}\,\tanh\left[\frac{t}{\tau} + \gamma(N_{\chi,0})\right], \tag{26}$$

where

$$\gamma(N_{\chi,0}) = \tanh^{-1}\left(\sqrt{\frac{C_\chi}{C_a}}\,N_{\chi,0}\right) \tag{27}$$

and

$$\tau^{-1} = \sqrt{C_\chi C_a}. \tag{28}$$

At $t = 0$, when the proto-NS is born, a typical progenitor may have already provided an initial population

$$N_{\chi,0} = 1.5 \times 10^{39}\left(\frac{\rho_\chi}{\rho_{\chi,0}^{\mathrm{ambient}}}\right)\left(\frac{1\,\mathrm{GeV}}{m_\chi}\right)\left(\frac{\sigma_s}{10^{-43}\,\mathrm{cm^2}}\right), \tag{29}$$

where $\sigma_s \equiv \sigma_{\chi-N}$ is the $\chi - N$ scattering cross section. As this quantity is currently unknown, only experimental constrains exist for it. In the range of DM masses used in this work $\sigma_s \in [10^{-46} - 10^{-33}]\,\mathrm{cm^{-2}}$ (Kavanagh 2017). Equation (29) assumes that the majority of the NS population can be found at galactocentric distances of a few kiloparsecs where $\rho_\chi \sim 10^2\rho_{\chi,0}^{\mathrm{ambient}}$. We use $\rho_{\chi,0}^{\mathrm{ambient}} \simeq 0.3\,\frac{\mathrm{GeV}}{\mathrm{cm^3}}$ as the solar-circle DM density value.

Let us mention that both capture and annihilation rates, will be intimately determined by the parameters of the model at hand, i.e., m_χ, m_a, g_0, g_χ (we set $g_f = 1$). In particular, the DM capture rate on the progenitor depends on the scattering cross section on nuclei (nucleons) that is proportional to the product of the couplings ($\sim g_0^2 g_\chi^2$) and the annihilation cross section proportional to the sum of ($\sim g_0^2 g_\chi^2$) and ($\sim g_\chi^4$) terms for the two reactions considered $\chi\chi \to f\bar{f}$ and $\chi\chi \to aa$, respectively (Buckley et al. 2015).

For the three models considered in this work appearing in Table 1, the average progenitor capture rate allows a nonvanishing initial DM population, $N_{\chi,0}$, since the annihilation rate, proportional to $n_\chi^2(r)$, is negligibly small at that stage. Later, in the NS collapsed state and at a given galactic location with a corresponding ambient DM density ρ_χ, the capture rate, C_χ, it is approximated up to factors of the order of unity by the expression (Gould 1987; de Lavallaz & Fairbairn 2010).

$$C_\chi \simeq 1.8 \times 10^{25}\left(\frac{1\,\mathrm{GeV}}{m_\chi}\right)\left(\frac{\rho_\chi}{\rho_{\chi,0}^{\mathrm{ambient}}}\right) f_{\chi,N}\ \mathrm{s^{-1}}. \tag{30}$$

A few remarks are due regarding this expression. $f_{\chi,N}$ denotes a phenomenological factor dealing with the opacity of stellar matter. $f_{\chi,N}$ depends on the ratio of the leading contribution of $\chi - N$ scattering cross section σ_s to the minimum geometrical cross section of an NS made of nucleons of mass m_N and defined as

$$\sigma_0 = \frac{m_N R^2}{M} \sim 10^{-45}\,\mathrm{cm^2}. \tag{31}$$

Thus this factor saturates to unity, $f_{\chi,N} \sim 1$, if $\sigma_s \gtrsim \sigma_0$. Otherwise, $f_{\chi,N} \sim \frac{\sigma_s}{\sigma_0}$. Using Boehm et al. (2014) and Appendix D in Dolan et al. (2015), we consider the scattering cross section (at one-loop) in the appropriate kinematical limit in our compact star so that for the parameters used in this work f_χ are effectively in the saturated regime.

The expressions in the literature for DM capture rates in dense objects are based on interactions with quarks (nucleons)

that in practice happen via a contact term (Freytsis & Ligeti 2011), possibly including form factors. Note that a more ellaborate treatment would involve the calculation of the nonrelativistic limit of the (full) series of operators included in the Lagrangian under study. Such a detailed analysis is beyond the scope of this work and remains to be done. The usual phenomenological treatment, through the $f_{\chi,N}$ factor, makes use of a lower bound to the global cross section with all relevant contributions in this realization picture. It is important to emphasize that the strength of the computed emissivity will depend on the number of DM particles remaining inside the star at any given time.

As thermalization times for DM particles in the light mass range we consider are consistently smaller than dynamical cooling times (Goldman & Nussinov 1989), inside the star the DM particle number density takes the form

$$n_\chi(r) = n_{0,\chi} e^{-\frac{m_\chi}{k_B T}\Phi(r)}, \tag{32}$$

where $n_{0,\chi}$ is the central value, T is the NS temperature, and k_B is the Boltzmann constant. The gravitational potential is given by

$$\Phi(r) = \int_0^r \frac{GM(r')dr'}{r'^2}, \tag{33}$$

where $M(r')$ is the NS mass inside a spherical volume of radius r'. So that assuming an approximately constant density core,

$$n_\chi(r) = n_{0,\chi} e^{-(r/r_{\rm th})^2}, \tag{34}$$

with a thermal radius

$$r_{\rm th} = \sqrt{\frac{3k_B T}{2\pi G \rho_N m_\chi}}. \tag{35}$$

Normalization requires $\int_0^R n_\chi(r)dV = N_\chi$ at a given time, as reflected by Equation (26). Note that potential limiting values of N_χ may arise from the fact that a fermionic χ would involve the existence of a Chandrasekhar critical mass for collapse (MacDermott et al. 2012). This possibility is safely not fulfilled as long as $N_\chi(t) < N_{\rm Ch}$, where $N_{\rm Ch} \sim (M_{\rm Pl}/m_\chi)^3 \sim 1.8 \times 10^{57}(1\,{\rm GeV}/m_\chi)^3$ with $M_{\rm Pl}$ the Planck mass.

Let us now comment on the fact that inside the star the tiny DM fraction can be described by a distribution function of a classical Maxwell–Boltzmann type

$$f_\chi = f_\chi^{\rm MB}(|\boldsymbol{p}_i|, r) = \left(\frac{1}{2\pi m_\chi k_B T}\right)^{\frac{3}{2}} n_\chi(r) e^{\frac{-|\boldsymbol{p}_i|^2}{2m_\chi T}},\ i = 1, 2, \tag{36}$$

and in the nonrelativistic scheme $E_i = \frac{\boldsymbol{p}_i^2}{2m_\chi}$, $i = 1, 2$. The annihilation rate, C_a, depends on the thermally averaged annihilation cross section inside the star, $\langle\sigma_a v\rangle$, for the two reactions considered in this work, see Figure 1. Therefore, the stellar χ-distribution contained in the thermal volume region $\sim r_{\rm th}^3$ determines the annihilation rate $C_a \sim \langle\sigma_a v\rangle/V_{\rm th}$ (Arina et al. 2015; Goncalves et al. 2017). Note that the presence of the phase space factor $f(f_1, f_2, f_3, f_4)$ in Equation (2) will introduce further DM density and T dependence into the vacuum standard calculation as a thermalized DM distribution exists inside the NS core. As for the outgoing fermions, the medium density effects will generally arise from the phase space blocking factors and collective effects (Cermeño et al. 2016a). In the case of neutrinos, we assume $f_\nu \sim 0$, although in cases where a trapped fraction $Y_\nu > 0$ exists it would further decrease the response.

3. Results

In this section, we explain our results regarding the emissivities in the NS astrophysical scenario particularizing to the case in which the final state fermions produced in the reactions depicted in Figure 1 are neutrino pairs. Neutrinos are weakly interacting SM fermions known to play a key role in the internal energy ;dynamics of a massive stellar progenitor undergoing gravitational collapse. In such an event, most of the gravitational binding energy is emitted into neutrinos (and antineutrinos) of the three families. A very efficient cooling scenario emerges in the first $\sim 10^5$ years. Standard processes such as those present in the URCA or the modified URCA (MURCA) cooling (Friman & Maxwell 1979; Yakovlev et al. 2005) among others can release neutrinos with associated emissivities $Q_E^{\rm URCA} \sim 10^{27}\mathcal{R}\left(\frac{T}{0.1\ {\rm MeV}}\right)^6\ {\rm erg\ cm^{-3}\ s^{-1}}$ and $Q_E^{\rm MURCA} \sim 10^{21}\mathcal{R}\left(\frac{T}{0.1\ {\rm MeV}}\right)^8\ {\rm erg\ cm^{-3}\ s^{-1}}$, respectively. Typical energetic scales can be obtained from the conversion factor $1\,{\rm MeV} \sim 10^{10}\,{\rm K}$. $\mathcal{R}$ is a reduction function of the order of unity describing the superfluid effects in the neutron and proton branches of those reactions (Yakovlev & Levenfish 1995). We must keep in mind the fact that these neutrinos effectively cool off the star as they leave, having scattered a few times with ordinary nucleon matter (Horowitz & Perez-Garcia 2003; Perez-Garcia 2010) after a first rapid trapping stage. In this way, processes with neutrino production in reactions involving nucleon components effectively release energy from the baryonic system as the associated neutrino mean-free path is relatively long $\lambda \sim 28\,{\rm cm}(100\,{\rm MeV}/{\rm E}_\nu)^2$. In analogy with what happens at the standard neutrino trapping stage in very young stars, when neutrinos have energies of dozens of MeV, it is expected that energetic neutrinos produced in reactions of DM annihilation could have mean-free paths that are very small, even at low stellar temperatures (in evolved stars) so they may not escape the dense medium so easily (Kouvaris 2008).

In Figure 2, the logarithm (base 10) of the energy emissivity for the process $\chi\chi \to \nu\bar{\nu}$ is shown as a function of temperature for the three sets of DM parameters A, B, and C in Table 1, with dashed, dotted, and dashed–dotted lines, respectively. Baryonic density is fixed at $2\rho_0$. We also fix (for reference) the assumed number of DM particles at initial instant $N_\chi = N_{0,\chi}$. Note, however, that N_χ is time (and model) dependent as it rapidly decreases when the self-annihilation sets in. We give below a suitable fit where the actual T and N_χ dependence is reflected. The baryonic density dependence is, however, weak. The standard physics cooling is depicted here by the MURCA emissivity (solid line) for the sake of comparison. Although the latter is not the only process that could possibly contribute to the effective standard cooling, all other processes capable of contributing are considered weaker at the temperature and density conditions considered in this work. Thus we take the standard processes to be represented by an upper limit to the currently used emissivities chosen as the MURCA processes. Note that we do not consider exotic meson codensates nor do we consider URCA emissivities, since stellar central densities required are usually higher than the one taken as reference here in order to provide the $Y_p \sim 11\%$–15% proton fraction

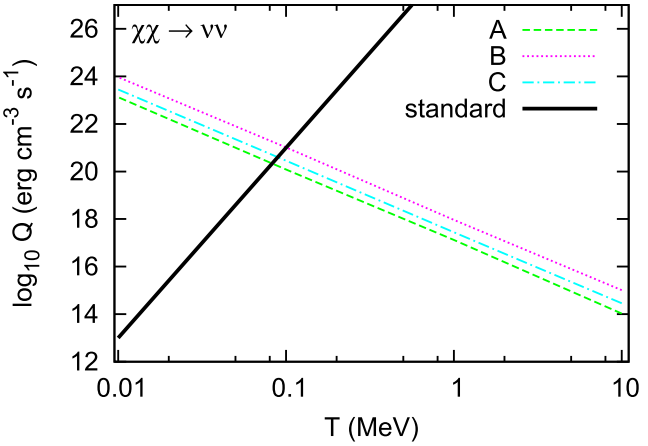

Figure 2. Energy emissivity from DM self-annihilation channel $\chi\chi \to \nu\nu$ as a function of temperature. Standard emission refers to MURCA processes. $N_\chi = N_{0,\chi}$ is assumed. See the text for details.

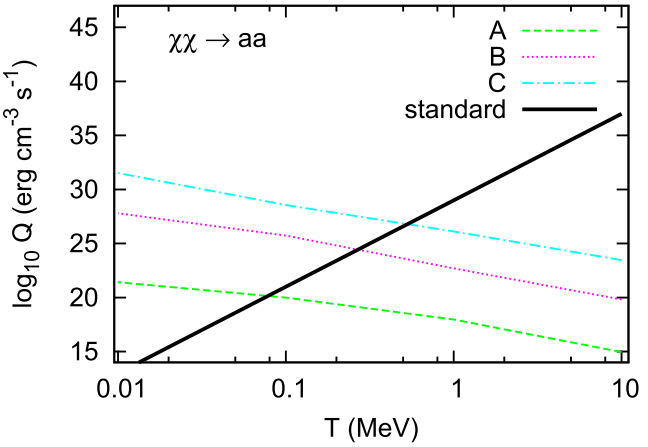

Figure 3. Energy emissivity from DM self-annihilation channel $\chi\chi \to aa$ with subsequent decay $a \to \nu\nu$ as a function of temperature. Standard emission refers to MURCA processes. $N_\chi = N_{0,\chi}$ is assumed. See the text for details.

(Lattimer et al. 1991) to sustain the fast reaction. Furthermore, we assume that a possible neutrino trapping phase will not be significant, particularly at low T. However, at high T it may produce a further reduction that has to be accounted for through a Pauli blocking factor. It must be included to take into account the time dependent nonvanishing leptonic fraction of the order of $Y_L \sim 0.1$ (Pons et al. 1999) until transparency sets in at $\sim$20 s.

The trends depicted in Figure 2 with temperature and DM particle population dependence for models A, B, and C and for both reaction channels can be fit as

$$Q_E(T, N_\chi) = Q_0 \left(\frac{N_\chi}{N_{0,\chi}}\right)^2 \left(\frac{T}{1\ \mathrm{MeV}}\right)^{-3}. \quad (37)$$

In Table 2, we give values for parameters Q_0 and $N_{0,\chi}$ for the reactions and models considered. We can see that around $T \sim 0.1$ MeV standard emissivities $\log_{10}(Q_E) \sim 21$ are as powerful as those from the DM annihilation processes in the thermal volume region $V_{\rm th} \sim r_{\rm th}^3$. However, since DM population is a decreasing function of time, one can expect that there will be a minimal number of N_χ population to beat the MURCA processes for $T < 0.1$ MeV. We find $Q_E(T, N_\chi) > Q_{\rm MURCA}$ for $T \in [0.01, 0.1]$ MeV for $N_\chi/N_{0,\chi} \gtrsim 10^{-5}$, 3.6×10^{-6}, 5.6×10^{-6} for A, B, and C models, respectively. One should note that the N_χ self-consistently depends on temperature and how it dynamically changes with time. A fully detailed cooling simulation would yield the temporal sequence to determine the complete behavior. As this is not the goal here, we give instead an estimate on the time duration of the dominance of the DM annihilation channel, i.e., where it could beat the local MURCA processes from Equation (26). We obtain $t \lesssim 50$ s for models A and B while this condition is true at all times for model C. We note that all timescales are thus overlapping the standard transparency window for SM neutrinos.

In Figure 3, the logarithm (base 10) is shown for the reaction $\chi\chi \to aa$ with subsequent decay $a \to \nu\nu$. The number of DM particles is also fixed $N_\chi = N_{0,\chi}$ for reference using the same argument as with the $\chi\chi \to \nu\nu$ reaction in Figure 2. In this case, for a population $N_{0,\chi}$, the neutrino emissivity is largely enhanced with respect to the direct production of neutrinos $\chi\chi \to \nu\nu$. For model C (dashed–dotted line), Q_E matches and surpasses the standard MURCA emission below $T \sim 0.5$ MeV, while for models B (dotted line) and A (dashed line) that happens for $T \sim 0.3$ MeV and $T \sim 0.1$ MeV, respectively. Values for the phenomenological fit in this channel are also provided in Table 2.

Table 2
Parameters Obtained for the Fit in Equation (37)

Channel	Model	$\log_{10} Q_0$ [erg cm^{-3} s^{-1}]	$N_{0,\chi}$
$\chi\chi \to \nu\nu$	A	17.3	4.1×10^{44}
$\chi\chi \to \nu\nu$	B	18	2.4×10^{44}
$\chi\chi \to \nu\nu$	C	17.6	5×10^{38}
$\chi\chi \to aa$[a]	A	18	4.1×10^{44}
$\chi\chi \to aa$	B	22.5	2.4×10^{44}
$\chi\chi \to aa$	C	27	5×10^{38}

Note.
[a] With subsequent decay $a \to \nu\nu$.

If we now consider the running character of DM population number as in the previous case we find $Q_E(T, N_\chi) > Q_{\rm MURCA}$ in the interval $T \in [0.01, 0.1]$ MeV for $N_\chi/N_{0,\chi} \gtrsim 3 \times 10^{-5}$ and model A, while for model B $Q(T, N_\chi) > Q_{\rm MURCA}$ in $T \in [0.01, 0.3]$ MeV when $N_\chi/N_{0,\chi} \gtrsim 5 \times 10^{-8}$. Finally $Q(T, N_\chi) > Q_{\rm MURCA}$ in $T \in [0.01, 0.5]$ MeV for $N_\chi/N_{0,\chi} \gtrsim 3 \times 10^{-10}$ for model C. This last ratio for model C is achieved during the entire lifetime of the star while not for the other cases. For the bi-pseudoscalar production reaction and at the thermodynamical conditions in the scenario considered we obtain that typical values obtained for the a-decay length are of the order of $\sim 10^2$ fm, making it a negligible contribution to the neutrino transport as their decay length is so tiny compared to stellar size.

At this point, it is worth noting that tighter restrictions on the validity of the coupling of DM to u–d–s quarks coming from including complementary experimental bounds, e.g., rare meson decays, could somewhat reduce the validity of models A and B. In addition, from isospin considerations, the χ coupling to neutrons and protons in the NS will also somewhat affect the results as the proton-to-neutron ratio inside the NS core is smaller than unity ($\sim 1/9$). As the ratio of coupling fulfills $|g_p/g_n| > 1$ when considering flavor-universal fermion couplings (Dolan et al. 2015) we expect

that the computed emissivities could be increased by a factor of ∼10–100.

We have considered the local emissivities of the novel reaction involving self-annihilating matter in the thermal volume. We must emphasize that since there is no uniform distribution of DM inside the star, neutrinos being produced from nuclear reactions in the majority of the core volume will wash out the dark contribution early, when the temperature is high enough. However, later, as temperature decreases there is an effective competition of the very efficient dark central engine (located in a few percent of the core volume) and the colder core emission.

The radial extent of the DM annihilating inner region is correlated to the ratio of the thermal radius to the NS radius. It is defined as $\xi = \sqrt{2}\, r_{\rm th}/R$ and indicates the radial fraction where DM particles can be found. Since the crust region has a tiny mass, we will not consider this refinement here (Cermeño et al. 2016b). For the parameterizations A, B, and C analyzed in this work this ratio takes values of, e.g., $\xi \in [0.03,\ 0.42]$ at $T \sim 1$ MeV, $\xi \in [0.007, 0.11]$ at $T \sim 0.1$ MeV and $\xi \in [0.003, 0.04]$ at $T \sim 0.01$ MeV. The volume where the dark emitting region resides shrinks as $\sim\sqrt{T}$.

As has been thoroughly studied, enhanced emissivities in the medium can have an impact on internal temperatures, temporal cooling sequence, and (un)gapped matter phases (Page & Reddy 2006; Page et al. 2013). In this regard, recent works (Page et al. 2011; Shternin et al. 2011) quote that the rapid cooling of the Cas A may be an indication of the existence of global neutron and proton superfluidity in the core. In addition, current observations of thermal relaxation of NS crusts indicates that even a small stellar volume fraction where fast neutrino emission reactions can take place would provide distinctive features. In detail, it has been shown (Brown et al. 2018) that even if there is a relatively small local volume where distortion from the standard energetic mechanisms is taking place inside the star, a fast neutrino reaction (Direct URCA) in a volume of ∼1% could explain the neutrino luminosities in the cooling curve of some particular objects like MXB 1659-29.

In the case presented in this work the long-term dark engine reaction $\chi\chi \rightarrow aa$ could provide emissivities $Q_E^{aa} \sim 4 \times 10^{22}\,{\rm erg\,cm^{-3}\,s^{-1}}$ for which the result is higher than that estimated for the $Q_{MX1659-29} \sim 1.7 \times 10^{21}\,{\rm erg\,cm^{-3}\,s^{-1}}$ for $T \sim 10^8$ K. The stellar volume affected in the annihilating DM mechanism is, nevertheless, much smaller for this range of temperatures but still providing the same powerful emission. Besides the process discussed in this work, other ones such as rotochemical heating (Fernández & Reisenegger 2005) or hot blobs located at different depths in the crust in young NS (Kaminker et al. 2014) have been also treated in the literature adding more sources of energetic variability based on SM matter.

It remains for further work to explore more exhaustively the precise relation between the model parameters m_χ, m_a, g_0, g_χ (and g_f) and the energetic efficiency of the emission. This will impact the duration of the dominance of such emission from DM annihilation over standard processes and thus its potential observability. We believe that the qualitatively different picture arising from the DM self-annihilation process inside NS may be worthwhile to explore.

4. Conclusions

We have calculated the energy emissivity of self-annihilating DM from an existing stellar distribution into final state SM fermions. A pseudoscalar-mediated DM interaction with the ordinary nucleon matter has been used. Later, as an astrophysically relevant case, we have particularized to neutrinos as final states, and we have considered in detail those produced from s-wave channels $\chi\chi \rightarrow \nu\nu$ or via pseudoscalar mediators p-wave $\chi\chi \rightarrow aa$, and subsequent decay $a \rightarrow \nu\nu$. In the inner stellar regions the radiation engine can encompass about $\lesssim$7% of the total stellar volume for $T \lesssim 10^{10}$ K and the energy emissivity can be enhanced by orders of magnitude compared to the MURCA standard neutrino processes for parameter sets respecting constraints of direct detection limits, cosmological bounds or even tighter rare meson decay bounds. We have provided a phenomenological fit of emissivities including dependence of temperature and DM particle number. Taking as reference the usual standard temporal sequence of NS cooling behavior, we expect that, for the models analyzed in this work, model C (with $m_\chi = 30$ GeV, $m_a = 1$ GeV) could be effectively active during the whole life of the star. Although a detailed solution of the full evolution equation is out of the scope of this work it is reasonable to foresee that the contribution of this new dark mechanism to the set of already known standard cooling reactions will drive the star into internal dynamical self-adjustment that is likely to emerge with a distinctive temperature sequence whose observability remains to be properly analyzed in future works.

We are thankful for useful discussions with J. Silk, J. Edsjö H. Grigorian, and C. Albertus. This work has been supported by PHAROS Cost action, MINECO Consolider-Ingenio Multidark CSD2009-00064, Junta de Castilla y León SA083P17 and FIS2015-65140-P projects. M.C. is supported by a fellowship from the University of Salamanca.

References

Aartsen, M. G., Ackermann, M., Adams, J., et al. 2017, EpJC, 77, 146
Abdullah, M., DiFranzo, A., Rajaraman, A., et al. 2014, PhRvD, 90, 035004
Ade, P. A. R., Aghanim, N., Arnaud, M., et al. [Planck Collaboration] 2016, A&A, 594, A13
Akerib, D. S., Alsum, S., Arajuo, H. M., et al. 2017, PhRvL, 118, 021303
Arina, C., Del Nobile, E., & Panci, P. 2015, PhRvL, 114, 011301
Baek, S., Ko, P., & Li, J. 2017, arXiv:1701.04131
Banerjee, S., Barducci, D., Bélanger, G., et al. 2017, JHEP, 1707, 080
Bauer, M., Haisch, U., & Kahlhoefer, F. 2017, arXiv:1701.07427
Belanger, G., Boudjema, F., Pukhov, A., & Semenov, A. 2010, arXiv:1005.4133v1
Bell, N. F., Cai, Y., Dent, J. B., Leane, R. K., & Weiler, T. J. 2017, PhRvD, 96, 023011
Bertone, G., & Hooper, D. 2016, arXiv:1605.04909v2
Bertone, G., Hooper, D., & Silk, J. 2005, PhR, 405, 279
Boehm, C., Dolan, M. J., McCabe, C., Spannowsky, M., & Wallace, C. J. 2014, JCAP, 1405, 009
Bringmann, T., Calore, F., Galea, A., & Garny, M. 2017, JHEP, 1709, 041
Brown, E. F., Cumming, A., Fattoyev, F. J., et al. 2018, PhRvL, 120, 182701
Buckley, M. R., Feld, D., & Gonçalves, D. 2015, PhRvD, 91, 015017
Cermeño, M., Perez-Garcia, M. A., & Silk, J. 2016a, PhRvD, 94, 023509
Cermeño, M., Perez-Garcia, M. A., & Silk, J. 2016b, PhRvD, 94, 063001
Cermeño, M., Pérez-García, M. A., & Silk, J. 2017, PASA, 34, e043
Cheng, H., & Chiang, C. 2012, JHEP, 07, 009
Chin, S. A. 1977, AnPhy, 108, 301
Chuzhoy, L. 2007, arXiv:0710.1856
de Lavallaz, A., & Fairbairn, M. 2010, PhRvD, 81, 123521

Dolan, M. J., Kahlhoefer, F., McCabe, C., & Schmidt-Hoberg, K. 2015, JHEP, 1503, 171
Esposito, S., Mangano, M., Miele, G., Picardi, I., & Pisanti, O. 2002, MPLA, 17, 491
Farzan, Y. 2003, PhRvD, 67, 073015
Fernández, R., & Reisenegger, A. 2005, ApJ, 625, 291
Freytsis, M., & Ligeti, Z. 2011, PhRvD, 83, 115009
Friman, B. L., & Maxwell, O. V. 1979, ApJ, 232, 541
Goldman, I., & Nussinov, S. 1989, PhRvD, 40, 3221
Goncalves, D., Machado, P. A. N., & No, J. M. 2017, PhRvD, 95, 055027
Gould, A. 1987, ApJ, 321, 571
Gresham, M., & Zurek, K. M. 2014, PhRvD, 89, 123521
Gusakov, M. E., Kaminker, A. D., Yakovlev, D. G., & Gnedin, O. Y. 2004, A&A, 423, 1063
Haber, H. E., & O'Neil, D. 2011, PhRvD, 83, 055017
Horowitz, C. J., & Perez-Garcia, M. A. 2003, PhRvC, 68, 025803
Ibarra, A., Totzauer, M., & Wild, S. 2013, JCAP, 12, 043
Ipek, S., McKeen, D., & Nelson, A. E. 2014, PhRvD, 90, 055021
Kaminker, A. D., Kaurov, A. A., Potekhin, A. Y., & Yakovlev, D. G. 2014, MNRAS, 442, 3484
Kavanagh, B. J. 2017, arXiv:1712.04901v3
Kouvaris, C. 2008, PhRvD, 77, 023006
Kouvaris, C., & Tinyakov, P. 2010, PhRvD, 82, 063531
Kouvaris, C., & Tinyakov, P. 2011, PhRvD, 83, 083512
Krauss, L. M., Srednicki, M., & Wilczek, F. 1986, PhRvD, 33, 2079
Lattimer, J. M., Pethick, C. J., Prakash, M., & Haensel, P. 1991, PhRvL, 66, 2701
MacDermott, S. D., Yu, H. B., & Zurek, K. M. 2012, PhRvD, 85, 023519
Mapelli, M., Ferrara, A., & Pierpaoli, E. 2006, MNRAS, 369, 1719
Matsui, T., & Serot, B. D. 1982, AnPhy, 144, 107
Page, D., Lattimer, J. M., Prakash, M., & Steiner, A. W. 2004, ApJ, 155 623
Page, D., Lattimer, J. M., Prakash, M., & Steiner, A. W. 2013, arXiv:1302.6626v2
Page, D., Prakash, M., Lattimer, J. M., & Steiner, A. W. 2011, PhRvL, 106, 081101
Page, D., & Reddy, S. 2006, ARNPS, 56, 327
Palomares-Ruiz, S., & Pascoli, S. 2008, PhRvD, 77, 025025
Perez-Garcia, M. A. 2010, EPJA, 44, 77
Perez-Garcia, M. A., & Silk, J. 2015, PhLB, 744, 13
Pons, J., Reddy, J., Prakash, M., Lattimer, J. M., & Miralles, J. A. 1999, ApJ, 513, 780
Rott, C., In, S., Kumar, J., & Yaylali, D. 2015, JCAP, 11, 039
Sedrakian, A. 2016, PhRvD, 93, 065044
Shternin, P. S., Yakovlev, D. G., Heinke, C. O., Ho, W. C. G., & Patnaude, D. J. 2011, MNRAS, 412, L108
Shternin, P. S., & Yakovlev, D. G. 2007, arXiv:0705.1963
Vigano, D., Rea, N., Pons, J. A., et al. 2013, MNRAS, 434, 123
Vincent, A. C., Scott, P., & Serenelli, A. 2015, PhRvL, 114, 081302
Wild, S. 2016, PhD thesis, Munich, Tech. U.
Yakovlev, D. G., & Levenfish, K. P. 1995, A&A, 297, 717
Yakovlev, D. G., Gnedin, O. Y., Gusakov, M. E., et al. 2005, NuPhA, 752, 590
Yuksel, H., & Beacom, J. F. 2007, PhRvD, 76, 083007
Zel'dovich, Y. B. 1965, ZhETF, 48, 986

Chapter 5

Gamma rays from dark mediators in white dwarfs

Resumen

En este trabajo se considera la autoaniquilación de DM, χ, en mediadores metaestables, Y, con su posterior decaimiento a fotones dentro de WDs. Nos centramos en reacciones del tipo $\chi\bar{\chi} \to$ YY, donde los mediadores, además de tener una vida media en reposo que verifica $\tau_{rest} \lesssim 1$ s, podrían sufrir pérdidas de energía en el medio antes de decaer a dos fotones, Y$\to \gamma\gamma$. Usando la aproximación de que la energía perdida por el mediador puede ser descrita de manera continua a través de las colisiones de éste con los núcleos del volumen estelar, hemos derivado las luminosidades internas teniendo en cuenta el efecto combinado de la atenuación y la vida media finita del mediador. Por último, hemos comparado las luminosidades con aquellas obtenidas a partir de medidas experimentales de WDs del cúmulo globular M4, obteniendo límites de exclusión para la vida media del mediador Y.

Gamma rays from dark mediators in white dwarfs

M. Cermeño[*] and M. A. Pérez-García[†]

Department of Fundamental Physics, University of Salamanca, Plaza de la Merced s/n, E-37008 Salamanca, Spain

(Received 9 July 2018; published 5 September 2018)

We consider self-annihilation of dark matter, χ, into metastable mediators, Y, and their subsequent decay into photons inside white dwarfs. We focus on reactions of the type $\chi\bar{\chi} \to YY$, where mediators, besides having a finite decay lifetime at rest $\tau_{\rm rest} \lesssim 1$ s, may suffer energy loss in the medium before they decay into photons, $Y \to \gamma\gamma$. We obtain attenuated gamma-ray luminosities arising from the combination of both effects. Using complementary sets of astrophysical measurements from cold white dwarfs in the M4 globular cluster as well as direct and indirect dark matter searches, we discuss further constraints on dark mediator lifetimes.

DOI: 10.1103/PhysRevD.98.063002

I. INTRODUCTION

Dark matter (DM) accumulation sites can provide a valid strategy to potentially identify hints of DM proper existence as well as its nature and properties. In particular, one could think of the concentration of this type of matter inside astrophysical bodies as a consequence of gravitational interaction and, provided suitable ranges of masses and cross sections, thermalization with ordinary—baryonic—matter constituting these objects. Effects such as self-annihilation and coannihilation with a different species or decay have been exhaustively studied as possible multimessenger signatures taking place in the Sun, planets, main sequence stars, and more compact objects like white dwarfs or even neutron stars [1–11].

Regarding DM itself, beyond standard model (BSM) candidates have flourished in the literature over the past decades. For a review, see, e.g., [12]. Some of them are now well constrained from the coordinated effort of different communities focusing on direct, indirect, and collider searches [13]. One of the currently accepted possible realizations considers that DM could generate a relic density via annihilation into so-called dark mediators and subsequent SM particles. These types of models are also referred to as "secluded" in the sense that DM dramatically reduces its couplings to SM states by an intermediate state, a decaying mediator, Y. Examples in the literature include coupling strengths ranging from weakly interacting DM particles [14] to strongly interacting ones [15]. According to the duration of a lifetime for these metastable particles, there is a further division among short-lived or long-lived mediators, each giving rise to dramatic differences in the predicted indirect signal [16,17]. Annihilation of DM into two generic different mediators $\chi\bar{\chi} \to M_1 M_2$ can take place in the s- or p-wave scheme, depending on the Lorentz structure of the DM-mediator interactions [18]. There are some works that have focused on particular realizations of these secluded models [19].

Indirect signals from DM could also be expected from the possibility of annihilation through long-lived mediators into gamma rays in astrophysical environments, the Galactic center, dwarf spheroidals, the CMB [14,20–22], and also into neutrinos [23,24]. From the experimental side, current DM searches are actively constraining the available mass and DM-nucleon cross-section, $m_\chi - \sigma_{\chi,N}$, phase space. Efforts include those from colliders like, e.g., Belle [25] or LHC [19]. Regarding indirect searches [26] in the neutrino channel, secluded DM models have been constrained by ANTARES [27], while in the gamma rays relevant searches are performed by Fermi, H.E.S.S., and AMS Collaborations [28].

On general grounds, considering dark metastable mediators enriches the picture by which DM interacts with ordinary SM matter. The main characteristic in this scenario comes from the fact that these particles have a finite lifetime. While short-lived mediators would be essentially indistinguishable in most of the searches from models where DM is not secluded, long-lived mediators allow an injection of SM states not directly related to places with enhanced DM density. Therefore, it could produce detectable signals far from the production site. Besides, this mechanism has been quoted [22] to introduce anisotropies

[*] marinacgavilan@usal.es
[†] mperezga@usal.es

of prompt species—positrons and photons—produced in the decays of long-lived mediators. Popular mediators such as the dark photon or the dark Higgs have been featured in a number of recently proposed dark sector models [29] although several model-independent DM scenarios also feature long-lived particles [30].

In this work, we consider the annihilation of light DM particles inside white dwarfs (WDs). We restrict our interest to dark candidates in the sub-GeV mass range as they can probe some particularly interesting astrophysical scenarios [31]. Recent constraints show a window for masses $m_\chi \lesssim 1$ GeV and $\chi - N$ cross sections $\sigma_{\chi,N} \lesssim 10^{-29}$ cm^2 (see Fig. 6 in [32]). Electrons are also relevant species inside WDs. However, their scattering cross section with sub-GeV DM is typically much smaller than that of nucleons [33] (less than $\sim 10^{-38}$ cm^2 for thermal DM when form factors do not play a role). Let us emphasize at this point that since the mass range beyond a few GeV is nowadays better probed, the less constrained light mass phase space seems the next interesting region to explore [34] with proposals allowing strongly interacting candidates (SIMPs) as recently described in [35].

The astrophysical scenario we consider is that of a WD where DM particles annihilate inside the stellar medium so that the metastable mediators produced in the reaction $\chi\bar{\chi} \to YY$ can lose energy while propagating (on-shell) outwards. Eventually, they will decay into photons, $Y \to \gamma\gamma$, either inside or outside the star, as this is governed by their energy-dependent lifetime and dissipation. White dwarfs are compact stars made mostly of carbon and oxygen and formed at the end of the lifetime of main sequence stars with masses up to $\sim 8 M_\odot$. They represent around ∼95% of all the stars in our Galaxy. It is believed that a fraction up to 20% may harbor magnetic fields with a strength up to several hundred MG. Since, at their final stages, no fusion reactions can happen in their interior, they are supported by electron pressure. Typical masses range $M_{\rm WD} \sim (0.3\text{–}1) M_\odot$ and radii $R_{\rm WD} \sim (0.01\text{–}0.03) R_\odot$. Thus, these stars are essentially cold, with effective temperatures $T \sim 10^3$–10^4 K, and dense enough $\rho \sim 10^4$–10^7 g/cm^3 so that density effects cannot be neglected. In order to avoid many of the limitations set by particular model settings, we will consider a generic scenario of annihilating fermionic DM into photons via dark mediators making a minimal set of assumptions. Depending on how long or short-lived these mediators are and the importance of dissipation, we will show how gamma ray emission and luminosities from WDs can end up being attenuated. For example, if the mediator lifetime is large enough, it could decay outside the stellar radius modifying the expected energy flux value with respect to that arising from decay in central regions. In this scenario, medium effects have to be dealt with as, generically, a mediator will loose energy when passing through the ordinary matter, provided the decay length, λ_D, is larger than the interaction length, λ_I. These boosted mediators will be produced with initial velocity, $v_{Y,0}$, that will be attenuated while propagating inside the star, thus affecting their survival probability and the energy deposited by them at the decaying site. However, let us emphasize that for less dense stellar bodies such as the sun or planets, average densities are less than $\sim 10^2$ g/cm^3, thus much lower than central densities in WDs and dissipation effects are less important.

The paper is structured as follows. In Sec. II, we describe the DM annihilation into dark mediators as well as particle energy losses inside the WD scenario. We calculate the survival probabilities for mediators with energy dependent lifetimes, their spectrum and the associated photon luminosities. In Sec. III, we show results concerning gamma-ray luminosities comparing to those for cold WDs in M4 globular cluster (GC) and further discuss possible constraints on dark mediator lifetimes. Finally, in Sec. IV, we conclude.

II. DARK MEDIATORS AND IN-MEDIUM INTERACTION

In this section, we describe the process where the photon emission arises from DM annihilation via dark mediators. We consider fermionic dark matter particles, χ, that annihilate into metastable mediators, Y, through reactions $\chi\chi \to YY$ with subsequent decay $Y \to 2\gamma$. Additional reactions from radiative emission processes or three body decay of mediators [36] induce small corrections, including anisotropies [22] that we will not consider here. It is well known that considering DM candidates not restricted to weakly interacting particles introduces the possibility that they could undergo self-interactions with 3-to-2 or 4-to-2 annihilations [15,37]; however, we expect our results will not be qualitatively modified as stellar DM densities remain small.

The metastable mediator has a lifetime at rest that can be related to its decay width as $\tau_{\rm rest} = \Gamma_Y^{-1}$ (we use $\hbar = c = 1$). As initially created in the boosted $2 \to 2$ process, they possess a Lorentz factor $\gamma_{Y,0} = \frac{1}{\sqrt{1-v_{Y,0}^2}} = m_\chi/m_Y$. In the stellar environment, the mediator will, in principle, interact with the medium decreasing its energy and velocity, v_Y, from initial values. Attenuation of dark candidates has been considered as a source of DM depletion on terrestrial detectors [38,39]. This stopping power is a crucial aspect that could largely impact the energetic yields of annihilation processes in a medium.

From the accumulated DM present inside the WD, dark mediators are produced from the two-body annihilation reaction $\chi\bar{\chi} \to YY$. Regarding the kinematics of the dark mediator propagation, we will use a radial treatment inside the star for the light DM mass range and (relatively) strong interacting cross sections motivated by previous findings of small-deflection angle approximation [38]. In the medium, they may suffer from interaction with ordinary matter

composed of nuclei and a gas of electrons. Such a possibility is realized when they live long enough to experience the scattering processes we consider, e.g., if their decay length λ_D is larger than the interaction length, $\lambda_I \sim \frac{1}{\sigma_{Y,i} n_i}$. n_i is the number density of scattering centers of ith-type in the stellar volume (nuclei of baryonic number A end electrons) and $\sigma_{Y,i}$ is the scattering cross section describing mediator interactions with those matter constituents. Besides, the possible interaction with electrons $\sigma_{Y,e}$ is unknown but we take it to be bounded by that of DM, i.e., $\sigma_{Y,e} \lesssim \sigma_{\chi,e}$ according to experimental constraints [33]. In the situation where scattering of DM with electrons is less frequent than for nuclei $\lambda_{\chi,e} > \lambda_{\chi,A}$ or, equivalently, $\sigma_{\chi,e} \lesssim 2A\sigma_{\chi,N}$, the effect of electrons can be safely neglected in the sub-GeV mass range. In this work, we will constrain all decaying mediators to have rest lifetimes $\tau_{\rm rest} < 1s$ to evade nucleosynthesis constraints [40].

As mentioned, inside the WD, we assume that a fraction of DM is present. The population number of DM particles inside the star, N_χ, will be the result of several processes. On one hand, the capture rate, $\Gamma_{\rm capt}$, collecting particles by gravitational capture from an existing galactic DM distribution. It is indeed expected at early ages for the star from the hydrogen dominated era, during the main sequence, and later, in the more compact configuration [5,41]. On the other hand, there are other processes yielding the opposite effect, such as annihilation and evaporation, each with a definite rate $\Gamma_{\rm ann}$, $\Gamma_{\rm evap}$, respectively. See, e.g., [42–45]. Let us emphasize that the strength of the possible (indirect) gamma ray signal is to be directly related to the amount of DM that the star is able to capture and retain.

During the WD stage the DM capture rate can be written [46,47] as

$$\Gamma_{\rm capt} = \frac{\sqrt{24\pi} G \rho_\chi M_{\rm WD} R_{\rm WD}}{m_\chi \bar{v}} f_{\chi,A} \left[1 - \frac{1 - e^{-B^2}}{B^2}\right], \quad (1)$$

where G is the gravitational constant, $M_{\rm WD}$ and $R_{\rm WD}$ are the WD mass and radius, ρ_χ is the local DM density, m_χ is the DM particle mass and $\bar{v}$ is the velocity dispersion between the DM particle and the WD. $f_{\chi,A}$ is the fraction of DM particles that undergo one or more scatterings with a nucleus of mass m_A and baryonic number A while inside the star. In our work, we set $A \sim 14$ to account for a mixed C-O composition. $f_{\chi,A}$ saturates to unity when it is larger than a typical scale $\sigma_{\rm sat} = \frac{\pi R_{\rm WD}^2 m_A}{M_{\rm WD}}$, known as geometrical cross section. Thus $f_{\chi,A} \sim 1$, if $\sigma_{\chi,A} \gtrsim \sigma_{\rm sat}$, where $\sigma_{\chi,A} \simeq A^2 \sigma_{\chi,N}$ is the DM-nucleus cross section [48–51], expressed in terms of the DM-nucleon cross section, $\sigma_{\chi,N}$. Otherwise, $f_{\chi,A} \sim \frac{\sigma_{\chi,A}}{\sigma_{\rm sat}}$. Finally, the bracketed term accounts for DM that scatters but it is not captured in the WD, being

$$B^2 = \frac{6 m_\chi v_{\rm esc}^2}{m_A \bar{v}^2 (\frac{m_\chi}{m_A} - 1)^2}, \quad (2)$$

and

$$v_{\rm esc} = \sqrt{\frac{2GM_{\rm WD}}{R_{\rm WD}}}, \quad (3)$$

the escape velocity.

Additional decay or even coannihilation with a different species could be possible but, for the sake of brevity, we will not consider those channels here. We assume no DM self-interaction exists. In order to check the consistency of our argument neglecting evaporation for light DM, we can estimate the limiting evaporation mass by demanding that the typical DM particle velocity, $v \sim \sqrt{\frac{T_c}{m_\chi}}$, at the WD central temperature, T_c, be less than the local escape velocity of the star, $v_{\rm esc}$. Thus, the evaporation mass value will somewhat depend on the thermodynamical properties of the star considered. For the WD masses $M_{\rm WD} \in [0.2M_\odot, 0.95M_\odot]$ and radii $R_{\rm WD} \in [1.2810^{-2}R_\odot, 2.1510^{-2}R_\odot]$, evaporation mass limits attain values $m_{\chi,\rm evap} \sim \frac{T_c}{v_{\rm esc}^2} \sim 2$ MeV when we set $T_c \sim 10^6$ K. The corresponding set of WD masses and radii have been obtained using the Lane-Emden solution for the nonrelativistic polytropic equation of state with $n = 3/2$ [52]. Inside WDs, mass density can be reasonably taken as a slowly variating radial function, approximately equal to the central density $\rho(r) \sim \rho_c$. In our case, the specific central density value range we use to obtain the selected $M_{\rm WD} - R_{\rm WD}$ parameter space is $\rho_c \in [1.66\times10^5, 3.78\times10^6]\,{\rm g/cm^3}$.

As explained, in the range of χ masses, we will consider, well above evaporation limits, the number of DM particles in the WD is obtained by solving the differential equation,

$$\frac{dN_\chi}{dt} = \Gamma_{\rm capt} - 2\Gamma_{\rm ann}, \quad (4)$$

where

$$\Gamma_{\rm ann} = \frac{1}{2}\int d^3\vec{r} n_\chi^2(\vec{r}) \langle\sigma_a v\rangle = \frac{1}{2} C_a N_\chi^2, \quad (5)$$

and $\langle\sigma_a v\rangle$ is the annihilation cross section averaged over the initial DM states and $n_\chi(\vec{r})$ is the DM number density inside the star, which verifies $\int d^3\vec{r} n_\chi(\vec{r}) = N_\chi$ at a given time. For simplicity, the $\langle\sigma_a v\rangle$ will be taken in what follows as that of a wimp-like candidate $\langle\sigma_a v\rangle \sim 10^{-26}$ cm^3/s but this parameter will indeed depend on the interacting nature of the DM candidate and will discuss later on its impact in our calculation. In particular, this value will assure that during the typical WD lifetime of ~Gyr, DM can effectively thermalize in the interior of the star. In such a case, the DM particle number density can be cast under a Gaussian form,

$$n_\chi(r) = n_{0,\chi} e^{-\left(\frac{r}{r_{\rm th}}\right)^2}, \tag{6}$$

where $n_{0,\chi}$ is the central number particle density value and the thermal radius is given [47,53] by

$$r_{\rm th} = \sqrt{\frac{9T}{8\pi G \rho_c m_\chi}}. \tag{7}$$

Using this expression, we can find an explicit form for $C_a \sim \langle \sigma_a v \rangle / r_{\rm th}^3$ in Eq. (5). Finally, solving Eq. (4), it is found that $\Gamma_{\rm ann} \simeq \frac{\Gamma_{\rm capt}}{2}$ for times much larger than the typical equilibrium time scale $\tau_{\rm eq} = 1/\sqrt{\Gamma_{\rm capt} C_a}$.

A. Dark mediator attenuation

In this paper, we are interested in the detectable signature of a mechanism of DM annihilation through dark mediators that subsequently decay to a photon pair, and its impact on the gamma ray luminosity and flux.

In [54], expressions for solar photon energy flux due to DM annihilation with free-streaming mediators were given

$$E_\gamma^2 \frac{d\Phi}{dE_\gamma} = \frac{\Gamma_{\rm ann}}{4\pi d^2} E_\gamma^2 \frac{dN_\gamma}{dE_\gamma} P^Y_{\rm d,out}, \tag{8}$$

where $P^Y_{\rm d,out}$ is the probability that the mediator decays at a distance d outside the WD. In what follows, we explain for our different scenario how we include attenuation and decay effects, as they are not explicitly reflected in Eq. (8). The energy spectrum in the decay process $Y \to \gamma\gamma$ is given by a box-type shape

$$\frac{dN_\gamma}{dE_\gamma} = \frac{4}{\Delta E} \Theta(E_\gamma - E_-)\Theta(E_+ - E_\gamma), \tag{9}$$

as described in [55,56], with $\Delta E = E_+ - E_-$ and

$$E_\pm = \frac{1}{\gamma_Y} \frac{m_Y}{2} (1 \mp v_Y)^{-1}. \tag{10}$$

In this last expression, the mediator velocity can be written as

$$v_Y = \frac{p_Y}{E_Y}, \tag{11}$$

where m_Y, p_Y, and E_Y are the mass, momentum modulus, and energy of the mediator in the medium, respectively. Note that each of the four photons emitted per annihilation has a monochromatic energy in the rest frame of the mediator,

$$E_{\gamma,\rm rest} = \frac{m_Y}{2}. \tag{12}$$

Therefore, in the laboratory frame, where DM particles move nonrelativistically, the photon energy can be written as

$$E_\gamma = \frac{1}{\gamma_Y} E_{\gamma,\rm rest} (1 - v_Y \cos\theta)^{-1}, \tag{13}$$

and, since the mediator decays isotropically, the resulting energy spectrum presents a box-shaped structure with a photon energy $E_\gamma \in [E_-, E_+]$ as obtained in Eq. (9).

In order to consider the fact that the mediator may suffer energy attenuation when passing through the medium, we consider that both momentum and energy will depend on the distance to the center of the star r, thus $p_Y \equiv p_Y(r)$ and $E_Y \equiv E_Y(r)$. It is important to remark here that, for the stellar conditions under inspection, $r_{\rm th} \ll R_{\rm WD}$ and, therefore, we will approximate DM particles annihilate at $r \sim 0$.

Under these circumstances when the mediator particle is created in the boosted scenario, we have, initially, the momentum modulus $p_{0,Y} = \sqrt{m_\chi^2 - m_Y^2}$. Later, when the mediator interacts inside the WD, it suffers a number of elastic scatterings that could be approximated as a continuous energy-loss with a small-deflection angle [3,38,39]. It is, therefore, reasonable to write the fractional momentum loss in terms of the variation of the mediator momentum prior to the interaction using a coefficient, $q \sim (m_A - m_Y)/m_A$ with $0 < q < 1$ parametrizing the collision so that when the Y particle has traveled a distance r,

$$\frac{dp_Y}{dr} = \frac{\Delta p_Y}{\lambda_I} = \frac{-(1-q)p_Y}{\lambda_I}, \tag{14}$$

where $\lambda_{\rm I} = \frac{1}{\sigma_{Y,A} n(r)}$, $\sigma_{Y,A}$ is the nucleus-mediator cross section. Assuming that the main contribution to the cross section of nuclei comes from the coherent enhancement of the spin-independent cross section, we can further consider $\sigma_{Y,A} = A^2 \sigma_{Y,N}$, being $\sigma_{Y,N}$ the nucleon-mediator cross section. At this point, we must note that while the DM-nucleon cross section is much constrained from current direct searches, it is scarcely tested for mediators. We will assume in what follows that due to the secluded nature of these type of DM mediators they will couple to nucleons with less (or up to the same) strength as compared to DM particles $\sigma_{Y,N} \sim (10^{-3} - 1)\sigma_{\chi,N}$.

We denote $n(r) = \frac{\rho_c}{A m_N} \int_0^r \omega(r')^{\frac{3}{2}} dr'$ the number density of nuclei in the stellar profile. Since the supporting pressure in the WD is provided by the degenerate electron fraction to obtain $n(r)$, we use a polytropic approach to the equation of state and approximate the analytic solution of the Lane-Emden equation with a polytropic index $n = \frac{3}{2}$ following [52] as

$$\omega(r) = -\alpha(1+B_{3/2}\xi^2)^{-2} + (1+\alpha)\left(1+\frac{1}{12}\xi^2\right)^{-2} + \frac{\alpha}{6}\xi^2\left(1+\frac{1}{12}\xi^2\right)^{-3} + \frac{4.6\times10^{-4}\xi^3}{(1+1.1\times10^{-3}\xi^2)^2}, \tag{15}$$

with $\xi = \frac{r}{a}$, $a^2 = \frac{5K}{8\pi G}\rho_c^{\frac{-1}{3}}$ and $K = P_c/\rho_c^{\frac{5}{3}}$, given the central density and pressure values ρ_c, $P_c = \frac{(3\pi^2)^{\frac{2}{3}}}{5m_e}[(\frac{Z}{A}\frac{\rho_c}{m_N})]^{\frac{5}{3}}$, respectively. m_e, m_N are the electron and nucleon masses. Using the prescribed fit with $\alpha = 0.481$, $B_{3/2} = \frac{18}{5}(\frac{4\alpha}{4+5\alpha})^4$, one can obtain a convenient approximation for the full numerical solution with an accuracy of 1%. Integrating Eq. (14), we obtain

$$p_Y(r) = \sqrt{m_\chi^2 - m_Y^2}\, e^{\frac{-(1-q)A\sigma_{Y,N}\rho_c}{m_N}\int_0^r \omega(r')^{\frac{3}{2}}dr'}, \tag{16}$$

and, accordingly, the radial dependent energy is given by $E_Y(r) = \sqrt{p_Y(r)^2 + m_Y^2}$. From this expression, it is clear that the energy spectrum, $E_\gamma^2\frac{dN_\gamma}{dE_\gamma}$, will be attenuated with radial distance from the production site inside the star.

In Fig. 1, we show the dark mediator attenuation from initial velocity $v_{Y,0} = \frac{\sqrt{m_\chi^2 - m_Y^2}}{m_\chi}$ as a function of the distance inside the WD for $m_\chi = 500$ MeV and $m_Y = 10$ MeV. We consider $\sigma_{Y,N} = \sigma_{\chi,N} = 10^{-38}$, 10^{-39}, 10^{-40} cm^2 depicted with dot-dashed, dotted, and dashed lines, respectively. The WD configuration corresponds to $\rho_c = 3.776\times10^6$ g/cm^3 and $R_{\rm WD} = 1.2810^{-2}R_\odot$, $M_{\rm WD} = 0.95\,M_\odot$. In order to emphasize the effect, we have imposed $\sigma_{Y,N} = \sigma_{\chi,N}$, but we will discuss later this dependence.

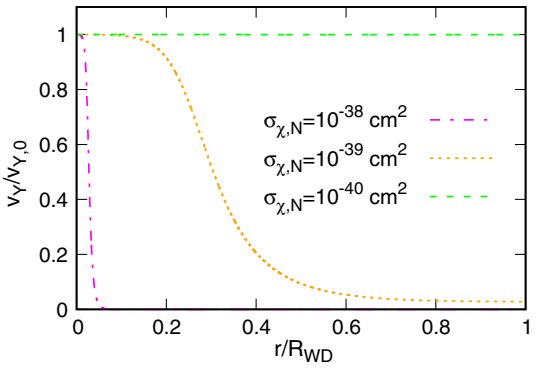

FIG. 1. In-medium dark mediator velocity as a function of the radial distance inside the WD for $m_\chi = 500$ MeV and $m_Y = 10$ MeV. We fixed $\sigma_{Y,N} = \sigma_{\chi,N} = 10^{-38}, 10^{-39}, 10^{-40}$ cm^2 with dot-dashed, dotted and dashed lines, respectively. See text for details.

B. Photon luminosity from dark decay

The equation which governs the decay probability density of the mediator inside the star can be written as

$$\frac{dP_{\rm dec}}{dr} = \frac{-P_{\rm dec}}{\gamma_Y\tau_{\rm rest}} = \frac{-P_{\rm dec}m_Y}{\tau_{\rm rest}E_Y(r)}, \tag{17}$$

where the relativistic decay length $\tau = \gamma_Y\tau_{\rm rest}$.

The decay probability must fulfill the normalization condition $\int_0^\infty P_{\rm dec}dr = 1$. Explicitly,

$$N\int_0^\infty e^{-\int_0^r \frac{m_Y dr'}{\tau_{\rm rest}E_Y(r')}}dr = 1, \tag{18}$$

where N is a normalization constant. Beyond the stellar radius, we will be assuming no energy losses such that the mediator will not be further attenuated and its energy remains quenched $E_Y(r) = E_Y(R_{\rm WD})$, $r > R_{\rm WD}$. If further scattering with an external agent was introduced an additional attenuation would arise [57]. For the sake of clarity we will not consider that refinement here.

From the integration in Eq. (18), we can obtain the actual form for the probability $P_{\rm dec,d>R_{WD}} \equiv P^Y_{\rm d,out}$ that the mediator decays outside the star, between $R_{\rm WD}$ and a generic distance $d > R_{\rm WD}$

$$P_{\rm dec,d>R_{WD}} = \int_{R_{\rm WD}}^d Ne^{-\int_0^r \frac{m_Y dr'}{\tau_{\rm rest}E_Y(R_{\rm WD})}}dr, \tag{19}$$

or explicitly,

$$P^Y_{\rm d,out} = \mathcal{P}\left(1 - e^{-\frac{m_Y(d-R_{\rm WD})}{\tau_{\rm rest}E_Y(R_{\rm WD})}}\right), \tag{20}$$

where we have used

$$\mathcal{P} = \frac{N\tau_{\rm rest}E_Y(R_{\rm WD})}{m_Y}e^{-\frac{m_Y R_{\rm WD}}{\tau_{\rm rest}E_Y(R_{\rm WD})}}. \tag{21}$$

On the other hand, the probability of decay $Y \to \gamma\gamma$ inside the WD ($r < R_{\rm WD}$) weighted with the position dependent spectrum in Eq. (9) will allow to obtain the photon luminosities deposited inside the stellar volume and extract valuable information of the strength of attenuation in the stellar medium.

The internal luminosity due to annihilation of DM particles into photons through dark mediators inside the stellar volume can be thus written as

$$L_\chi = \Gamma_{\rm ann}\int_0^{R_{\rm WD}} Ne^{-\int_0^r \frac{m_Y dr'}{\tau_{\rm rest}E_Y(r')}}\left[\int_{E_-(r)}^{E_+(r)} E_\gamma\frac{dN_\gamma(r)}{dE_\gamma}dE_\gamma\right]dr, \tag{22}$$

where now dependencies are made explicit. On one hand, the dependence on the radial coordinate of the energy

spectrum of photons produced inside the WD as a result of the finite lifetime of the mediators and, on the other hand, the medium interaction of the mediators from the spatially dependent limiting values in the energy interval, $E_{\pm}(r)$. When $\sigma_{Y,N} \to 0$, we recover the case $p_Y(r) = p_{Y,0}$ where no attenuation is present.

III. RESULTS

In this section, we analyze the results obtained for the photon luminosity and flux to compare with existing experimental measurements of the coldest WDs. By comparing the expected internal warming due to the dark mediator in-medium decay, one could obtain some constraints to the lifetime of the mediator in the scenario considered. In order to maximize the possible DM effects in the stellar warming, we consider those WDs present in the M4 GC [58] where, in line with [6], we assume a DM density $\rho_\chi = 2660\rho_{\chi,0}$, being $\rho_{\chi,0} = 0.3$ GeV cm^{-3} the solar-circle value, usually taken as reference in our Galactic DM distribution. The quoted value in M4 GC refers to the density at the largest radius where the WD data are observed [2,6], having a velocity dispersion of $\bar{v} = 20$ km/s. It is important to mention that in this GC the age of the WDs is set to $t = 12.7 \pm 0.7$ Gyr [59], so that the assumption that the DM particles which have some impact on the luminosity through annihilation are those which are captured in the WD stage seems a reasonable hypothesis. Along the same lines, it is clear that at this age $t > \tau_{\rm eq}$ and they are indeed thermalized.

In Fig. 2, we show the energy flux due to annihilation of DM with $m_\chi = 800$ MeV and $m_Y = 100$ MeV as a function of the photon energy at distance $d = 2R$ for a WD with mass $M_{\rm WD} = 0.28\ M_\odot$ and radius $R_{\rm WD} = 0.04 R_\odot$ and normalized to the product $2\Gamma_{\rm ann} m_\chi$. We consider two different values of $\tau_{\rm rest} = 0.8$ s (solid lines) and $\tau_{\rm rest} = 0.1$ s (dashed lines) and $\sigma_{\chi,N} = 10^{-39}$ cm^2 (green) and $\sigma_{\chi,N} = 5 \times 10^{-39}$ cm^2 (magenta). We assume $\sigma_{\chi,N} = \sigma_{Y,N}$ and $q = 0.5$. The case where more attenuation is obtained is that of the larger cross section where the available energy window for photoproduction is small and centered about $E_\gamma = m_Y/2$. For the considered cases it is fulfilled that $\lambda_D > 2R$ and as $\tau_{\rm rest}$ grows the flux obtained is smaller since less mediators have been able to decay into photons at the radial distance $2R$. Let us note at this point that, in principle, some modulating geometrical factors would be needed in order to precisely account for decays from mediators beyond stellar radius. As we will see later, since most lifetime values allowed are in the region $\tau > 0.1$ s, around one order of magnitude larger than the typical WD radius, we expect this approximate treatment not to substantially change our conclusions.

In Fig. 3, we show the WD internal luminosity, i.e., energy per unit time deposited inside the stellar volume, due to the annihilation of DM as a function of the WD mass for $m_\chi = 500$ MeV and $m_Y = 375$ MeV (solid lines) and $m_Y = 10$ MeV (dash-dotted lines). We set different lifetimes $\tau_{\rm rest} = 0.001$, 0.01, 0.1, 1 s. We fix $\sigma_{\chi,N} = \sigma_{Y,N} = 10^{-39}$ cm^2 and $q = 0.5$. We can see that the more similar to the DM particle mass, m_χ, the mediator mass, m_Y, is, the higher the luminosity is. This happens because the mediator is produced almost at rest and it is equivalent to a prompt photoproduction (there is no energy attenuation for the mediator). Moreover, the luminosity decreases when $\tau_{\rm rest}$ increases due to the fact that the higher $\tau_{\rm rest}$ is, the smaller the probability of decaying inside the object. It is clear from the figure that we can exclude sets of parameters that yield an internal luminosity L_χ higher than that experimentally

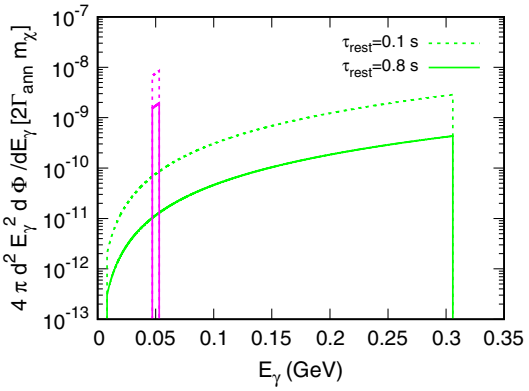

FIG. 2. Energy flux at distance $d = 2R$ due to DM annihilation as a function of the photon energy for different values of $\tau_{\rm rest} = 0.8$ s (solid lines) and $\tau_{\rm rest} = 0.1$ s (dashed lines). It is normalized to the product $2\Gamma_{\rm ann} m_\chi$. We consider two values for the $\sigma_{\chi,N} = 10^{-39}$ cm^2 (green) and $\sigma_{\chi,N} = 5 \times 10^{-39}$ cm^2 (magenta). We assume $\sigma_{\chi,N} = \sigma_{Y,N}$ and fix $m_\chi = 800$ MeV and $m_Y = 100$ MeV. See text for details.

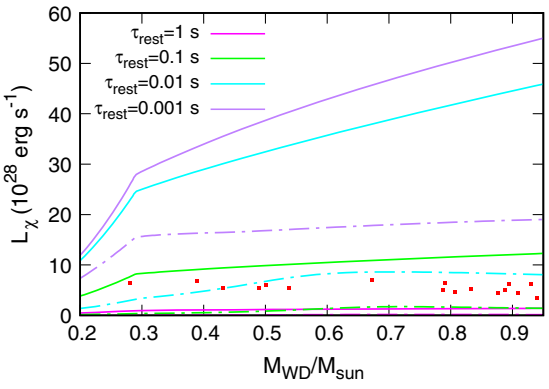

FIG. 3. WD internal luminosity due to DM annihilation as a function of the WD mass for different values of $\tau_{\rm rest} = 0.001$, 0.01, 0.1, 1 s using $m_\chi = 500$ MeV and mediator masses, $m_Y = 375$ MeV (solid lines) and $m_Y = 10$ MeV (dash-dotted lines). We fixed $\sigma_{\chi,N} = \sigma_{Y,N} = 10^{-39}$ cm^2. Red points are experimental data for M4 GC from [6].

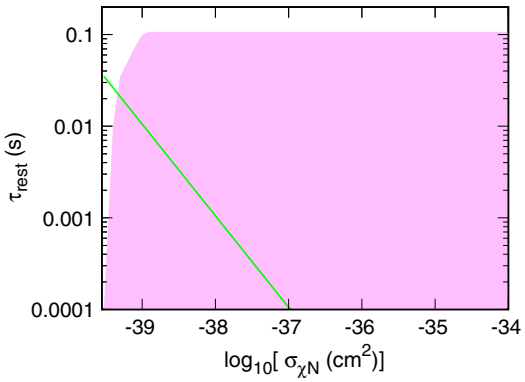

FIG. 4. Constraints for the mediator lifetime as a function of DM-nucleon cross section for the case $m_Y/m_\chi \to 1$. We fixed $\sigma_{\chi,N} = \sigma_{Y,N}$. Colored region depicts the excluded parameter space, see the text for more details. Green line is a lower limit signaling where the mediator scatters at least once in the WD.

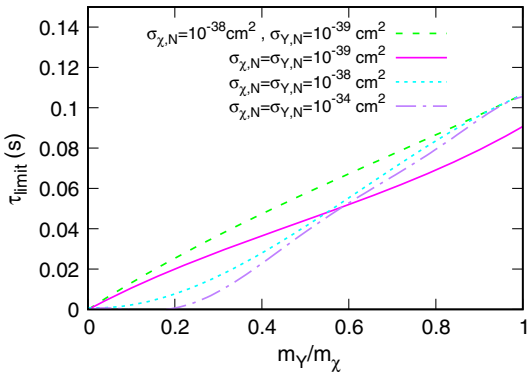

FIG. 5. $\tau_{\rm limit}$ (boundary of excluded $\tau_{\rm rest}$ region) as a function of the ratio m_Y/m_χ for different values of $\sigma_{\chi,N}$,$\sigma_{Y,N}$. See text for details.

extracted for WDs in M4 GC (red points as given by [6]). In other words, for fixed values of m_χ, m_Y and $\sigma_{\chi,N}$ (that is fixed to be equal to $\sigma_{Y,N}$) there will be a limiting lower value of $\tau_{\rm rest}$ below which the luminosity would be higher than that deduced from experimental data.

In order to analyze these specific constraints, we plot in Fig. 4, the excluded values of $\tau_{\rm rest}$ (colored region) as a function of the logarithm (base 10) of $\sigma_{\chi,N}$ for $m_Y/m_\chi \to 1$. Being conservative, we exclude values of $\tau_{\rm rest}$ which provide luminosities beyond a 50% tolerance for the complete set of all experimental data, i.e., $L_\chi > 1.5 L_{\rm exp}$. We fix this error band since experimentally deduced luminosities for WDs are accurate only to the first or second significant figures. Incidentally, this happens for luminosities above 50% of the value for the first experimental data point considered in the series ($M_{\rm WD} = 0.28\ M_\odot$, $R_{\rm WD} = 2.7 \times 10^9$ cm for $\rho \sim 3.3 \times 10^5$ g/cm^3). On this plot we show the boundary of the colored region, whose physical meaning is that of the minimum value of $\tau_{\rm rest}$ below which lifetimes for a decaying mediator produced at rest are not allowed for a given $\sigma_{\chi,N}$. In this case, since the mediator decays at rest, it does not suffer attenuation so that there is no dependence on $\sigma_{Y,N}$. As it is obtained, it is indeed a lower limit of allowed $\tau_{\rm rest}$ independent on m_χ, m_Y, and $\sigma_{Y,N}$. Besides, the green line indicates the corresponding Y-lifetime where $\tau_{\rm rest} = \lambda_{Y,A}$, i.e., the value for which at least one scattering between the mediator Y and a nucleus A inside the WD will take place, assuming $\sigma_{Y,N} = \sigma_{\chi,N}$. Below this limiting value situation is equivalent to that with no energy losses. In the figure, it is shown that for saturated values of the capture rate in the WD, i.e., $\sigma_{\chi,N} > \sigma_{\rm sat} = 1.1 \times 10^{-39}$ cm^2 there is no further change in the limiting value of $\tau_{\rm rest}$. We refer to this as $\tau_{\rm limit}$. For smaller values $\sigma_{\chi,N} < \sigma_{\rm sat}$ there is a quenching of $\tau_{\rm limit}$ as smaller values of $\tau_{\rm rest}$ are not excluded from luminosity constraints. We expect that our results could be, in principle, extended up to $\sigma_{\chi,N} \sim 10^{-29}$ cm^2 covering the targeted region in the phase space for sub-GeV DM as we comment in the Introduction. In other more general cases, for a fixed value of $\sigma_{\chi,N}$ and given m_χ, m_Y the maximum excluded value of τ_{rest}, $\tau_{\rm limit}$, will be lower than that obtained in the extreme $m_Y \sim m_\chi$ case. In other words, the most restrictive $\tau_{\rm rest}$ limit would be that in which is independent on $\sigma_{Y,N}$ and m_χ, m_Y.

In Fig. 5, $\tau_{\rm limit}$ (boundary of the excluded region for $\tau_{\rm rest}$) is shown as a function of the ratio m_Y/m_χ for different values of $\sigma_{\chi,N}$, $\sigma_{Y,N}$. In these cases, when $m_Y/m_\chi \neq 1$, there is effective contribution from energy attenuation and decay effects. We fixed $\sigma_{\chi,N} = \sigma_{Y,N} = 10^{-39}$ cm^2 (solid lines), $\sigma_{\chi,N} = \sigma_{Y,N} = 10^{-38}$ cm^2 (short-dashed lines), $\sigma_{\chi,N} = \sigma_{Y,N} = 10^{-34}$ cm^2 (dash-dotted lines) and $\sigma_{\chi,N} = 10\sigma_{Y,N} = 10^{-38}$ cm^2 (long-dashed lines). We can see that the smaller the ratio m_Y/m_χ is, the smaller the lifetime limit is, since the photons would yield luminosities compatible with experimental bounds, thus being a weak constraint. In the case of $\sigma_{\chi,N} \lesssim 1.1 \times 10^{-39}$ cm^2 (solid line), there is a further effect not present in the other cases considered due to the reduction of the WD capture rate of DM as the saturation factor $f_{\chi,A} < 1$. It can be seen that the effect of reducing $\sigma_{Y,N}$ fixing $\sigma_{\chi,N}$ is quenching $\tau_{\rm limit}$. Although all decay probabilities are naturally allowed in our setting, let us remind that results shown in Figs. 3–5 dealing with the internal luminosity will effectively be sensitive to decays only inside the stellar radius, by construction, while those in Fig. 2 consider decays both inside and outside the stellar volume.

IV. CONCLUSIONS

We have studied the gamma ray emission in WDs from annihilation of DM in their interior through metastable mediators. We have considered the combined effect of energy attenuation and finite decaying lifetime. Using an

approximation where the energy loss can be described in a continuous way through mediator scattering with nuclei inside the stellar volume we have derived the internal luminosities and fluxes. We have compared these luminosities to those from cold WDs in M4 GC. We find that in the case where $\sigma_{\chi,N} \lesssim 10^{-40}$ cm^2 the attenuation is negligible and the only effect comes determined from the lifetime. However, for larger cross sections, up to $\sigma_{\chi,N} \sim 10^{-29}$ cm^2, there are nontrivial effects that further constrain the lifetime bounds with a monotonic increase in the m_Y/m_χ ratio. The effect of the expected seclusion of DM from nucleons can be seen by imposing the nondegeneracy of $\sigma_{\chi,N}$ and $\sigma_{Y,N}$ values. We find that the smaller the $\sigma_{Y,N}$ is the less restrictive effect on the allowed Y-lifetimes. Note that the annihilation rate of DM or, in other words, the value of the thermally averaged annihilation cross section could somewhat modify our results concerning obtained luminosities and flux (and lifetimes) as an increase factor would yield larger values of $\tau_{\rm limit}$. As for energy flux, we find the more attenuation there is, the sharper the photoproduction results. Let us keep in mind that the considerations in the discussion about the restrictions on the decaying mediator lifetimes in cold WDs must also include, apart from other astrophysical scenarios, current efforts from colliders. As a new strategy to follow, they have shifted towards an alternative simplified model paradigm that includes these additional mediators and the search for a displaced secondary vertex, characterised by the mass of the particle and its lifetime, see [60]. This has led to an extensive effort amongst both theorists and experimentalists at the LHC to establish a systematic program to characterize DM searches using simplified models. A multidirectional and complementary approach from different search contexts will most surely provide valuable information on this type of model.

ACKNOWLEDGMENTS

We thank R. Lineros, M. Ardid, M. A. Sánchez-Conde, and J. Silk for useful discussions. This work has been supported by Junta de Castilla y León SA083P17, FIS2015-65140-P projects and by PHAROS CA COST Action CA16214. We also thank the Spanish Red Consolider MultiDark FPA2017 90566 REDC for support. M. C. is supported by a fellowship from the University of Salamanca.

[1] J. Silk, K. A. Olive, and M. Srednicki, Phys. Rev. Lett. **55**, 257 (1985).
[2] D. N. Spergel and W. H. Press, Astrophys. J. **294**, 663 (1985).
[3] S. Ritz and D. Seckel, Nucl. Phys. **B304**, 877 (1988).
[4] C. Kouvaris, Phys. Rev. D **77**, 023006 (2008).
[5] A. Gould, Astrophys. J. **321**, 571 (1987).
[6] M. McCullough and M. Fairbairn, Phys. Rev. D **81**, 083520 (2010).
[7] M. A. Pérez-García, F. Daigne, and J. Silk, Astrophys. J. **768**, 145 (2013).
[8] M. Cermeño, M. A. Perez-Garcia, and J. Silk, Phys. Rev. D **94**, 023509 (2016).
[9] M. Cermeño, M. A. Perez-Garcia, and J. Silk, Phys. Rev. D **94**, 023509 (2016).
[10] M. Cermeño, M. A. Perez-Garcia, and R. A. Lineros, Astrophys. J. **863**, 157 (2018).
[11] M. Cermeño, M. A. Perez-Garcia, and J. Silk, Pub. Astron. Soc. Aust. **34**, e043 (2017).
[12] G. Bertone and D. Hooper, arXiv:1605.04909v2.
[13] T. J. Sumner, Living Rev. Relativity 5 (**2002**) 4.
[14] M. Pospelov, A. Ritz, and M. Voloshin, Phys. Lett. B **662**, 53 (2008); **671**, 391 (2009).
[15] Y. Hochberg, E. Kuflik, T. Volansky, and J. G. Wacker, Phys. Rev. Lett. **113**, 171301 (2014).
[16] I. Z. Rothstein, T. Schwetz, and J. Zupan, J. Cosmol. Astropart. Phys. 07 (2009) 018.
[17] M. Lucente, C. Arina, M. Backovic, and J. Heisig, Proc. Sci. EPS-HEP2017 (**2017**) 628.
[18] N. F. Bell, Y. Cai, J. B. Dent, R. K. Leane, and T. J. Weiler, Phys. Rev. D **96**, 023011 (2017).
[19] T. Plehn, J. M. Thompson, and S. Westhoff, Phys. Rev. D **98**, 015012 (2018).
[20] S. Profumo, F. S. Queiroz, J. Silk, and C. Siqueira, J. Cosmol. Astropart. Phys. 03 (**2018**) 010.
[21] M. Escudero, S. J. Witte, and D. Hooper, J. Cosmol. Astropart. Phys. 11 (2017) 042.
[22] X. Chu, S. Kulkarni, and P. Salati, J. Cosmol. Astropart. Phys. 11 (2017) 023.
[23] M. Ardid, I. Felis, A. Herrero, and J. A. Martinez-Mora, J. Cosmol. Astropart. Phys. 04 (**2017**) 010.
[24] N. F. Bell and K. Petraki, J. Cosmol. Astropart. Phys. 04 (2011) 003.
[25] I. Jaegle *et al.* (Belle Collaboration), Phys. Rev. Lett. **114**, 211801 (2015).
[26] M. Cirelli, Proc. Sci. CORFU2015 (**2015**) 026.
[27] S. Adrian-Martinez *et al.*, J. Cosmol. Astropart. Phys. 05 (2016) 016.
[28] J. M. Gaskins, Contemp. Phys. **57**, 496 (2016).
[29] N. Arkani-Hamed, D. P. Finkbeiner, T. R. Slatyer, and N. Weiner, Phys. Rev. D **79**, 015014 (2009).
[30] K. Agashe, Y. Cui, L. Necib, and J. Thaler, J. Cosmol. Astropart. Phys. 10 (2014) 062; D. Pappadopulo, J. T. Ruderman, and G. Trevisan, Phys. Rev. D **94**, 035005 (2016).

[31] J. M. Cline and A. R. Frey, Phys. Lett. B **706**, 384 (2012).
[32] B. J. Kavanagh, Phys. Rev. D **97**, 123013 (2018).
[33] R. Essig, T. Volansky, and T. T. Yu, Phys. Rev. D **96**, 043017 (2017).
[34] D. Hooper and S. D. McDermott, Phys. Rev. D **97**, 115006 (2018).
[35] J. I. Collar, Phys. Rev. D **98**, 023005 (2018).
[36] D. Kim, J.-C. Park, and S. Shin, J. High Energy Phys. 04 (2018) 093.
[37] J. Herms, A. Ibarra, and T. Toma, arXiv:1802.02973.
[38] G. D. Starkman, A. Gould, R. Esmailzadeh, and S. Dimopoulos, Phys. Rev. D **41**, 3594 (1990).
[39] C. Kouvaris and I. M. Shoemaker, Phys. Rev. D **90**, 095011 (2014).
[40] F. Chen, J. M. Cline, and A. R. Frey, Phys. Rev. D **80**, 083516 (2009).
[41] R. Garani and S. Palomares-Ruiz, J. Cosmol. Astropart. Phys. 05 (2017) 007.
[42] A. R. Zentner, Phys. Rev. D **80**, 063501 (2009).
[43] C. Kouvaris and P. Tinyakov, Phys. Rev. D **82**, 063531 (2010).
[44] L. M. Krauss, M. Srednicki, and F. Wilczek, Phys. Rev. D **33**, 2079 (1986).
[45] K. Griest and D. Seckel, Nucl. Phys. **B283**, 681 (1987).
[46] J. Bramante, Phys. Rev. Lett. **115**, 141301 (2015).
[47] C. Kouvaris and P. Tinyakov, Phys. Rev. D **83**, 083512 (2011).
[48] G. Panotopoulos and I. Lopes, Phys. Rev. D **96**, 063003 (2017).
[49] T. J. Hurst, A. R. Zentner, A. Natarajan, and C. Badenes, Phys. Rev. D **91**, 103514 (2015).
[50] P. Amaro-Seoane, J. Casanellas, R. Schödel, E. Davidson, and J. Cuadra, Mon. Not. R. Astron. Soc. **459**, 695 (2016).
[51] J. Cembranos, J. L. Diaz-Cruz, and L. Prado, Phys. Rev. D **84**, 083522 (2011).
[52] F. K. Liu, Mon. Not. R. Astron. Soc. **281**, 1197 (1996).
[53] P. Baratella, M. Cirelli, A. Hektor, J. Pata, M. Piibeleht, and A. Strumia, J. Cosmol. Astropart. Phys. 03 (2014) 053.
[54] R. K. Leane, K. C. Y. Ng, and J. F. Beacom, Phys. Rev. D **95**, 123016 (2017).
[55] A. Ibarra, S. López, and M. Pato, J. Cosmol. Astropart. Phys. 07 (2012) 043.
[56] A. Ibarra, H. M. Lee, S. L. Gehler, W.-I. Park, and M. Pato, J. Cosmol. Astropart. Phys. 05 (2013) 016.
[57] G. Ingelman and M. Thunman, arXiv:hep-ph/9604286v1.
[58] L. R. Bedin, M. Salaris, G. Piotto, J. Anderson, I. R. King, and S. Cassisi, Astrophys. J. **697**, 965 (2009).
[59] B. M. S. Hansel, J. Brewer, G. G. Fahlman, B. K. Gibson, R. Ibata, M. Limongi, R. Michael Rich, H. B. Richer, M. M. Shara, and P. B. Stetson, Astrophys. J. **574**, L155 (2002).
[60] O. Buchmueller, A. De Roeck, K. Hahn, M. McCullough, P. Schwaller, K. Sung, and T.-T. Yu, J. High Energy Phys. 09 (2017) 076.

Chapter 6

Fermionic Light Dark Matter Particles and the New Physics of Neutron Stars

Resumen

En este artículo se presenta un repaso sobre trabajos relacionados con DM capturada por NSs. Las condiciones extremas de la materia ordinaria, altas densidades y presiones, en NSs hacen que estos objetos sean aptos para acumular gravitacionalmente una gran cantidad de DM. En esta contribución, consideramos diferentes modelos fenomenológicos para la DM de los innumerables actualmente permitidos y repasamos aspectos astrofísicos de interés basándonos en su interacción con la materia ordinaria para un amplio rango de densidades de la materia bariónica. Nos centramos en el interior del medio nuclear, tanto en el núcleo y como en las capas externas de una NS discutiendo el impacto de un nuevo sector oscuro en cantidades estelares relevantes para el transporte de (calor) energía, como son la conductividad térmica o las emisividades.

Publications of the Astronomical Society of Australia (PASA), Vol. 34, e043, 11 pages (2017).

doi:10.1017/pasa.2017.38

Fermionic Light Dark Matter Particles and the New Physics of Neutron Stars

M. Cermeño[1,5], M. Ángeles Pérez-García[1] and Joseph Silk[2,3,4]

[1]Department of Fundamental Physics, University of Salamanca, Plaza de la Merced s/n 37008, Spain
[2]Institut d'Astrophysique, UMR 7095 CNRS, Université Pierre et Marie Curie, 98bis Blvd Arago, 75014 Paris, France
[3]Department of Physics and Astronomy, The Johns Hopkins University, Homewood Campus, Baltimore, MD 21218, USA
[4]Department of Physics, Beecroft Institute of Particle Astrophysics and Cosmology, University of Oxford, Oxford OX1 3RH, UK
[5]Email: marinacgavilan@usal.es

(Received August 1, 2017; Accepted August 29, 2017)

Abstract

Dark Matter constitutes most of the matter in the presently accepted cosmological model for our Universe. The extreme conditions of ordinary baryonic matter, namely high density and compactness, in Neutron Stars make these objects suitable to gravitationally accrete such a massive component provided interaction strength between both, luminous and dark sectors, at current experimental level of sensitivity. We consider several different DM phenomenological models from the myriad of those presently allowed. In this contribution, we review astrophysical aspects of interest in the interplay of ordinary matter and a fermionic light Dark Matter component. We focus in the interior nuclear medium in the core and external layers, i.e. the crust, discussing the impact of a novel dark sector in relevant stellar quantities for (heat) energy transport such as thermal conductivity or emissivities.

Keywords: dark matter – dense matter – stars: neutron

1 INTRODUCTION

As early as 1933, the discovery made by F. Zwicky about visible matter being only a tiny fraction of the matter in our Universe, evidenced that our understanding of the cosmos was far from being complete. Since that date a variety of further indications including galactic rotation curves, anisotropies in the cosmic microwave background, distribution of galaxies, etc., points to the existence of cold non-luminous sector of particles, i.e. Dark Matter (DM), see Hubble & Humason (1931), Rubin & Ford (1970), and Clowe et al. (2006). Nowadays, this paradigm is well accepted by the scientific community and we know DM constitutes the most abundant type of matter in our Universe, being its density experimentally well-determined, $\Omega_{\rm CDM}h^2 = 0.1199 \pm 0.0027$ by the Planck Collaboration et al. (2014), although its true identity remains unknown, see for example, a discussion in Bertone & Hooper (2016).

The Standard Model (SM) of particle physics alone is not capable to explain the nature of this DM, suggesting that it must be extended. Current experimental constraints come from attempting different strategies. Direct detection searches of thermalised galactic DM (χ) are mainly based on nuclear recoils on selected targets. For the interaction cross-sections with nuclear matter (i.e. nucleons, N), there are at least five orders of magnitude remaining to be fully tested, namely $\sigma_{\chi N} \sim 10^{-43}$–$10^{-48}$ cm^2 in the $m_\chi \sim$ few GeV mass scale. DM particle existence could also be deduced from their annihilation products in indirect search experiments. In the case of a Majorana candidate, the indirect signal expected at Earth involving detection of gamma rays or neutrino final products is still under debate, see Cirelli (2012). A possible (tiny) modification of standard physics in systems of interest is another way to indirectly detect its presence. Along this direction rely other lines of research such as the modification of the emissivity of SM neutrinos (or steriles) in solar reaction chains that have been suggested by Lopes & Silk (2010). In addition, colliders aim to produce DM candidates through decay or annihilation of SM particles (Khachatryan et al. 2015; Aad et al. 2015).

In the light (low) mass region of DM candidates (LDM), $m_\chi \lesssim 1$ GeV c $-$ 2, cosmological, astrophysical, and collider constraints seem to be the most significant, due to the fact that particles with masses smaller than that of the nucleon can only provide kinematical recoil energies a the ∼eV range, below the ∼keV threshold for current conventional terrestrial searches in direct detection experiments, see Lin, Yu, & Zurekl (2012). If one, instead, considers

LDM scattering off bound electrons, energy transfer can cause excitation or even ionisation and thus seems promising for exploring the phase space in a complementary way, as explained in Essig et al. (2016). Contrary to what has been done in cosmological analysis, the importance of the dark sector component on celestial body scales has been less extensively studied and only recently has focused on the sun (Press & Spergel 1985), planets, or to a lesser extent on white dwarfs (McCullough & Fairbairn 2010; Hooper et al. 2010) and compact stars (Goldman et al. 1989; Kouvaris 2008).

2 CAPTURE OF DARK MATTER BY NEUTRON STARS

DM reaching terrestrial targets is expected to have low velocities $\beta_{\rm Earth} = \sqrt{\frac{2GM_{\rm Earth}}{R_{\rm Earth}}} = v_\chi \sim 10^{-3}$ (taking $c = \hbar = 1$ units and being G the gravitational constant) due to the fact that the gravitational boost is small for the Earth and, accordingly, the Lorentz factor $\gamma_{\rm Earth} = 1/\sqrt{1-\beta^2_{\rm Earth}} \sim 1$. Instead, for more compact objects, i.e. with a larger ratio M/R, the boosting capability increases. For neutron stars (NSs) with masses $M_{\rm NS} \simeq 1.5\,{\rm M}_\odot$ and radius $R_{\rm NS} \simeq 12$ km, $\gamma_{\rm NS} \sim 1.26$ or $v_\chi \sim 0.6$, providing thus a mechanism to attain higher χ kinetic energies.

It is important to remark that DM could be in principle accreted (and retained) by the star not only during the collapsed stage but also during most of the previous stellar lifetime, being the capture rate, C_χ, provided the interaction strength with ordinary matter is not negligible. Different particle candidates display interaction couplings in a wide range (Bertone & Hooper 2016). Regarding the progenitor stages, the progressively denser central core allows the rise of a finite spatial number density, $n_\chi(r)$, over time. Later, when a compact object is formed, the efficiency changes and the capture rate enhances, see for example, Gould (1987) and Kouvaris & Tinyakov (2011a). In this way, assumed an equation of state for regular SM matter in the interior of the NS, at a given galactic location, and with a corresponding ambient DM mass density $\rho_\chi \sim m_\chi n_\chi$, following Kouvaris (2008) and Guver et al. (2014), the capture rate can be written for a weakly interacting DM particle as

$$C_\chi = \frac{8}{3}\pi^2 \frac{\rho_\chi}{m_\chi} \frac{GM_{\rm NS}R_{\rm NS}}{1-\frac{2GM_{\rm NS}}{R_{\rm NS}}} \bar{v}^2 \left(\frac{3}{2\pi\bar{v}^2}\right)^{\frac{3}{2}} f_\chi$$
$$\simeq 1.8\times 10^{25} \left(\frac{1\,{\rm GeV}}{m_\chi}\right)\left(\frac{\rho_\chi}{\rho_{\chi,0}}\right) f_\chi \ {\rm s}^{-1}, \quad (1)$$

where $\bar{v}$ is the average χ velocity in the existing distribution, with a local value $\rho_{\chi,0} \simeq 0.3\ \frac{\rm GeV}{\rm cm^3}$ and f_χ is the fraction of particles that undergo one or more scatterings while inside the star. It saturates to $f_\chi \sim 1$ if $\sigma_{\chi N} \gtrsim \sigma_0$, otherwise $f_\chi \sim 0.45\frac{\sigma_{\chi N}}{\sigma_0}$, being $\sigma_0 = \frac{m_n R^2_{\rm NS}}{M_{\rm NS}} \sim 10^{-45}$ cm^2 the geometrical cross-section. As thermalisation times for $m_\chi \sim 1$ GeV particles are much smaller than dynamical cooling times, see Goldman et al. (1989), once inside, DM is believed to diffuse towards the denser central stellar regions according to the exponential law

$$n_\chi(r) = n_{0,\chi} e^{-\frac{m_\chi}{k_B T}\Phi(r)} \quad (2)$$

with $n_{0,\chi}$ the central value and $\Phi(r) = \int_0^r \frac{GM(r')dr'}{r'^2}$ the gravitational potential. Finally, $n_\chi(r) = n_{0,\chi} e^{-(r/r_{\rm th})^2}$ with a thermal radius $r_{\rm th} = \sqrt{\frac{9k_BT}{8\pi G\rho_n m_\chi}}$, where ρ_n is the barionic density. Normalisation requires $\int_0^{R_{\rm NS}} n_\chi(r){\rm d}V = N_\chi$ at a given time. N_χ is the number of DM particle population which resides inside. This number will depend, in general, on the capture, annihilation (or decay), and evaporation rates C_χ, C_a, C_s, respectively, see for example, Zentner (2009). But, for DM particles with masses larger than ~ 2 keV, evaporation effects can be ignored as it is shown in Kouvaris & Tinyakov (2011b) and Krauss, Srednicki, & Wilczek (1986). Then, as a function of time t, capture and annihilation processes compete to yield a population

$$N_\chi(t) = \sqrt{C_\chi/C_a}\tanh(t/\tau + \gamma(N_{\chi,0})), \quad (3)$$

where $\gamma(N_{\chi,0}) = \tanh^{-1}(\sqrt{C_a/C_\chi}N_{\chi,0})$ and $\tau = 1/\sqrt{C_\chi C_a}$. For a typical progenitor of a compact star, one can estimate $N_{\chi,0} \sim 10^{39}(\frac{m_\chi}{1\,{\rm GeV}})$, see Kouvaris & Tinyakov (2010), assuming that local densities for average NS galactic distances peak around $\sim$2 kpc where $\rho_\chi \sim 10^2\rho_{\chi,0}$. For times $t \gtrsim \tau \sim 10^4$ yr, the equilibrium sets $N_\chi(t) \sim \sqrt{C_\chi/C_a}$.

In the case of asymmetric DM candidates, accretion of DM mass beyond a critical value, i.e. the Chandrasekhar mass, could destroy (collapse) the star over time as it has been studied in Kouvaris & Tinyakov (2011a), McDermott, Yu, & Zurek (2012), and Bramante, Fukushima, & Kumar (2013). Possible limiting values of N_χ arising from a fermionic nature provide a value of Chandrasekhar number $N_{\rm Ch} \sim (M_{\rm Pl}/m_\chi)^3 \sim 1.8\times 10^{54}\,(1\,{\rm TeV/m}_\chi)^3$ with $M_{\rm Pl}$ the Planck mass.

Another way quoted to limit the dark sector population and thus collapse the whole star stems from the fact that quark deconfinement could be triggered via DM seeding. Energy release from self-annihilating DM could induce spark formation energetic enough to nucleate stable bubbles of deconfined quark matter leading to a softening of the nucleon equation of state. This has been invoked as a mechanism that could drive NS to quark star (QS) conversion, see Pérez-García, Silk, & Stone (2010), Pérez-García & Silk (2012), and Pérez-García, Daigne, & Silk (2013). In addition, arguments along the same line state that unstable DM can also be constrained by structural stability of accreting objects (Pérez-García & Silk 2015).

3 LIGHT DARK MATTER SCATTERING AT HIGH DENSITIES

The DM capture rate Equation (1) mainly determines the magnitude of the novel effects due to the interplay of both

matter sectors. For a given DM candidate, the interaction with the relevant degrees of freedom of the system considered will be crucial. This, in turn, comes phenomenologically described through couplings and mathematical operators in the underlaying theory. So far, no satisfactory answers exist coming from a unique model description, although there is a general consensus that the particle or particles in the dark sector should be electrically neutral and cold. The most popular extension to the SM, supersymmetry (SUSY), predicts that each particle has a partner of different spin but similar interactions. The lightest superpartner or LSP is stable in many cases and is often a neutralino, constituting an excellent DM candidate (Bertone & Hooper 2016).

In a nuclear medium such as the core of a compact-sized (spherical) object of mass M and radius R, the (in) elastic scattering of χ out of nucleons, $\sigma_{\chi N}$, mainly determines the relative fraction of DM to ordinary matter. In general, most of the works calculate this quantity without considering *in-medium* effects, and obtain the mean free path of these DM particles, λ_χ, approximating as $\lambda_\chi \simeq 1/\sigma_{\chi N} n$, where n is the ordinary nucleon number density, see for example, Spergel & Press (1985). This is usually considered as being sufficient to obtain knowledge about the internal processed happening inside the most efficient opaque environments. It is also important to know that the isospin charge is relevant as the coupling strengths to protons or neutrons may not be the same or even suffer from cancellations.

In the central core in an NS (with a content $\gtrsim 90\%$ neutrons), is described as having densities higher than several times nuclear saturation density $n_0 \simeq 0.17$ fm^{-3}. By neglecting medium corrections, one misses important features and qualitative insight into the system. Let us briefly comment on some of the possible issues. To begin with, Fermi-blocking, due to partial restriction of the outgoing nucleon phase space, can play a role diminishing the χN scattering cross-section. Finite temperature effects will allow the population of higher energy states in the nucleon sector with respect to the case in which no temperature effects are considered. It is important to note here that temperatures in the range $T \lesssim 50$ MeV are usually achieved in the very early stages of proto-NS evolution, see for example, Page et al. (2004). Later, after a primary neutrino cooling era, temperatures fall to the $\sim$ keV range. This will effectively set at large times a $T \approx 0$ configuration, as thermal energies are indeed much smaller than nucleon Fermi energies $k_{\rm B}T \ll E_{\rm FN}$ in the dense medium ($k_{\rm B}$ is the Boltzman constant). These in-medium effects are taken into account, for example, in Bertoni, Nelson, & Reddy (2013), Cermeño, Pérez-García, & Silk (2016a), and Cermeño, Pérez-García, & Silk (2016b).

As we have mentioned before, usually, the incoming DM particle is supposed to be thermalised in the galaxy with the Maxwellian mean velocities $v_\chi \sim 10^{-3}$. However, if the scenario considered is an accreting dense NS, the associated wavelength of the incoming DM particle decreases as $\lambda = \frac{2\pi}{\sqrt{\gamma^2-1}\, m_\chi}$. This expression sets, in practice, a measure of the validity of the quasielastic approximation, DM particles see nucleons as a whole, since matter is tested to sizes around $\lambda \sim 1$ fm, i.e. in the light DM mass range $m_\chi \lesssim 5$ GeV. Although further modelling would be required for the description of the inner hadron structure, for this mass range, a monopolar form factor in momentum space, $F(|\vec{q}|) = \frac{\Lambda^2}{\Lambda^2+q^2}$ with a cut-off parameter $\Lambda = 1.5$ GeV can be used, so that $F(0) = 1$, which can somewhat mitigate the short-range correlations arising in the calculation.

To check the importance of the modifications of the medium in the LDM scattering events, one has to calculate the differential cross-section per unit volume for the interaction between a fermionic particle of Dirac type, χ, and a nucleon field N (protons and neutrons). It is necessary to use the general expression, which can be found in Patrignani & Particle Data Group (2016),

$$\mathrm{d}\sigma = \frac{|\overline{\mathcal{M}}_{\chi \mathrm{N}}|^2 |F(|\vec{q}|)|^2}{4\sqrt{(p_N p_\chi)^2 - m^{*2}_N m^2_\chi}} \mathrm{d}\Phi(p_N, p'_N, p_\chi, p'_\chi) \mathcal{F}_{\mathcal{FB}}, \tag{4}$$

where the phase space volume element is

$$\mathrm{d}\Phi(p_N, p'_N, p_\chi, p'_\chi) = (2\pi)^4 \delta^{(4)}(p_N + p_\chi - p'_N - p'_\chi) \times \frac{\mathrm{d}^3 \vec{p'_N}}{(2\pi)^3 2E'_N} \frac{\mathrm{d}^3 \vec{p'_\chi}}{(2\pi)^3 2E'_\chi}. \tag{5}$$

$p'^\mu_N = (E'_N, \vec{p'_N})$ and $p^\mu_N = (E_N, \vec{p_N})$ are the four momenta for the outgoing and incoming nucleon, and $p'^\mu_\chi = (E'_\chi, \vec{p'_\chi})$ and $p^\mu_\chi = (E_\chi, \vec{p_\chi})$ those analogous for the DM particle, respectively. Momentum transfer is denoted by $q^\mu = p'^\mu_\chi - p^\mu_\chi$. In this way, $q_0 = E'_N - E_N = E_\chi - E'_\chi$ and $\vec{q} = \vec{p'_N} - \vec{p_N} = \vec{p_\chi} - \vec{p'_\chi}$. The four-dimensional delta assures the energy and momentum conservation in the collision and $|\overline{\mathcal{M}}_{\chi \mathrm{N}}|^2$ is the squared matrix element for the interaction considered. The factor $\mathcal{F}_{\mathcal{FB}} = f(E_N)(1 - f(E'_N))$, with $f(E_i) = \frac{1}{1+e^{(E_i - \mu^*_i)/k_B T}}$ $i =$ p,n, and μ^*_i the effective nucleon chemical potential for a particle with isospin of ith-type, see Reddy, Prakash, & Lattimer (1998), accounts for the Fermi blocking term. It takes into account the occupation of states and in this scenario affecting only to the nucleons. For the dark sector, it can be assumed that all outgoing DM particles states are in principle allowed and $1 - f_\chi(E) \approx 1$ since the fraction of DM inside the star remains tiny at all times. The validity of this approximation is discussed in Cermeño et al. (2016a). Let us mention here that effective values of nucleon mass and chemical potential define the *quasi-particle* nature of the nucleon in the medium and differ from the nude values by the presence of average meson fields (Serot & Walecka 1986).

When discussing the effect of density (and T) in the diffusion of DM in NSs, the quantity we should analyse is the mean free path λ_χ to be obtained from the integrated cross-section per unit volume $\frac{\sigma(E_\chi)}{V}$, as $\lambda_\chi = (\frac{\sigma(E_\chi)}{V})^{-1}$.

In a previous step, one obtains the differential value as

$$\frac{1}{V}\frac{\mathrm{d}\sigma}{\mathrm{d}\Omega \mathrm{d}q_0} = \frac{1}{(2\pi)^4}\int_{|\vec{p}_-|}^{\infty}\frac{\mathrm{d}|\vec{p_N}||\vec{p_N}|}{4E'_N}\frac{m^*_N|\vec{p'_\chi}||F(|\vec{q}|)|^2}{|\vec{q}|} \times\delta(\cos\theta-\cos\theta_0)\Theta(|\vec{p_N}|^2-|\vec{p_N}_-|^2) \times\frac{|\overline{\mathcal{M}}_{\chi\mathcal{N}}|^2 f(E_N)(1-f(E'_N))}{4\sqrt{E_N^2E_\chi^2-m^{*2}_N m_\chi^2}}, \quad (6)$$

where only the lowest order terms are retained. Since $v_\chi^2 \sim v_N^2 \ll 1$ given $\frac{|\vec{p_i}|}{E_i} = v_i, i = \chi, N$ and nucleon Fermi velocities $v_N \sim v_{\rm FN} = p_{\rm FN}/E_{\rm FN}$. On the other hand, expressing the energy conservation as a function of the dispersion angle for the outgoing DM particle θ, one obtains the minimun value of $\vec{p_N}$

$$\cos\theta_0 = \frac{m^*_N}{|\vec{p}||\vec{q}|}\left(q_0-\frac{|\vec{q}|^2}{2m^*_N}\right), \quad (7)$$

and

$$|\vec{p}_-|^2 = \frac{m^{*\,2}_N}{|\vec{q}|^2}\left(q_0-\frac{|\vec{q}|^2}{2m^*_N}\right)^2. \quad (8)$$

These expressions, Equations (7) and (8), are discussed step by step in Cermeño et al. (2016a).

We have to remark that this scenario is restricted to temperatures and densities typical for the thermodynamical evolution of the stellar core region, that is $T \lesssim 50$ MeV and $n \simeq (1-3)n_0$. Let us note that if finite temperature is considered, a detailed balance factors must be added to the medium response to weak probes (Horowitz & Pérez-García 2003; Horowitz & Wehrberger 1991) under the form

$$S(q_0, T) = \frac{1}{1-e^{-\frac{|q_0|}{k_B T}}}. \quad (9)$$

This factor provides the relation between the dynamical nuclear structure factor for positive and negative energy transfers q_0 as the thermodynamic environment can donate energy to the outgoing particle.

Now, to obtain the total cross-section per unit volume and the inverse of it, i.e. the mean free path, the integrations over all possible outgoing energy transfer values and solid angle have to be performed. In this way,

$$\frac{\sigma(E_\chi)}{V} = \frac{m^*_N}{4(2\pi)^3}\int_0^{E_\chi-m_\chi}\mathrm{d}q_0\int_{|\vec{p'_\chi}|-|\vec{p'_\chi}|}^{|\vec{p'_\chi}|+|\vec{p'_\chi}|}\mathrm{d}|\vec{q}||F(|\vec{q}|)|^2 \times\int_{|\vec{p}_-|}^{\infty}\mathrm{d}|\vec{p_N}|\frac{|\overline{\mathcal{M}}_{\chi\mathcal{N}}|^2|\vec{p_N}|f(E_N)(1-f(E'_N))S(q_0,T)}{4E'_N|\vec{p'_\chi}|\sqrt{E_N^2E_\chi^2-m^{*\,2}_N m_\chi^2}}. \quad (10)$$

When particularising the calculation for a spin-independent (scalar-vector) interaction model, the interaction Lagrangian is $\mathcal{L}_\mathcal{I} = \sum_{N=n,p} g_{s,N}\chi\overline{\chi}N\overline{N} + g_{v,N}\chi\gamma^\mu\overline{\chi}N\gamma_\mu\overline{N}$, where $g_{s,N}$ ($g_{v,N}$) are the effective scalar (vector) couplings of the DM particle to the N field.

The effect of the Pauli blocking can be seen, for example, in Figure 1 of Cermeño et al. (2016a) where the differential cross-section per unit volume as a function of the energy transfer q_0 for different values of the transferred momentum $|\vec{q}|$ is shown for a pure neutron system. We use $n = n_0$, setting $T = 0$ and $m_\chi = 0.5$ GeV. The limiting upper value of the energy transfer is $E_\chi - m_\chi \approx 130$ MeV. This is because, in general, $-\infty < q_0 < E_\chi - m_\chi$, since $m_\chi < E'_\chi < \infty$. Instead, at $T = 0$, the energy transfer cannot be negative, so that $q_0 > 0$ and $0 < q_0 < E_\chi - m_\chi$. The triangular shape is due to the Heaviside Fermi distribution at $T = 0$. Beyond q_0 values limited by real-valued angles in Equation (7), the scattered states are not allowed since it is kinematically impossible to scatter a nucleon due to lack of empty states. To understand the value of the maxima of this plot, we have to remind ourselves that at $T = 0$ our allowed states will be given by the factor $\Theta(E_F - E_N)\Theta(1 - f_N(E_F - E'_N))$, and, on the other hand, there is a minimum allowed value for $\vec{p_N}$ given by the kinematics of the interaction, $|\vec{p}_-|$. Then, it is easy to verify that maximum values are reached when $|\vec{p}_-| = |\vec{p_N}|$ being $|\vec{p_N}|$ the value of $|\vec{p_N}|$ when $|\vec{p'}_N| = |\vec{p}_F|$.

Finite temperature effects can be observed in Figure 2 where the detailed balance factors have been included and

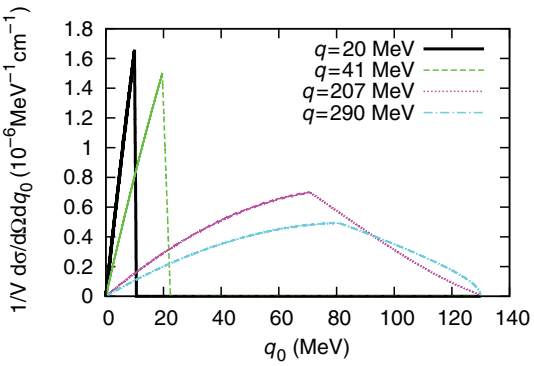

Figure 1. Differential cross-section per unit volume as a function of the energy transfer q_0 for values of $|\vec{q}| = 20, 41, 207$, and 290 MeV. The DM particle mass is $m_\chi = 0.5$ GeV and $T = 0$ at $n = n_0$. From Cermeño et al. (2016a).

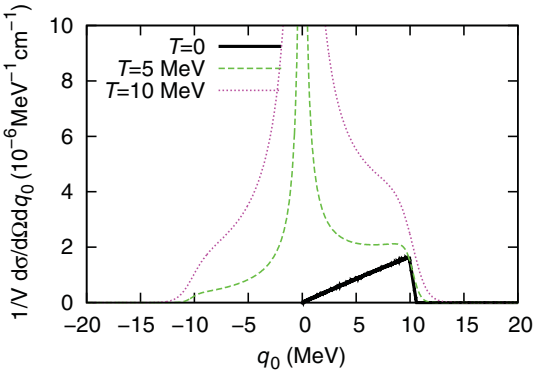

Figure 2. Differential cross-section per unit volume as a function of the energy transfer q_0 at $T = 0, 5, 10$ MeV for a nucleon density $n = n_0$. We set $|\vec{q}| = 20$ MeV and $m_\chi = 0.5$ GeV. From Cermeño et al. (2016a).

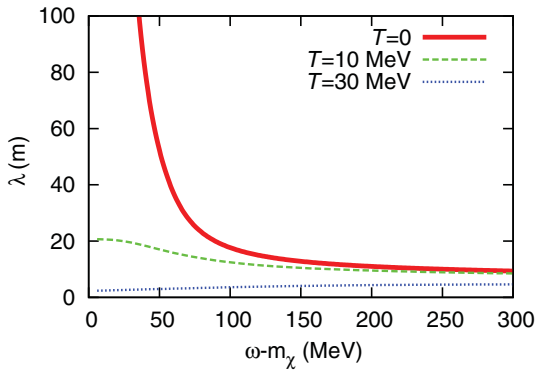

Figure 3. DM particle mean free path as a function of kinetic energy for $m_\chi = 1$ GeV at $n = n_0$ for $T = 0$, 10, 30 MeV. From Cermeño et al. (2016a).

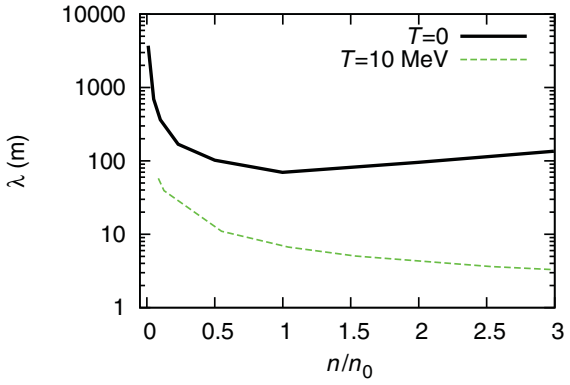

Figure 4. DM particle mean free path as a function of density (in units of n_0) for two values of temperature, $T = 0$ and $T = 10$ MeV. Effective (naked) nucleon mass has been used in the zero (finite) T calculation. From Cermeño et al. (2016a).

the transferred momentum $|\vec{q}| = 20$ MeV, chemical potential $\mu = E_{\rm FN}$, DM particle mass $m_\chi = 0.5$ GeV and nucleon density $n = n_0$ are fixed.

At temperatures $T > 0$, the negative energy transfer states get increasingly populated and the sharp nucleon distribution is smoothed. As $q_0 \to 0$, the inverse detailed balance factor $S^{-1}(q_0, T) \to 0$. The corresponding divergence will, however, be integrable in order to obtain a finite integrated cross-section. This, can be seen, for example, in Figure 3, where the mean free path for the χ particle as a function of kinetic energy $K_\chi = E_\chi - m_\chi$ for temperatures $T = 0$ (solid line) $T = 10$ MeV (dashed line) and $T = 30$ MeV (dotted line) is plotted. $m_\chi = 1$ GeV and $n = n_0$ are considered. The notation used states that $E_\chi \equiv \omega$. Note that for $T = 0$ in the limit of vanishing kinetic energy for the incoming DM particle $E_\chi \to m_\chi$, the phase space available for the outgoing particles vanishes as the energy transferred $q_0 \to 0$ due to filled population levels, therefore providing a null cross-section, while this is not true in the finite T case as more channels are available.

In Figure 4, we show the variation of the DM particle mean free path as a function of density (in units of n_0) for two values of temperature and fixing $m_\chi = 1$ GeV considering effective nucleon masses for the $T = 0$ case while not for the finite temperature case. We can see competitive effects from the temperature and effective mass. A steady decrease is obtained in case the naked nucleon mass is considered. Temperature effects, which are relevant in the early stages of dense star evolution, tend to increase the opacity of nucleon matter to prevent DM nearly free streaming. The cross-section is greatly affected by the finite density of matter, namely by the effect of a smaller effective nucleon mass $m_N^* < m_N$. Temperature effects are important although to a lesser extent relative to density ones.

It is important to point out that in this LDM mass range, scattering is diffusive to very good approximation as $\lambda_\chi / R_{\rm NS} \ll 1$. On the other hand, for the choice of couplings strengths consistent with collider constraints as Khachatryan et al. (2015) and Aad et al. (2015), once fixed K energy, an SM neutrino displays typical mean free path somewhat smaller, see Reddy et al. (1998), Horowitz & Wehrberger (1991), and Horowitz & Pérez-García (2003).

4 LIGHT DARK MATTER SCATTERING AT LOW DENSITIES

At low densities, $\lesssim 10^{13}$ g cm $-$ 3 inside the star crust matter arranges in a series of irregular shapes or structures called generically *pasta phases* (Horowitz, Pérez-García, & Piekarewicz 2004). In particular, the outer crusts in NSs are formed by periodically arranged nuclei with typical densities ranging from $\rho \simeq 2 \times 10^6$–$4 \times 10^{11}$ g cm^3. In the single-nucleus description, see Rüster, Hempel, & Schaffner-Bielich (2006), a series of nuclei with increasing baryonic number, A, from Fe to Kr form a lattice before neutrons start to leak out of nuclei. At these high densities, electrons form a degenerate Fermi sea. Around $\rho_0 \simeq n_0 m_N \simeq 2.4 \times 10^{14}$ g cm^3, and beyond that, matter can be considered a homogeneous system.

When the phase space is restricted to fermionic DM particles with masses $m_\chi \lesssim 100$ MeV, the relevant cross-section of the interaction between DM particles and the outer stellar layers is that scattering off nuclei. Taking this into account, the possibility of production of quantised lattice vibrations (phonons) in the periodically arranged structures in the NS outer crust by LDM scattering, arises. These extra phonons can impact subsequent quantities of interest, such as the ion thermal conductivity, that are relevant for computing the cooling behaviour of NSs.

Phonons are quantised vibrational modes characterised by a momentum $\vec{k}$ and polarisation vector $\vec{\epsilon}_\lambda$ appearing in a nuclear periodic system, as it can be seen in Ziman (1960). They can have a number of different sources. They can be excited due to non-zero temperature T in the medium. The Debye temperature allows us to evaluate the importance of the ion motion quantisation. For a bcc lattice, see Carr (1961), $T_{\rm D} \simeq 0.45 T_{\rm p}$, being $T_{\rm p} = \omega_{\rm p}/k_{\rm B} = \sqrt{\frac{4\pi n_A Z^2 e^2}{k_{\rm B}^2 m_A}}$ the plasma temperature associated to a medium of ions with number

density n_A, baryonic number A, electric charge Ze and mass m_A. At low temperatures $T < T_{\rm D}$, the quantisation becomes increasingly important and the thermal phonons produced are typically acoustic modes, following a linear dispersion relation $\omega_{k,\lambda} = c_{l,\lambda}|\vec{k}|$, where $c_l = \frac{\omega_{\rm p}/3}{(6\pi^2 n_A)^{1/3}}$ is the sound speed. In addition, phonon production can be caused by an external scattering agent, for example, SM neutrinos. In this respect, weak probes such as cosmological neutrinos with densities $n_\nu \sim 116\,{\rm cm}^{-3}$ per flavour have been shown to provide small phonon production rates in a crystal target, see Ferreras & Wasserman (1995). Due to the tiny mass of the neutrino, the experimental signature of this effect seems however hard to confirm.

The single phonon excitation rate (per unit volume) is obtained as Cermeño et al. (2016b)

$$R_k^{(0)} = \frac{8\pi^4 n_A^2}{(2\pi)^6 m_\chi^2 m_A c_l} \int_0^\infty |\vec{p_\chi}|{\rm d}|\vec{p_\chi}| f_\chi(\vec{p_\chi}) |E_\chi - |\vec{k}| c_l| a^2, \tag{11}$$

where $f_\chi(\vec{p_\chi}) = \frac{n_\chi \mu}{4\pi m_\chi^3 K_2(\mu)} e^{-\mu\sqrt{1+\frac{|\vec{p_\chi}|^2}{m_\chi^2}}}$ is the Maxwell–Juttner distribution (Juttner 1911) function for relativistic incoming DM particles. With $\mu = \frac{m_\chi}{k_B T} \approx 6.7$ for $\sqrt{< v^2 >} \sim 0.6$, see Hakim (2011) and Cercignani & Kremer (2002), and $K_2(\mu)$ the modified Bessel function of second kind. The value of a takes into account the length of the interaction when a DM particle approaches a nucleus in the periodic lattice. Using the Born approximation for the cross-section (off protons and neutrons) in the centre of mass frame, it can be written as

$$4\pi a^2 = m_A^2 \frac{\left(\frac{Z}{m_{\rm p}}\sqrt{|\tilde{\mathcal{M}}_{\rm p}|^2} + \frac{(A-Z)}{m_n}\sqrt{|\tilde{\mathcal{M}}_n|^2}\right)^2}{16\pi(m_\chi + m_A)^2}, \tag{12}$$

with $\int_{-1}^{1} 2\pi {\rm d}(\cos\,\theta_\chi)|\overline{\mathcal{M}}_{\chi{\rm N}}|^2 \equiv |\tilde{\mathcal{M}}_{\rm N}|$ and the averaged matrix element considering a prescribed model interaction. In this expression, Pauli blocking effects are not considered but, as an approximation, density dependence can be retained using a parameterisation of the nuclear Fermi momentum $|\vec{p}_{\rm FN}| \sim (3\pi^2 n_0 Y_N)^{1/3}$ and the nuclear fractions $Y_{\rm p} = Z/A$, $Y_{\rm n} = (A-Z)/A$. It is important to say that the allowed values for the phonon momentum are restricted for the Born approximation, $|\vec{k}| \ll \frac{1}{a}$, as well as for kinematical restrictions when energy conservation is imposed, $0 \leq |\vec{k}| \leq 2\left(\frac{c_l E_\chi}{(c_l^2-1)} + \frac{|\vec{p_\chi}|}{|c_l^2-1|}\right)$.

The single phonon excitation rate (per unit volume) $R_k^{(0)}$ due to the accretion of DM particles is almost constant with $|\vec{k}|$, whereas for neutrinos $R_\nu^0(|\vec{k}|) = R_{\nu 0} e^{-b|\vec{k}|}$ with b a constant which depends on neutrino mass. This means that, for a fixed value of $|\vec{k}|$, contribution from DM particles to the phonon excitation rate will be much higher than neutrino contribution.

Now, it will be important to discuss the astrophysical impact of these phonons. As we have mentioned before, phonon production can be crucial for determining further transport properties, in particular, thermal conductivity in an ion-electron system such as that in the outer NS crust. As an important contribution to the total ion conductivity, κ_i, partial ion conductivities due to ion–ion, $\kappa_{\rm ii} \equiv \kappa_{\rm ph}$, and ion-electron collisions, $\kappa_{\rm ie}$, must be added, see for example, Chugunov & Haensel (2007), under the prescription $\kappa_{\rm i}^{-1} = \kappa_{\rm ii}^{-1} + \kappa_{\rm ie}^{-1}$. Standard mechanisms to produce lattice vibrations include thermal excitations, as analysed in detail in previous works (Negele & Vautherin 1973; Potekhin, Chabrier, & Yakovlev 1997; Baiko et al. 1998). In an NS, the outer crust can be modelled under the one-component-plasma description. This low-density solid phase can be classified according to the Coulomb coupling parameter $\Gamma = Z^2 e^2/ak_{\rm B}T$, where $a = (4\pi n_A/3)^{1/3}$ is the ion sphere radius. It is already known that typically for $\Gamma \geqslant \Gamma_{\rm m} \simeq 175$, or below melting temperature $T < T_{\rm m}$, single-ion systems crystallise, see Nagara, Nagata, & Nakamura (1987).

There are a number of processes that can affect thermal conductivity in the medium. The so-called U-processes are responsible for modifying the electron conductivity such that for high temperatures, $T > T_{\rm U}$, electrons move almost freely, more details in Ziman (1960). Assuming a bcc lattice, $T_{\rm U} \simeq 0.07 T_{\rm D}$. Thus, in the scenario depicted here, the temperature range must be $T_{\rm U} < T < T_{\rm D} < T_{\rm m}$ for each density considered. According to kinetic theory, the thermal conductivity can be written in the form

$$\kappa_{\rm ii} = \frac{1}{3} k_{\rm B} C_A n_A c_l L_{\rm ph}, \tag{13}$$

as it can be seen in Ziman (1960), where $C_A = 9\left(\frac{T}{T_{\rm D}}\right)^3 \int_0^{T_{\rm D}/T} \frac{x^4 e^x {\rm d}x}{(e^x-1)^2}$ is the phonon (dimensionless) heat capacity (per ion) and $L_{\rm ph}$ is an effective phonon mean free path that includes all scattering processes considered: U-processes and impurity (I) scattering processes (both dissipative) and the phonon normal (N) scattering which are non dissipative $L_{\rm ph}^{-1} = L_{\rm U}^{-1} + L_{\rm I}^{-1} + L_{\rm N}^{-1}$. Typically, the thermal conductivity is related to the thermal phonon number at temperature T, $L_{\rm ph} \sim 1/N_{0,k\lambda}$, where $N_{0,k\lambda} = (e^{\omega_{k\lambda}/k_{\rm B}T} - 1)^{-1}$. The contribution from DM can be obtained by the net number of phonons that results from the competition between thermal phonons and scattering excitation and stimulated emission, as it is shown in Ferreras & Wasserman (1995), in a 4-volume $\delta V \delta t$. Using the averaged rate per unit volume and weighting with the incoming distribution providing the frequencies of different values of momenta, the total number of phonons can be written as

$$N_{k\lambda} \simeq N_{0,k\lambda} + R_k^{(0)} \delta V \delta t - \int \frac{{\rm d}^3\vec{p}}{n_\chi} f_\chi(\vec{p}) \tilde{R}_k^{(0)} N_{0,k\lambda} e^{(\omega_{k,\lambda} + \vec{k}.\vec{v})/K_\chi} \delta V \delta t, \tag{14}$$

see Cermeño et al. (2016b). Where $\tilde{R}_k^{(0)}$ is the single phonon excitation rate for each particular momentum value (not averaged over incoming χ momenta). Since the source (NS) is in relative motion to the LDM flux, there is a Doppler shift characterised by the source velocity $v \equiv v_{\rm NS} \sim 10^{-2}$ i.e. galactic NS drift velocity. As we have mentioned before, the distribution of NSs in our galaxy peak at distances $\lesssim$ few kpc

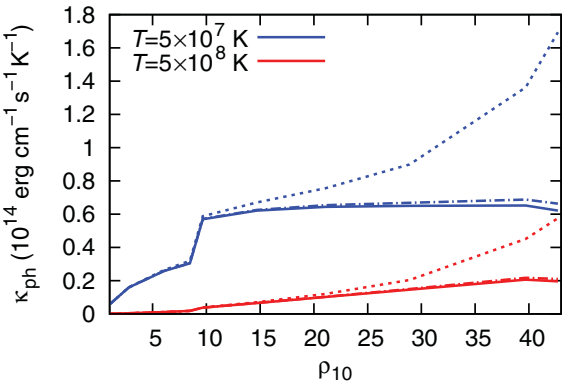

Figure 5. Phonon thermal conductivity as a function of density (in units of 10^{10} g cm^3) for temperatures $T = 510^7$ K (blue), 510^8 K (red), and m_χ = 100 MeV. Dash-dotted and dashed lines depict the impact of a LDM density $n_\chi/n_{0\chi} = 10, 100$. Solid lines are the standard thermal result with no DM for each case. From Cermeño et al. (2016b).

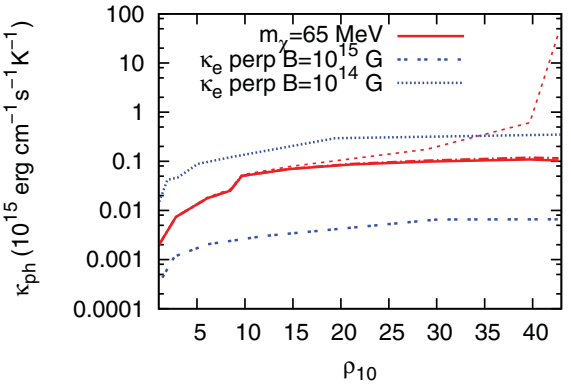

Figure 6. Phonon thermal conductivity as a function of density (in units of 10^{10} g cm^3) at $T = 10^8$ K and $m_\chi = 65$ MeV. Solid, dot-dashed, and dashed lines correspond to cases with no DM, $n_\chi/n_{0,\chi} = 10, 100$. Perpendicular electron thermal conductivity is also shown for $B = 10^{14}$, 10^{15} G. From Cermeño et al. (2016b).

((Lorimer et al. 2006)) where the DM density is enhanced with respect to the solar neighbourhood value.

In Figure 5, the phonon thermal conductivity as a function of barionic density is shown for two different typical temperatures for the base of the crust, using $m_\chi = 100$ MeV. Solid lines are the standard thermal result with no DM. Dash-dotted and dashed lines correspond to $n_\chi/n_{0,\chi} = 10, 100$, respectively. It is clear to see that at the largest LDM local densities considered, there is an enhancement over the thermal result well inside the outer crust. This corresponds to the site where the DM-induced effects have the most influence ((Pérez-Azorín, Miralles, & Pons 2006)) as this is the most massive part of the outer crust. Although, below these densities, there is a negligible change. At lower T, the effect of a perturbation over the thermal phonon population is more important. Enhanced (decreased) conductivities at moderate LDM densities are due to a net reduction (increase) of the number of phonons in the lattice as a result of cancellation of modes.

The same type of plot can be shown in Figure 6 in a more realistic stellar context. Here, the phonon thermal conductivity as a function of baryonic density at $T = 10^8$ K and $m_\chi = 65$ MeV can be seen. Solid, dot-dashed, and dashed lines correspond to cases with no DM, $n_\chi/n_{0,\chi} = 10, 100$, respectively. Electron thermal conductivity is also shown for magnetised realistic scenarios in the perpendicular direction to a magnetic field B of strength $B = 10^{14}$ G (dotted) and $B = 10^{15}$ G (doble dotted), these NSs with so high magnetic fields are called magnetars and they are being studied by many groups, see for example, a review from Turolla, Zane, & Watts (2015). Ions are mostly not affected by the presence of a magnetic field for the range of temperatures and magnetic fields considered, this can be checked in Chugunov & Haensel (2007). The parallel direction electronic contribution is not depicted here since it is typically much larger $k_{e\|} \sim 10^{17} - 10^{19}$ erg cm^{-1} s^{-1} K^{-1}. Values of electronic contribution have been obtained from Viganò (2013). Since the global conductivity is $\kappa = \kappa_e + \kappa_{ph}$, this result is expected to contribute to the reduction of the difference in heat conduction in both directions and thus to the isotropisation of the NS surface temperature pattern, which is studied for example in Perna et al. (2013) and Viganò et al. (2014), as it would be smoothly driven towards more isothermal profiles for latitudes among pole and equator. It is already known, see for example, Kaminker et al. (2007), that the outer crust plays an important role in regulating the relation among temperature in the base of it and the surface. The detailed calculation remains, however, for future works.

5 IN-MEDIUM ENERGY RELEASE FROM ANNIHILATING DARK MATTER

In previous sections, we consider a scattering interaction between DM and ordinary matter. Apart from the spin-independent interaction model considered before (corresponding to effective scalar and vector couplings), more effective operators for fermionic DM particles can be studied. For example, the so-called Coy DM model proposed by Boehm et al. (2014) which belongs to the family of simplified models, see for instance, Dolan et al. (2015), Bauer, Haisch, & Kahlhoefer (2017), and Baek, Ko, & Li (2017), includes two new particles to the SM, i.e. a Dirac fermion DM candidate, χ which interacts with a boson a, with mass m_a, through the pseudoscalar coupling of strength g_χ as proposed in Arina, Del Nobile, & Panci (2015). The interaction lagrangian of the model reads

$$\mathcal{L}_\mathcal{I} = -i\frac{g_\chi}{\sqrt{2}} a\bar{\chi}\gamma_5\chi - ig_0\frac{g_f}{\sqrt{2}} a\bar{f}\gamma_5 f. \qquad (15)$$

A final state of fermion–antifermion is formed through the boson mediator. The vertex involves a pseudoscalar coupling with the SM fermions f with strength $g_0 g_f$, where g_f denotes a multiplicative factor common to all couplings of a with

SM fermions. The most common type of couplings are the flavour-universal coupling $g_f = 1$, independent of the fermion type, and Higgs-like coupling, proportional to the fermion mass $g_f = \frac{m_f}{174\,\mathrm{GeV}}$. However, there are other schemes where a couples either to quarks or leptons exclusively, and with a flavour structure (Dolan et al. 2015).

An existing DM distribution inside the star capable of self-annihilating can be a source of energy emission for the dynamical cooling behaviour, once the star is formed. In the range $m_\chi < m_{\mathrm{Higgs}}$ and $m_a < m_\chi$, the relevant annihilation processes are $\chi\chi \to f\bar{f}$ and $\chi\chi \to aa$, see Arina et al. (2015).

In this context, these annihilation reactions, $\chi\chi \to f\bar{f}$ and $\chi\chi \to aa$, with subsequent decay $a \to f\bar{f}$ can be considered to explore possible astrophysical consequences in the neutrino fermionic channel as dense stars are efficient DM accretors. One of the key quantities that can govern the internal stellar energetic balance is the local energy emissivity, $Q_{\mathrm{E}} = \frac{\mathrm{d}E}{\mathrm{d}V\mathrm{d}t}$, which can be understood as the energy emitted per unit volume per unit time, through a prescribed particle physics reaction.

Considering the above quoted reactions which involve annihilating DM accreted by a NS, with baryonic density $\rho_b \sim 2\rho_0$, from an existing galactic distribution. Q_{E} denotes the energy emission rate per volume due to fermionic or pseudoscalar pair emission in the final states. In general, its expression can be written under the form (Esposito et al. (2002))

$$Q_{\mathrm{E}} = 4\int \mathrm{d}\Phi(E_1+E_2)\,|\overline{\mathcal{M}}|^2\, f(f_1,f_2,f_3,f_4), \tag{16}$$

with $\mathrm{d}\Phi = \frac{\mathrm{d}^3p_1}{2(2\pi)^3E_1}\frac{\mathrm{d}^3p_2}{2(2\pi)^3E_2}\frac{\mathrm{d}^3p_3}{2(2\pi)^3E_3}\frac{\mathrm{d}^3p_4}{2(2\pi)^3E_4}(2\pi)^4\delta^4(p_1+p_2-p_3-p_4)$ the 4-body ($12 \to 34$) phase space element and $|\overline{\mathcal{M}}|^2$ the spin-averaged squared matrix element of the reaction considered. The additional factor $f(f_1, f_2, f_3, f_4)$ accounts for the initial and final particle distribution functions contribution which will be different for each annihilation channel. The notation used is the following $p_1 = (E_1, \vec{p_1})$, $p_2 = (E_2, \vec{p_2})$ as the incoming 4-momenta while $p_3 = (E_3, \vec{p_3})$, $p_4 = (E_4, \vec{p_4})$ are the outgoing 4-momenta, respectively. Feynman diagrams and matrix elements can be seen in Cermeño, Pérez-García, & Lineros (2017).

For the case of annihilation into fermionic pairs $f(f_1, f_2, f_3, f_4) = f_\chi(E_1)f_{\bar{\chi}}(E_2)(1 - f_f(E_3))(1 - f_{\bar{f}}(E_4))$ and f_χ, f_f are the local stellar distribution functions for DM and fermionic particles, respectively, containing density and temperature dependence. Whereas for the annihilation into pseudoscalars, the factor $f(f_1, f_2, f_3, f_4) = f_\chi(E_1)f_{\bar{\chi}}(E_2)f_a(E_3)$ $f_a(E_4)$. Given the fact that inside the star, the small DM fraction provides a Fermi energy $E_{\mathrm{F},\chi} \ll k_{\mathrm{B}}T$, in both reactions, its distribution function can be approximated by a classical Maxwell–Boltzmann type $f_\chi = f_\chi^{\mathrm{MB}}(|\vec{p}_i|) = \left(\frac{1}{2\pi m_\chi k_B T}\right)^{\frac{3}{2}} n_\chi(r) e^{\frac{-|\vec{p}_i|^2}{2m_\chi T}}$. We can see that the phase space factor $f(f_1, f_2, f_3, f_4)$ in Equation (16) introduces DM density and T dependence into the calculation as a thermalised DM distribution exists inside the NS core.

Table 1. Parameters used in this work as appearing in the interaction lagrangian in Equation (15). $g_f = 1$ is taking. From Cermeño et al. (2017).

	m_χ [GeV]	m_a [GeV]	g_χ	g_0
A	0.1	0.05	7.5×10^{-3}	7.5×10^{-3}
B	1	0.05	1.2×10^{-1}	2×10^{-3}
C	30	1	6×10^{-1}	5×10^{-5}

For the outgoing fermions, the medium density effects have to be taken into account too through the phase space blocking factors as we have reviewed in Section 3, whereas for the outgoing pseudoscalars (bosons) no blocking has to be considered.

In order to analyse an interesting astrophysical consequence, Cermeño et al. (2017) restrict the analysis to three different sets of flavour-universal ($g_f = 1$) parameters that are not in conflict with existing phenomenology of direct detection experiments (Bertone & Hooper 2016) nor cosmological bounds (Zeldovich 1965; Zeldovich, Okun, & Pikelner 1965). The masses and couplings considered can be seen in Table 1. Models A and B are mainly determined by DM relic abundance due to the fact that the DM mass is in the region where direct detection experiments are less restrictive but can be more constrained with Kaon decays. On the contrary, the couplings in set C are constrained by LUX results, Akerib et al. (2017), in spin-independent and spin-dependent cross-sections. For more details, see Cermeño et al. (2017). On the other hand, they fixed the final fermion states to neutrinos. These weakly interacting SM fermions play a key role in releasing energy from NSs. At the end of the life of a very massive star, the central core collapses gravitationally and it is well known that its gravitational binding energy is emitted in neutrinos (and antineutrinos) of the three families. A very efficient cooling scenario emerges in the first $\sim 10^5$ yr. Standard processes such as the URCA cooling or the modified URCA (MURCA) cooling, see Friman & Maxwell (1979) and Yakovlev & Levenfish (1995), can release neutrinos with associated emissivities $Q_{\mathrm{E}}^{\mathrm{URCA}} \sim 10^{27} R(\frac{k_{\mathrm{B}}T}{0.1\,\mathrm{MeV}})^6$ erg cm^{-3} s^{-1} and $Q_{\mathrm{E}}^{\mathrm{MURCA}} \sim 10^{21} R(\frac{k_{\mathrm{B}}T}{0.1\,\mathrm{MeV}})^8$ erg cm^{-3} s^{-1}, respectively. R is a control function of order unity. These standard processes release energy from the baryonic system, having a very different effect in the energetic balance when compared to average energy injection from stellar DM annihilation processes (Kouvaris 2008). It is important to remark that in this scenario, it can be assumed that neutrinos do not get trapped after being produced and therefore their Fermi-Dirac distributions fulfill $f_\nu \sim 0$.

In this context, to compare the result with the standard physics cooling, in the left panel of Figure 7, the energy emissivity for the process $\chi\chi \to \nu\nu$ as a function of temperature for three sets of DM parameters in Table 1 is shown. The MURCA energy emissivity (solid line) is plotted too for the sake of comparison. Although this latter is not the only

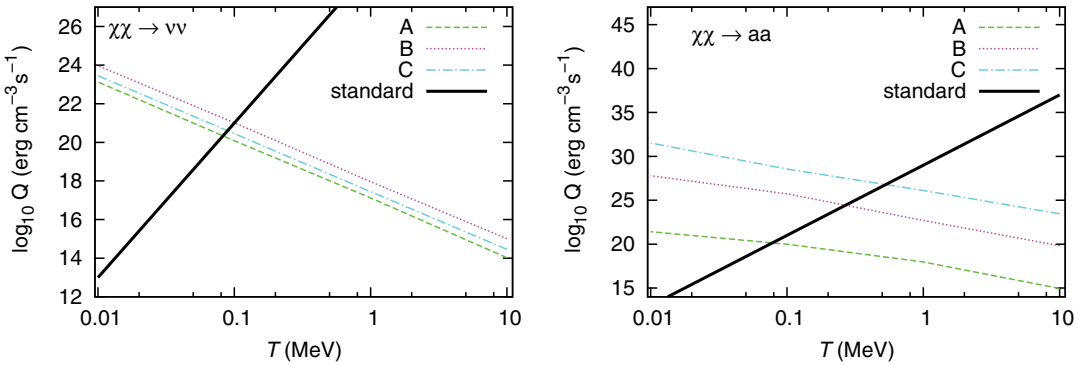

Figure 7. Energy emissivity from channels $\chi\chi \to \nu\nu$ (left) and via pseudoscalar mediators $\chi\chi \to aa$ (right) with subsequent decay $a \to \nu\nu$ as a function of temperature. Standard emission refers to MURCA processes. From Cermeño et al. (2017).

process contributing to the effective cooling, it sets an upper limit to standard emissivities in the scenario depicted due to the fact that to sustain the URCA fast reaction central densities must be higher to provide the ∼11% protons fraction required (Lattimer et al. 1991). It is easy to see that around $T \sim 0.1$ MeV local central emissivities $\log_{10}(Q_{\rm E}) \sim 21$–22 are balanced by the heating processes. It is important to remind ourselves that $T \sim 0.01$ MeV for a NS of $\sim 10^5$ yr. But the most important result is obtained for the reaction $\chi\chi \to aa$ with subsequent decay $a \to \nu\nu$, Figure 7, right panel. In this case, the neutrino emissivity is largely enhanced with respect to the direct production of neutrinos $\chi\chi \to \nu\nu$. For model C (somewhat heavier DM particles), $Q_{\rm E}$ matches and surpasses the standard MURCA emission at $T \lesssim 1$ MeV while model B has analogous behaviour for $T \lesssim 0.3$ MeV. Note that both models provide larger emissivities in this channel than the direct neutrino pair emission in the analysed T range in spite of being in a different range of masses. Model A provides similar results for both emission reactions, however. This effect of enhanced emissivities can have an impact on internal temperatures and matter phases depending critically on them, as can be seen in Page et al. (2014). In this sense, works as Page et al. (2011) and Shternin et al. (2011) quote that the rapid cooling of the Cas A may be an indication of the existence of global neutron and proton superfluidity in the core.

As most of the fraction of DM particles will be in the central region of the NS, characterised by the length $r_{\rm th}$, the impact of the radial extent of an emitting inner region through these new processes can be correlated to the ratio $\xi = (\sqrt{2} r_{\rm th}/R_b)$, which make reference to the fraction where 95% of the approximately Gaussian distribution of DM particles can be found, versus $R_b \sim 9$ km, radial extent of the boundary, or limit of the core-to-crust region. Since the crust region has a tiny mass, in this scenario, it is not necessary to consider the refinement which it is taken into account in Cermeño et al. (2016b). For the models analysed in Cermeño et al. (2017), this fraction ranges from $\xi \in [0.03, 0.42]$ at $T \sim 1$ MeV to $\xi \in [0.01, 0.14]$ at $T \sim 0.1$ MeV.

Focusing in a fixed stellar evolutionary time, t, to analyse the temperature evolution, the radial (internal) heat equation $r < R_b$ can be written as

$$\frac{2}{r} T'(r) + T''(r) = \kappa^{-1}[Q_\nu - H(r)], \tag{17}$$

where κ is the thermal conductivity given by a contribution from baryons and another from electrons Shternin & Yakovlev (2007) $\kappa = \kappa_b + \kappa_e$ and Q_ν is the standard MURCA emissivity, $Q_\nu \sim Q_{\rm E}^{\rm MURCA}$. The DM heating term, $H(r)$, has the radial dependence induced by the DM density so that $H(r) = H_0 e^{-(r/r_0)^2}$ with $H_0 = Q_{\rm E}^{aa} n_{0,\chi}^2$ and $r_0 = r_{\rm th}(T)/\sqrt{2}$. Although a detailed solution of the full evolution equation remains for future works that should consider the dynamical part, in Cermeño et al. (2017) an study of the radial T-profile at different fixed evolutionary times is done solving Equation (17) and assuming a flat initial profile to see how it is distorted from the presence of internal cooling and heating terms. They find that, for example, fixing a value $T(r) \equiv \bar{T}$ for $r \in [0, R_b]$ the central value T_0 is related to it through the approximate solution $T(r) = T_0 + \alpha \frac{r^2}{6} - \beta \frac{r_0^2}{2}[1 - \sqrt{\pi} \frac{r_0}{2} \frac{\mathrm{erf}(r/r_0)}{r}]$, where erf (x) is the error function and $\alpha = Q_\nu(\bar{T})/\kappa(\bar{T})$ and $\beta = H_0(\bar{T})/\kappa(\bar{T})$ are coefficients that can be approximated at $\bar{T}$. Typical values can be seen in Cermeño et al. (2017). The important thing here is that if we fixed, for example, $\bar{T} = 10^9 K \sim 0.1$ MeV, one can verify that the net effect of models B and C is heating the central volume while model A provides net cooling. However, it is important to remark that the star will self-adjust in a consisting way that has to be dynamically determined to see at what extent the subsequent thermal evolution is affected in the stellar volume. This could be studied through a full dynamical simulation to see how the cooling mechanisms adjust inside the star as a temporal sequence.

6 CONCLUSIONS

In summary, in this contribution, we have reviewed some astrophysical consequences of the possible existence of DM by its interaction with ordinary matter ranging from low to high densities. In the parameter space of DM mass to cross-section off nucleons, we have first considered fermionic DM particles

in the light (low) mass region $m_\chi \lesssim 5$ GeV. We discuss the importance of in-medium effects, density, and temperature, in DM-nucleon scattering when DM particles are gravitationally boosted into a dense compact object, where core densities typically exceed a few times n_0 and temperatures $T \lesssim 50$ MeV.

Density effects have to be included through Fermi-Dirac distributions for the nucleon sector, which restrict the parameter space, and effective values for the nucleon mass and its chemical potential, while temperature effects are present through the detailed balance factor, which takes into account the energy gained or lost due during the interaction. Temperature effects have been found to be important although to a lesser extent relative to density ones. The differential and integrated cross-sections are greatly affected by the finite density of matter, namely by the effect of a smaller effective nucleon mass $m_N^* < m_N$. The mean free path for a DM particle is found to be larger than the typical values of those found for SM neutrinos with vector-axial couplings. From these values obtained for the mean free path, it can be concluded that the diffusive behaviour approximation at finite density and temperature in the interior of NS is well grounded and DM can contribute to the energy transport in their interior. The simplified estimate for the mean free path, $\lambda_\chi \simeq 1/\sigma_{\chi N} n$, lacks the rich dependence on the phase space of the scattering process.

Then, restricting more the range of masses $m_\chi \lesssim$ 100 MeV, the interaction between DM particles and the periodically arrange of nuclei in the NS outer crust at lower ordinary densities can be studied. From this interaction, phonons can be created in the lattice. Calculating the phonon excitation rate, it can be seen that this rate is much larger than for cosmological neutrinos. As an astrophysical consequence of this new source of phonons, the ion thermal conductivity in the outer envelope is modified founding that it can be largely enhanced at the highest LDM density $n_\chi \sim 100 n_{0,\chi}$ due to a net modification of the acoustic phonon population. Besides, comparing this result with electronic contribution to the conductivity for magnetised NSs in the perpendicular direction to the magnetic field, an enhanced with respect to electron contribution in this direction can be found. This means that perpendicular thermal conductivity in these scenarios will be higher, and, although a detailed study of the quantitative effect in the surface temperature pattern remains to be undertaken, it is expected that this enhancement allows a reduction of the difference of heat transport among parallel and perpendicular directions to the magnetic field. Based on previous works, as Perna et al. (2013) and Viganò et al. (2014), only including standard thermal contributions we expect that, as a natural consequence, the surface temperature profile would be more isotropic yielding flatter profiles for intermediate latitudes.

Another impact of this dark sector in stellar quantities of NSs is considered for a model of annihilating LDM. We use the Coy DM model, where the energy emissivity due to the annihilation of DM particles into neutrinos through a pseudoscalar interaction is taken into account. In this context and considering not only LDM particles, it is shown that in the inner stellar regions where most of the DM population distribution exists, the emissivity into neutrinos can be enhanced orders of magnitude with respect to the MURCA standard neutrino processes for parameter sets respecting constraints of direct detection limits and cosmological bounds. This novel mechanism of energy release may lead to enhanced cooling features. A detailed analysis is missing to determine whether locally warmer inner temperature stellar profiles that can affect the onset of superfluid phases at typical temperatures $T_c \sim 5 \times 10^9$ K. Although some other heating processes have been quoted in the literature (rotochemical heating, Fernández & Reisenegger (2005), or hot blobs located at different depths in the crust in young NS, Kaminker et al. (2014)) the qualitative picture arising from the DM annihilation process is different, as this heating in the inner region can produce thermal instabilities in the inner core. This could be an interesting field to explore in the future.

ACKNOWLEDGEMENTS

We thank useful discussions with R. Lineros, J. Edsjo, and C. Albertus. This work has been supported by NewCompstar and MINECO Consolider-Ingenio Multidark CSD2009-00064 and FIS2015-65140-P projects. M. Cermeño is supported by a fellowship from the University of Salamanca.

REFERENCES

Aad, G., et al. (ATLAS Collaboration) 2015, PhRvD, 91, 012008
Akerib, D. S., et al. 2017, PhRvL, 118, 021303
Arina, C., Del Nobile, E., & Panci, P. 2015, PhRvL, 114, 011301
Baek, S., Ko, P., & Li, J. 2017, PhRvD, 95, 075011
Baiko, D. A., Kaminker, A. D., Potekhin, A. Y., & Yakovlev, D. G. 1998, PhRvL, 81, 5556
Bauer, M., Haisch, U., & Kahlhoefer, F. 2017, JHEP, 2017, 138
Bertone, G., & Hooper, D. 2016, arXiv:1605.04909v2
Bertoni, B., Nelson, A. E., & Reddy, S. 2013, PhRvD, 88, 123505
Boehm, C., Dolan, M. J., McCabe, C., Spannowsky, M., & Wallace, C. J. 2014, JCAP, 2014, 009
Bramante, J., Fukushima, K., & Kumar, J. 2013, PhRvD, 87, 055012
Carr, W. J. 1961, PhRv, 122, 1437
Cercignani, C., & Kremer, G. M. 2002, The Relativistic Boltzmann Equation: Theory and Applications (Berlin: Birkhuser Verlag)
Cermeño, M., Pérez-García, M. A., & Silk, J. 2016a, PhRvD, 94, 023509
Cermeño, M., Pérez-García, M., & Silk, J. 2016b, PhRvD, 94, 063001
Cermeño, M., Pérez-García, M. A., & Lineros, R. A. 2017, arXiv:1705.03012
Chugunov, A. I., & Haensel, P. 2007, MNRAS, 381, 1143
Cirelli, M. 2012, Pramana, 79, 1021
Clowe, D., Brada, M., Gonzalez, A. H., Markevitch, M., Randall, S. W., Jones, C., & Zaritsky, D. 2006, ApJL, 648, L109
Dolan, M. J., Kahlhoefer, F., McCabe, C., & Schmidt-Hoberg, K. 2015, JHEP, 2015, 171
Esposito, S., Mangano, G., Miele, G., Picardi, I., & Pisanti, O. 2002, MPLA, 17, 491
Essig, R., et al. 2016, JHEP, 5, 46

Fernández, R., & Reisenegger, A. 2005, ApJ, 625, 291
Ferreras, I., & Wasserman, I. 1995, PhRvD, 52, 5459
Friman, B. L., & Maxwell, O. V. 1979, ApJ, 232, 541
Goldman Itzhak Nussinov 1989, PhRvD, 40, 3221
Gould, A. 1987, ApJ, 321, 571
Guver, T., Erkoca, A. E., Reno, M. H., & Sarcevic, I. 2014, JCAP, 2014, 013
Hakim, R. 2011, Introduction to Relativistic Statistical Mechanics Classical and Quantum (Singapore: World Scientific)
Hooper, D., Spolyar, D., Vallinotto, A., & Gnedin, N. Y. 2010, PhRvD, 81, 103531
Horowitz, C., & Wehrberger, K. 1991, PhRvB, 266, 236
Horowitz, C. J., & Pérez-García, M. A. 2003, PhRvC, 68, 025803
Horowitz, C. J., Pérez-García, M. A., & Piekarewicz, J. 2004, PhRvC, 69, 045804
Hubble, E., & Humason, M. L. 1931, ApJ, 74, 43
Juttner, F. 1911, Ann. Phys. Chem., 339, 856
Kaminker, A. D., Kaurov, A. A., Potekhin, A. Y., & Yakovlev, D. G. 2014, MNRAS, 442, 3484
Kaminker, A. D., Yakovlev, D. G., Potekhin, A. Y., Shibazaki, N., Shternin, P. S., & Gnedin, O. Y. 2007, Ap&SS, 308, 423
Khachatryan, V., et al. 2015, EPJC, 75, 235
Kouvaris, C. 2008, PhRvD, 77, 023006
Kouvaris, C., & Tinyakov, P. 2010, PhRvD, 82, 063531
Kouvaris, C., & Tinyakov, P. 2011a, PhRvD, 83, 083512
Kouvaris, C., & Tinyakov, P. 2011b, PhRvL, 107, 091301
Krauss, L. M., Srednicki, M., & Wilczek, F. 1986, PhRvD, 33, 2079
Lattimer, J. M., Pethick, C. J., Prakash, M., & Haensel, P. 1991, PhRvL, 66, 2701
Lin, T., Yu, H., & Zurekl, K. M. 2012, PhRvD, 85, 063503
Lopes, I., & Silk, J. 2010, Science, 330, 462
Lorimer, D. R., et al. 2006, MNRAS, 372, 777
McCullough, M., & Fairbairn, M. 2010, PhRvD, 81, 083520
McDermott, S. D., Yu, H.-B., & Zurek, K. M. 2012, PhRvD, 85, 023519
Nagara, H., Nagata, Y., & Nakamura, T. 1987, PhRvA, 36, 1859
Negele, J. W., & Vautherin, D. 1973, NuPhA, 207, 298
Page, D., Lattimer, J. M., Prakash, M., & Steiner, A. W. 2004, ApJS, 155, 623
Page, D., Lattimer, J. M., Prakash, M., & Steiner, A. W. 2014, in Novel Superfluids, Vol. 2, eds. Karl-Heinz Bennemann & John B. Ketterson (Oxford: Oxford University Press), chap. 21
Page, D., Prakash, M., Lattimer, J. M., & Steiner, A. W. 2011, PhRvL, 106, 081101
Patrignani, C., Particle Data Group 2016, ChPhC, 40, 100001
Pérez-Azorín, J. F., Miralles, J. A., & Pons, J. A. 2006, A&A, 451, 1009
Pérez-García, M. A., Daigne, F., & Silk, J. 2013, ApJ, 768, 145
Pérez-García, M. A., & Silk, J. 2012, PhLB, 711, 6
Pérez-García, M. A., & Silk, J. 2015, PhLB, 744, 13
Pérez-García, M. A., Silk, J., & Stone, J. R. 2010, PhRvL, 105, 141101
Perna, R., Viganò, D., Pons, J. A., & Rea, N. 2013, MNRAS, 434, 2362
Planck Collaboration et al. 2014, A&A, 571, A16
Potekhin, A. Y., Chabrier, G., & Yakovlev, D. G. 1997, A&A, 323, 415
Press, W. H., & Spergel, D. N. 1985, ApJ, 296, 679
Reddy, S., Prakash, M., & Lattimer, J. M. 1998, PhRvD, 58, 013009
Rubin, V. C., & Ford, W. K. Jr. 1970, ApJ, 159, 379
Rüster, S. B., Hempel, M., & Schaffner-Bielich, J. 2006, PhRvC, 73, 035804
Serot, B., & Walecka, J. D. 1986, Advances in Nuclear Physics, Vol. 16 (New York: Plenum Press)
Shternin, P. S., & Yakovlev, D. G. 2007, PhRvD, 75, 103004
Shternin, P. S., Yakovlev, D. G., Heinke, C. O., Ho, W. C. G., & Patnaude, D. J. 2011, MNRAS: Letters, 412, L108
Spergel, D. N., & Press, W. H. 1985, ApJ, 294, 663
Turolla, R., Zane, S., & Watts, A. L. 2015, RPPh, 78, 116901
Viganò, D. 2013, PhD thesis, Universiy of Alicante, arXiv: 1310.1243
Viganò, D., Perna, R., Rea, N., & Pons, J. A. 2014, MNRAS, 443, 31
Yakovlev, D. G., & Levenfish, K. P. 1995, A&A, 297, 717
Zeldovich, Y. B. 1965, ZhETF, 48, 986
Zeldovich, Y. B., Okun, L., & Pikelner, S. B. 1965, UsFiN, 84, 113
Zentner, A. R. 2009, PhRvD, 80, 063501
Ziman, J. M. 1960, Electrons and Phonons (Oxford: Oxford University Press)

Chapter 7

Modified Gravity at Astrophysical Scales

Usando una aproximación perturbativa, en esta contribución se resuelven las ecuaciones de estructura estelar para estrellas de tipo solar, cuyo interior es descrito por una ecuación de estado politrópica de índice $n = 3$, en el contexto de teorías de MG. En lugar de centrarnos en un modelo determinado de los existentes en la literatura, hacemos un estudio general en el que las desviaciones de la teoría de GR están descritas por un único parámetro ξ. Tras esto, obtenemos que, para escalas de longitud de $\sqrt{\xi}$ entre uno y dos órdenes de magnitud menores que los radios estelares obtenidos usando GR, las modificaciones introducidas por las teorías de MG afectan a los valores de las masas y los radios de las estrellas haciendo que los diagramas $M - R$ difieran del caso constante obtenido para GR. Encontramos que para $\xi > 0$ las masas aumentan al disminuir el radio, siendo el aumento mayor para radios pequeños. Además, valores de ξ negativos proporcionan configuraciones estelares metaestables, de modo que pueden considerarse excluidos. Como consecuencia a estas modificaciones de M y R, tanto la temperatura como la luminosidad se ven afectadas, aumentado la pendiente de ésta última con respecto a la temperatura efectiva un $\sim 0.6\%$ con respecto al caso de GR. Finalmente, discutimos las posibles implicaciones de estas teorías para estrellas de mayores densidad (WDs) y la observabilidad de estos efectos.

The Astrophysical Journal, 872:130 (7pp), 2019 February 20 https://doi.org/10.3847/1538-4357/ab001c

Modified Gravity at Astrophysical Scales

M. Cermeño[1], J. Carro[2], A. L. Maroto[2], and M. A. Pérez-García[1]
[1] Department of Fundamental Physics, University of Salamanca, Plaza de la Merced s/n, E-37008 Salamanca, Spain; marinacgavilan@usal.es, mperezga@usal.es
[2] Departamento de Física Teórica and UPARCOS, Universidad Complutense de Madrid, E-28040 Madrid, Spain; maroto@ucm.es
Received 2018 November 26; revised 2019 January 17; accepted 2019 January 17; published 2019 February 19

Abstract

Using a perturbative approach we solve stellar structure equations for low-density (solar-type) stars whose interior is described with a polytropic equation of state in scenarios involving a subset of modified gravity (MG) theories. Rather than focusing on particular theories, we consider a model-independent approach in which deviations from General Relativity are effectively described by a single parameter ξ. We find that for length scales below those set by stellar General Relativistic radii the modifications introduced by MG can affect the computed values of masses and radii. As a consequence, the stellar luminosity is also affected. We discuss possible further implications for higher-density stars and observability of the effects previously described.

Key words: cosmological parameters – gravitation – stars: general

1. Introduction

It is well established that General Relativity (GR) provides an accurate description of the gravitational interaction from the submillimeter scales probed by torsion balance experiments (Adelberger et al. 2003, 2009) to kiloparsec distances as confirmed by recent observations of strong gravitational lensing of extragalactic objects (Collett et al. 2018). These tests probe the weak-field regime of the theory, and so far no discrepancy with respect to the predictions of GR has been found. For strong fields, the theory is still poorly tested, but the recent discovery of gravitational waves produced in the merger processes of black holes (Abbott et al. 2016) or neutron stars (Abbott et al. 2017) has opened a new avenue to explore this regime of the theory. Despite the success of GR on small (subgalactic) scales, the difficulties of accommodating the observed accelerated expansion of the universe within the theory has led to the suggestion that the universal attractive character of gravity could break down on cosmological scales. Several modified gravity (MG) theories have been proposed in the last few years that introduce additional degrees of freedom, typically scalars, that mediate the gravitational interaction, thus changing its behavior on very large scales.

On small scales, the new degrees of freedom are usually screened (Vainshtein 1972; Khoury & Weltman 2004; Hinterbichler & Khoury 2010) so that the agreement of standard GR with observations is not spoiled (Joyce et al. 2015; Burrage & Sakstein 2018). However, in certain modified gravities, such as beyond Horndeski models (Zumalacárregui & García-Bellido 2014; Gleyzes et al. 2015), the screening mechanism is only partially operational, and, in particular, it could break down (Koyama & Sakstein 2015; Saito et al. 2015) inside astrophysical objects, such as stars, where a weakening of the gravitational interaction is predicted (Kobayashi et al. 2015). This possible modification has also been studied in other approaches (Pérez-García & Martins 2012). Such deviations from Newton's law can produce modifications in the internal stellar structure. This fact has motivated the use of different types of stars, i.e., main sequence (Koyama & Sakstein 2015; Sakstein 2015a; Velten et al. 2016), white dwarfs (WDs; Sakstein 2015b; Babichev et al. 2016; Jain et al. 2016), or neutron stars (Babichev et al. 2016; Capozziello et al. 2016; Velten et al. 2016), as probes for alternative gravitational models.

Despite the fact that some of the theories beyond that of Horndeski have been practically ruled out by the observation of the GW170817 event, some of them are still viable modifications of gravity (Ezquiaga & Zumalacárregui 2017, 2018). For a discussion see Baker et al. (2017), Creminelli & Vernizzi (2017), and Sakstein & Jain (2017). Thus, in such theories the equation for hydrostatic equilibrium in the nonrelativistic regime is modified in such a way that (Koyama & Sakstein 2015)

$$\frac{dP}{dr} = -\rho\frac{Gm(r)}{r^2} - \frac{\rho\Upsilon G}{4}\frac{d^2m(r)}{dr^2}, \tag{1}$$

where P is the pressure, $m(r)$ is the mass inside a radius r, ρ is the energy density, G is the gravitational constant (Patrignani & Particle Data Group 2016), and Υ is a constant parameterizing the deviation with respect to GR. Existing bounds $-0.22 < \Upsilon < 1.6$ are set by the Chandrasekhar limit on WD stars (Babichev et al. 2016; Jain et al. 2016) and the minimum mass of main-sequence stars (Sakstein 2015a; Babichev et al. 2016; Saltas et al. 2018).

On more general grounds, effective descriptions of alternative gravity theories have been developed in recent years aiming to encapsulate in a few parameters all the relevant modifications at a given scale (Clifton et al. 2012; Silvestri et al. 2013). These parameterizations have been widely employed in the analysis of structure and lensing data of galaxy surveys (Amendola et al. 2018).

In this work, we will explore the implications for stellar structure of one of the simplest and most widely used effective parameterizations considered in the literature (Bertschinger & Zukin 2008; Silvestri et al. 2013). For a wide class of theories of gravity with one additional scalar degree of freedom, assuming the quasi-static approximation and not higher than second-order equations of motion, it can be seen that all the relevant modifications can be encoded in an effective Newton's

constant parameterized in Fourier space by $\mu(k) = G_{\rm eff}(k)/G$, with G as the ordinary Newton's constant, and a gravitational slip parameter $\gamma(k) = \phi(k)/\psi(k)$. The $\mu(k)$ parameter changes the hydrostatic equilibrium equation introducing, generically, a new length scale in the dynamics and leading to expressions that can deviate from Equation (1). This effective approach will allow us to analyze the potential modifications in the stellar structure, including radius, mass, luminosity, and temperature of stars, in a largely model-independent way.

The manuscript is structured as follows. In Section 2, we briefly review and expose the main features of the MG theories we consider in our analysis of the changes induced in the stellar structure equations. We also present the main scenario we explore, i.e., low-density stars, and discuss the validity of our approach. The results are then detailed in Section 3, and final conclusions are drawn in Section 4.

2. Stellar Structure Equations

In this section, we start by presenting the standard setup of the calculation for the structure of a stellar object of mass M and radius R in GR. We consider for the sake of simplicity a nonrelativistic and nonrotating object. Following Silvestri et al. (2013) we consider a spherical Minkowski metric with linear scalar perturbations through the introduction of two radial potentials, $\psi(r)$ and $\phi(r)$, both fulfilling the condition of weak-field approximation, i.e., $\psi(r) \ll 1$, $\phi(r) \ll 1$. The interval $d\tau^2 = g_{\mu\nu}dx^\mu dx^\nu$ is written as

$$d\tau^2 = -(1 + 2\psi(r))dt^2 + (1 - 2\phi(r))(dr^2 + r^2 d\Omega^2), \quad (2)$$

where the four coordinates of x^μ are t, r, θ, and ϕ.

From the selected metric, $g_{\mu\nu}$, and using the approximation of a perfect fluid, the energy momentum tensor can be written as

$$T_{\mu\nu} = (\rho + P)U_\mu U_\nu + P g_{\mu\nu}. \quad (3)$$

U^μ is the fluid four-velocity. We assume static solutions with $U_\mu = (U_t, 0, 0, 0)$ and impose $U^\mu U_\mu = -1$. We can obtain the Einstein's equations $G_{\mu\nu} = 8\pi G T_{\mu\nu}$ with $G_{\mu\nu} = R_{\mu\nu} - \frac{1}{2}g_{\mu\nu}R$ the Einstein's tensor given by the Ricci tensor, $R_{\mu\nu}$, and the Ricci scalar, R, for this metric. Explicitly, these expressions read to first order in metric perturbations

$$2\phi'(r) + r\phi''(r) = 4\pi G r \rho(r), \quad (4)$$

$$(\psi(r) - \phi(r))' = 4\pi G r P(r), \quad (5)$$

and

$$(\psi(r) - \phi(r))' + r(\psi''(r) - \phi''(r)) = 8\pi G r P(r). \quad (6)$$

In addition, for the spatial diagonal component of the energy momentum tensor we can approximate to first order in metric perturbations $T_{ii} = P(1 - 2\phi) \simeq P$, being $i = 1, 2, 3$ a spatial index.

As obtained, it is clear that Equation (4) is the Poisson equation for ϕ,

$$\nabla^2\phi = 4\pi G\rho. \quad (7)$$

If we take into account the mass relation

$$\frac{dm}{dr} = 4\pi r^2 \rho, \quad (8)$$

then from Equation (7) we obtain

$$\frac{d\phi}{dr} = \frac{Gm(r)}{r^2}. \quad (9)$$

On the other hand, using Equations (5) and (9) we obtain

$$\frac{d\psi}{dr} = \frac{Gm(r) + 4\pi G r^3 P}{r^2}. \quad (10)$$

Now, if we use the continuity equation $\nabla_\mu T^{\mu\nu} = 0$, we finally obtain

$$\frac{dP}{dr} = -(\rho + P)\frac{d\psi}{dr}. \quad (11)$$

It is important to note that Equations (10) and (11) along with the mass equation Equation (8) are the structure equations for the potential, pressure, and mass in the star. Besides, using Equations (5) and (6) we get $\psi - \phi = C_1 + C_2 r^2$, with C_1 and C_2 as constants. If we impose the existence of a finite solution when $r \to \infty$, it follows that $C_2 = 0$. On the other hand, for $r > R$ we have to recover the Schwarzschild metric, which means $\psi = \phi$. In this way, $C_1 = 0$ and $\psi - \phi = 0$, making $P = 0$. This result is due to the fact that we obtain a first-order perturbation solution, being $\psi \sim \phi \sim \frac{-Gm(r)}{r}$. Then, whereas ρ and ψ are first-order functions in perturbation theory, P is a second-order function in perturbations. We can thus rewrite Equations (10) and (11) as

$$\frac{d\psi}{dr} = \frac{Gm(r)}{r^2} \quad (12)$$

and

$$\frac{dP}{dr} = -\rho\frac{d\psi}{dr}, \quad (13)$$

retaining only the leading contributions, i.e., first and the second order, respectively. From Equation (12) the mass of the star can be solved as

$$m(r) = \frac{r^2}{G}\psi'(r). \quad (14)$$

2.1. Input from MG Theories

In the context of MG theories and for static configurations following Silvestri et al. (2013), we introduce two functions, $\mu(k)$ and $\gamma(k)$, in the Fourier k-space whose effect is modifying the equations governing the solution of the potentials ψ, ϕ. We can write

$$\nabla^2\psi = 4\pi G\mu\rho \quad (15)$$

and

$$\phi = \gamma\psi. \quad (16)$$

The physical meaning of the $\mu(k)$ function is that of providing an effective value of the gravitational constant, G. Instead, $\gamma(k)$ establishes a relationship between the two potentials, ψ and ϕ. When $\mu = \gamma = 1$, we recover GR equations. The most general expression for $\mu(k)$ in theories with one extra scalar degree of freedom and modified Einstein's equations involving up to second-order derivatives can be cast into the rational form

(Silvestri et al. 2013)

$$\mu(k) = \frac{1 + p_3 k^2}{p_4 + p_5 k^2}. \tag{17}$$

The previous step stems from the fact that it is indeed equivalent to rewrite Equation (15) as

$$p_4 \nabla^2 \psi - p_5 \nabla^4 \psi = 4\pi G(\rho - p_3 \nabla^2)\rho, \tag{18}$$

which is a local expression. Keeping this in mind we can now obtain the expression of μ in position space as

$$\mu(r) = \frac{1 - p_3 \nabla^2}{p_4 - p_5 \nabla^2}, \tag{19}$$

with p_3, p_4, p_5 as constant parameters. Thus, for example, by defining $\beta_1 = p_3/p_5$ it has been shown (Bertschinger & Zukin 2008; Giannantonio et al. 2010) that several models such as $f(R)$ or certain Chameleon theories correspond to $\beta_1 = 4/3$. The parameter values corresponding to other models like Yukawa-type theories belong to the interval $0.75 < \beta_1 < 1.25$. Furthermore, as we will show below, $\gamma(k)$ plays no role in our study, so we do not provide any particular parameterization for it. In any case, we should keep in mind that more general parameterizations exist (Hojjati et al. 2014) that could also include additional vector degrees of freedom (Resco & Maroto 2018).

As can be readily seen, under the conventions used, p_3 and p_5 have units of squared length, while p_4 is dimensionless. Using Equation (19) we can rewrite Equation (15) as

$$\psi'' + \frac{2}{r}\psi' = 4\pi G\left(\frac{1 - p_3 \nabla^2}{p_4 - p_5 \nabla^2}\right)\rho, \tag{20}$$

which generalizes the Poisson equation in our post-Newtonian scenario (Pani et al. 2011).

As we want to consider small perturbations from GR, in what follows we demand p_4 does not depart largely from unity and $p_3 \nabla^2 \ll 1$ and $p_5 \nabla^2 \ll 1$. In this scenario, for spherically symmetric configurations, Equation (8) now takes the form

$$\frac{dm}{dr} = \frac{r^2}{G}\mu^{-1}\left[\frac{1}{r^2}(r^2\psi')'\right], \tag{21}$$

where the differential operator μ^{-1} is given to first order in the perturbative expansion by

$$\mu^{-1} = p_4(1 - \xi \nabla^2), \tag{22}$$

where

$$\xi = -p_3 + \frac{p_5}{p_4}. \tag{23}$$

From integration of Equation (21) we get to first order

$$m(r) = \frac{p_4}{G} r^2 \psi'(r) - \frac{p_4 \xi}{G} r^2 \left(\frac{1}{r^2}(r^2\psi')'\right)'. \tag{24}$$

In addition, we can also write

$$\frac{d\psi}{dr} = \frac{Gm(r)}{p_4 r^2} + \frac{\xi G}{p_4}\left(\frac{m''(r)}{r^2} - \frac{2m'(r)}{r^3}\right), \tag{25}$$

which is the modified version of Equation (12). Finally,

$$\frac{dP}{dr} = -\rho\frac{Gm(r)}{p_4 r^2} - \frac{\xi \rho G}{p_4}\left(\frac{m''(r)}{r^2} - \frac{2m'(r)}{r^3}\right). \tag{26}$$

At this point it is important to notice that the subset of MG models we are considering only hold in the linear regime, which we assume to be the one valid inside solar-type stars (and other high-density stars such as WDs). In this sense, we must emphasize that some proposed modifications of gravity on cosmological scales that rely on screening mechanisms (Koyama & Sakstein 2015; Saito et al. 2015) through nonlinear effects on astrophysical scales are not covered by this approach.

Notice that because of the form of the effective operator μ, the structure of the pressure equation is different from that shown in Equation (1). A few comments are in order. For simplicity we have limited ourselves to the case in which the parameters p_3, p_4, and p_5 are just object-independent constants. In the most general case, for the spherically symmetric configurations considered in the work and unlike the cosmological case discussed in Silvestri et al. (2013), these parameters could be general functions of the stellar radius. Thus, for example, the p_4 parameter related to the effective Newton's constant could interpolate between different values in the interior and exterior of the star. However, in our case with constant p_4, matching with the laboratory-measured value of Newton constant G imposes $p_4 = 1$. Thus, the combination G/p_4 appearing in the obtained structure equations inside the stellar body will effectively take the value G. The possibility of changing the effective Newton's constant in astrophysical objects as compared to the laboratory value has been considered phenomenologically in previous works in non-weak-field limits; see, for instance, Velten et al. (2016) and references therein, where an α parameter is used analogously to our p_4 or in cosmological contexts, and see Planck Collaboration et al. (2016) for explicit measurements of μ_0.

2.2. Perturbative Solution for a Polytropic Star

We have seen that the potential ψ, the density ρ, and the pressure P are related through Equation (13). In this way, given an equation of state (EoS) determining a relation between P and ρ we could, in principle, obtain an expression for $\psi(\rho)$.

In this work, we use a polytropic EoS that can be considered a reasonable description for main-sequence (solar-type) stars (Hansen et al. 1994). In addition, we will also consider the higher-density case of WDs. No dark matter presence is assumed (Pérez-García et al. 2013; Cermeño & Pérez-García 2018) in this context. As mentioned, a generic polytropic EoS takes the simple form

$$P = K\rho^{1+\frac{1}{n}}, \tag{27}$$

where n is the so-called polytropic index, which is related to the internal constituents of the star, and K is a constant with appropriate units. In this work, we use CGS units.

Therefore, using Equations (13) and (27), for $n > 0$ we have

$$\rho = \left(\frac{-\psi}{(n+1)K}\right)^n, \tag{28}$$

whereas for $n = 0$ the equation simply takes the form $\rho = \rho_c$, with ρ_c as the central density of the star. The equation for the ψ

potential can be written under the form

$$\psi'' + \frac{2}{r}\psi' = 4\pi G\mu\left(\frac{-\psi}{(n+1)K}\right)^n. \quad (29)$$

In order to solve the differential equation in Equation (29) using a perturbative approach, one can propose a solution under the form $\psi = \psi_0 + \psi_1$, with $|\psi_1| \ll |\psi_0|$. Thus, a set of two differential equations is obtained, one for each component, ψ_0, ψ_1:

$$\psi_0'' + \frac{2}{r}\psi_0' = 4\pi G\left(\frac{-\psi_0}{(n+1)K}\right)^n, \quad (30)$$

and

$$\psi_1'' + \frac{2}{r}\psi_1' = \frac{4\pi G}{(n+1)^n K^n}[\xi\nabla^2(-\psi_0)^n - n(-\psi_0^{n-1})\psi_1]. \quad (31)$$

Let us mention that this same result would follow from the alternative calculation using a perturbative expansion of ψ and ρ in Equation (18). Notice that the perturbative approach allows us to solve separately the gravitational potential equation from the conservation equation shown in Equation (13), which remains unchanged with respect to the ordinary GR case.

In order to calculate the radius R and mass M we must first obtain the solution $\psi(r)$, which will provide us the density ρ through Equation (28). By imposing $\psi(R) = 0$, the radius R will be calculated from the usual consideration that both pressure and density vanish for $r = R$.

Accordingly, the total mass of the star, $M(R)$, is obtained using Equation (28) and integrating Equation (8), so finally

$$M(R) = \int_0^R 4\pi r^2\rho dr. \quad (32)$$

It is important to note that if we impose $\xi = 0$ we will recover the GR case. In order to be more definite we now particularize to the perturbative solution for a polytropic $n = 3$ star focusing on the case of low-mass solar-type stars $M \lesssim M_\odot$. Most of the internal description is reasonably well described by a polytrope with an $n = 3$ index. Refinements to this description would involve, at least, the use of several polytropes or, more appropriately, an improved version (Hansen et al. 1994) of the standard solar model (SSM; Turck-Chieze & Couvidat 2011). Note, however, that the goal of our calculation is not a detailed modeling of the stellar object but rather showing the effects of selected MG models, thus we will restrict to a single polytropic EoS. Therefore, in this case, it can be written as

$$P = K\rho^{\frac{4}{3}}. \quad (33)$$

In addition, Equations (30) and (31) for this specific polytrope take the form

$$\psi_0'' + \frac{2}{r}\psi_0' = \frac{-\pi G}{16}\left(\frac{\psi_0}{K}\right)^3 \quad (34)$$

and

$$\psi_1'' + \frac{2}{r}\psi_1' = \frac{-\pi G}{16K^3}[\xi\nabla^2(\psi_0)^3 + 3(\psi_0)^2\psi_1]. \quad (35)$$

The density profile and the mass can be obtained as

$$\rho(r) = \left(\frac{-\psi}{4K}\right)^3, \quad (36)$$

from which the radius R is derived through the relation it must fulfill, $\rho(R) = 0$, which is needed to calculate the stellar mass

$$M = \frac{-\pi}{16K^3}\int_0^R \psi^3(r)r^2dr. \quad (37)$$

For reference, solutions for the radii and masses of solar-type configurations in the GR case we consider in this work have been obtained using $K = 3.8\ \mathrm{cm^3\ g^{-\frac{1}{3}}\ s^{-2}}$ so that we can recover values close to those of the Sun, $M_0 = 1.95674 \times 10^{33}\ \mathrm{g}$ and $R_0 = 6.8141 \times 10^{10}\ \mathrm{cm}$. A central density value $\rho_c = \rho_0 = 80\ \mathrm{g\ cm^{-3}}$ has been used.

In addition, stellar luminosity, L, can be derived by considering the energetics taking place inside the stellar volume through the differential law

$$dL = \epsilon dm, \quad (38)$$

where ϵ is the nuclear energy generation rate in units of $\mathrm{erg\ g^{-1}\ s^{-1}}$. In general, ϵ can display a rather complicated expression, but its main contribution can be parameterized for a low-mass solar-type star with an active *pp* chain under the form (Maciel 2016)

$$\epsilon(r) = 2.46 \times 10^6\ \mathrm{erg\ g^{-1}\ s^{-1}}\,\rho(r) \times X^2\left(\frac{T(r)}{10^6\ \mathrm{K}}\right)^{-\frac{2}{3}} e^{-33.81\left(\frac{T(r)}{10^6\ \mathrm{K}}\right)^{-\frac{1}{3}}}, \quad (39)$$

where X is the proton fraction and T is the temperature of the star. Thus, the luminosity (in $\mathrm{erg\ s^{-1}}$) can be derived as

$$L = \int_0^R 4\pi r^2\rho(r)\epsilon(r)dr. \quad (40)$$

For most stars (with the exception of very low mass stars and stellar remnants) the ions and electrons can be treated as an ideal gas and quantum effects do not critically affect their behavior. In our treatment and in order to keep our modelization simplified, we will consider that the radiation pressure is much smaller than that of the gas of ions and electrons in the stellar plasma, i.e., $P_r \ll P_{\mathrm{gas}}$. Note that for the particular example of the Sun core $P_r \sim 10^{-4}P_{\mathrm{gas}}$. As mentioned, a more general treatment (Koyama & Sakstein 2015) would involve considering a mixture of both pressure components.

Therefore, in our scenario, the stellar conditions are dominated by the gas pressure $P \approx P_{\mathrm{gas}} = \frac{\rho k_{\mathrm{B}} T}{\bar{\mu} m_{\mathrm{H}}}$, with $\bar{\mu}$ the mean molecular weight, m_{H} the hydrogen mass, and k_{B} the Boltzmann constant. Then, the temperature can be written for the $n = 3$ polytropic star as

$$T = \frac{\bar{\mu} m_{\mathrm{H}} K\rho^{\frac{1}{3}}}{k_{\mathrm{B}}}. \quad (41)$$

3. Results

In this section, we analyze the results obtained for several magnitudes of interest we have calculated in the context of the MG modelizations under study. In order to solve

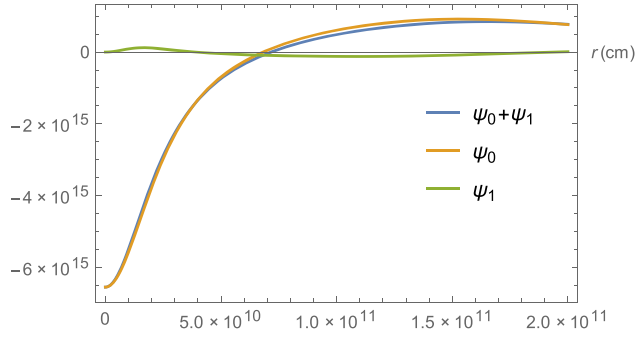

Figure 1. Potential $\psi = \psi_0 + \psi_1$, constructed from the unperturbed potential ψ_0 and the perturbation ψ_1 as a function of r for $\xi = -2.67 \times 10^{18}\,\mathrm{cm}^2$. We take $\rho_c = \rho_0 = 80\,\mathrm{g\,cm}^{-3}$.

Equations (34) and (35), we take $K = 3.8\,\mathrm{cm}^3\,\mathrm{g}^{-\frac{1}{3}}\,\mathrm{s}^{-2}$ so that we can recover typical values of radius and mass of solar-type stars, R_0 and M_0, used as normalization. Although we do not attempt to accurately model stellar values of relevant magnitudes, it is worth mentioning at this point that in our polytropic description most of the stars, i.e., in the region $r < 0.7\,R_\odot$, are well approximated by a polytrope of index $n = 3$, while for the outer region, with convective behavior, it would be better described by a polytrope of index $n = 1.5$. The latter corresponds, however, only to 0.6% of the mass.

In Figure 1, we consider the case of a low-density solar-type model with a central density $\rho_c = \rho_0$ ($\rho_0 = 80\,\mathrm{g\,cm}^{-3}$). We show the solution potentials, i.e., the potential before introducing the perturbation, ψ_0, and the perturbation, ψ_1, fulfilling $|\psi_1| \ll |\psi_0|$, as well as their sum $\psi = \psi_0 + \psi_1$, as functions of the radial coordinate r for $\gamma = 1$ and $\xi = -2.67 \times 10^{18}\,\mathrm{cm}^2$. More generally, we obtain that only for values of $|\xi| \lesssim 1.225 \times 10^{19}\,\mathrm{cm}^2$ does a perturbative correction $|\psi_1| \leqslant 0.1|\psi_0|$ indeed justify our framework.

As we have mentioned before, the radius of the star in this approach can be obtained as the first zero of the full potential solution, $\psi(R) = 0$. Once we know this value, the mass of the star is obtained as $M = M(R) = \int_0^R 4\pi r^2 \rho dr$.

In Figure 2, we plot the M–R relationship for $|\xi| = 4 \times 10^{18}\,\mathrm{cm}^2$. We normalize to values obtained in the solar-type case R_0 and M_0. The solid line corresponds to the case in which $\xi > 0$ and the dashed line to $\xi < 0$. We take $\rho_c \in [0.05, 5]\rho_0$ to generate our data points. We can see that in all cases corresponding to MG the relation gets distorted from the $n = 3$ GR case in which M is constant when varying ρ_c. Objects along the M–R curve with a positive slope $dM/dR > 0$ denote metastable configurations so that in our analysis they are discarded.

In Figure 3, the M–R diagram is shown. It has been obtained by varying the central density value in the interval $\rho_c \in [0.05, 5]\rho_0$. We use $\xi = 2.5 \times 10^{17}\,\mathrm{cm}^2$ (solid line) and $\xi = 10^{18}\,\mathrm{cm}^2$ (dashed line). We can observe how the shape of the M–R diagram slightly changes (compared to the flat $M/M_0 = 1$ result from GR) for different values of ξ, being more significant for objects with lower radii. The star will achieve a more massive configuration as ξ increases.

Stellar mass and radius can be described with an approximate fit as functions of (ξ, ρ_c). In this way, the stellar radius

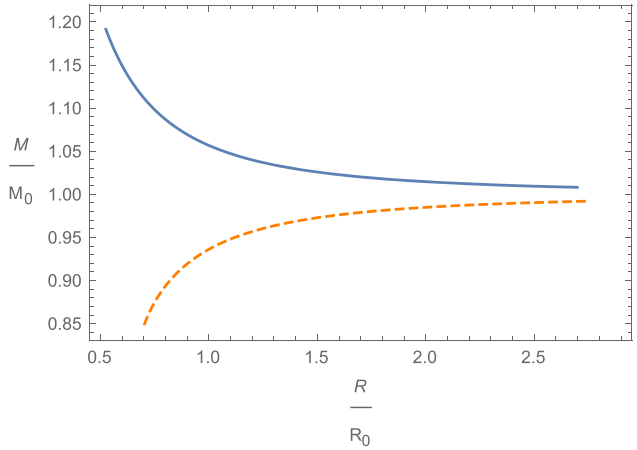

Figure 2. Mass–radius relationship for $|\xi| = 4 \times 10^{18}\,\mathrm{cm}^2$. Solid line corresponds to the case in which $\xi > 0$ and dashed line to $\xi < 0$. We use $\rho_c \in [0.05, 5]\rho_0$. See the text for details.

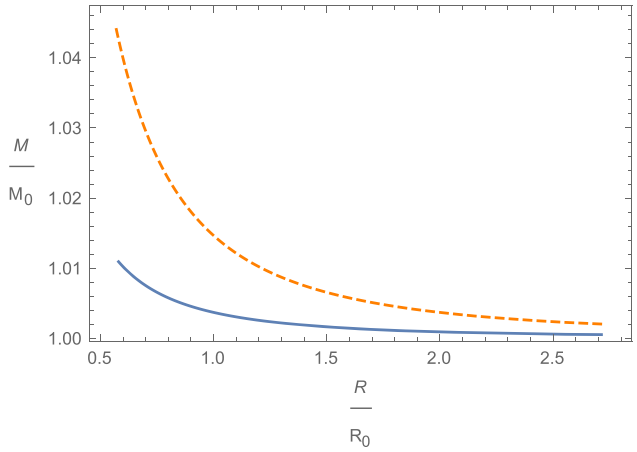

Figure 3. Mass–radius relationship for values $\xi = 2.5 \times 10^{17}\,\mathrm{cm}^2$ (solid line) and $\xi = 10^{18}\,\mathrm{cm}^2$ (dashed line). We use $\rho_c \in [0.05, 5]\rho_0$. See the text for details.

$R(\xi, \rho_c)$ is given by

$$\frac{R}{R_0} = \left(1 + \frac{\xi}{10^{19}\,\mathrm{cm}^2}\right)^{-0.116} \left(\frac{\rho_c}{\rho_0}\right)^{-0.333 - 0.075 \frac{\xi}{10^{19}\,\mathrm{cm}^2}}. \quad (42)$$

For masses $M(\xi, \rho_c)$, instead, the corresponding fit is

$$\frac{M}{M_0} = \left(1 + \frac{\xi}{10^{19}\,\mathrm{cm}^2}\right)^{0.15} \left(\frac{\rho_c}{\rho_0}\right)^{0.1 \frac{\xi}{10^{19}\,\mathrm{cm}^2}}. \quad (43)$$

Using this fit, GR solutions $M/M_0 = 1$ and $R/R_0 = 1$ are obtained when $\xi = 0$ and $\rho_c = \rho_0$.

In Figure 4, we plot stellar density and temperature (normalized to the central values) as a function of r/R_0, fixing $\rho_c = \rho_0$ for $\xi = 9 \times 10^{18}\,\mathrm{cm}^2$ (solid lines) and $\xi = 0$ (dashed lines), the latter corresponding to the GR case. Central temperature is obtained using Equation (41) with $\bar{\mu} = 0.61$, corresponding to hydrogen, helium fractions of solar-type stars $X \sim 0.7$, $Y \sim 0.3$ yielding a central value $T_c \sim 1.21 \times 10^7\,\mathrm{K}$. As can be seen, the value of the density (temperature) profile for the MG case of $\xi = 9 \times 10^{18}\,\mathrm{cm}^2$ is only slightly changed when compared to the GR case. The temperature radial profile,

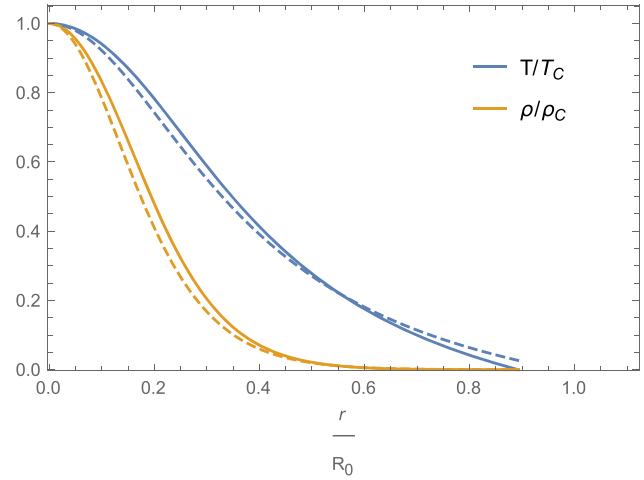

Figure 4. Density and temperature as a function of r/R_0 for a solar-type star. We take $\xi = 9 \times 10^{18}$ cm^2 (solid lines) and $\xi = 0$ (dashed lines) to compare with the GR case.

$T(r)$, also governs the change in the luminosity of (low-mass) solar-type stars.

In Figure 5, we plot stellar luminosity as a function of ξ. We consider $\rho_c = \rho_0$ (solid line) and $\rho_c = 100\,\mathrm{g\,cm^{-3}}$ (dashed line). From considerations relative to solar emission uncertainties, a $\sim\pm 1\%$ flux accuracy in the SSM could accommodate variations of GR taking place below length scales $\sqrt{\xi} \sim 10^9$ cm. Although variations expected for some objects may be indeed larger, it may be extremely difficult to disentangle the presence of such a component from an ordinary variation due to the complex dynamics of the stellar (solar) interior.

In order to size the impact of the models under study in the MG scenario on the luminosity and temperature, a prescribed correspondence with a blackbody spectrum $L = 4\pi R^2 T_{\rm eff}^4$ has been used in Figure 6. We plot stellar luminosity as a function of effective temperature, $T_{\rm eff}$. We consider values $\xi = -4\times 10^{18}$, 0, and 4×10^{18} cm^2 (blue, orange, and green lines, respectively). Values $\xi < 0$ would correspond to metastable stellar configurations, but they are shown for the sake of completeness. We set values for the central density in the interval $\rho_c \in [0.1, 3]\rho_0$. We can see there is a correlation of luminosity–temperature, as expected, and thus a nontrivial dependence on the effective parameter of our MG modelization, ξ, which is clear for $T_{\rm eff} > 6000$ K. Spectral types O, B, A, and F for main-sequence stars can display such high temperatures. Although we cannot expect to recover the meaningful (GR) Hertzsprung–Russell diagram with our simplified approach, the analogous logarithmic correlation we find under the form $\mathrm{Log}\, L = \alpha \mathrm{Log}\,[T_{\rm eff}(R)] + C$ yields a weak variation in the slope, $\alpha(\xi)$, for this case at the $\sim$0.6%. See some values listed for reference in Table 1. One important difference obtained in our calculation with respect to the usual approach where ($T_{\rm eff}$, R) are noncorrelated variables is that for the GR case we do not recover the familiar value $\alpha = 4$, as in our treatment $T_{\rm eff}$ is obtained from the R-dependent value of the luminosity. In other words, the MG model used determines the variation in the radius R, and thus the luminosity. Therefore, values shown in Table 1 are by no means a predictive output of the model, but rather an indication of the weak dependence of the ξ parameter.

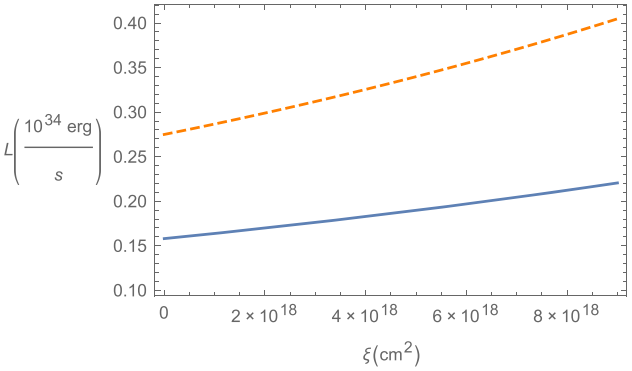

Figure 5. Stellar luminosity for a solar-type star as a function of ξ for two different values of $\rho_c = \rho_0$ (solid line) and $\rho_c = 100\,\mathrm{g\,cm^{-3}}$ (dashed line).

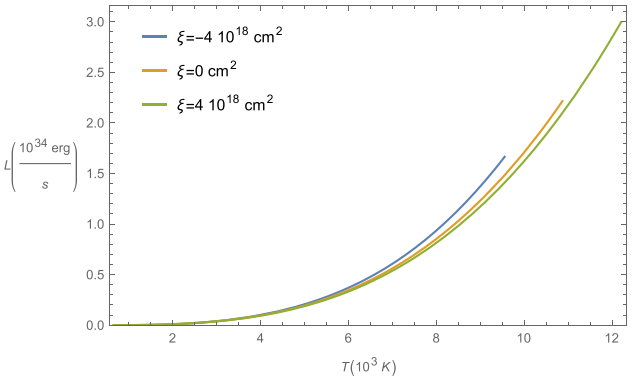

Figure 6. Stellar luminosity for a solar-type star as a function of effective temperature $T_{\rm eff}$ for $\xi = -4 \times 10^{18}$, 0 (GR case), and 4×10^{18} cm^2. We take $\rho_c \in [0.1, 3]\rho_0$.

Table 1
Slope values $\alpha(\xi)$ in the Correlation L vs. $T_{\rm eff}$ for Solar-type Stars

ξ(cm^2)	α
-4×10^{18}	3.234
0	3.1904
4×10^{18}	3.1702

Note. See the text for details.

In order to explore the variations introduced by the subset of the MG model we study in this work let us consider a higher-density stellar object such as a WD. To model this kind of object we use a relativistic Fermi gas simplified EoS dominated by an electron component using a polytrope with $n = 3$ and $K = 4.8 \times 10^{14}\,\mathrm{cm^3\,g^{-\frac{1}{3}}\,s^{-2}}$. In this way, we recover solutions to the structure equations Equations (34) and (35) yielding masses up to the maximum theoretical limit $M = 1.44\,M_\odot$ (Chandrasekhar mass). Note that when using GR with an $n = 3$ polytropic EoS, M values (but not radii) are constant when varying ρ_c.

In Figure 7, we plot the WD mass–radius relationship for $|\xi| = 10^{16}$ cm^2. Solid (dashed) lines corresponds to the case in which $\xi < 0$ ($\xi > 0$). We use $\rho_c \in [0.01, 9]\rho_{c,I}$ where $\rho_{c,I} = 10^6\,\mathrm{g\,cm^{-3}}$ is a typical WD central density. As before, we keep for reference M_0 and R_0 for normalization in the axis labels using those given by solar-type stars. If we further restrict to models in which $\xi \geqslant 0$, which are those that provide

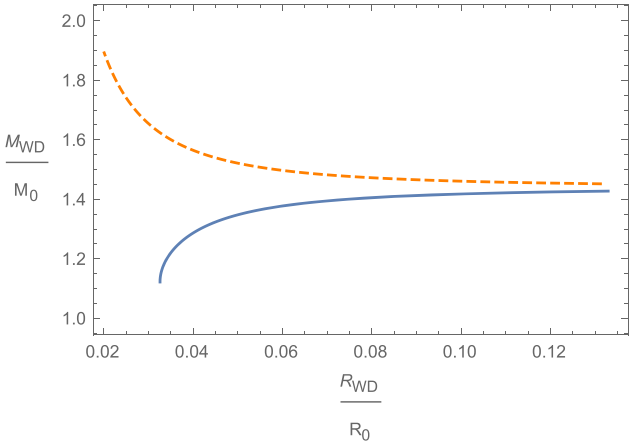

Figure 7. WD mass–radius relationship for $|\xi| = 10^{16}\,\mathrm{cm}^2$. The solid line corresponds to the case in which $\xi < 0$ and the dashed line to $\xi > 0$. We use $\rho_c \in [0.01, 9]\rho_{c,I}$ where $\rho_{c,I} = 10^6\,\mathrm{g\,cm}^{-3}$.

stable stellar configurations of $M(R)$, it is clear that, given a ξ value, the maximum mass (M_{Ch}) will be obtained for the highest possible value of ρ_c provided the perturbative solution still holds. Because the heaviest WD reported in the literature has a mass $M/M_\odot \simeq 1.37$ (Hachisu & Kato 2000), and the GR M_{Ch} value is even higher than this, $\sim 1.44\,M_\odot$, all values obtained in this perturbative framework are allowed. Thus, in the high-density setting presented the ξ parameter remains unconstrained.

4. Conclusions

Using a model-independent approach, we have studied the effects of a subset of MG theories involving one extra scalar degree of freedom on stellar structure. We use a perturbative technique capable of solving in a linearized regime. We have selected our main scenario concerning the application to low-density stellar objects. First, in a perturbative approach, we have obtained mass and radius solutions for low-mass solar-type objects using a polytropic $n = 3$ EoS. We have analyzed how internal temperature profiles and stellar luminosities are affected with respect to the reference case of GR. We provide a fit for masses and radii provided a central density value, i.e., $M(\xi, \rho_c)$, $R(\xi, \rho_c)$. We obtain that a change in the curvature of $M(R)$ results when ξ changes from positive to negative values, connecting the latter to metastable stellar configurations. We also find that MG can affect stellar luminosity from its ξ dependence. Globally, the effective temperature from a $L \propto T_{\mathrm{eff}}^4$ law results in a linear Log L–Log T_{eff} behavior with a weak dependence on ξ. We anticipate that this could result in objects appearing brighter (as L is increased with any stable configuration $\xi > 0$, but this seems hard to measure experimentally as internal stellar dynamics is complex. Furthermore, it seems challenging to disentangle this effect from other standard effects such as proper fluctuations of the star. Even the Sun is a weakly variable star, with its major source of fluctuation coming from the 11-year solar cycle and revealing a smaller periodic variation of about $\sim\pm 0.1\%$. It is nevertheless worth pointing out that both effects, involving standard and new physics, could indeed be present and need to be further studied. When a particular case of a high-density star is considered (WDs), we find that no constraint appears on the ξ parameter from calculated values of the Chandrasekhar mass as it is always larger than the GR value in the perturbative approach we use. Our treatment for both low- and high-density stellar case examples can help to understand the behavior of MG on small (not cosmological) scales.

We thank M. Fairbairn for useful comments. This work has been supported by Junta de Castilla y León SA083P17, Spanish MINECO grant FIS2016-78859-P(AEI/FEDER, UE), and by PHAROS Cost action. We also thank the support of the Spanish Red Consolider MultiDark FPA2017-90566-REDC. M.C. is supported by a fellowship from the University of Salamanca.

References

Abbott, B. P., Abbott, R., Abbott, T. D., et al. (LIGO Scientific and Virgo Collaborations) 2016, PhRvL, 116, 061102
Abbott, B. P., Abbott, R., Abbott, T. D., et al. (LIGO Scientific and Virgo Collaborations) 2017, PhRvL, 119, 161101
Adelberger, E. G., Gundlach, J. H., Heckel, B. R., Hoedl, S., & Schlamminger, S. 2009, PrPNP, 62, 102
Adelberger, E. G., Heckel, B. R., & Nelson, A. E. 2003, ARNPS, 53, 77
Amendola, L., Appleby, S., Avgoustidis, A., et al. 2018, LRR, 21, 2
Babichev, E., Koyama, K., Langlois, D., Saito, R., & Sakstein, J. 2016, CQGra, 33, 235014
Baker, T., Bellini, E., Ferreira, P. G., et al. 2017, PhRvL, 119, 251301
Bertschinger, E., & Zukin, P. 2008, PhRvD, 78, 024015
Burrage, C., & Sakstein, J. 2018, LRR, 21, 1
Capozziello, S., De Laurentis, M., Farinelli, R., & Odintsov, S. D. 2016, PhRvD, 93, 023501
Cermeño, M., & Pérez-García, M. A. 2018, PhRvD, 98, 063002
Clifton, T., Ferreira, P. G., Padilla, A., & Skordis, C. 2012, PhR, 513, 1
Collett, T. E., Oldham, L. J., Smith, R. J., et al. 2018, Sci, 360, 1342
Creminelli, P., & Vernizzi, F. 2017, PhRvL, 119, 251302
Ezquiaga, J. M., & Zumalacárregui, M. 2018, FrASS, 5, 44
Ezquiaga, J. M., & Zumalacárregui, M. 2017, PhRvL, 119, 251304
Giannantonio, T., Martinelli, M., Silvestri, A., & Melchiorri, A. 2010, JCAP, 1004, 030
Gleyzes, J., Langlois, D., Piazza, F., & Vernizzi, F. 2015, PhRvL, 114, 211101
Hachisu, I., & Kato, M. 2000, ApJ, 540, 447
Hansen, C. J., Kawaler, S. D., & Trimble, V. 1994, Stellar Interiors—Physical Principles, Structure, and Evolution (2nd ed.; New York: Spinger)
Hinterbichler, K., & Khoury, J. 2010, PhRvL, 104, 231301
Hojjati, A., Pogosian, L., Silvestri, A., & Zhao, G. B. 2014, PhRvD, 89, 083505
Jain, R. K., Kouvaris, C., & Nielsen, N. G. 2016, PhRvL, 116, 151103
Joyce, A., Jain, B., Khoury, J., & Trodden, M. 2015, PhR, 568, 1
Khoury, J., & Weltman, A. 2004, PhRvL, 93, 171104
Kobayashi, T., Watanabe, Y., & Yamauchi, D. 2015, PhRvD, 91, 064013
Koyama, K., & Sakstein, J. 2015, PhRvD, 91, 124066
Maciel, W. J. 2016, Introduction to Stellar Structure (Berlin: Springer)
Pani, P., Cardoso, V., & Delsate, T. 2011, PhRvL, 107, 031101
Patrignani, C., & Particle Data Group 2016, ChPhC, 40, 100001
Pérez-García, M. A., Daigne, F., & Silk, J. 2013, ApJ, 768, 145
Pérez-García, M. A., & Martins, C. J. A. P. 2012, PhLB, 718, 241
Planck Collaboration, Ade, P. A. R., Aghanim, N., et al. 2016, A&A, 594, A14
Resco, M. A., & Maroto, A. L. 2018, JCAP, 1810, 014
Saito, R., Yamauchi, D., Mizuno, S., Gleyzes, J., & Langlois, D. 2015, JCAP, 1506, 008
Sakstein, J. 2015a, PhRvL, 115, 201101
Sakstein, J. 2015b, PhRvD, 92, 124045
Sakstein, J., & Jain, B. 2017, PhRvL, 119, 251303
Saltas, I. D., Sawickia, I., & Lopes, I. 2018, JCAP, 05, 028
Shapiro, S. L., & Teukolsky, S. A. 1983, Black Holes, White Dwarfs and Neutron Stars: The Physics of Compact Objects (New York: Wiley)
Silvestri, A., Pogosian, L., & Buniy, R. V. 2013, PhRvD, 87, 104015
Turck-Chieze, S., & Couvidat, S. 2011, RPPh, 74, 086901
Vainshtein, A. I. 1972, PhL, 39B, 393
Velten, H., Oliveira, A. M., & Wojnar, A. 2016, PoS, 2015, 025, https://pos.sissa.it/262/025/pdf
Zumalacárregui, M., & García-Bellido, J. 2014, PhRvD, 89, 064046

Bibliography

1. F. Zwicky, *Helvetica Physica Acta* **6**, 110 (1933).
2. F. Zwicky, *Astrophysical Journal* **86**, 217 (1937).
3. V. C. Rubin, W. K. Ford, *Astrophys. J* **159**, 379 (1970).
4. M. Markevitch *et al.*, *The Astrophysical Journal* **606**, 819, (http://stacks.iop.org/0004-637X/606/i=2/a=819) (2004).
5. D. Clowe, A. Gonzalez, M. Markevitch, *The Astrophysical Journal* **604**, 596, (http://stacks.iop.org/0004-637X/604/i=2/a=596) (2004).
6. D. Clowe *et al.*, *The Astrophysical Journal Letters* **648**, L109, (http://stacks.iop.org/1538-4357/648/i=2/a=L109) (2006).
7. D. Scott, G. Smoot, eprint: astro-ph/0406567 (2004).
8. N. S. W. Hu, J. Silk, *Nature* **386**, 37, (http://link.aip.org/link/?RSI/72/4477/1) (1997).
9. W. Hu, S. Dodelson, *Ann. Rev. Astron. Astrophys.* **40**, 171, (http://link.aip.org/link/?RSI/72/4477/1) (2002).
10. A. Liddle, *An Introduction to Modern Cosmology (2nd ed.), edited by Wiley* (2003).
11. Planck Collaboration *et al.*, eprint: arXiv:1807.06209[astro-ph.CO] (2018).
12. G. Bertone, D. Hooper, eprint: arXiv:1605.04909v2[astro-ph.CO] (2016).
13. K. G. Begeman, A. H. Broeils, R. H. Sanders, *MNRAS* **249**, 523 (1991).
14. R. Scarpa, *AIP Conference Proceedings* **822**, 253, eprint: https://aip.scitation.org/doi/pdf/10.1063/1.2189141, (https://aip.scitation.org/doi/abs/10.1063/1.2189141) (2006).
15. B. Famaey, S. S. McGaugh, *Living Reviews in Relativity* **15**, 10, (https://doi.org/10.12942/lrr-2012-10) (2012).
16. D. J. Fixsen, *The Astrophysical Journal* **707**, 916, (https://doi.org/10.1088%2F0004-637x%2F707%2F2%2F916) (2009).
17. (http://ramanujan25449.blogspot.com.es/2014/02/lentes-gravitacionales-lostelescopios).
18. C. Skordis, D. F. Mota, P. G. Ferreira, C. Bœhm, *Phys. Rev. Lett.* **96**, 011301, (https://link.aps.org/doi/10.1103/PhysRevLett.96.011301) (2006).
19. S. DODELSON, *International Journal of Modern Physics D* **20**, 2749, eprint: https://doi.org/10.1142/S0218271811020561, (https://doi.org/10.1142/S0218271811020561) (2011).
20. L. Bernard, L. Blanchet, *Phys. Rev. D* **91**, 103536, (https://link.aps.org/doi/10.1103/PhysRevD.91.103536) (2015).
21. J. Khoury, *Phys. Rev. D* **91**, 024022, (https://link.aps.org/doi/10.1103/PhysRevD.91.024022) (2015).

22. J. Khoury, *Phys. Rev. D* **93**, 103533, (https://link.aps.org/doi/10.1103/PhysRevD.93.103533) (2016).
23. J. I. Read, M. G. Walker, P Steger, *Monthly Notices of the Royal Astronomical Society*, sty3404, eprint: /oup/backfile/content_public/journal/mnras/pap/10.1093_mnras_sty3404/1/sty3404.pdf, (http://dx.doi.org/10.1093/mnras/sty3404) (2019).
24. L. Roszkowski, E. M. Sessolo, S. Trojanowski, *Reports on Progress in Physics* **81**, 066201, (http://stacks.iop.org/0034-4885/81/i=6/a=066201) (2018).
25. S. W. Randall, M. Markevitch, D. Clowe, A. H. Gonzalez, M. Bradač, *The Astrophysical Journal* **679**, 1173, (http://stacks.iop.org/0004-637X/679/i=2/a=1173) (2008).
26. Y. Hochberg, E. Kuflik, T. Volansky, J. G. Wacker, *Phys. Rev. Lett.* **113**, 171301, (https://link.aps.org/doi/10.1103/PhysRevLett.113.171301) (2014).
27. Y. Hochberg, E. Kuflik, H. Murayama, T. Volansky, J. G. Wacker, *Phys. Rev. Lett.* **115**, 021301, (https://link.aps.org/doi/10.1103/PhysRevLett.115.021301) (2015).
28. N. Bernal, X. Chu, *Journal of Cosmology and Astroparticle Physics* **2016**, 006.
29. J. Herms, A. Ibarra, T. Toma, *Journal of Cosmology and Astroparticle Physics* **2018**, 036, (http://stacks.iop.org/1475-7516/2018/i=06/a=036) (2018).
30. J. B. Muñoz, A. Loeb, *Nature* **557**, 684 (2018).
31. E. Fermi, *Il Nuovo Cimento (1924-1942)* **11**, 1, (https://doi.org/10.1007/BF02959820) (1934).
32. X. Chu, T. Hambye, M. H. Tytgat, *Journal of Cosmology and Astroparticle Physics* **2012**, 034, (https://doi.org/10.1088%2F1475-7516%2F2012%2F05%2F034) (2012).
33. G. D. Starkman, A. Gould, R. Esmailzadeh, S. Dimopoulos, *Phys. Rev. D* **41**, 3594, (https://link.aps.org/doi/10.1103/PhysRevD.41.3594) (1990).
34. G. D. Mack, J. F. Beacom, G. Bertone, *Phys. Rev. D* **76**, 043523, (https://link.aps.org/doi/10.1103/PhysRevD.76.043523) (2007).
35. M. S. Mahdawi, G. R. Farrar, *Journal of Cosmology and Astroparticle Physics* **2017**, 004, (http://stacks.iop.org/1475-7516/2017/i=12/a=004) (2017).
36. C. Muñoz, *EPJ Web Conf.* **136**, 01002, (https://doi.org/10.1051/epjconf/201713601002) (2017).
37. J. Magaña, T. Matos, *Journal of Physics: Conference Series* **378**, 012012, (http://stacks.iop.org/1742-6596/378/i=1/a=012012) (2012).
38. M. Pospelov, A. Ritz, M. Voloshin, *Physics Letters B* **662**, 53, (http://www.sciencedirect.com/science/article/pii/S0370269308002402) (2008).
39. S. Liem *et al.*, *Journal of High Energy Physics* **2016**, 77, (https://doi.org/10.1007/JHEP09(2016)077) (2016).
40. J. Brod, A. Gootjes-Dreesbach, M. Tammaro, J. Zupan, *Journal of High Energy Physics* **2018**, 65, (https://doi.org/10.1007/JHEP10(2018)065) (2018).
41. N. F. Bell, Y. Cai, J. B. Dent, R. K. Leane, T. J. Weiler, *Phys. Rev. D* **96**, 023011, (https://link.aps.org/doi/10.1103/PhysRevD.96.023011) (2017).
42. B. Batell, M. Pospelov, A. Ritz, Y. Shang, *Phys. Rev. D* **81**, 075004, (https://link.aps.org/doi/10.1103/PhysRevD.81.075004) (2010).

43. N. F. Bell, K. Petraki, *Journal of Cosmology and Astroparticle Physics* **2011**, 003, (http://stacks.iop.org/1475-7516/2011/i=04/a=003) (2011).
44. R. K. Leane, K. C. Y. Ng, J. F. Beacom, *Phys. Rev. D* **95**, 123016, (https://link.aps.org/doi/10.1103/PhysRevD.95.123016) (2017).
45. I. Z. Rothstein, T. Schwetz, J. Zupan, *Journal of Cosmology and Astroparticle Physics* **2009**, 018, (http://stacks.iop.org/1475-7516/2009/i=07/a=018) (2009).
46. S. Profumo, F. S. Queiroz, J. Silk, C. Siqueira, *Journal of Cosmology and Astroparticle Physics* **2018**, 010, (http://stacks.iop.org/1475-7516/2018/i=03/a=010) (2018).
47. E. Morgante, eprint: arXiv:1804.01245[hep-ph] (2018).
48. C. Boehm, M. J. Dolan, C. McCabe, M. Spannowsky, C. J. Wallace, *Journal of Cosmology and Astroparticle Physics* **2014**, 009, (http://stacks.iop.org/1475-7516/2014/i=05/a=009) (2014).
49. C. Arina, E. Del Nobile, P. Panci, *Phys. Rev. Lett.* **114**, 011301, (https://link.aps.org/doi/10.1103/PhysRevLett.114.011301) (2015).
50. M. Bauer, U. Haisch, F. Kahlhoefer, *Journal of High Energy Physics* **2017**, 138, (https://doi.org/10.1007/JHEP05(2017)138) (2017).
51. S. Baek, P. Ko, J. Li, *Phys. Rev. D* **95**, 075011, (https://link.aps.org/doi/10.1103/PhysRevD.95.075011) (2017).
52. M. J. Dolan, F. Kahlhoefer, C. McCabe, K. Schmidt-Hoberg, *Journal of High Energy Physics* **2015**, 171, (https://doi.org/10.1007/JHEP03(2015)171) (2015).
53. E. Izaguirre, G. Krnjaic, B. Shuve, *Phys. Rev. D* **90**, 055002, (https://link.aps.org/doi/10.1103/PhysRevD.90.055002) (2014).
54. M. Cermeño, M. A. Pérez-García, J. Silk, *Phys. Rev. D* **94**, 023509, (https://link.aps.org/doi/10.1103/PhysRevD.94.023509) (2016).
55. M. Cermeño, M. Pérez-García, J. Silk, *Phys. Rev. D* **94**, 063001, (https://link.aps.org/doi/10.1103/PhysRevD.94.063001) (2016).
56. M. Cermeño, M. A. Pérez-García, R. A. Lineros, *The Astrophysical Journal* **863**, 157, (https://doi.org/10.3847%2F1538-4357%2Faad1ec) (2018).
57. M. Cermeño, M. A. Pérez-García, *Phys. Rev. D* **98**, 063002, (https://link.aps.org/doi/10.1103/PhysRevD.98.063002) (2018).
58. S. Scopel, K.-H. Yoon, J.-H. Yoon, *Journal of Cosmology and Astroparticle Physics* **2015**, 041, (http://stacks.iop.org/1475-7516/2015/i=07/a=041) (2015).
59. J. Goodman *et al.*, *Phys. Rev. D* **82**, 116010, (https://link.aps.org/doi/10.1103/PhysRevD.82.116010) (2010).
60. T. M. Undagoitia, L. Rauch, *Journal of Physics G: Nuclear and Particle Physics* **43**, 013001, (http://stacks.iop.org/0954-3899/43/i=1/a=013001) (2016).
61. J. H. Davis, *International Journal of Modern Physics A* **30**, 1530038, eprint: https://doi.org/10.1142/S0217751X15300380, (https://doi.org/10.1142/S0217751X15300380) (2015).
62. B. J. Kavanagh, *Phys. Rev. D* **97**, 123013, (https://link.aps.org/doi/10.1103/PhysRevD.97.123013) (2018).

63. M. G. Aartsen *et al.*, *The European Physical Journal C* **78**, 831, (https://doi.org/10.1140/epjc/s10052-018-6273-3) (2018).
64. J. Zornoza, C. Toennis, *Journal of Physics: Conference Series* **888**, 012206, (http://stacks.iop.org/1742-6596/888/i=1/a=012206) (2017).
65. E. Charles *et al.*, *Physics Reports* **636**, Sensitivity Projections for Dark Matter Searches with the Fermi Large Area Telescope, 1, (http://www.sciencedirect.com/science/article/pii/S0370157316300916) (2016).
66. M. Aguilar *et al.*, *Phys. Rev. Lett.* **117**, 091103, (https://link.aps.org/doi/10.1103/PhysRevLett.117.091103) (2016).
67. A. Boveia, C. Doglioni, *Annual Review of Nuclear and Particle Science* **68**, 429, eprint: https://doi.org/10.1146/annurev-nucl-101917-021008, (https://doi.org/10.1146/annurev-nucl-101917-021008) (2018).
68. E. Bagnaschi, et al., eprint: arXiv:1508.01173[hep-ph] (2015).
69. F. Kahlhoefer, *International Journal of Modern Physics A* **32**, 1730006, eprint: https://doi.org/10.1142/S0217751X1730006X, (https://doi.org/10.1142/S0217751X1730006X) (2017).
70. M. Crisler *et al.*, *Phys. Rev. Lett.* **121**, 061803, (https://link.aps.org/doi/10.1103/PhysRevLett.121.061803) (2018).
71. T. Basak, 2053-2571, 2–1 to 2–9, (http://dx.doi.org/10.1088/978-1-64327-132-3ch2) (2018).
72. M. Freytsis, Z. Ligeti, *Phys. Rev. D* **83**, 115009, (https://link.aps.org/doi/10.1103/PhysRevD.83.115009) (2011).
73. T. Li, *Physics Letters B* **782**, 497, (http://www.sciencedirect.com/science/article/pii/S0370269318304374) (2018).
74. (https://upload.wikimedia.org/wikipedia/commons/9/9e/Neutron_star_cross_section.svg).
75. W. Baade, F. Zwicky, *Proceedings of the National Academy of Science* **20**, 254 (1934).
76. A. Hewish, *Annual Review of Astronomy and Astrophysics* **8**, 265, eprint: https://doi.org/10.1146/annurev.aa.08.090170.001405, (https://doi.org/10.1146/annurev.aa.08.090170.001405) (1970).
77. N. K. Glendenning, *Compact stars: Nuclear physics, particle physics, and general relativity, New York: Springer* (1997).
78. N. Chamel, P. Haensel, *Living Reviews in Relativity* **11**, 10, (https://doi.org/10.12942/lrr-2008-10) (2008).
79. D. G. Yakovlev *et al.*, *Nuclear Physics A* **752**, 590 (2005).
80. D. D. Ofengeim, D. G. Yakovlev, *MNRAS* **467**, 3598 (2017).
81. D. Koester, G. Chanmugam, *Reports on Progress in Physics* **53**, 837 (1990).
82. S. D. Kawaler, I. Novikov, G. Srinivasan, ed. by G. Meynet, D. Schaerer (1997).
83. G. Fontaine, F. Wesemael, in *Encyclopedia of Astronomy and Astrophysics*, ed. by P. Murdin, p. 1894.
84. Haensel, P., *EAS Publications Series* **7**, 249, (https://doi.org/10.1051/eas:2003043) (2003).

85. S. D. Kawaler, I. Novikov, G. Srinivasan, G. Meynet, D. Schaerer, *Stellar Remnants*.
86. C. J. Hansen, S. D. Kawaler, V. Trimble, *Stellar interiors : physical principles, structure, and evolution, 2nd ed., New York: Springer-Verlag* (2004).
87. W. J. Maciel, *Introduction to Stellar Structure, Edited by Springer* (2016).
88. M. I. Nouh *et al.*, *Astrophysics* **59**, 540, (https://doi.org/10.1007/s10511-016-9456-3) (2016).
89. A. Gould, *Astrophysical Journal* **321**, 571 (1987).
90. D. N. Spergel, W. H. Press, *Astrophysical Journal* **294**, 663 (1985).
91. D. R. Lorimer *et al.*, *Monthly Notices of the Royal Astronomical Society* **372**, 777, eprint: astro-ph/0607640 (2006).
92. R. Catena, P. Ullio, *Journal of Cosmology and Astroparticle Physics* **2010**, 004, (https://doi.org/10.1088%2F1475-7516%2F2010%2F08%2F004) (2010).
93. L. R. Bedin *et al.*, *The Astrophysical Journal* **697**, 965, (https://doi.org/10.1088%2F0004-637x%2F697%2F2%2F965) (2009).
94. G. Bertone, M. Fairbairn, *Phys. Rev. D* **77**, 043515, (https://link.aps.org/doi/10.1103/PhysRevD.77.043515) (2008).
95. M. McCullough, M. Fairbairn, *Phys. Rev. D* **81**, 083520, (https://link.aps.org/doi/10.1103/PhysRevD.81.083520) (2010).
96. H. B. Richer *et al.*, *The Astrophysical Journal* **484**, 741, (https://doi.org/10.1086%2F304379) (1997).
97. F. Camilo, F. A. Rasio, presented at the Binary Radio Pulsars, ed. by F. A. Rasio, I. H. Stairs, vol. 328, p. 147, eprint: astro-ph/0501226.
98. C. Kouvaris, P. Tinyakov, *Phys. Rev. D* **83**, 083512, (https://link.aps.org/doi/10.1103/PhysRevD.83.083512) (2011).
99. T. Güver, A. E. Erkoca, M. H. Reno, I. Sarcevic, *Journal of Cosmology and Astroparticle Physics* **2014**, 013, (http://stacks.iop.org/1475-7516/2014/i=05/a=013) (2014).
100. J. Bramante, *Phys. Rev. Lett.* **115**, 141301, (https://link.aps.org/doi/10.1103/PhysRevLett.115.141301) (2015).
101. C. Kouvaris, P. Tinyakov, *Phys. Rev. D* **82**, 063531, (https://link.aps.org/doi/10.1103/PhysRevD.82.063531) (2010).
102. M. Ángeles Pérez-García, J. Silk, *Physics Letters B* **744**, 13, (http://www.sciencedirect.com/science/article/pii/S0370269315001896) (2015).
103. A. R. Zentner, *Phys. Rev. D* **80**, 063501, (https://link.aps.org/doi/10.1103/PhysRevD.80.063501) (2009).
104. P. Baratella *et al.*, *Journal of Cosmology and Astroparticle Physics* **2014**, 053, (http://stacks.iop.org/1475-7516/2014/i=03/a=053) (2014).
105. S. D. McDermott, H.-B. Yu, K. M. Zurek, *Phys. Rev. D* **85**, 023519, (https://link.aps.org/doi/10.1103/PhysRevD.85.023519) (2012).
106. J. Bramante, K. Fukushima, J. Kumar, *Phys. Rev. D* **87**, 055012, (https://link.aps.org/doi/10.1103/PhysRevD.87.055012) (2013).
107. M. Cermeño, M. A. Pérez-García, J. Silk, *Publications of the Astronomical Society of Australia* **34**, e043 (2017).

108. M. Cermeño, J. Carro, A. L. Maroto, M. A. Pérez-García, *The Astrophysical Journal* **872**, 130 (2019).

109. B. D. Serot, J. D. Walecka, *Advances in Nuclear Physics, edited by J. W. Negele and E. Vogt Plenum* (1986).

110. C. J. Horowitz, M. A. Pérez-García, *Phys. Rev. C* **68**, 025803, (https://link.aps.org/doi/10.1103/PhysRevC.68.025803) (2 2003).

111. M. Tanabashi *et al.*, *Phys. Rev. D* **98**, 030001, (https://link.aps.org/doi/10.1103/PhysRevD.98.030001) (2018).

112. A. Gould, G. Raffelt, *Astrophysical Journal* **352**, 654 (1990).

113. W. J. Carr, *Phys. Rev.* **122**, 1437, (https://link.aps.org/doi/10.1103/PhysRev.122.1437) (5 1961).

114. F. Jüttner, *Annalen der Physik* **339**, 856, (https://onlinelibrary.wiley.com/doi/abs/10.1002/andp.19113390503) (1911).

115. R. Hakim, *Introduction to Relativistic Statistical Mechanics Classical and Quantum (World Scientific, Singapore)* (2011).

116. C. Cercignani, G. M. Kremer, *The Relativistic Boltzmann Equation: Theory and Applications, edited by Birkhäuser Verlag* (2002).

117. I. Ferreras, I. Wasserman, *Phys. Rev. D* **52**, 5459, (https://link.aps.org/doi/10.1103/PhysRevD.52.5459) (1995).

118. M. Hedman, *Journal of Cosmology and Astroparticle Physics* **2013**, 029, (https://doi.org/10.1088%2F1475-7516%2F2013%2F09%2F029) (2013).

119. J. M. Ziman, *Electrons and Phonons (Oxford University Press, Oxford)* (1960).

120. A. I. Chugunov, P. Haensel, *Monthly Notices of the Royal Astronomical Society* **381**, 1143, eprint: http://oup.prod.sis.lan/mnras/article-pdf/381/3/1143/3654270/mnras0381-1143.pdf, (https://doi.org/10.1111/j.1365-2966.2007.12301.x) (2007).

121. J. F. Pérez-Azorín, J. A. Miralles, J. A. Pons, *Astronomy and Astrophysics* **451**, 1009, eprint: astro-ph/0510684 (2006).

122. D. Viganò *et al.*, *Monthly Notices of the Royal Astronomical Society* **434**, 123, arXiv: 1306.2156 [astro-ph.SR] (2013).

123. D. Viganò, R. Perna, N. Rea, J. A. Pons, *Monthly Notices of the Royal Astronomical Society* **443**, 31, eprint: http://oup.prod.sis.lan/mnras/article-pdf/443/1/31/4290053/stu1109.pdf, (https://dx.doi.org/10.1093/mnras/stu1109) (2014).

124. S. Esposito, G. Mangano, G. Miele, I. Picardi, O. Pisanti, *Modern Physics Letters A* **17**, 491, eprint: https://doi.org/10.1142/S0217732302006643, (https://doi.org/10.1142/S0217732302006643) (2002).

125. B. L. Friman, O. V. Maxwell, *Astrophysical Journal* **232**, 541 (1979).

126. D. Yakovlev *et al.*, *Nuclear Physics A* **752**, Proceedings of the 22nd International Nuclear Physics Conference (Part 2), 590, (http://www.sciencedirect.com/science/article/pii/S0375947405002162) (2005).

127. J. M. Lattimer, C. J. Pethick, M. Prakash, P. Haensel, *Phys. Rev. Lett.* **66**, 2701, (https://link.aps.org/doi/10.1103/PhysRevLett.66.2701) (1991).

128. E. F. Brown *et al.*, *Phys. Rev. Lett.* **120**, 182701, (https://link.aps.org/doi/10.1103/PhysRevLett.120.182701) (18 2018).

129. F. K. Liu, *MNRAS* **281**, 1197, eprint: astro-ph/9512061 (1996).

130. T. G. Cowling, *Quarterly Journal of the Royal Astronomical Society* **7**, 121 (1966).

131. A. Hojjati, L. Pogosian, G.-B. Zhao, *Journal of Cosmology and Astroparticle Physics* **2011**, 005 (2011).

132. A. Hojjati *et al.*, *Phys. Rev. D* **85**, 043508, (https://link.aps.org/doi/10.1103/PhysRevD.85.043508) (4 2012).

133. A. Silvestri, L. Pogosian, R. V. Buniy, *Phys. Rev. D* **87**, 104015, (https://link.aps.org/doi/10.1103/PhysRevD.87.104015) (2013).

134. A. D. Simone, A. Monin, A. Thamm, A. Urbano, *Journal of Cosmology and Astroparticle Physics* **2013**, 039, (http://stacks.iop.org/1475-7516/2013/i=02/a=039) (2013).